

MONTICELLO
NUCLEAR GENERATING PLANT
RELOAD SAFETY EVALUATION METHODS

Docket # 50-263
Control # 8610150527
Date 10/2/86 of Document
REGULATORY DOCKET FILE

Septem

NORTHERN STATE
NUCLEAR ANAL

NSI

— NOTICE —

THE ATTACHED FILES ARE OFFICIAL RECORDS OF THE
DIVISION OF DOCUMENT CONTROL. THEY HAVE BEEN
CHARGED TO YOU FOR A LIMITED TIME PERIOD AND
MUST BE RETURNED TO THE RECORDS FACILITY
BRANCH 016. PLEASE DO NOT SEND DOCUMENTS
CHARGED OUT THROUGH THE MAIL. REMOVAL OF ANY
PAGE(S) FROM DOCUMENT FOR REPRODUCTION MUST
BE REFERRED TO FILE PERSONNEL.

DEADLINE RETURN DATE _____

RECORDS FACILITY BRANCH

8610150529 861002
PDR ADOCK 05000263
P PDR

NSPNAD8608

RELOAD SAFETY EVALUATION METHODS

FOR

APPLICATION TO THE MONTICELLO NUCLEAR GENERATING PLANT

NSPNAD-8608

September 1986

Revision 0

Prepared By

Dave Rautmann

Date

9/15/86

Reviewed By

C. J. Giedyl

Date

09/15/86

Approved By

Roger O. Anderson

Date

9/19/86

Reload Safety Evaluation Methods

for

Application to the Monticello Nuclear
Generating Plant

NSPNAD-8606

September 1986

Revision 0

Principal Contributors

Northern States Power Company

Craig Gantner

Jon Kapitz

Craig Nierode

Dave Rautmann

Pat Riedel

Utility Associate International

Dr. Richard Kern

LEGAL NOTICE

This report was prepared by or on behalf of Northern States Power Company (NSP). Neither NSP, nor any person acting on behalf of NSP:

- a. Makes any warranty or representation, express or implied, with respect to the accuracy, completeness, usefulness, or use of any information, apparatus, method or process disclosed or contained in this report, or that the use of any such information, apparatus, method, or process may not infringe privately owned rights; or
- b. Assumes any liabilities with respect to the use of, or for damages resulting from the use of, any information, apparatus, method, or process disclosed in the report.

Table of Contents

	<u>Page</u>
1.0 Introduction and Summary	15
2.0 DYNODE-B Code Description	16
2.1 General Description	16
2.2 Specific Model Descriptions	17
2.2.1 Core Model	17
2.2.2 Reactor Vessel Fluid Model	19
2.2.3 Main Steam System Model	20
2.2.4 Safety System	21
2.2.5 Control Systems	22
2.2.6 Integration Scheme	23
2.3 Comparisons with other Approved Licensing Codes	24
2.3.1 Core Neutronics	24
2.3.2 Steam Lines	25
2.3.3 Reactor Vessel Pressure Distribution	25
3.0 DYNODE-B Code Qualification	27
3.1 Nuclear Model Comparisons	27
3.1.1 Scram Reactivity	28
3.1.2 Void Reactivity	28

Table of Contents (continued)

	<u>Page</u>
3.2 Thermal-Hydraulic Comparisons	29
3.2.1 Code-Code Comparisons	29
3.2.1.1 General Electric REDY Code	29
3.2.1.1.1 Turbine Trip Without Bypass	31
3.2.1.1.2 Turbine Trip With Bypass	32
3.2.1.1.3 Generator Trip	33
3.2.1.1.4 Closure of All Main Steam Isolation Valves	34
3.2.1.1.5 Feedwater Controller Malfunction, Maximum Demand	35
3.2.1.1.6 Loss of Feedwater	37
3.2.1.1.7 Loss of Feedwater Heating	38
3.2.1.1.8 Pressure Regulator Fails Open	39
3.2.1.1.9 Recirculation Pump Seizure	40
3.2.1.1.10 Two Recirculation Pump Drive Motor Trip	41
3.2.1.1.11 Recirculation Flow Controller Failure, Increase Demand	42
3.2.1.1.12 Recirculation Flow Controller Failure, Decrease Demand	43
3.2.1.1.13 Improper Start of an Inactive Recirculation Loop	44
3.2.1.2 General Electric ODYN Code	47
3.2.1.2.1 Load Rejection without Bypass	48
3.2.1.2.2 Feedwater Controller Malfunction, Maximum Demand	50
3.2.1.2.3 MSIV Closure (Flux Scram)	52

Table of Contents (continued)

	<u>Page</u>
3.2.2 Code-Data Comparisons	53
3.2.2.1 Peach Bottom Unit 2 EOC2 Turbine Trip Tests	54
3.2.2.1.1 Test Summary	54
3.2.2.1.2 Model Inputs	54
3.2.2.1.3 Data Comparison	56
3.2.2.2 Monticello Start Up Tests	59
3.2.2.2.1 Turbine Trip with Bypass at 100% Power (STP 16)	60
3.2.2.2.2 Closure of 4/4 Main Steam Isolation Valves at 75% Power (STP 11)	61
3.2.2.2.3 2/2 Recirculation Pump Trip (STP 14)	63
3.2.2.2.4 Automatic Flow Decrease at 100% Power (STP 15)	64
3.2.2.2.5 Pressure Regulator Setpoint Step at 100% Power (STP 18)	66
3.2.2.2.6 Feedwater Controller Level Setpoint Step at 100% Power (STP 20)	68
4.0 Reload Safety Evaluation Methods	161
4.1 Model/Event Application	162

Table of Contents (continued)

	<u>Page</u>
4.2 Input Parameters	164
4.2.1 Kinetics Parameters	165
4.2.1.1 Bundle Power	166
4.2.1.2 Control Rod Worths	167
4.2.1.3 Void Reactivity	168
4.2.1.4 Doppler Reactivity	170
4.2.1.5 Delayed Neutrons	171
4.2.1.6 Neutron Source Lifetime	173
4.2.2 CRD Scram Time	174
4.2.3 Critical Power Ratio	176
4.3 Limiting Acceptance Criteria	177
4.3.1 Thermal Limits	177
4.3.2 ASME Vessel Overpressure	178
4.3.3 System Stability	179
4.4 Evaluation and Application of Uncertainties	180
4.4.1 Thermal Limits	180
4.4.2 ASME Vessel Overpressure	181
4.4.3 System Stability	182
5.0 Conclusions	200
6.0 References	201

List of Figures

	<u>Page</u>
2.1-1 Schematic of DYNODE-B BWR NSSS Representation	26
3.1-1 NDH-DNB Comparison - Relative Power	74
3.1-2 NDH-DNB Comparison - Relative Power	74
3.1-3 NDH-DNB Comparison - Delta Rho	75
3.1-4 NDH-DNB Comparison - Delta Rho Error	75
3.2-1 Turbine Trip without Bypass - Steam Dome Pressure	76
3.2-2 Turbine Trip without Bypass - Relative Power	76
3.2-3 Turbine Trip without Bypass - Core Average Heat Flux	77
3.2-4 Turbine Trip without Bypass - Core Inlet Flow	77
3.2-5 Turbine Trip without Bypass - Main Steam Line Flow	78
3.2-6 Turbine Trip without Bypass - Feedwater Flow	78
3.2-7 Turbine Trip without Bypass - Sensed Level	79
3.2-8 Turbine Trip with Bypass - Steam Dome Pressure	80
3.2-9 Turbine Trip with Bypass - Relative Power	80
3.2-10 Turbine Trip with Bypass - Core Average Heat Flux	81
3.2-11 Turbine Trip with Bypass - Core Inlet Flow	81
3.2-12 Turbine Trip with Bypass - Main Steam Line Flow	82
3.2-13 Turbine Trip with Bypass - Feedwater Flow	82
3.2-14 Turbine Trip with Bypass - Sensed Level	83
3.2-15 Generator Trip - Sensed Level	84
3.2-16 Generator Trip - Steam Dome Pressure	84
3.2-17 Generator Trip - Core Inlet Flow	85
3.2-18 Generator Trip - Core Average Heat Flux	85
3.2-19 Generator Trip - Relative Power	86
3.2-20 Generator Trip - Feedwater Flow	86
3.2-21 Generator Trip - Main Steam Line Flow	87
3.2-22 Closure of All Main Steam Isolation Valves - Steam Dome Pressure	88
3.2-23 Closure of All Main Steam Isolation Valves - Relative Power	88
3.2-24 Closure of All Main Steam Isolation Valves - Core Average Heat Flux	89
3.2-25 Closure of All Main Steam Isolation Valves - Core Inlet Flow	89

Figures (continued)

	<u>Page</u>
3.2-26 Closure of All Main Steam Isolation Valves - Main Steam Line Flow	90
3.2-27 Closure of All Main Steam Isolation Valves - Feedwater Flow	90
3.2-28 Closure of All Main Steam Isolation Valves - Sensed Level	91
3.2-29 Feedwater Controller Malfunction, Maximum Demand - Sensed Level	92
3.2-30 Feedwater Controller Malfunction, Maximum Demand - Steam Dome Pressure	92
3.2-31 Feedwater Controller Malfunction, Maximum Demand - Core Inlet Flow	93
3.2-32 Feedwater Controller Malfunction, Maximum Demand - Core Average Heat Flux	93
3.2-33 Feedwater Controller Malfunction, Maximum Demand - Relative Power	94
3.2-34 Feedwater Controller Malfunction, Maximum Demand - Feedwater Flow	94
3.2-35 Feedwater Controller Malfunction, Maximum Demand - Main Steam Line Flow	95
3.2-36 Loss of Feedwater - Sensed Level	96
3.2-37 Loss of Feedwater - Steam Dome Pressure	96
3.2-38 Loss of Feedwater - Core Inlet Flow	97
3.2-39 Loss of Feedwater - Core Average Heat Flux	97
3.2-40 Loss of Feedwater - Relative Power	98
3.2-41 Loss of Feedwater - Feedwater Flow	98
3.2-42 Loss of Feedwater - Main Steam Line Flow	99
3.2-43 Loss of Feedwater Heating - Sensed Level	100
3.2-44 Loss of Feedwater Heating - Steam Dome Pressure	100
3.2-45 Loss of Feedwater Heating - Core Inlet Flow	101
3.2-46 Loss of Feedwater Heating - Core Average Heat Flux	101
3.2-47 Loss of Feedwater Heating - Relative Power	102
3.2-48 Loss of Feedwater Heating - Feedwater Flow	102
3.2-49 Loss of Feedwater Heating - Main Steam Line Flow	103
3.2-50 Pressure Regulator Fails Open - Steam Dome Pressure	104
3.2-51 Pressure Regulator Fails Open - Relative Power	104
3.2-52 Pressure Regulator Fails Open - Core Average Heat Flux	105
3.2-53 Pressure Regulator Fails Open - Core Inlet Flow	105
3.2-54 Pressure Regulator Fails Open - Main Steam Line Flow	106
3.2-55 Pressure Regulator Fails Open - Feedwater Flow	106
3.2-56 Pressure Regulator Fails Open - Sensed Level	107

Figures (continued)

	<u>Page</u>
3.2-57 Recirculation Pump Seizure - Sensed Level	108
3.2-58 Recirculation Pump Seizure - Steam Dome Pressure	108
3.2-59 Recirculation Pump Seizure - Core Inlet Flow	109
3.2-60 Recirculation Pump Seizure - Core Average Heat Flux	109
3.2-61 Recirculation Pump Seizure - Relative Power	110
3.2-62 Recirculation Pump Seizure - Feedwater Flow	110
3.2-63 Recirculation Pump Seizure - Main Steam Line Flow	111
3.2-64 Two Recirculation Pump Drive Motor Trip - Sensed Level	112
3.2-65 Two Recirculation Pump Drive Motor Trip - Steam Dome Pressure	112
3.2-66 Two Recirculation Pump Drive Motor Trip - Core Inlet Flow	113
3.2-67 Two Recirculation Pump Drive Motor Trip - Core Average Heat Flux	113
3.2-68 Two Recirculation Pump Drive Motor Trip - Relative Power	114
3.2-69 Two Recirculation Pump Drive Motor Trip - Feedwater Flow	114
3.2-70 Two Recirculation Pump Drive Motor Trip - Main Steam Line Flow	115
3.2-71 Recirculation Flow Controller Failure, Increase Demand - Sensed Level	116
3.2-72 Recirculation Flow Controller Failure, Increase Demand - Steam Dome Pressure	116
3.2-73 Recirculation Flow Controller Failure, Increase Demand - Core Inlet Flow	117
3.2-74 Recirculation Flow Controller Failure, Increase Demand - Core Average Heat Flux	117
3.2-75 Recirculation Flow Controller Failure, Increase Demand - Relative Power	118
3.2-76 Recirculation Flow Controller Failure, Increase Demand - Feedwater Flow	118
3.2-77 Recirculation Flow Controller Failure, Increase Demand - Main Steam Line Flow	119
3.2-78 Recirculation Flow Controller Failure, Decrease Demand - Sensed Level	120
3.2-79 Recirculation Flow Controller Failure, Decrease Demand - Steam Dome Pressure	120
3.2-80 Recirculation Flow Controller Failure, Decrease Demand - Core Inlet Flow	121
3.2-81 Recirculation Flow Controller Failure, Decrease Demand - Core Average Heat Flux	121
3.2-82 Recirculation Flow Controller Failure, Decrease Demand - Relative Power	122
3.2-83 Recirculation Flow Controller Failure, Decrease Demand - Feedwater Flow	122
3.2-84 Recirculation Flow Controller Failure, Decrease Demand - Main Steam Line Flow	123

Figures (continued)

	<u>Page</u>
3.2-85 Improper Start of an Inactive Recirculation Loop - Sensed Level	124
3.2-86 Improper Start of an Inactive Recirculation Loop - Steam Dome Pressure	124
3.2-87 Improper Start of an Inactive Recirculation loop - Core Inlet Flow	125
3.2-88 Improper Start of an Inactive Recirculation Loop - Core Average Heat Flux	125
3.2-89 Improper Start of an Inactive Recirculation Loop - Relative Power	126
3.2-90 Improper Start of an Inactive Recirculation Loop - Feedwater Flow	126
3.2-91 Improper Start of an Inactive Recirculation Loop - Main Steam Line Flow	127
3.2-92 Load Rejection w/o Bypass - Relative Power	128
3.2-93 Load Rejection w/o Bypass - Core Average Heat FLux	128
3.2-94 Load Rejection w/o Bypass - Steam Dome Pressure	129
3.2-95 Load Rejection w/o Bypass - Sensed Level	129
3.2-96 Load Rejection w/o Bypass - Vessel Steam Flow	130
3.2-97 Load Rejection w/o Bypass - Feedwater Flow	130
3.2-98 Load Rejection w/o Bypass - Core Inlet Flow	131
3.2-99 Feedwater Controller Failure - Relative Power	132
3.2-100 Feedwater Controller Failure - Core Average Heat Flux	132
3.2-101 Feedwater Controller Failure - Steam Dome Pressure	133
3.2-102 Feedwater Controller Failure - Sensed Level	133
3.2-103 Feedwater Controller Failure - Vessel Steam Flow	134
3.2-104 Feedwater Controller Failure - Feedwater Flow	134
3.2-105 Feedwater Controller Failure - Core Inlet Flow	135
3.2-106 MSIV Closure - Relative Power	136
3.2-107 MSIV Closure - Core Average Heat Flux	136
3.2-108 MSIV Closure - Steam Dome Pressure	137
3.2-109 MSIV Closure - Sensed Level	137
3.2-110 MSIV Closure - Vessel Steam Flux	138
3.2-111 MSIV Closure - Feedwater Flow	138
3.2-112 MSIV Closure - Core Inlet Flow	139
3.2-113 Peach Bottom Test TT1 - Steam Dome Pressure	140
3.2-114 Peach Bottom Test TT1 - Relative Power	140
3.2-115 Peach Bottom Test TT1 - Turbine Throttle Pressure	141
3.2-116 Peach Bottom Test TT2 - Steam Dome Pressure	142

Figures (continued)

	<u>Page</u>
3.2-117 Peach Bottom Test TT2 - Relative Power	142
3.2-118 Peach Bottom Test TT2 - Turbine Throttle Pressure	143
3.2-119 Peach Bottom Test TT3 - Steam Dome Pressure	144
3.2-120 Peach Bottom Test TT3 - Relative Power	144
3.2-121 Peach Bottom Test TT3 - Turbine Throttle Pressure	145
3.2-122 Turbine Trip with Bypass - Steam Dome Pressure	146
3.2-123 Turbine Trip with Bypass - Relative Power	146
3.2-124 Turbine Trip with Bypass - Main Steam Line Flow	147
3.2-125 Turbine Trip with Bypass - Feedwater Flow	147
3.2-126 Turbine Trip with Bypass - Sensed Water Level	148
3.2-127 Turbine Trip with Bypass - Vessel Flow	148
3.2-128 4/4 MSIV Closure - Steam Dome Pressure	149
3.2-129 4/4 MSIV Closure - Relative Power	149
3.2-130 4/4 MSIV Closure - Sensed Water Level	150
3.2-131 4/4 MSIV Closure - Main Steam Line Flow	150
3.2-132 4/4 MSIV Closure - Feedwater Flow	151
3.2-133 2/2 Pump Trip - Vessel Flow	152
3.2-134 2/2 Pump Trip - Average Heat Flux	152
3.2-135 Automatic Flow Decrease - Steam Dome Pressure	153
3.2-136 Automatic Flow Decrease - Relative Power	153
3.2-137 Automatic Flow Decrease - Main Steam Line Flow	154
3.2-138 Automatic Flow Decrease - Feedwater Flow	154
3.2-139 Automatic Flow Decrease - Sensed Water Level	155
3.2-140 Automatic Flow Decrease - Vessel Flow	155
3.2-141 Pressure Regulator Setpoint Step - Steam Dome Pressure	156
3.2-142 Pressure Regulator Setpoint Step - Relative Power	156
3.2-143 Pressure Regulator Setpoint Step - Main Steam Line Flow	157
3.2-144 Pressure Regulator Setpoint Step - Feedwater Flow	157
3.2-145 Pressure Regulator Setpoint Step - Sensed Water Level	158
3.2-146 Feedwater Controller Level Setpoint Step - Steam Dome Pressure	159
3.2-147 Feedwater Controller Level Setpoint Step - Relative Power	159
3.2-148 Feedwater Controller Level Setpoint Step - Feedwater flow	160
3.2-149 Feedwater Controller Level Setpoint Step - Sensed Water Level	160

List of Tables

		<u>Page</u>
3.1-1	NDH-DYNODE-B Void Reactivity Comparison	70
3.2-1	Peach Bottom-2 Turbine Trip Transient Test Actual Conditions	71
3.2-2	Peach Bottom-2 Turbine Trip Transient Test Peak Measured and Calculated Responses	72
3.2-3	Peach Bottom-2 Turbine Trip Transient Test Critical Power Ratio Response	73
4.1-1	Spectrum of Events for Thermal Limits Acceptance Criteria Evaluation	184
4.1-2	Spectrum of Events for ASME Vessel Overpressurization Acceptance Criteria Evaluation	187
4.1-3	Spectrum of Events for System Stability Acceptance Criteria Evaluation	188
4.1-4	DYNODE-B Model Option Selection for Licensing Application	189
4.1-5	Sensitivity of CPR to Various Thermal-Hydraulic Parameters	191
4.2-1	Initial Conditions and Input Parameters for Monticello Reload Safety Evaluation Model	192
4.2-2	Axial Power Factors for the Hot Channel Model	194
4.2-3	Steady State Critical Power Ratio Comparisons	195
4.3-1	Fuel Cladding Integrity Limit MCPR for Monticello	196

List of Tables (continued)

		<u>Page</u>
4.4-1	Comparison of Measured Versus Calculated Transient Δ CPR/ICPR	197
4.4-2	Comparison of Measured Versus Calculated Transient Maximum Steam Dome Pressure	198
4.4-3	Comparison of Measured Versus Calculated Transient Power Decay Ratio	199

1.0 INTRODUCTION AND SUMMARY

This report addresses the methods developed by Northern States Power Co. Nuclear Analysis Department (NSPNAD) to perform Reload Safety Evaluations and other licensing transient analyses for the Monticello Nuclear Generating Plant.

Section 2 of this report describes the DYNODE-B (DNB) computer program. DYNODE-B is a transient simulator of the Nuclear Steam Supply System (NSSS) of a BWR. This program simulates all the important features of a BWR design which significantly influence the response of the NSSS to transient conditions. The NSPNAD version of DYNODE-B includes a hot channel model which uses the General Electric GEXL Correlation to calculate Critical Power Ratio.

Section 3 describes the code qualification benchmark analysis done with DYNODE-B. This includes comparisons to other approved licensing codes; i.e. GE REDY and ODYN codes, as well as comparisons to data; i.e. Monticello Start Up tests and the Peach Bottom Turbine Trip tests. In all cases, DYNODE-B provides acceptable results.

Section 4 describes the methodology that will be used to perform licensing analyses. This includes: a description of the models and input parameters used, the spectrum of events to which the methodology applies, a description of the application of uncertainties and conservatisms, a description of the applicable acceptance criteria, and an evaluation of margin.

The methodology described in this document used in conjunction with the DYNODE-B computer code provides a conservative evaluation of margins with respect to thermal limits (CPR), ASME overpressure limits, and system stability limits.

2.0 DYNODE-B CODE DESCRIPTION

2.1 GENERAL DESCRIPTION

The DYNODE-B computer program [6] is a transient simulator of the Nuclear Steam Supply System (NSSS) of a Boiling Water Reactor (BWR). This program represents all the important features of current types of BWR design which significantly influence the response of the NSSS to transient conditions. The major components of a BWR which are simulated are shown in Figure 2.1-1.

Each major component is represented by a set of time-dependent differential equations. A self-initialization procedure is carried out for each of the component models in DYNODE-B at the beginning of each initial case. This self-initialization procedure is consistent with specified initial conditions.

The major technical features of DYNODE-B are as follows:

- Provision for simulating a wide variety of transient conditions.
- Provisions for a representation of all current types of BWR design.
- Multinode radial fuel rod and multinode axial coolant channel representations in core.
- Point kinetics, one-dimensional (axial) space-time kinetics, or power-forced options for core power transients.
- Solution to conservation equations of mass, energy, volume, and momentum for the reactor vessel fluid and main steam system regions.

- Explicit representation of the main steam system relief, isolation, bypass, and turbine valves.
- Representation of the turbine.
- Representation of heat transfer with the structural metal components of NSSS.
- Representation of the reactor protective and safety injection systems.
- Representation of the major control systems.
- Complete self-initialization.
- Full range of water properties.

2.2 SPECIFIC MODEL DESCRIPTIONS

2.2.1 CORE MODEL

The core model consists of the neutronic and thermal-hydraulic analysis of the fuel and coolant. The average fuel rod is represented radially by a set of equal volume nodes in the uranium dioxide (maximum of 8) and two nodes in the cladding. The axial representation consists of a set of equal volume nodes with a maximum of 25. The heat conduction model allows temperature-dependent conductivity and heat capacity for the uranium dioxide. The gap is represented by an effective heat transfer coefficient which is a function of the average fuel temperature. The power distribution across the uranium dioxide is also modeled. The core heat generation in the moderator is dependent on the coolant void fraction. Heating of the bypass water region is also represented. The surface heat transfer coefficient is based on the Thom correlation.

The conservation of mass and energy equations are solved in the coolant channel for a set of equal volume axial nodes subject to the core flow, pressure, and inlet subcooling boundary conditions which are obtained from the reactor vessel model which is described later. The core pressure is assumed to be spatially uniform. Several void fraction models are available; the preferred model is a profile-fit model to compute the flow quality, which is then used to calculate the void fraction from a modified Zuber-Findlay drift-flux relationship.

The Critical Power Ratio (CPR) for a number of limiting bundles is obtained using the GEXL correlation to compute the critical quality.

The core power transient is optionally based on a point or a one-dimensional (axial) space-time kinetics model. The power transient can also be specified by the user. The kinetics models account for the important reactivity components which are void (density), fuel temperature (Doppler), and rod motion (scram). In addition, the user may specify a reactivity forcing function. The delayed neutrons are represented by a maximum of six precursors, and the decay heat is also explicitly modeled. The core may be initially subcritical. The one-dimensional kinetics model is based on the total fission source and a nodal representation for the average fuel and coolant channel. The nuclear parameters (K^∞ and M^2) are obtained from a comparable three-dimensional model [1] in which a collapsing procedure is used to obtain the radially averaged values. Individual and groups of control rods (maximum of 10) may be represented. The collapsing procedure is used to obtain the initial condition parameters as well as the feedback parameters for the transient solution. Spatial variation of the total delayed neutron fraction and prompt neutron lifetime are represented. The initial power distribution is based on the solution of the neutron source equations with all time-derivatives set to zero.

2.2.2 REACTOR VESSEL FLUID MODEL

The reactor vessel (RV) excluding the core is represented by six fluid regions: upper downcomer, lower downcomer, lower plenum, bypass, riser (outlet plenum and separators), and steam dome. The conservation equations of mass and energy are solved for each region based on the boundary flows and enthalpies. Heat conduction with metal structural components is also considered. The pressure distribution is assumed to be spatially uniform. The RV pressure is obtained from a consideration of the mass and energy balance in the steam dome which accounts for non-equilibrium effects. A separate model is provided to calculate the water level in the steam dome which accounts for steam carryunder in the recirculation water and area variations due to the steam separator geometry. Level sensing is also represented.

The RV flow is either user-specified or calculated from the conservation of momentum equations. In this latter case, the dynamics of the recirculation pumps (RP's) are also taken into consideration, and a wide variety of pump transients can be represented. The pump heat is included in the model. The hydraulic model for the RP's is based on homologous relationships. The hydraulic model represents the flow in the two individual recirculation loops and considers forward and reverse suction and drive line flows. Automatic RP trip on low RV level or high RV pressure can be specified. The initial suction and drive flows are specified, and the suction flow path loss coefficient is computed to provide momentum balance. This loss coefficient is assumed constant during the transient. Two phase pressure drop and fluid inertial effects in the core, outlet plenum and steam separators are modeled. The transient core bypass flow fraction is computed based on the conservation of momentum equations. The initial pump status is arbitrary. The pump motor electrical torque is obtained from the output of the motor/generator (M/G) flow control system, which is described later.

It should be noted that, when the dynamic flow calculation is used, the temperature (enthalpy) distribution within the downcomer, recirculation lines, and jet pumps is represented in detail to provide an accurate model of the changes in core inlet subcooling due to changes in feedwater, HPCIS, and RCICS flows and enthalpies.

The feedwater flow is assumed to enter the top of the downcomer. The feedwater flow can be specified by the user or controlled by a three-element control system which is described later. The feedwater enthalpy is user-specified.

The safety/relief valves (S/RV's) are represented as individual valves. Account is taken for accumulation and blowdown, valve opening/closing delays, and valve stroking.

2.2.3 MAIN STEAM SYSTEM MODEL

The main steam system consists of the main steam lines, main steam line isolation valves (MSIV's), bypass, turbine control and stop valves, and the turbine.

The main steam lines can be represented by either a lumped parameter model or a detailed model.

For the lumped parameter model, the steam line portion on the RV side of the MSIV's is included in the definition of the steam dome, and the remainder is represented by a single volume. The flow through the MSIV's is calculated from an orifice equation so that the steam inertial effects are neglected. The steam dome pressure is obtained from the RV model as described earlier, and the steam line pressure is based on conservation of mass assuming saturation conditions.

In the detailed model, the main steam system representation begins at the RV exit and consists of seven pipe segments per steam line. These seven segments consist of four in the main steam line (RV exit to S/RV location, S/RV to MSIV, MSIV to bypass valve location and bypass valve to turbine valve location), the relief valve line, the safety valve line; and the bypass valve line. Each pipe segment is subdivided into a finer mesh with a maximum of 11 mesh points per segment. The conservation equations for mass, energy and momentum are solved at each mesh point based on the Method of Characteristics (MOC). The MOC model provides for realistic modeling of the pressure waves within the main steam system resulting from rapid valve motion with minimal numerical dispersion. The solution of the MOC model is based on the appropriate boundary conditions which consist of the steam dome pressure and the S/R, bypass, and turbine valve flow rates.

Closure of the MSIV's is automatically initiated by any of the following three signals: low RV level; high steam flow; or low RV pressure. Appropriate time delays and valve closure rates are user specified.

The bypass valve flow is based on the bypass valve position (and hence area), which can be specified by the user or controlled by the Pressure Regulator Control System which is described later. Similar treatments are used for the turbine control and stop valves. Automatic bypass valve opening can be actuated on turbine stop valve closure.

The turbine model provides a representation of the turbine speed based on the angular momentum equation solution. The driving torque is related to the turbine inlet steam flow. The turbine speed can be used to simulate frequency changes for the M/G drive motor torque.

2.2.4 SAFETY SYSTEMS

The high pressure coolant injection system (HPCIS) model is based on a flow versus back pressure curve with a user-specified enthalpy. Automatic actuation with an appropriate time delay is provided based on either low RV water level or pressure.

The reactor core isolation cooling system (RCICS) is modeled in a similar manner to the HPCIS.

The reactor protective system represents five explicit trip functions: high neutron power, high RV pressure, low RV Level, high RV level, and MSIV closure fraction. The flow dependence of the High neutron power trip is represented based on the sensed recirculation drive line flow. Each trip function has a unique time delay.

2.2.5 CONTROL SYSTEMS

The main feedwater controller is based on a three-element system with the sensed reactor vessel water level, sensed main steamline flow and the feedwater flow as the three input signals. The control system adjusts the feedwater valve position to attempt to obtain a zero error signal. RV back pressure effects on flow rate can be represented.

The M/G flow controller accepts the coupler scoop tube position and output signal from the turbine speed governor as input and adjusts the scoop tube position to maintain the appropriate setpoint. Control is provided for each loop independently. The M/G dynamic model is based on solving the conservation of angular momentum for the motor and generator separately. Idle loop recirculation pump startup can be modeled. Automatic drive motor trip on high RV pressure can be specified.

The pressure regulator control system accepts the sensed RV pressure and the turbine speed governor output signal as input. This system controls the turbine control and bypass valve positions to maintain the RV pressure at the appropriate setpoint. RV back pressure effects on steam flow can be represented.

2.2.6 INTEGRATION SCHEME

The reactor core model equations are integrated by using a fifth-order Runge-Kutta-Merson method in which the time step is automatically selected to achieve a user-specified accuracy limit. This same method is used to integrate the dynamic flow equations for the RV flow rates. Note that the core and RV time step sizes are usually different with the former being smaller. The MOC solution in the steam lines is carried out over a user-specified fraction of the RV time step using an explicit integration technique and linear variation of the boundary conditions over the RV time step.

2.3

COMPARISONS WITH OTHER APPROVED LICENSING CODES

This section provides a comparison with two other approved licensing codes: REDY [8] and ODYN [9].

In general, the development of DYNODE-B paralleled the evolution of these two codes from the standpoint of applications to licensing analyses. Early versions of DYNODE-B were patterned after REDY, based on the information provided in Reference 8, so that the models, assumptions, and approximations in these early versions are similar to those of REDY. The advanced versions incorporated more sophisticated models in the areas of the core kinetics (1-D axial) and steam line hydraulics, following the improvements of ODYN over REDY. The nature of the DYNODE-B enhancements are similar to those of ODYN, but slightly different in implementation, as discussed later.

The remainder of this section presents the major technical differences between ODYN and DYNODE-B.

2.3.1 CORE NEUTRONICS

ODYN is based on one-group diffusion theory, in which the cross sections are a function of coolant density, fuel temperature, and control state. DYNODE-B is based on the total fission source nodal formulation, in which neutron migration is represented by coupling coefficients between adjacent nodes. The coupling coefficients are functions of the migration area, M^2 . Local neutron multiplication is given in terms of the infinite multiplication factor, K^∞ . The forms of the equations for these two models are similar in nature, and the DYNODE-B nodal formulation can be derived from the one-group equations. The treatment of the delayed neutrons is identical in the two codes. The DYNODE-B model treats decay heat precursors in conformance with the 1971 ANS Standard while ODYN uses a simple exponential decay heat model. The radial collapsing procedures used to develop the one-dimensional parameters are identical in nature.

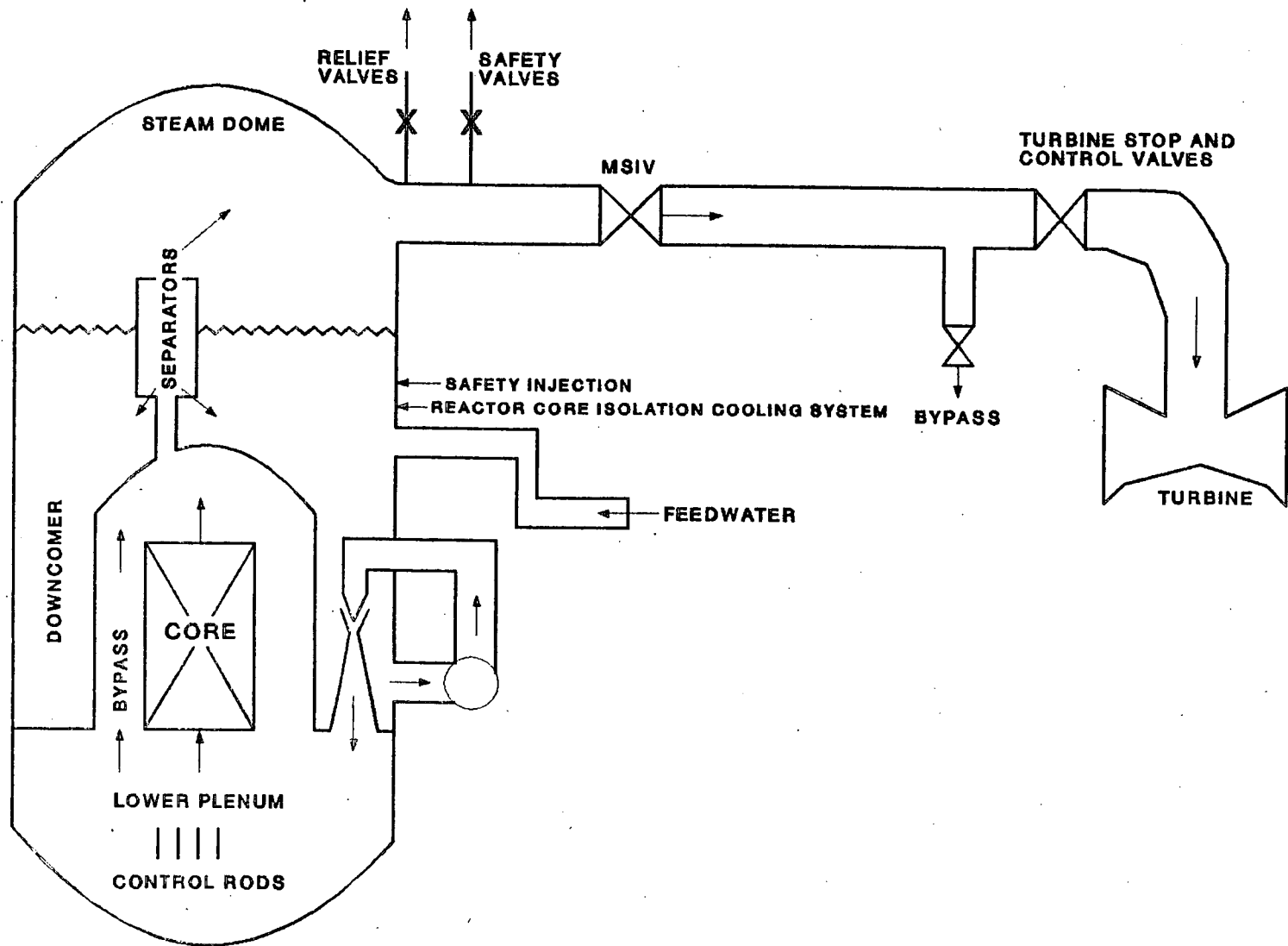
2.3.2 STEAM LINES

ODYN is based on a single-phase, one-dimensional nodal representation of the steam line (8 nodes) in which the steam is assumed to behave isentropically. DYNODE-B is based on a Method of Characteristic (MOC) solution to the one-dimensional conservation equations for mass, energy, momentum, and state. The MOC methodology is more rigorous and does not assume a priori that the steam is isentropic. The MOC method was used as a reference in establishing the validity of the ODYN model.

2.3.3 REACTOR VESSEL PRESSURE DISTRIBUTION

ODYN explicitly calculates the pressure at the reactor inlet and the RV dome. DYNODE-B calculates the pressure in the RV dome. The reactor core pressure is obtained by simulating the appropriate transport delay between the dome and the core outlet based on the sonic velocity and the distance between these two points.

Figure 2.1-1
Schematic of BWR NSSS Representation



3.0 DYNODE-B CODE QUALIFICATION

This section discusses the benchmark analyses performed to qualify the DYNODE-B computer code for BWR analysis.

The nuclear models (1-D kinetics parameters) are compared to results from the 3-D simulator [1] in Section 3.1.

The thermal-hydraulic models are compared to other approved licensing codes, i.e., GE's REDY and ODYN codes, and to test data, i.e., Peach Bottom turbine trip tests, Monticello start-Up tests, and Monticello operational transients. These results are shown in Section 3.2.

It is the intent of this section to determine the applicability of the DYNODE-B code models to BWR analysis only. The application of DYNODE-B to licensing analysis and an evaluation of margin is contained in Section 4.

3.1 NUCLEAR MODEL COMPARISONS

The 1-D kinetics parameters which are input to DYNODE-B (DNB) are derived from a radial collapsing of the 3-D results from the corresponding NDH parameters (Reference 1). Since the NDH model has been qualified against plant measurements, the accuracy of the 3-D parameters is well founded, and thus the only other uncertainty/bias associated with the 1-D parameters is that which is introduced by the collapsing process. This additional uncertainty/bias can be assessed by direct comparisons of reactivity changes between NDH and DYNODE-B results for comparable changes in the neutronics parameters. This assessment has been made for the void and scram reactivity components, since the dominant reactivity changes occur due to these two components during events analyzed with the 1-D model (overpressurization events). It should be noted that any non-conservative uncertainty/bias which is associated with the collapsing procedure is added to those which are applied to the kinetics parameters based on the qualification of the NDH model against measurements (See Section 4.2.1).

The results of specific comparisons for Monticello Cycle 10 are presented in the following sections to demonstrate the nature of this process.

3.1.1 SCRAM REACTIVITY

The scram reactivities, calculated with NDH and DYNODE-B, for the case of ARO to ARI are shown in Figure 3.1-3. The difference between these two curves is presented in Figure 3.1-4, which indicates that the DYNODE-B result is slightly non-conservative. Thus in this particular case, the scram reactivity parameters which are derived from the collapsing procedure must be corrected prior to use in any licensing transient analysis to be performed with DYNODE-B (See Section 4.2.1).

3.1.2 VOID REACTIVITY

The calculated values for $K_{\text{effective}}$ between NDH and DYNODE-B for a change in subcooling and pressure are shown in Table 3.1-1.

The corresponding power distributions are shown on Figures 3.1-1, 3.1-2. These results show that the DYNODE-B result for void reactivity feedback is slightly more conservative, so that no additional uncertainty needs to be applied (See Section 4.2.1).

3.2 THERMAL - HYDRAULIC COMPARISONS

This section is intended to benchmark the thermal hydraulic models in the DYNODE-B code. This is accomplished by benchmarking to other approved licensing codes and to test data. The test data benchmarks provide the primary checkout. The code benchmarks provide a secondary check of the overall behavior, however exact comparisons are not expected, due to modeling and input differences. Essentially, these benchmarks provide a full system checkout of the models in DYNODE-B, including the main models described in Section 2.

In order to provide an accurate comparison, an effort was made to duplicate the comparative conditions as closely as possible, i.e. models used in the case of benchmark codes and the measured test conditions for data comparisons.

These benchmarks are meant only to test the modeling of the DYNODE-B code. The methodology used for Reload Safety Evaluations is described in Section 4, and these results are referenced where applicable.

3.2.1 — CODE-CODE COMPARISONS

In this section the DYNODE-B code is benchmarked to the General Electric REDY code [8], FSAR analysis [2], and the ODYN code [9] Cycle 11 analysis [4].

3.2.1.1 GENERAL ELECTRIC REDY CODE

The models described in Reference 8 were duplicated as closely as possible for these cases.

The major discrepancies in the code modeling are: REDY uses a second order sweep model to calculate the dynamic void effects, whereas DYNODE-B uses a Pofile Fit Non-Equilibrium Flow Quality Void Model; REDY calculates decay heat from the Stehn-Clancey correlation [8], whereas DYNODE-B calculates decay heat as part of the kinetics equations; and REDY assumes a constant value of cladding surface heat transfer coefficient throughout the transient, whereas DYNODE-B assumes the heat transfer coefficient to behave according to the Thom correlation.

The input from Reference 13 was used wherever possible. In cases where the REDY input value was unknown; typical or actual plant values were used in the DYNODE-B models. In particular, the majority of the controller (flow, pressure, and level) model inputs to REDY were not known.

Fourteen transients from the FSAR [2] were benchmarked. The following sections describe each transient and document the benchmark analysis results.

3.2.1.1.1 TURBINE TRIP WITHOUT BYPASS

Description Of The Accident

This transient is a severe abnormal event which results directly in a primary system pressure increase. It represents the sequence of events that would follow an assumed (instantaneous) loss of condenser vacuum, which automatically initiates closure of the turbine stop valves. For this event, the turbine bypass valves are assumed to be inoperable because of the loss of condenser vacuum. Reactor scram is initiated by position switches on the turbine stop valves.

Summary Of Accident Analysis

The reactor is assumed initially to be at rated power (1670 MWt). The turbine stop valves are taken to close in a conservatively short duration (0.1 second), and the insertion of scram reactivity is limited to the rate of insertion allowed by the Technical Specifications with the most reactive rod stuck out. The fuel temperature reactivity is assumed to correspond to its least negative time in life, while the void reactivity is taken as the most negative to maximize the power spike and pressure increases which result from the stop valve closure. The transient is mitigated by the action of the safety/relief valves, which are taken to open at the maximum pressure permitted by the Technical Specifications. Initial system pressure is conservatively placed 25 psi above the nominal operating pressure.

Figures 3.2-1 through 3.2-7 show the DYNODE-B versus GE REDY results for the Turbine Trip without Bypass transient.

The results show excellent comparison. DYNODE-B slightly overpredicts the peak power, and hence pressure, response (344% nominal versus 321% from REDY). Both codes predict the same initial water level response, though REDY predicts a stronger recovery of level. This is due to the differences in the transient void models.

DYNODE-B accurately reproduces the REDY results. The minor discrepancies that exist are due to code modeling differences. This case therefore provides an acceptable benchmark.

3.2.1.1.2 TURBINE TRIP WITH BYPASS

Description of the Accident

The sequence of events for the turbine trip with bypass malfunction are similar to that for the turbine trip without bypass (Section 3.2.1.1.1), except that the condenser heat sink is presumed to be available and hence the turbine bypass valves are operable. Following stop valve closure, the pressure regulator controls react to open the bypass valves and relieve steam to the condenser.

Summary of Accident Analysis

The reactor is assumed initially to be at rated power (1670 MWt). The turbine stop valves are taken to close in a conservatively short duration (0.1 second), and the insertion of scram reactivity is limited to the rate of insertion allowed by the Technical Specifications with the most reactive rod stuck out. The fuel temperature reactivity is taken to be at its least negative time in life while the void reactivity is at its most negative value. A rapid power spike and pressure increase follow the valve closure. The transient is terminated by the reactor scram, opening of the turbine bypass valves, and by the safety/relief valves whose opening setpoints are presumed at the maximum value permitted by the Technical Specifications. The initial system pressure is conservatively assumed to be 25 psi above the nominal setpoint.

Figures 3.2-8 through 3.2-14 show the DYNODE-B versus GE REDY results for the Turbine Trip with Bypass transient.

The results show excellent comparison. DYNODE-B slightly overpredicts the power, and hence pressure, response. Both codes predict the same initial water level response, though REDY predicts a stronger recovery of level. This is due to the differences in the transient void models. The increased level predicted by REDY in turn causes the feedwater controller to cut back on flow. This effect is not seen in DYNODE-B, since the level does not recover to the same degree.

DYNODE-B accurately reproduces the REDY results. The minor discrepancies that exist are due to code modeling differences. This case therefore provides an acceptable benchmark.

3.2.1.1.3 GENERATOR TRIP

Description of the Accident

The generator trip transient is a severe overpressurization transient which is similar in nature to the turbine trip. It represents the sequence of events which would follow rapid closing of the turbine control valves, which could follow a complete loss of electrical load. Reactor scram is initiated automatically by relays which sense the fast turbine control valve closure.

Summary of Accident Analysis

The reactor is assumed initially to be at rated power (1670 MWt). The turbine control valves are taken to close in a conservatively short duration (0.2 second), and the insertion of scram reactivity is limited to the rate of insertion allowed by the Technical Specifications with the most reactive rod stuck out. A rapid pressure increase follows the valve closure, the magnitude of which depends principally on the scram reactivity insertion rate and the void reactivity. The fuel temperature reactivity is conservatively taken at its least negative time in life, while the void reactivity is at its most negative to maximize the power excursion. The transient is mitigated by opening of the turbine bypass valves and the safety/relief valves.

Figures 3.2-15 through 3.2-21 show the DYNODE-B versus GE REDY results for the Generator Trip with Bypass transient.

The results show excellent comparison for all variables except water level and feedwater flow. Both codes predict the same initial water level response, though REDY predicts a stronger recovery of level. This is due to the differences in the transient void models. The increased level predicted by REDY in turn causes the feedwater controller to cut back on flow. This effect is not seen in DYNODE-B, since the level does not recover to the same degree.

DYNODE-B accurately reproduces the REDY results. The minor discrepancies that exist are due to code modeling differences. This case therefore provides an acceptable benchmark.

3.2.1.1.4 CLOSURE OF ALL MAIN STEAM ISOLATION VALVES

Description of the Accident

Closure of all the main steam isolation valves (MSIV) while the reactor is at power can result in a significant overpressure transient in the reactor vessel. The MSIV's can be closed directly by operator action while at power. Normally, as the valves close in all four steamlines, a reactor scram is initiated by position switches which sense the closure. As the system isolates, pressure rises in the vessel until the safety/relief valves open to mitigate the accident.

Summary of Accident Analysis

The reactor is assumed to be at rated power (1670 MWt). The MSIVs are taken to close in three seconds with a nonlinear valve flow characteristic. Fuel temperature reactivity is taken to be at its least negative time in life, while the void coefficient is at the most negative to maximize pressurization. Position switches on each MSIV will cause a reactor scram when valves in three of the four steamlines reach approximately 10% closed. This results in a scram before any significant steam flow interruption takes place. System pressure rises due to heat stored in the core. Insertion of scram reactivity is limited to the rate allowed by the Technical Specifications with the most reactive rod stuck out. The transient is mitigated by opening of the safety/relief valves, with lift setpoints assumed at the maximum Technical Specification limit. Initial system pressure is assumed 25 psi above the nominal value.

Figures 3.2-22 through 3.2-28 show the DYNODE-B versus GE REDY results for the MSIV Closure transient.

The DYNODE-B results show excellent comparison for all variables. The peak pressure predicted by REDY is approximately 10 psi greater than predicted by DYNODE-B. This difference can be caused by slight differences in the non-linear MSIV position versus area curve input.

DYNODE-B accurately reproduces the REDY results. The minor discrepancies that exist are due to code modeling and input differences. This case therefore provides an acceptable benchmark.

3.2.1.1.5 FEEDWATER CONTROLLER MALFUNCTION, MAXIMUM DEMAND

Description of the Accident

Failure of the feedwater controller in the direction of increased feedwater flow results in a moderator temperature and void decrease and a reactor power increase through the effect of the negative reactivity void coefficient. Water level increases during the initial part of the transient until the high water level turbine trip setpoint is reached. The turbine and feedwater pump trips, the reactor scrams, and an overpower and overpressure transient occurs.

Summary of Accident Analysis

The reactor is taken to be at rated power (1670 Mwt). The feedwater controller is assumed to fail in such a manner as to cause the feedwater flow to increase to its full run-out value. The water level and core inlet subcooling increase, causing reactor power to increase until the high water level turbine trip setpoint is reached, causing a turbine trip, feedwater pump trip, and a subsequent reactor scram due to turbine stop valve closure. Fuel temperature reactivity is taken at its least negative time in life, while the void reactivity is at its most negative to maximize the power and pressure transient. The insertion of scram reactivity is limited to the rate of insertion allowed by the Technical Specifications with the most reactive rod stuck out. The transient is mitigated by opening the turbine bypass valves and the safety/relief valves. The safety/relief valves are assumed to open at the maximum pressure permitted by the Technical Specifications.

Figures 3.2-29 through 3.2-35 show the DYNODE-B versus GE REDY results for the Feedwater Controller Failure - Maximum Demand transient.

The results show excellent comparison for all variables. The predicted scram time is slightly later in DYNODE-B. This is due to the fact that REDY assumes an instantaneous increase in feedwater flow whereas DYNODE-B assumes the feedwater control valve opens at the maximum rate. The peak pressure predicted by REDY is approximately 25 psi greater than predicted by DYNODE-B. This is due to the fact that the slight differences in the steam line models cause DYNODE-B to open the bypass valves, whereas REDY predicts they stay closed.

DYNODE-B accurately reproduces the REDY results. The minor discrepancies that exist are due to code modeling differences. This case therefore provides an acceptable benchmark.

3.2.1.1.6 LOSS OF FEEDWATER

Description of the Accident

A loss of feedwater flow results in a situation where the mass of steam leaving the reactor vessel exceeds the mass of water entering the vessel, resulting in a net decrease in the coolant inventory available to cool the core. Feedwater control system failures or feedwater pump trips can lead to partial or complete loss of feedwater flow. Feedwater flow would decay over a few seconds and the recirculation flow control system would ramp the pumps down to about 20% speed when the feedwater flow falls below 20% of rated. Water level declines rapidly and a reactor scram takes place when the low level trip setpoint is reached. The system subsequently closes the main steam isolation valves (MSIV's), and actuation of the high pressure coolant injection (HPCI) and reactor core isolation cooling (RCIC) systems on low level setpoints terminate the transient.

Summary of Accident Analysis

The reactor is taken to be at rated power (1670 MWt). The loss of feedwater is modeled as taking place over a three second period. When the feedwater flow reaches 20% of normal, the recirculation pump speed demand is set to 20%. The power level and system pressure decline in a fashion which depends principally on the void reactivity coefficient.

Figures 3.2-36 through 3.2-42 show the DYNODE-B versus GE REDY results for the Loss of Feedwater transient.

The DYNODE-B results show excellent comparison for all variables. The only minor discrepancy is that REDY predicts a reactor scram on low water level at approximately 13 seconds. DYNODE-B does not predict the scram throughout the 16 seconds simulated. This is due to the fact that the low water level scram input to REDY is 9 inches above that used in DYNODE-B.

DYNODE-B accurately reproduces the REDY results for this transient. The only discrepancy is caused by the input difference mentioned above. This case therefore provides an acceptable benchmark.

3.2.1.1.7 LOSS OF FEEDWATER HEATING

Description of the Accident

A loss of feedwater heating event can occur as the result of a loss of extraction steam to a feedwater heater. An alternative, but generally less severe, loss of heating can result from inadvertent actuation of high pressure coolant injection, (HPCI) which delivers relatively cool water to the reactor through the feedwater sparger. Reduction in feedwater temperature follows, with a gradual rise in reactor power as the moderator temperature declines and reduces the core void fraction. If neutron power exceeds the reactor trip setpoint, a scram occurs; otherwise the system settles to a steady-state high-power condition until the operator intervenes.

Summary of Accident Analysis

The reactor is taken to be at rated power (1670 Mwt). The feedwater temperature change is modeled as a 100 °F decline with a 30-second exponential time constant. This is more severe than any loss of feedwater heating which can result from a single system malfunction. Fuel temperature reactivity is chosen at its least negative time in life, while void reactivity is at its most negative to maximize the power increase. Scram insertion, should it occur, is limited to the insertion rate permitted by the Technical Specifications.

Figures 3.2-43 through 3.2-49 show the DYNODE-B versus GE REDY results for the Loss of Feedwater Heating transient.

The DYNODE-B results show excellent comparison for all variables. DYNODE-B predicts a more conservative increase in power and average surface heat flux. This case therefore provides an acceptable benchmark of DYNODE-B's capabilities to reproduce the REDY code predictions.

3.2.1.1.8 PRESSURE REGULATOR FAILS OPEN

Description of the Accident

In the event that either the electrical or mechanical pressure regulator were to fail such that the turbine control and/or bypass valves were opened, steam flow from the reactor would increase. System pressure would drop, causing an increase in core voids and a consequent drop in reactor power. Depressurization would continue until the main steam isolation valve closure setpoint was reached, resulting in closure of the valves and a reactor scram. Decay heat then would cause the system to repressurize, limited by opening of the automatic safety relief valves until cooldown was initiated.

Summary of Accident Analysis

The reactor is taken to be at rated power (1670 MWt). The pressure regulator is taken to fail in such a way that the turbine control valves and/or bypass valves are opened to 110% steam demand (the maximum permitted by the control system). The excess demand depressurizes the system until the main steam isolation valves close and the reactor scrams. Thereafter, the pressure rises due to decay heat, and the automatic safety/relief valves lift intermittently until cooldown is initiated.

Figures 3.2-50 through 3.2-56 show the DYNODE-B versus GE REDY results for the Pressure Regulator Fails Open transient.

DYNODE-B follows the REDY predicted steam dome pressure very closely with the exception that DYNODE-B predicts the MSIV closure on low turbine throttle pressure to occur approximately 2 seconds after REDY. This is due to differences in the steam line model. The same initial depressurization causes a greater void increase in REDY than in DYNODE-B due to the differences in the void models. This in turn causes the REDY predicted core power and core inlet flow to drop faster than DYNODE-B.

DYNODE-B accurately reproduces the REDY results for this transient. The discrepancies are caused by code modeling differences. This case therefore provides an acceptable benchmark.

3.2.1.1.9 RECIRCULATION PUMP SEIZURE

Description of the Accident

The recirculation pump seizure is a nearly instantaneous stoppage of a recirculation pump shaft and impeller. This stoppage results in a very rapid reduction in core flow and a subsequent decline in core power. Because the heat flux at the fuel pin surface declines more slowly than the core flow, there is a potential degradation of thermal margin. No reactor scram results, and the system settles to reduced power.

Summary of Accident Analysis

The reactor is taken to be at rated power (1670 MWt). The affected pump speed is instantaneously set to zero and the drive flow abruptly decays. Jet pump flow in the seized loop reverses in less than 1 second. As a result, core flow decreases, causing an increase in void fraction and a consequent reduction in reactor power. The degree of reduction in power depends principally on the void coefficient of reactivity, which is taken at its least negative time in life, while Doppler reactivity is at its most negative to maximize the heat flux to flow ratio during the transient. Heat flux from the fuel pins lags the core power decline, and the system relaxes to a reduced power steady state.

Figures 3.2-57 through 3.2-63 show the DYNODE-B versus GE REDY results for the Recirculation Pump Seizure transient.

The DYNODE-B results show excellent comparison for all variables. This case therefore provides an acceptable benchmark of DYNODE-B's capabilities to reproduce the REDY code predictions.

3.2.1.1.10 TWO RECIRCULATION PUMP DRIVE MOTOR TRIP

Description of the Accident

In the event that the power supply to both recirculation pump motor/generator (M/G) sets were lost, the pumps would coast down and coolant flow to the core would decline. Core voids would then increase and power would decline. The system settles to a natural circulation condition where core flow is provided through the jet pump suction path by the weight of subcooled water in the downcomer. Heat flux decline lags power and core flow, so there is a potential degradation of thermal margin limits.

Summary of Accident Analysis

The reactor is taken to be at rated power (1670 MWt). The transient is initiated by setting the recirculation pump drive motor torques to zero. The inertia of the M/G sets is included in the analysis because there is no single event which would result in simultaneously opening the pump generator breakers to both pumps. The void reactivity is taken at its least negative time in life, while fuel temperature reactivity is at its most negative to maximize the power to flow ratio during the event. The pumps, core flow, power, pressure, and steam flow all decline to steady-state, natural-circulation conditions.

Figures 3.2-64 through 3.2-70 show the DYNODE-B versus GE REDY results for the Two Recirculation Pump Drive Motor Trip transient.

DYNODE-B compares very well with the REDY-predicted core inlet flow during the initial flow coastdown. As the transient progresses, REDY predicts a slightly lower core inlet flow. This could be caused by differences in the pump model input. The lower core inlet flow predicted by REDY causes increased voiding and hence a greater power decrease and more level holdup. The lower power causes lower heat flux and lower pressure. The higher level causes a greater feedwater decrease in an attempt by the feedwater controller to compensate.

In general, DYNODE-B follows the same trends and reproduces the REDY result for this transient. The discrepancies are caused by code modeling difference. This case therefore provides an acceptance benchmark.

3.2.1.1.11 RECIRCULATION FLOW CONTROLLER FAILURE, INCREASE DEMAND

Description of the Accident

There are several possible failures which can result in an increase in core coolant flow. The most severe of these occurs when a motor/generator (M/G) set fluid coupler for one recirculation pump attempts to achieve full speed at maximum acceleration. The result is a surge of additional coolant through the core and a consequent power increase. If the neutron flux increases to the high power trip setpoint, the reactor scrams. The possibility of a large power increase allows for potential degradation of thermal margin.

Summary of Accident Analysis

The most severe initial condition for the increasing recirculation flow transient is near the low end of the automatic recirculation flow control range, where reactor power is approximately 65% of rated power and core flow is approximately 50% of rated flow. The pumps are operating at approximately 45% speed, and the relative M-G set fluid coupler scoop tube position is approximately 20%. The transient is modeled by moving the scoop tube position at its maximum rate to the maximum coupling position. Void reactivity is taken at its most negative time in life, while fuel temperature reactivity is at its least negative to maximize the power increase. As the pump speed increases, core flow and power increase and, if the power increase is sufficient, a scram occurs. The system then settles to a steady state until the operator intervenes.

Figures 3.2-71 through 3.2-77 show the DYNODE-B versus GE REDY results for the Recirculation Flow Controller Failure - Increased Demand transient.

The DYNODE-B results show excellent comparison for all variables. Minor discrepancies in the level response are caused by the transient void model differences.

DYNODE-B accurately reproduces the REDY results for this transient. The minor discrepancies are caused by code modeling differences. This case therefore provides an acceptance benchmark.

3.2.1.1.12 RECIRCULATION FLOW CONTROLLER FAILURE, DECREASE DEMAND

Description of the Accident

The failure of one recirculation pump motor/generator (M/G) set speed controller could cause the scoop tube position to move at its maximum speed in the direction of zero pump speed and flow. As a result, core flow, power, steam flow, and pressure all decrease. Because the decline in heat flux lags that of core flow and power, there is a potential degradation in thermal margin.

Summary of Accident Analysis

The reactor is taken to be at rated power (1670 MWt). The transient is initiated by forcing the scoop tube position of the affected loop M-G set from its initial value to zero at the maximum rate. Core flow, power, steam generation, and pressure all decline, and the system settles to a steady state at reduced power with reverse flow through the inactive jet pumps. Void reactivity is taken at the least negative time in life while fuel temperature reactivity is at the most negative to maximize the power to flow ratio during the transient.

Figures 3.2-78 through 3.2-84 show the DYNODE-B versus GE REDY results for the Recirculation Flow Controller Failure - Decreased Demand transient.

The DYNODE-B results show excellent comparison for all variables. The DYNODE-B predicted core inlet flow drops slightly lower than the REDY-predicted flow. This can be due to minor input differences in the coupler torque versus slip and coupling function. All of the other discrepancies are insignificant and attributable to the void model differences.

DYNODE-B accurately reproduces the REDY results for this transient. The slight discrepancies are caused by code modeling or input differences. This case therefore provides an acceptance benchmark.

3.2.1.1.13. IMPROPER START OF AN INACTIVE RECIRCULATION LOOP

Description of the Accident

Improper start of an inactive recirculation loop involves activating an improperly warmed idle recirculation pump while the reactor is at power. Depending on the initial reactor condition, this incident can cause a significant power increase and reduction of thermal margin. The system settles out to an increased power steady state or, in the event the high neutron power trip setpoint is reached, the reactor scrams.

Summary of Accident Analysis

The initial conditions of the system substantially affect the results of the transient. One recirculation pump is presumed operating at full speed while the second pump is stopped. The idle loop pump discharge valve is taken to be initially closed with the discharge bypass valve open. The inactive drive line is assumed to be filled with cold (100 °F) water. Reactor power and core flow are conservatively placed at midrange values with analyses performed to determine the most adverse conditions. The motor/generator (M/G) set fluid coupler for the idle pump is initially set for 50% speed demand.

The transient sequence of events is as follows:

- A. At $t = 0$, the idle M/G set drive motor breaker is closed.
- B. The drive motor reaches near-synchronous speed quickly, while the generator reaches approximately 80% speed in 5 seconds.
- C. At 5 seconds the generator field breaker is closed, loading the generator and applying starting torque to the pump motor. Generator speed decreases, the pump breaks into rotation and builds up speed.

D. Generator speed demand is programmed back to 20% starting at 8 seconds.

E. The pump discharge valve/drive motor interlock is cleared, and the valve opens with a 60-second stroke time.

The transient system behavior depends, to a great degree, on initial system power. At relatively high power, the pressure drop across the core becomes large and the starting pump does not develop sufficient head to reverse the backflow through the idle loop diffusers. Consequently, the water injected out the idle drive lines is swept back into the downcomer, where it is heated before eventually returning to the lower plenum through the active loop. In contrast, at low power, the starting pump may cause the jet pump flow to become positive, sending the cold water directly into the immediate core flow path and resulting in a substantial core power increase and a possible reactor trip on high flux.

Following the pump start, core flow abruptly increases, causing a power increase. If the reactor does not trip, the power peaks and then settles to a new level. As the pump discharge valve opens, power will increase as the valve permits flow to increase. If the reactor does trip, the scram terminates the power increase and causes the system to settle to zero power conditions. In either case, heat flux will increase to a maximum value at which time thermal margin will reach a minimum, and then the heat flux will decline.

Figures 3.2-85 through 3.2-91 show the DYNODE-B versus GE REDY results for the Improper Start of an Inactive Recirculation Loop transient.

The DYNODE-B results show the same general trends for all parameters as those predicted by GE REDY, although the magnitudes of the responses are different. This is due primarily to an apparent discrepancy between GE's written description of this transient and the plotted results (Reference 2). In the description, it is stated that the active pump initially produces 115% of normal rated flow in its associated jet pumps; in the figure, a flow of 150% is indicated. In either case, the core receives 54% of its normal rated flow, and all remaining flow from the active loop appears as reverse flow through the inactive loop. Therefore, the reverse flow through the inactive loop is much higher in the case of 150% active pump flow. The DYNODE-B analysis uses 115% active loop flow, per the written description.

Because of the initially high reverse flow in the GE REDY case, the inactive pump is unable to establish positive flow during the transient. As a result, the cold water in the loop is swept up into the downcomer, where it mixes with the bulkwater before being pumped through the core by the active loop. This causes a relatively gradual reactivity insertion, so that the resulting power spike and rise in heat flux are mild.

In contrast, the reverse flow in the DYNODE-B case is low enough so that the idle pump does establish positive flow upon starting up. The cold water is therefore pumped directly into the lower plenum and through the core, causing a faster reactivity insertion than in the GE REDY case. At the same time, establishing positive flow through the idle loop means an additional power increase because of the higher core flow. As a result, the power spike and the rise in heat flux are higher in the DYNODE-B case. The responses of other parameters are correspondingly altered.

Despite this input difference which causes DYNODE-B to predict a more severe transient than REDY, both codes predict the same trends and show the same general results for this transient. This case therefore provides an acceptance benchmark.

3.2.1.2

GENERAL ELECTRIC ODYN CODE

The models described in Reference 9 were duplicated as closely as possible for these cases. Major differences in the code models are described in Section 2.3.

Wherever possible, the input from the Monticello Cycle 11 ODYN analysis [4] was used. The major input discrepancy in these cases is that the 1-D kinetics inputs used by the ODYN code were unknown and had to be estimated.

Three transients from the Cycle 11 Supplemental Reload Analysis [4] were benchmarked. The following sections describe each transient and document the benchmark analysis results.

3.2.1.2.1 LOAD REJECTION WITHOUT BYPASS

Description of the Accident

Fast closure of the turbine control valves is initiated whenever electrical grid disturbances occur which result in significant loss of load on the generator. The turbine control valves are required to close as rapidly as possible to prevent overspeed of the turbine generator rotor. The closing causes a sudden reduction of steam flow which results in a nuclear system pressure increase. The reactor is scrammed by the fast closure of the turbine control valves.

Summary of Accident Analysis

The reactor and turbine/generator are initially operating at full power when the load rejection occurs. The power/load unbalance device steps the load reference signal to zero and closes the turbine control valves at the earliest possible time. The turbine accelerates at a maximum rate until the valves start to close. The turbine control valves close in 0.25 sec.

Reactor scram is initiated upon sensing control valve fast closure. The insertion of scram reactivity is limited to the rate of insertion allowed by the Technical Specifications with the most reactive rod stuck out. A rapid pressure increase follows the valve closure, the magnitude of which principally depends on the scram reactivity insertion rate and the void reactivity. If the pressure rises to the pressure relief set point, some or all of the relief valves open, discharging steam to the suppression pool. If the pressure rises to ≥ 1150 psig, trip of the M/G set breaker occurs.

Figures 3.2-92 through 3.2-98 show the DYNODE-B calculated results versus the General Electric ODYN results.

DYNODE-B underpredicts the ODYN power and hence heat flux, increase. This is due to differences in the void and scram reactivity functions. It is impossible to accurately reproduce the 1-D reactivity inputs used by General Electric based on the limited information available. A better response can be achieved by

performing sensitivity studies for the kinetics parameters. However, since the purpose of these benchmarks is only to perform a general check on the models used in DYNODE-B (the data comparisons in Section 3.2.2 perform the primary check), the benchmarks were left as is. It is sufficient to understand discrepancies due to input differences in this case.

Most of the remaining differences are attributable to the difference in the heat flux response. The larger heat flux predicted by ODYN causes the pressure to hang up for a longer time and the water level to recover more quickly due to a larger core resistance. Note that GE plots actual water level and DYNODE-B sensed water level which is the source of the difference in the initial values. Faster recovery of the water level causes the feedwater controller to ramp down the feedwater sooner.

The differences in core inlet flow response are partially attributable to the heat flux differences and partially due to code modeling differences. In DYNODE-B, the pressure difference between the core outlet plenum and the steam dome is not explicitly calculated. Thus, for the recirculation flow rate calculation, this pressure difference is computed from the momentum equation in which the steam separator flow acceleration term is obtained by assuming that the separator flow is replaced by the total core flow. This assumption is equivalent to assuming that the core fluid is incompressible. Thus, in cases of rapid void collapse in the core, this acceleration term does not play a significant role. The effect of this assumption is expected to be small, since the core void fraction is primarily responding to changes in pressure which are being taken into account properly. For this transient, this assumption results in DYNODE-B underpredicting the core inlet flow increase during the initial pressurization. The impact of this effect on ΔCPR is insignificant.

This benchmark represents a positive check of DYNODE-B's capabilities to perform BWR transient calculations. The differences between the DYNODE-B and ODYN results are well understood and do not reflect deficiencies in the DYNODE-B code.

3.2.1.2.2 FEEDWATER CONTROLLER FAILURE - MAXIMUM DEMAND

Description of the Accident

This event is postulated on the basis of a single failure of a control device, specifically one which can directly cause an increase in coolant inventory by increasing the feedwater flow. The most severe applicable event is a feedwater controller failure resulting in maximum flow demand, which causes an increase of feedwater flow to the reactor vessel. This excess flow results in an increase in core subcooling, which results in a core power rise, and a rise in the reactor vessel water level.

The rise in the reactor vessel water level eventually leads to high water level turbine trip, feedwater pump trip, and reactor scram trip.

Summary of Accident Analysis

The reactor is taken to be initially at 98% rated power (1634 MWt) and 100% flow. This point was found to be more conservative than the 100% power/100% flow point (Ref. 4).

The reactor is operating in a manual flow control mode which provides for the most severe transient. The feedwater controller is assumed to fail during the maximum flow demand. Maximum feedwater pump run out is assumed. The influx of excess feedwater flow results in an increase in core subcooling which reduces the void fraction and thus induces an increase in reactor power. The excess feedwater flow also results in a rise in the reactor vessel water level which eventually leads to high water level; main turbine and feedwater trip and turbine bypass valves are actuated. Reactor scram trip is actuated from main turbine stop valve position switches. Relief valves open as steamline pressures reach relief valve setpoints. If the pressure rises to ≥ 1150 psig, trip of the M/G set breakers occurs.

Figures 3.2-99 through 3.2-105 show the DYNODE-B calculated results versus the General Electric ODYN results.

The DYNODE-B results compare very well to the ODYN results. The same input and modeling differences exist as in the previous benchmark (Section 3.2.1.2.1 Load Rejection without Bypass). The Feedwater Controller Failure transient is not as sensitive to void reactivity as is the Load Rejection transient and hence provides a much better code comparison.

The DYNODE-B results are slightly time shifted (approximately 0.5 sec). This is due to the fact that General Electric assumes instantaneous feedwater runout flow, whereas DYNODE-B opens the feedwater control valves at the maximum rate to runout flow. Time to runout in DYNODE-B is 1.1 sec.

This case provides an excellent check of DYNODE-B's capabilities to perform BWR transient analysis. The differences between the ODYN and DYNODE-B results, for this transient, are insignificant.

3.2.1.2.3 MSIV CLOSURE (FLUX SCRAM)

Description of the Accident

This event is performed to show compliance with the ASME Vessel Pressure Code. The MSIV's can be closed directly by operator action while at power. Closure of all main steam isolation valves (MSIV) while at power can result in a significant overpressure transient in the reactor vessel. Normally, as the MSIV's close, a reactor scram is initiated by position switches which sense closure.

In addition, a secondary reactor scram will be initiated on high neutron flux. As the system isolates, pressure rises in the vessel until the safety/relief valves open to mitigate the accident.

Summary of Accident Analysis

The reactor is assumed initially to be at rated power (1670 MWt). The MSIV's are taken to close in three seconds with a non-linear valve flow characteristic. A reactor scram on MSIV position is conservatively ignored. Reactor scram is initiated on high neutron flux. The insertion of scram reactivity is limited to the rate of insertion allowed by the Technical Specifications with the most reactive rod stuck out. A rapid pressure increase follows closure of the MSIV's. If the pressure rises to the pressure relief set point, some or all of the relief valves open, discharging steam to the suppression pool. If the pressure rises to ≥ 1150 psig, trip of the M/G set breakers occurs.

Figures 3.2-106 through 3.2-112 show the DYNODE-B calculated results versus the General Electric ODYN results.

The DYNODE-B results compare favorably to the ODYN results. The same input and modeling differences exist as in the Load Rejection without Bypass benchmark (Section 3.2.1.2.1) since the two transients are very similar in response. The MSIV closure transient pressurizes more slowly and therefore is less sensitive to void reactivity and hence the DYNODE-B and ODYN results compare more closely. The maximum increase in the reactor vessel pressures are within 10 psi. The differences between the DYNODE-B and ODYN responses to this transient are insignificant.

3.2.2 CODE-DATA COMPARISONS

In this section the DYNODE-B code is benchmarked to three Peach Bottom turbine trip tests [16] and six Monticello start-up tests [14]. The purpose of these benchmarks is to qualify the models used in DYNODE-B and to quantify the conservatism in the DYNODE-B code. Section 4 discusses the quantification of the code conservatisms.

3.2.2.1 PEACH BOTTOM 2 EOC 2 TURBINE TRIP TESTS

Three instrumented turbine trips were carried out at the Peach Bottom-2 reactor during April 1977. These tests were conducted with the direct scram on stop valve position bypassed so that a trip on high flux was obtained. This departure from the normal reactor condition was required to obtain a sufficiently large flux response to allow a more complete model-test comparison. A detailed description of the test conditions and measurement process can be found in Reference 16.

3.2.2.1.1 TEST SUMMARY

The initial power and flow conditions for each test are shown in Table 3.2-1. These test conditions were selected in order of increasing power along a line of constant reactor flow. Prior to the second turbine trip test, it was necessary to reduce core flow to obtain the power to within 1% of planned test power level due to the xenon level in the core at the time of the test. In each of the three tests, the trip scram was disabled and the flux scram setpoint was reduced. The scram setpoints are also listed in Table 3.2-1.

A total of 153 signals were recorded by a digital data acquisition system. The comparisons presented here will concentrate on those parameters which affect the transient Δ CPR.

3.2.2.1.2 MODEL INPUTS

The DYNODE-B program has been used to model the three Peach Bottom 2 End of Cycle 2 (PB2EOC2) turbine trip tests (TT1, TT2, and TT3) for the purpose of benchmarking against overpressure transients which result in a rapid power increase. This benchmark effort began with an early version of DYNODE-B which did not have a one-dimensional kinetics or a detailed steam line model, so that these results were based on point kinetics and the lumped steam line models. This same model was used in pre-test predictions which validated the corresponding REDY results. Subsequently, the latest version of DYNODE-B was used to incorporate spatial kinetics and steam line momentum effects. The development process is described below.

The initial modeling of PB2 EOC2 was accomplished by utilizing design data and operational characteristics published in Reference 11 for the Reactor Coolant System (RCS). The point kinetics parameters were generated with a full 3-D nodal model of the core, similar to the models for Monticello described in Reference 1, using the actual initial test conditions. This work was performed by UAI (formerly NAI) and documented in Reference 10. This Best Estimate model utilized the MOC solution for the steam line momentum effects as well as actual APRM trip setpoints, actual turbine and bypass valve positions, scram velocities, and recorded initial test conditions (RV pressure and flow, core power, steam flow, and core inlet subcooling) from Reference 16.

The results of these comparisons provided satisfactory agreement with the measured core power and pressure transient data.

Later on, after the one-dimensional kinetics model had been implemented in DYNODE-B, the benchmarks were repeated. However, for these analyses, the one-dimensional kinetics could not be obtained directly from the 3-D model, since the model is no longer available. Thus, an approximate approach was taken in which the reactivity dependencies on void, fuel temperature, and control state were established to give results which were comparable with the point kinetics data. The void dependency was then adjusted until the peak power matched the test data, and the scram worth was adjusted until the integrated power matched the test data. This procedure effectively eliminates the uncertainty due to the kinetics parameters. The test data comparisons thus represent differences due to the DYNODE-B computer code uncertainties only. Therefore, these tests therefore represent a way to quantify these uncertainties (See Section 4.4).

3.2.2.1.3 DATA COMPARISONS

This section describes the calculated to measured comparisons for the most important transient parameters; neutron flux, steam dome pressure, turbine throttle pressure, and critical power ratio. Table 3.2-1 summarizes the comparisons. A detailed description of each of the above four parameters follows.

Neutron Flux Comparisons

The neutron flux transient is initiated by the main steam line pressure rise due to turbine stop valve (TSV) closure. Normally a reactor scram on TSV position would occur at 10% closure of three out of four valves. This scram signal was bypassed for these tests. A pressure wave, due to TCV closure, travels down the steamline and into the core, causing void collapse and a flux increase. The largest flux rise occurs near the top of the core, which has the largest void fraction and the largest void coefficient. The flux increase causes a reactor scram on high neutron flux. The power peaks and turns around due to the insertion of scram reactivity as well as a decrease in the void reactivity and an increase in the negative Doppler reactivity. For the Peach Bottom Test conditions, the scram reactivity is the dominant contributor to the flux transient turn-around. This is due to the fact that many control rods are inserted in the core, initially giving rise to a strong scram reactivity.

Figures 3.2-114, 3.2-117 and 3.2-120 show the calculated versus measured responses of the relative neutron flux (APRM Channel A from Reference 16) for tests TT1, TT2, and TT3, respectively. The uncertainties in void reactivity and scram reactivity have been factored out as discussed previously. Therefore, as would be expected, the DYNODE-B results show excellent comparison in the peak flux, flux slopes, and widths of the flux peak.

Transient Pressure Comparisons

Dynamic pressure measurements were recorded at the turbine inlet, in the steamline 90 ft downstream from the vessel, the vessel dome, and near the core exit plenum. In all of the pressure comparisons listed in this section, the data shown are the unfiltered data as recorded by the pressure sensors. The sensors are connected to the appropriate measurement locations by water-filled sensor lines. These sensor lines have their own second-order response which can often give rise to oscillations in the recorded data. Further discussion of the sensor line effects is contained in Reference 16.

Figures 3.2-115, 3.2-118 and 3.2-121 show the calculated versus measured response of the turbine throttle pressure for TT1, TT2, and TT3, respectively. DYNODE-B accurately predicts the initial pressure oscillation in both timing and magnitude, indicating that the initial time effects; i.e. delays, rise times, and frequencies; are well modeled. As the transient progresses, the calculated wave frequencies are accurately predicted, though the wave amplitudes are greater. The increased amplitude does not appreciably affect the transient results with respect to CPR. The overall magnitude of the turbine throttle pressure is conservatively overpredicted for the latter part of the transients.

Figures 3.2-113, 3.2-116 and 3.2-119 show the calculated and measured steam dome pressures follow the same trends as the turbine throttle pressures; the initial pressure rise and wave frequency are well predicted, the wave amplitudes are slightly over predicted, and the overall magnitude is conservatively overpredicted.

Critical Power Ratio

Critical Power Ratio is defined as the ratio of the bundle power which would produce onset of transition boiling to the actual bundle power. A good measure of the relative severity of a particular reactor transient is the maximum change of CPR, divided by the initial or steady-state CPR (ICPR). The "measured" CPR is taken from Reference 9 and is determined as follows:

"For the Peach Bottom turbine trips, the CPR comparisons have been made by driving a hot channel transient thermal-hydraulic calculation with experimentally determined inlet flow, pressure, and fuel heat generation rate. The pressure input was taken from the core pressure signal, which was filtered with a 5 Hz low pass filter. The transient fuel heat generation rate was taken to be proportional to the total APRM response. Core flow was obtained from pressure drop measurements taken across four of the jet pumps throughout the three turbine trips. Changes in core flow can be detected by assuming the jet pump pressure drop to be proportional to the square of the flow. In practice, however, this is not an accurate measure of core flow because of the large amount of noise in the jet pump pressure drop signal. In this case, a 5 Hz filter was applied to the four jet pump signals to reduce the noise component and then averaged to obtain a pressure drop. The steady-state flow was normalized to the recorded flow at the beginning of each transient.

For the transient CPR calculations driven by the experimental data, uncertainties in the input quantities will contribute to an uncertainty in the ratio $\Delta\text{CPR}/\text{ICPR}$. Reference 16 quotes a ± 2 psi uncertainty in core pressure. This pressure uncertainty, coupled with a $\pm 3\%$ uncertainty in flow, results in a ± 0.01 uncertainty in the ratio $\Delta\text{CPR}/\text{ICPR}$. This CPR uncertainty is obtained from sensitivity calculations carried out on pressurization type transients."

The calculated CPR is determined from a hot-channel model in DYNODE-B using the GEXL correlation. The hot-channel dimensions are taken from Reference 11. The initial hot-channel bundle power was forced to give the correct ICPR.

In both cases, the initial conditions, channel properties, and the CPR correlation are identical. Only the transient forcing functions, i.e., power, pressure, flow, and inlet enthalpy are different, so that a good measure of the CPR uncertainty due to code model uncertainty is obtained.

The calculated versus measured CPR results are shown in Table 3.2-3. For each transient, the calculated $\Delta\text{CPR}/\text{ICPR}$ is approximately 10% greater than the measured value. This indicates that the DYNODE-B code model uncertainties provide a conservative 10% bias on transient $\Delta\text{CPR}/\text{ICPR}$.

3.2.2.2 MONTICELLO START UP TESTS

The DYNODE-B code has been used to model six Monticello Start-Up Tests. These tests are described and documented in Reference 14.

The modeling of these tests was done using best-estimate input parameters. A 1-D kinetics model was used for the MSIV closure and Turbine Trip transients. Point kinetics were used for the remaining four cases. This is in accordance with the guidelines in Section 4.1.

The results for each transient are discussed in the following sections.

3.2.2.2.1 TURBINE TRIP WITH BYPASS AT 100% POWER (STP 16)

Description of the Test

The purpose of this test was to determine the response of the reactor system to a turbine trip.

The turbine was tripped with the Turbine Emergency Trip Switch at 1656 MWt. Reactor pressure peaked at 1115 psig, an increase of 105 psi. The M/G set breakers were tripped on turbine trip causing a flow coastdown. All four relief valves opened to terminate the pressure transient. A power increase was not observed on the APRMs.

Summary of the Test Analysis

Figures 3.2-122 through 3.2-127 show the calculated versus measured results for the Turbine Trip Start Up Test.

DYNODE-B overpredicts the core power response with a peak relative power of approximately 300 percent. The data does not show a power increase during the initial pressurization. This is probably due to a faster/stronger scram than was assumed in the analysis. Since DYNODE-B overpredicts the integrated power, it also overpredicts the vessel pressure response. Both the calculated and measured results show that all four relief valves open, but DYNODE-B predicts a peak vessel pressure of 1154 psia compared to the measured value of 1130 psia.

DYNODE-B conservatively predicts the vessel flow coastdown and does a good job of tracking level.

A "measured" Critical Power Ratio was calculated by forcing the DYNODE-B hot channel model with the measured data. This resulted in a "measured" $\Delta\text{CPR}/\text{ICPR}$ of 0.003. The DYNODE-B calculated results give a $\Delta\text{CPR}/\text{ICPR}$ of 0.156. This is due mainly to the difference in the power response.

This transient provides a good benchmark of DYNODE-B's capability to conservatively predict reactor vessel pressure and transient ΔCPR . It also provides an excellent benchmark of DYNODE-B's capability to model transient vessel flow response.

3.2.2.2.2 CLOSURE OF 4/4 MAIN STEAM ISOLATION VALVES AT 75% POWER (STP 11)

Description of the Test

The purpose of this test was to functionally check the main steam line isolation valves for proper operation, demonstrate the capability to perform isolation valve test closures without threatening reactor safety or causing a reactor scram, determine reactor transient behavior following simultaneous full closure of all MSIV's, and determine isolation valve closure times.

The full isolation test was done at 75% power by tripping the relays in the RCICS circuit with a special test switch to give a full isolation and subsequent scram. Following the full isolation at 75% power, reactor pressure increased 69 psi to 1069 psig two seconds after the MSIV's had closed.

Summary of the Test Analysis

Figures 3.2-128 through 3.2-132 show the calculated versus measured results for the MSIV Closure Start Up Test.

The measured feedwater flow did not behave as would be expected from automatic controller action. Therefore it was presumed that the feedwater was controlled manually during the test and the measured feedwater flow was forced onto the DYNODE-B solution. The measured steam flow shows unexplainable behavior and was assumed to be bad data. The two most important input parameters, MSIV closure time and scram time, are unknown and were assumed to match the nominal values in the DYNODE-B calculation.

Both the measured and calculated results show a rapid increase in pressure due to the MSIV closure. DYNODE-B predicts a faster initial rise than the data (50 psi/sec versus 30 psi/sec). The data shows that the pressure peaks at about 1080 psia (15 psi below the relief valve setpoint) and then slowly decays. DYNODE-B predicts that the pressure rises to the relief valve setpoint, cycling the relief valves to control pressure. The differences in pressure response could be attributable to several different factors; the test may have a slower MSIV closure than assumed, a faster scram than assumed, the MSIV valves may not have closed completely, or there may be a steam condensation effect due to uncovering of the feedwater sparger. In any case, there is insufficient data available to determine a cause and effect.

This test does not provide a very good benchmark due to the poor quality of the data. It does show that DYNODE-B tracks the water level very well during the initial pressurization and that DYNODE-B conservatively overpredicts the peak transient pressure.

3.2.2.2.3 2/2 RECIRCULATION PUMP TRIP (STP 14)

Description of the Test

The purposes of this test were to evaluate the recirculation flow and core power transients following trips of both of the recirculation pumps, calibrate the reactor core flow measurement system, and measure the reactor core flow by performing mass and energy balances on the reactor downcomer.

Both individual and dual pump trip transients were recorded. For the purposes of this analysis, only the two-pump trip case was examined, since this represents a more severe transient than the single pump trip. Prior to tripping the pumps, core performance data were taken to enable the peak heat flux and MCHFR to be evaluated. A recording was taken which included a trace of the core flow and the simulated heat flux.

Summary of the Test Analysis

Figures 3.2-133 and 3.2-134 show the calculated versus measured results for 2/2 Pump Trip Start Up Test.

DYNODE-B conservatively overpredicts the vessel flow coastdown, i.e., DYNODE-B predicts lower flow than the data. Also, DYNODE-B conservatively overpredicts the core average heat flux. Since these are the only variables available for comparison, it is concluded that DYNODE-B provides a conservative prediction of Critical Power Ratio for this transient.

3.2.2.2.4 AUTOMATIC FLOW DECREASE AT 100% POWER (STP 15)

Description of the Test

The purpose of this test was to determine the plant response to changes in the recirculation flow and to demonstrate the plant load-following capability.

To determine the plant response to changes in the recirculation flow, the master flow controller setpoint was stepped a nominal $\pm 10\%$ of full scale. At each test condition, the test was repeated with several controller settings to aid in optimizing the response of the system. Initial individual loop control settings were at 500% proportional band and 15 repeats per minute reset. The optimized controller settings were arrived at during testing at 50% power, where the proportional band of both loops were set to 450%, loop A reset was set at 40 repeats per minute, and loop B reset was set at 20 repeats per minute. The initial master controller settings were 400% proportional band and 8 repeats per minute based on results obtained during 50% power testing. Instabilities which occurred during flow ramp testing between 75 and 100% power on the 100% power-flow line were corrected by reducing the resets to 2 repeats per minute.

The upper and lower speed demand limits were set to 93% and 58% speed, respectively. This placed the limits of automatic and master manual flow control to a range from 75% to 100% power in the 100% power rod pattern.

The automatic flow control flow ramp tests were performed with the Electrical Pressure Regulator (EPR) setpoint adjuster gain (POT150P) at 3.0 psi/% and a time constant (POT162P) of 20 seconds.

To demonstrate plant load-following capability, the fast flow changes were made with the final control system settings described above. The load changes were made first in the Master Manual mode and then in the Automatic Flow Control mode. In the Automatic mode, the load changes were caused by ramping the turbine speed/load changer. Turbine load could be dropped very rapidly by the automatic opening of the bypass valves.

For the purposes of this analysis only the Pump Flow Decrease in Automatic Manual from 100% to 75% power was examined since this represents the most severe transient in the series.

As the flow controller responds to the setpoint step, the vessel flow ramps down and core power decreases due to the increased void feedback. The entire system decays to a new steady state. An APRM decay ratio of 0.25 was calculated based on the measured data.

Summary of the Test Analysis

Figures 3.2-135 through 3.2-140 show the calculated versus measured results for the Auto Flow Decrease Start Up Test.

The DYNODE-B predicted results show excellent comparison during the first 20 sec of the transient, tracking all variables very closely. Beyond this point, the DYNODE-B results deviate slightly. The data settles out to a new steady state condition very quickly, with a decay ratio of 0.25 calculated from the APRM response. DYNODE-B conservatively predicts a decay ratio of 0.89 and a longer frequency (approximately 30 sec versus 10 sec from the data).

This transient provides an excellent benchmark of DYNODE-B's capability to conservatively predict decay ratio.

3.2.2.2.5 PRÉSSURE REGULATOR SETPOINT STEP AT 100% POWER (STP 18)

Description of the Test

The purpose of this test was to determine the reactor and pressure control system responses to pressure regulator setpoint changes, to demonstrate the stability of the reactivity void feedback loop to pressure perturbations, and to optimize the pressure regulator setpoints.

Pressure setpoint changes were made with both the Electrical Pressure Regulator (EPR) and the Mechanical Pressure Regulator (MPR) to determine reactor and turbine system responses and to demonstrate the stability of the reactivity void feedback loop to pressure perturbations.

The pressure disturbances were obtained by changing the regulator setpoint downward and then upward as fast as possible to produce a nominal 10 psi change in reactor pressure. This was done with the load limits out of the way (load limiter set well above the reactor power level) and repeated with the load limits incipient (load limiter set at the reactor power level).

The changes in the EPR setpoint were made from a special test circuit located in the cable spreading room, which initiated a step change in the setpoint.

For the purposes of this analysis, only the -10 psi step of the EPR setpoint at 100% power was examined, since this represents the most severe transient in the series.

The pressure controller responds to -10 psi step by opening the turbine control valves to drop the turbine throttle pressure by 10 psi. As the pressure drops the core power drops due to increased voiding. The entire system decays to a new steady state with a period of approximately 8 seconds.

The stability of the reactivity void feedback loop was clearly demonstrated at this test condition.

Summary of the Test Analysis

Figures 3.2-141 through 3.2-145 show the calculated versus measured results for the Pressure Setpoint Step Start Up Test.

The DYNODE-B predicted results show excellent comparison to the test results. The predicted results exhibit approximately the same period with a slightly greater amplitude. The reported APRM decay ratio is zero, based on the measured data. DYNODE-B calculates a decay ratio of 0.21 for relative power.

This transient provides an excellent benchmark of DYNODE-B's capability to conservatively predict decay ratio.

3.2.2.2.6 FEEDWATER CONTROLLER LEVEL SETPOINT STEP AT 100% POWER (STP 20)

Description of the Test

The purposes of this test were to determine the effect of changes in subcooling on reactor power and steam pressure and to demonstrate that reactor responses to changes in subcooling are stable at all power levels.

The changes in subcooling were introduced by varying the vessel water level setpoint (3 and 6-inch changes), and the resulting transients were recorded.

Testing at all power levels, in three-element and one-element level control and automatic and manual recirculation flow control, yielded stable plant responses to changes in subcooling. Decay ratios of primary variables were less than 0.25 for all of these tests.

For the purposes of this analysis, only the 6 inch level step at 100% power in three-element control and automatic flow control was examined, since this represents the most severe transient in this series.

The feedwater controller responds to the 6-inch setpoint drop by cutting back the feedwater flow to attempt to balance the level error. As the feedwater flow drops, the core power and vessel pressure drop slightly due to the decreased inlet subcooling. As the level drops, the controller error goes to zero and the feedwater flow and all other core parameters return to their original level.

The stability of the reactor in response to subcooling changes was clearly demonstrated at this test condition.

Summary of the Test Analysis

Figures 3.2-146 through 3.2-149 show the calculated versus measured results for the Feedwater Controller Level Setpoint Step Start Up Test.

The DYNODE-B predicted results show excellent comparison to the test results. The predicted level response and feedwater flow track very closely. Both DYNODE-B and the data show a decay ratio of zero for the core power. There are no significant deviations between the predicted and measured results.

This transient provides an excellent benchmark of DYNODE-B's capability to predict decay ratio and to track water level.

Table 3.1-1

NDH - DYNODE-B VOID REACTIVITY COMPARISON

<u>Dome Pressure</u> <u>(psia)</u>	<u>Subcooling</u> <u>(Btu/lbm)</u>	K_{eff}	
		<u>NDH</u>	<u>DYNODE-B</u>
1038	24.42	0.99833	0.99811
1238	53.20	<u>1.01991</u>	<u>1.02003</u>

Reactivity Change = .0212 0.0215

$$\Delta\rho = K_1 - K_2 / K_1 K_2$$

Table 3.2-1

PEACH BOTTOM-2 TURBINE TRIP TRANSIENT
TEST ACTUAL CONDITIONS

Test Number	Reactor Power		Core Flow Rate		Core Pressure
	(Mwt)	(% Rated)	(10 ⁶ lb/h)	(% Rated)	(psia)
TT1	1562	47.4	101.3	98.8	1005
TT2	2030	61.6	82.9	80.9	995
TT3	2275	69.1	101.9	99.4	1005

Test Number	Core Inlet Enthalpy (Btu/lb)	APRM Trip Set Point (% Rated)
TT1	528.4	85
TT2	519.8	95
TT3	523.6	77

Table 3.2-2

PEACH BOTTOM-2
TURBINE TRIP TRANSIENT TEST
PEAK MEASURED AND CALCULATED RESPONSES

Variable	TT1		TT2		TT3	
	Data	DYNODE-B	Data	DYNODE-B	Data	DYNODE-B
Average Neutron Flux (% Rated)	239	239	280	281	339	342
Core Exit Pressure (psia)	1036	1053	1034	1066	1072	1088
Reactor Vessel Pressure (psia)	1031	1047	1038	1062	1061	1082

Data from Reference 16

Table 3.2-3

PEACH BOTTOM-2
TURBINE TRIP TRANSIENT TEST
CRITICAL POWER RATIO RESPONSE

Variable	TT1		TT2		TT3	
	Data	DYNODE-B	Data	DYNODE-B	Data	DYNODE-B
ICPR	2.536	2.536	2.115	2.115	2.048	2.048
Δ CPR	0.431	0.474	0.288	0.315	0.270	0.305
Δ CPR/ICPR	0.170	0.187	0.136	0.149	0.132	0.149

Data from Reference 9

Monticello Cycle 10 NDH - DNB Comparison

Figure 3.1-1
Relative Power

DNB053/86

NDH 85-536

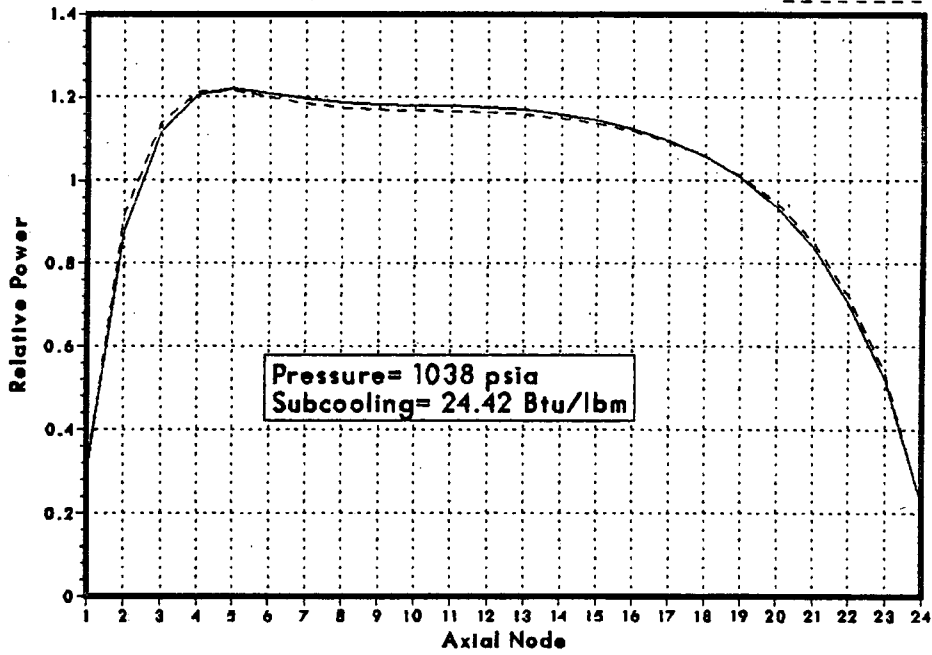
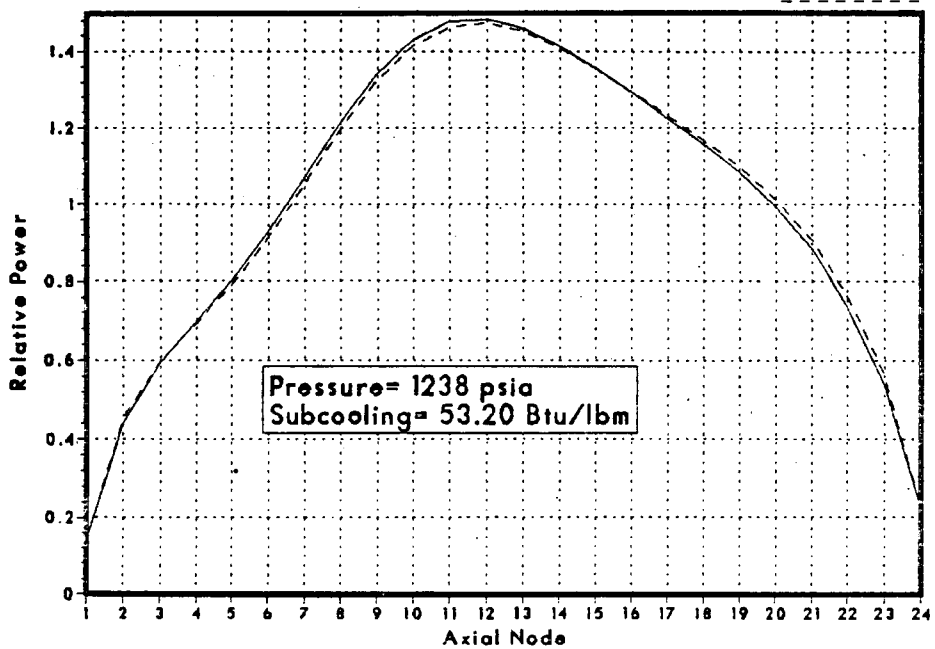


Figure 3.1-2
Relative Power

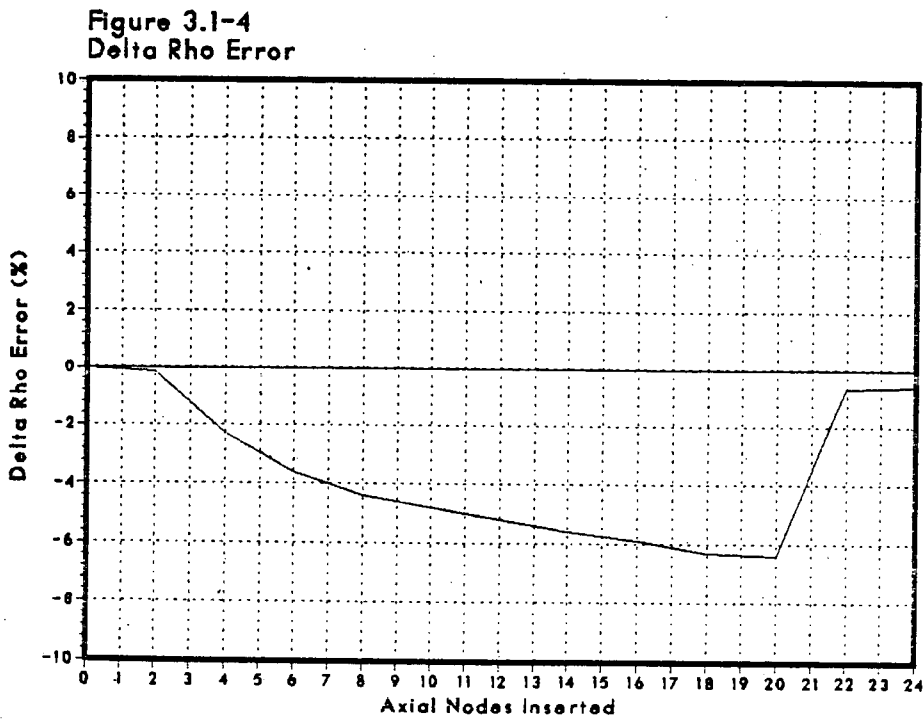
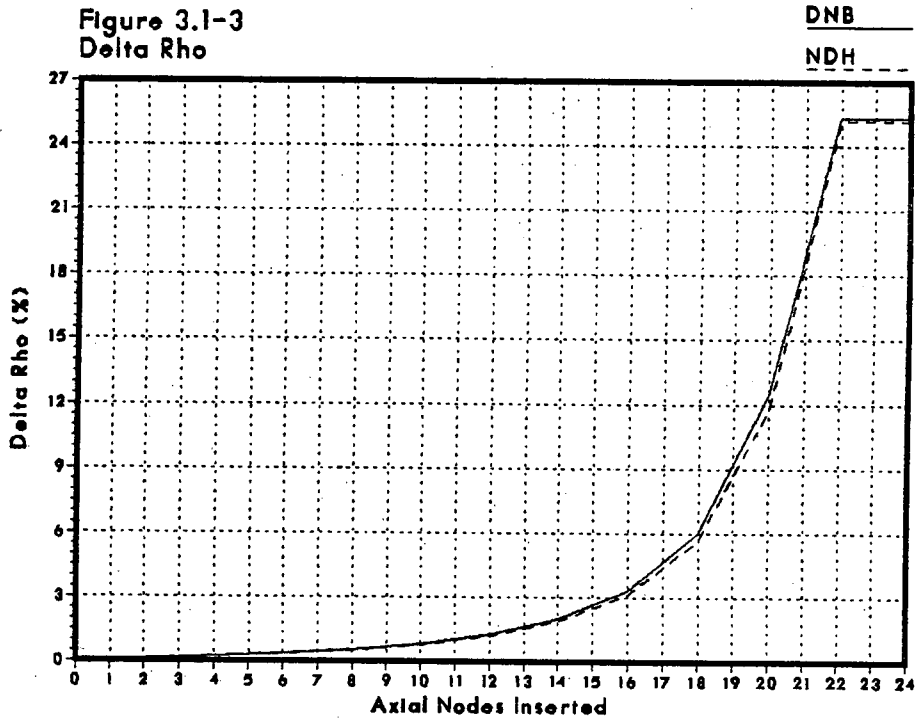
DNB054/86

NDH 85-589



NSP

Monticello Cycle 10 NDH - DNB Comparison



NSP

Monticello FSAR Benchmark Turbine Trip w/o Bypass

Figure 3.2-1
Steam Dome Pressure

DNB063/86

FSAR

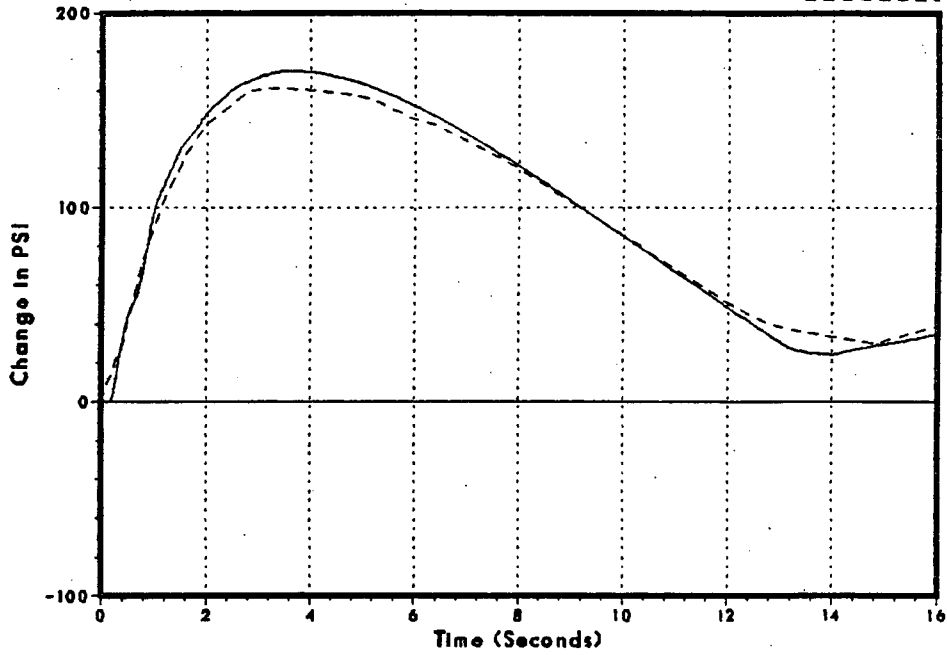
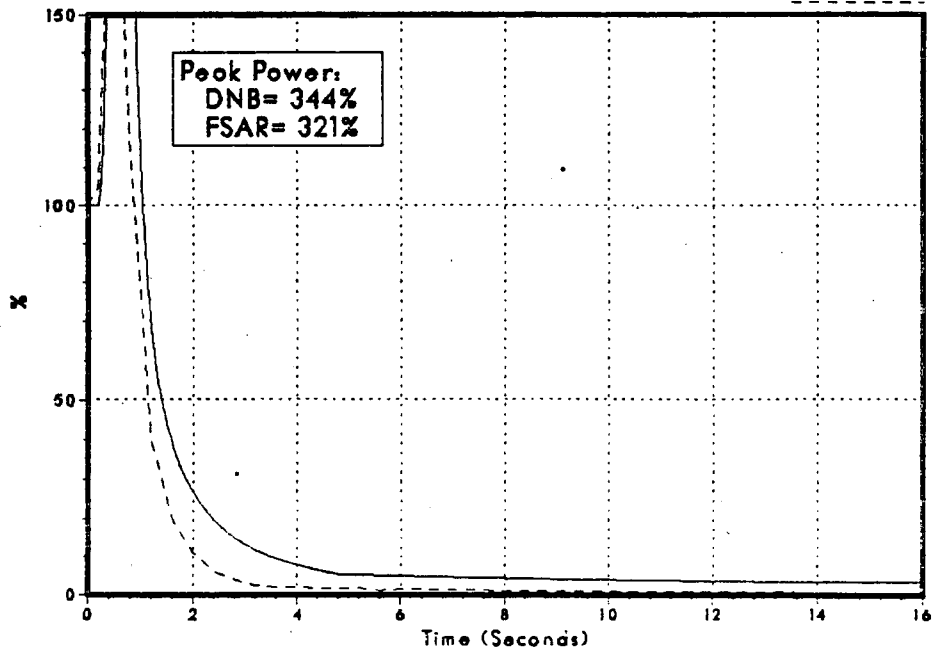


Figure 3.2-2
Relative Power

DNB063/86

FSAR



Monticello FSAR Benchmark Turbine Trip w/o Bypass

Figure 3.2-3
Core Average Heat Flux

DNB063/86
FSAR

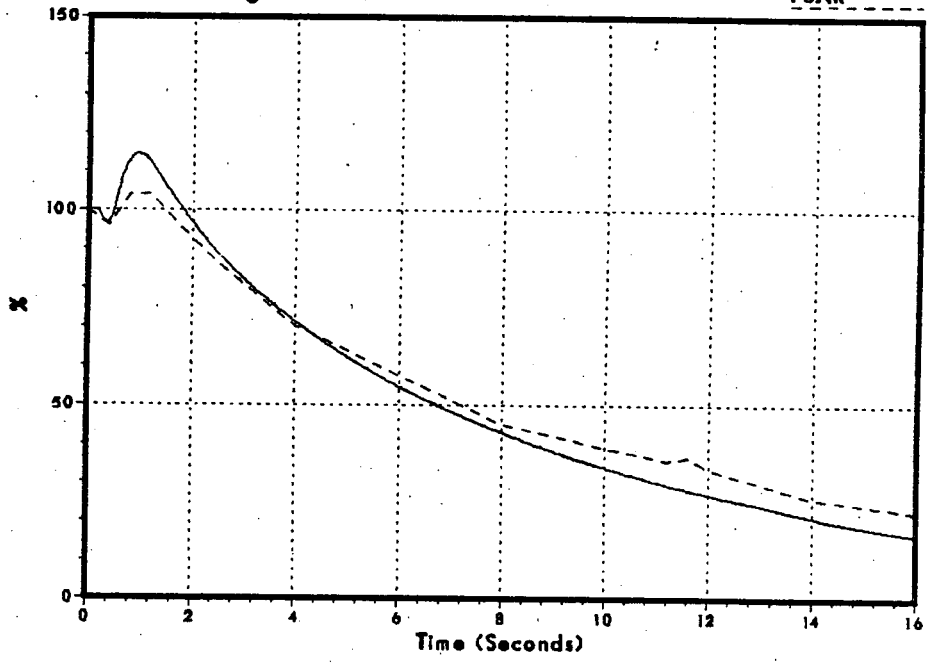
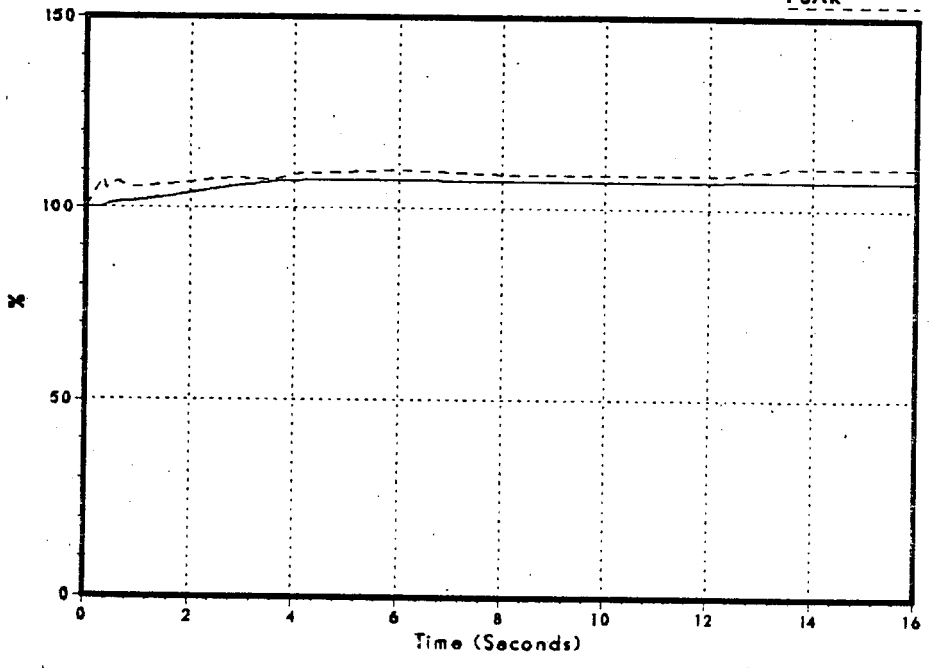


Figure 3.2-4
Core Inlet Flow

DNB063/86
FSAR



PREPARED BY NSP SAFETY ANALYSIS. 6/27/86



Monticello FSAR Benchmark Turbine Trip w/o Bypass

Figure 3.2-5
Main Steam Line Flow

DNB063/86

FSAR

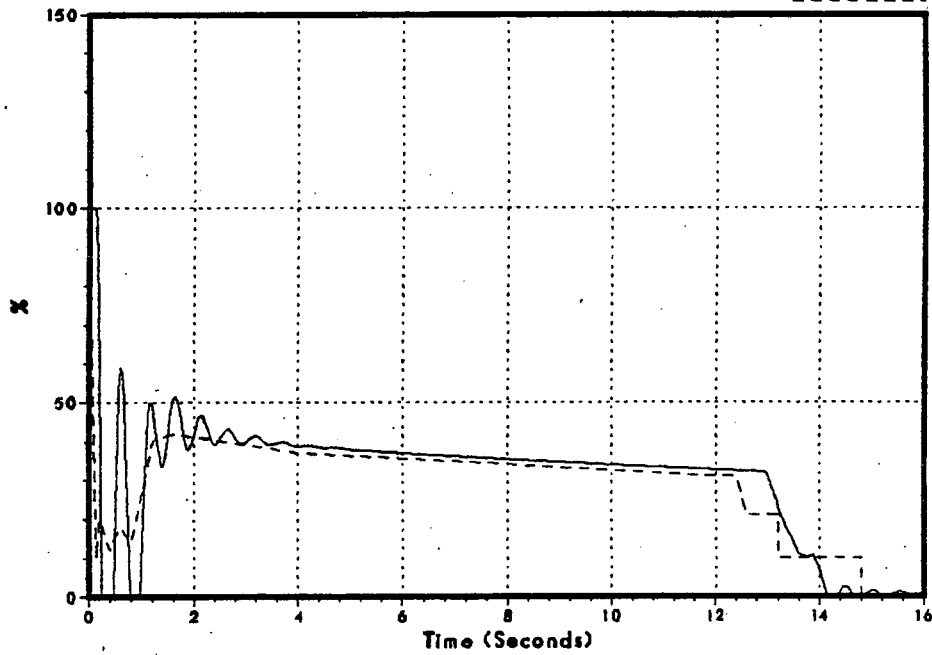
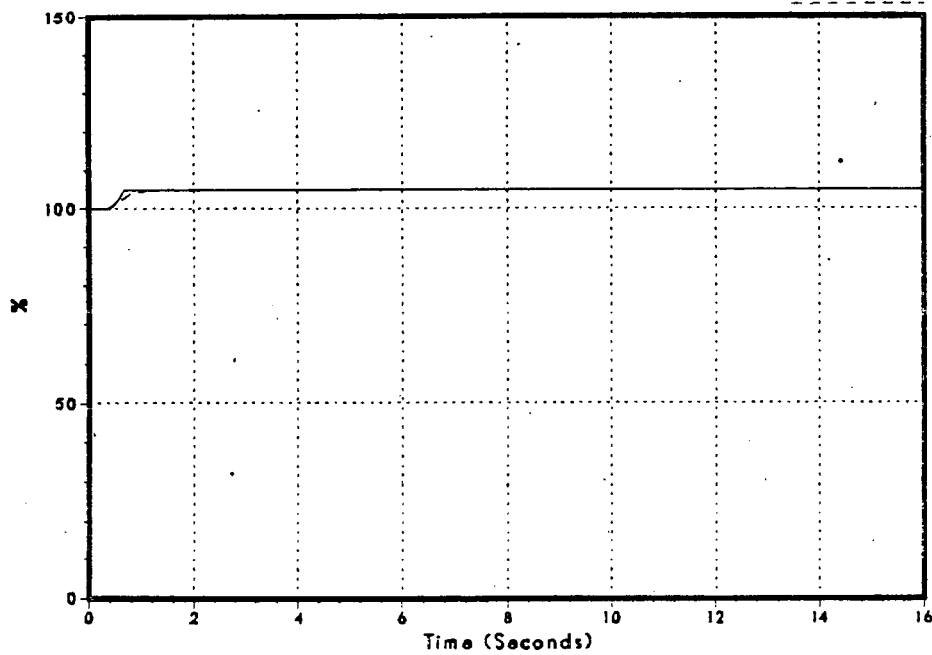


Figure 3.2-6
Feedwater Flow

DNB063/86

FSAR

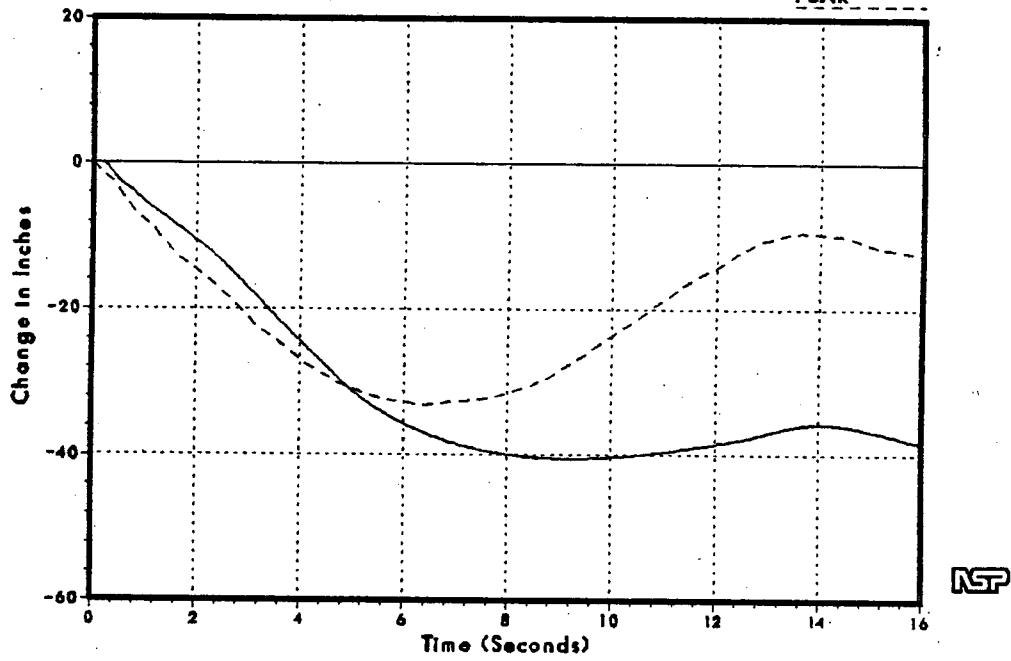


Monticello FSAR Benchmark Turbine Trip w/o Bypass

Figure 3.2-7
Sensed Level

DNB063/86

FSAR



Monticello FSAR Benchmark Turbine Trip w/ Bypass

Figure 3.2-8
Steam Dome Pressure

DNB070/86

FSAR

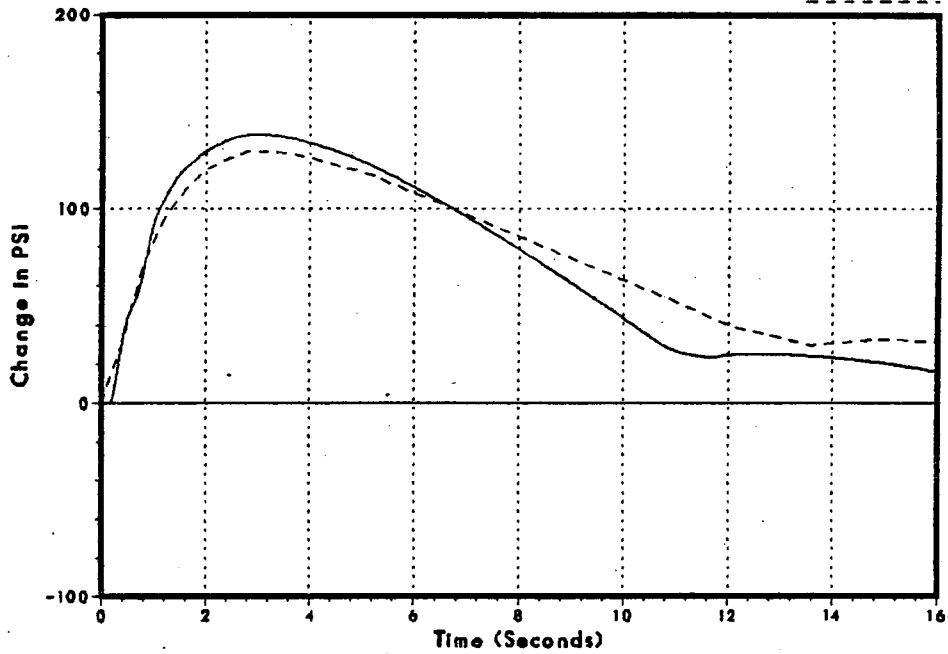
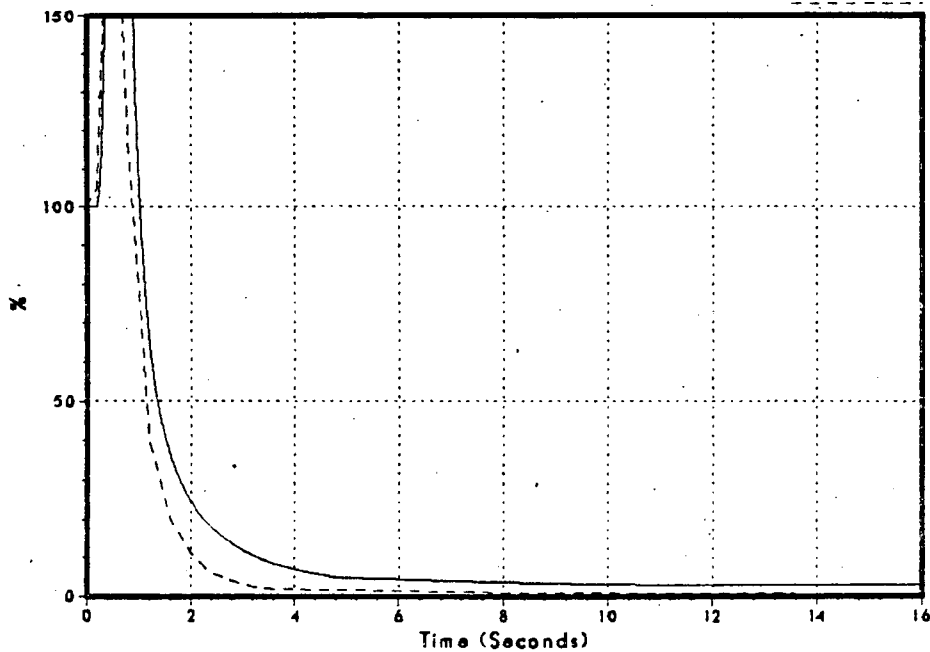


Figure 3.2-9
Relative Power

DNB070/86

FSAR



Monticello FSAR Benchmark Turbine Trip w/ Bypass

Figure 3.2-10
Core Average Heat Flux

DNB070/86

FSAR

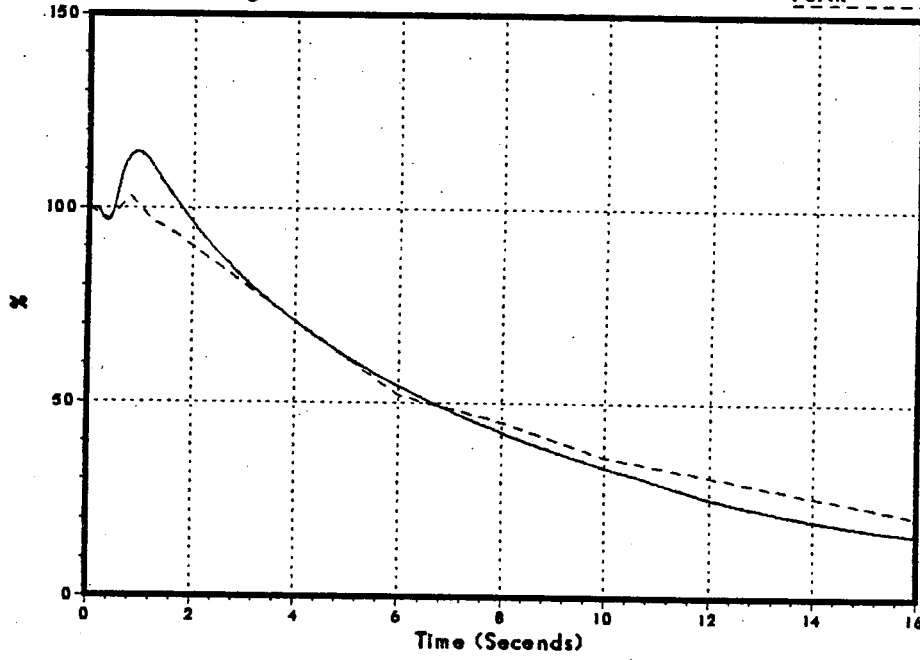
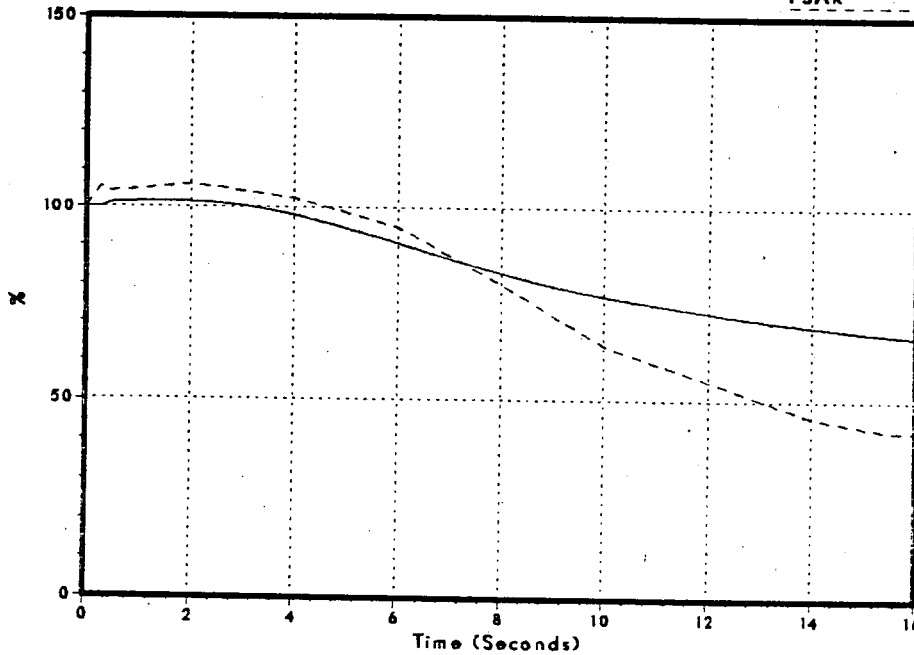


Figure 3.2-11
Core Inlet Flow

DNB070/86

FSAR



NSP

Monticello FSAR Benchmark Turbine Trip w/ Bypass

Figure 3.2-12
Main Steam Line Flow

DNB070/86

FSAR

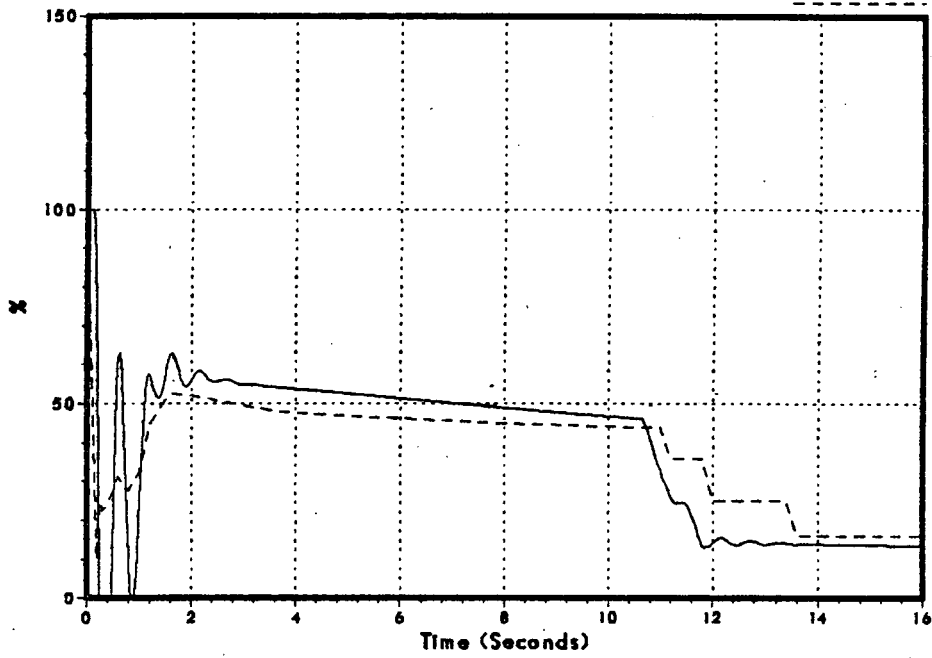
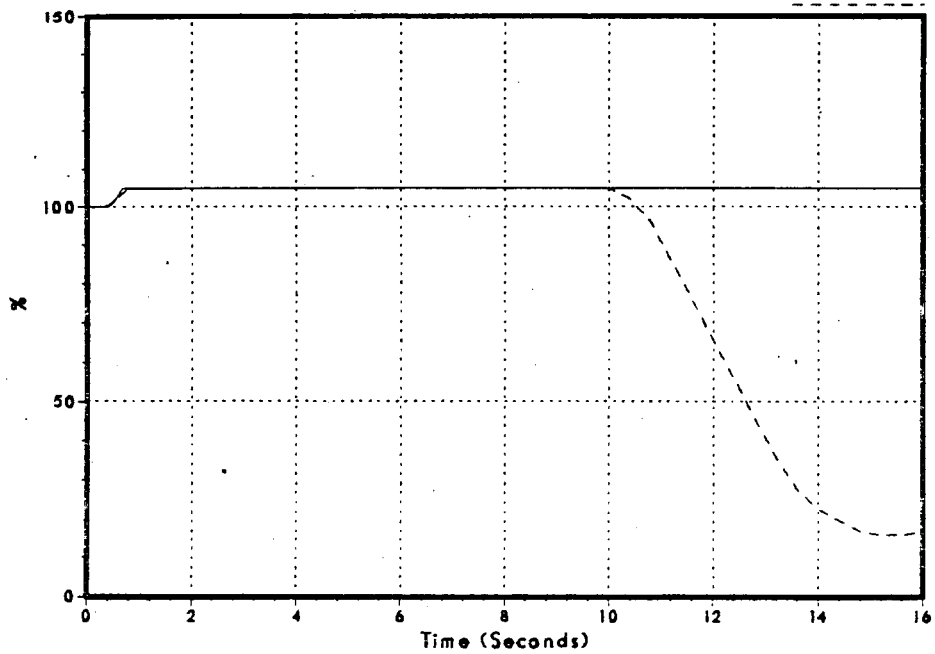


Figure 3.2-13
Feedwater Flow

DNB070/86

FSAR

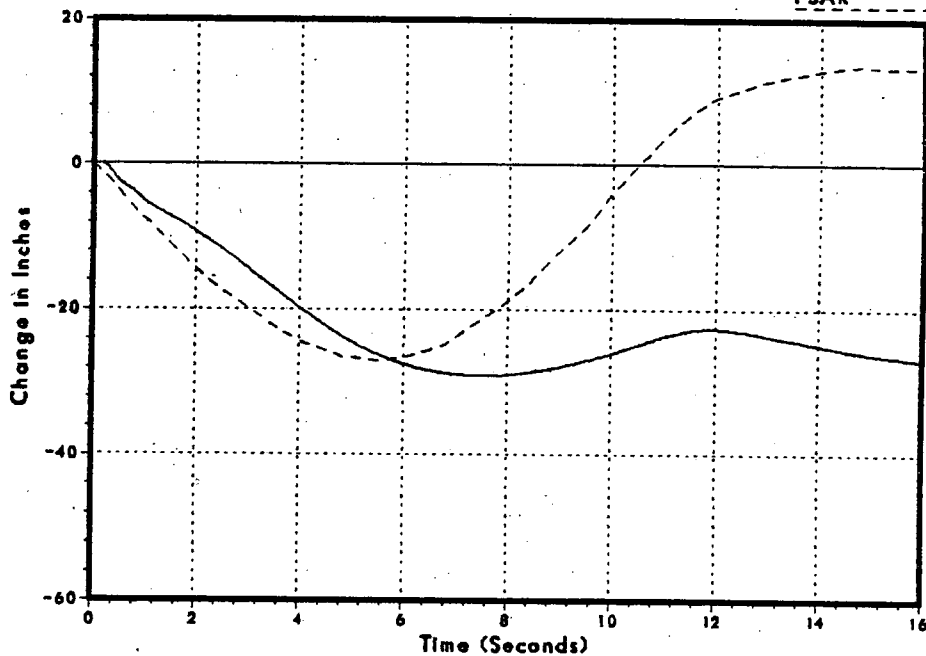


Monticello FSAR Benchmark Turbine Trip w/ Bypass

Figure 3.2-14
Sensed Level

DNB070/86

FSAR



NSP

Monticello FSAR Benchmark Generator Trip w/ Bypass

Figure 3.2-15
Sensed Level

DNB069/86

FSAR

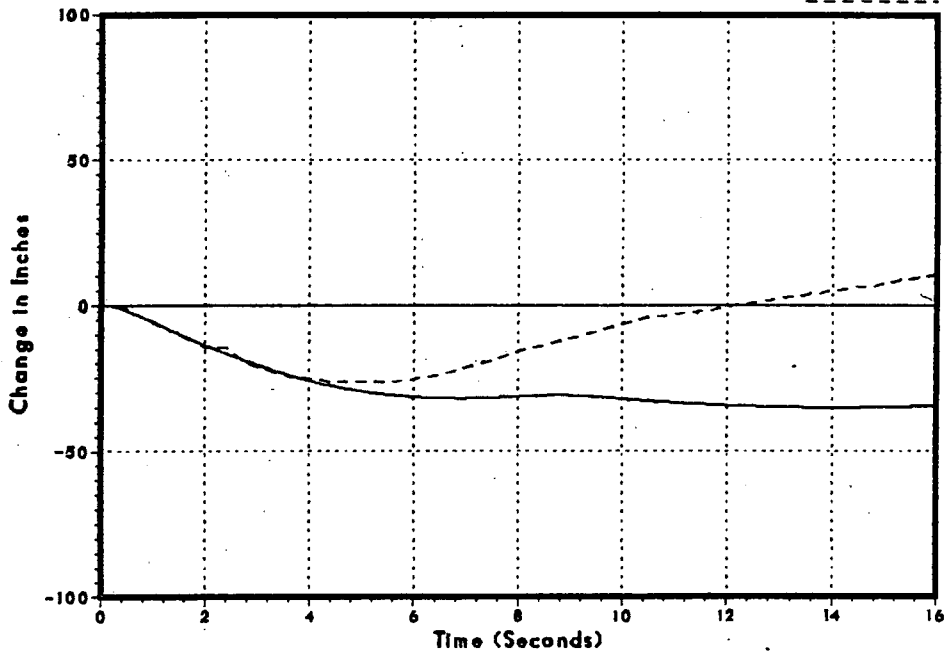
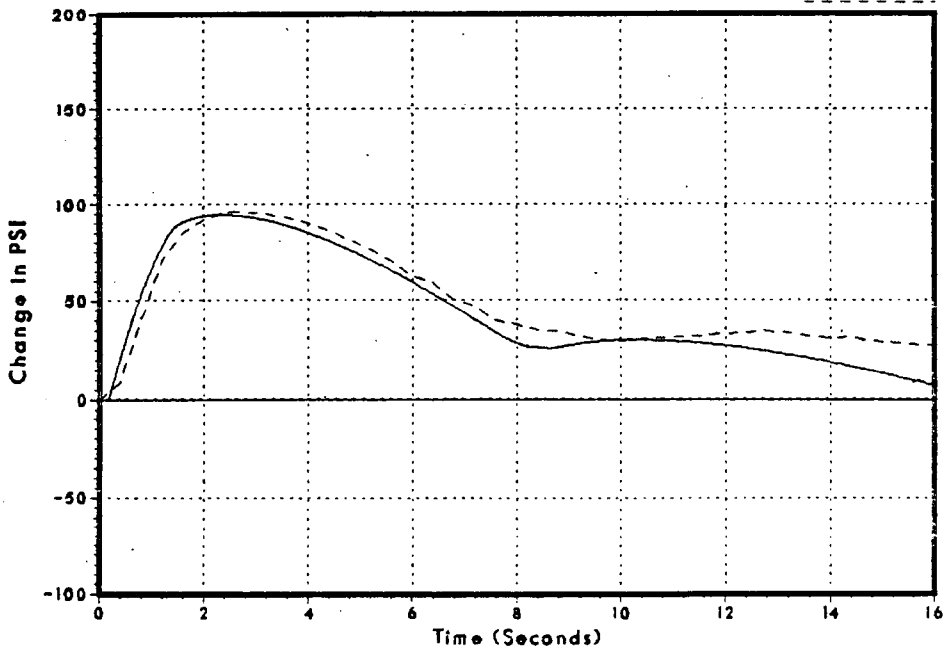


FIGURE 3.2-16
STEAM DOME PRESSURE

DNB069/86

FSAR



Monticello FSAR Benchmark Generator Trip w/ Bypass

Figure 3.2-17
Core Inlet Flow

DNB069/86

FSAR

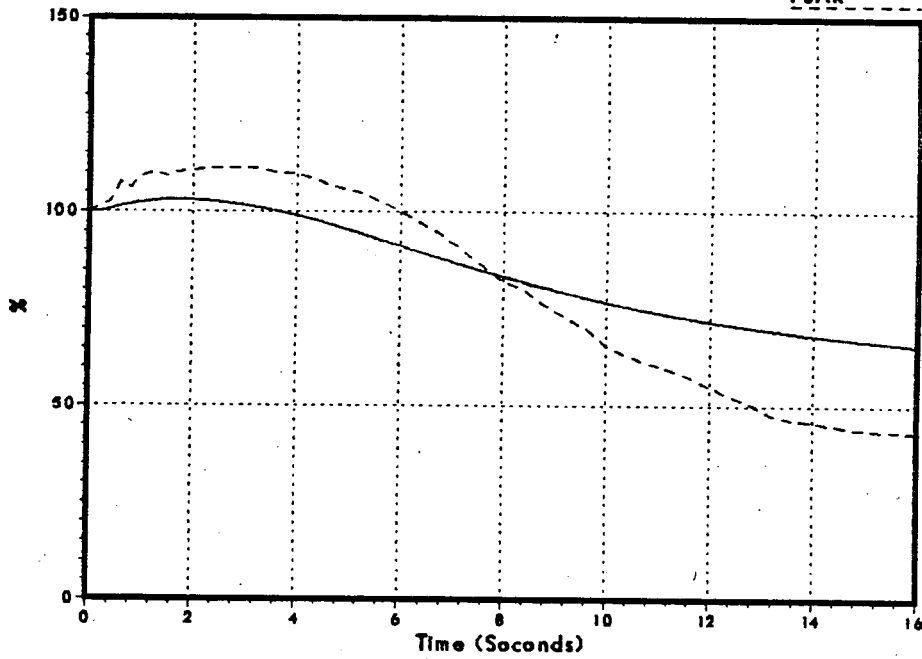
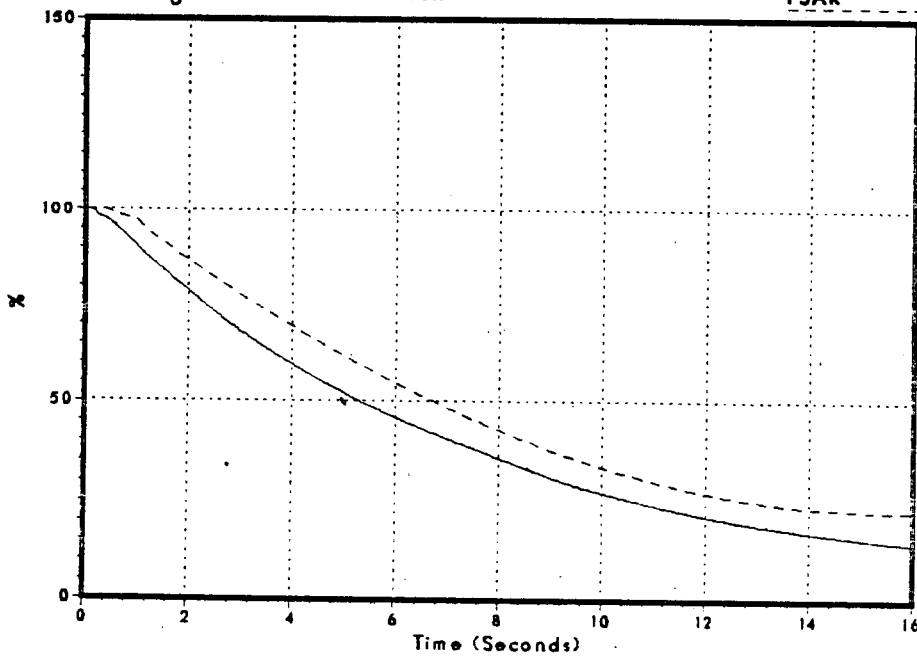


Figure 3.2-18
Average Surface Heat Flux

DNB069/86

FSAR



Monticello FSAR Benchmark Generator Trip w/ Bypass

Figure 3.2-19
Relative Power

DNB069/86

FSAR

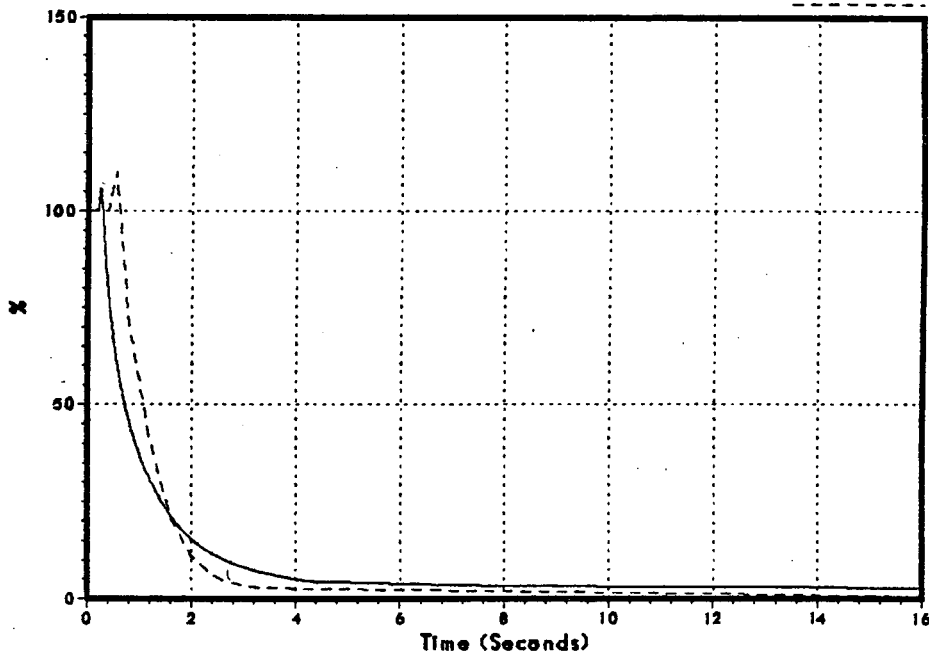
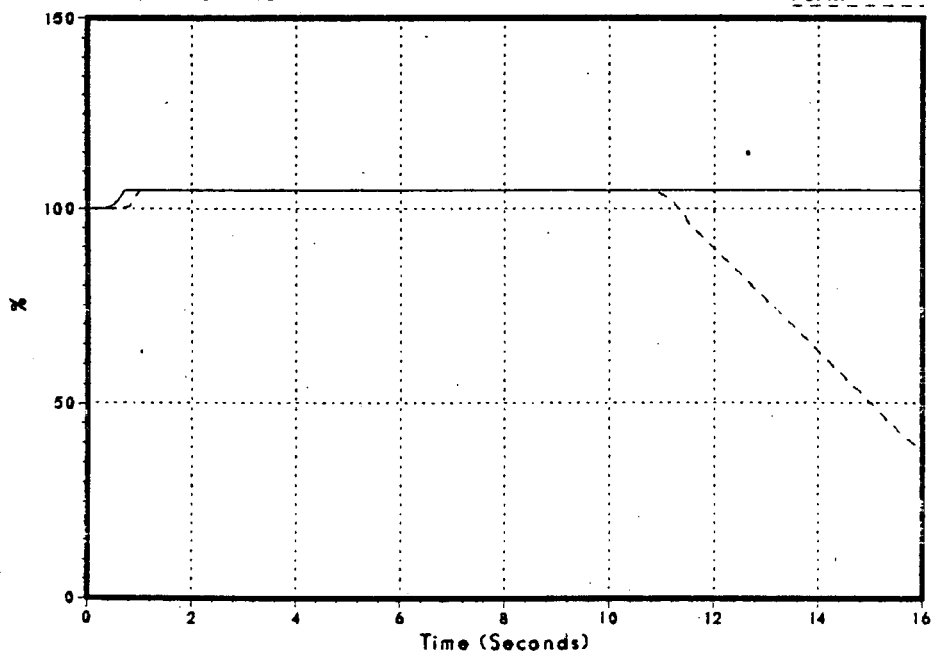


Figure 3.2-20
Feedwater Flow

DNB069/86

FSAR

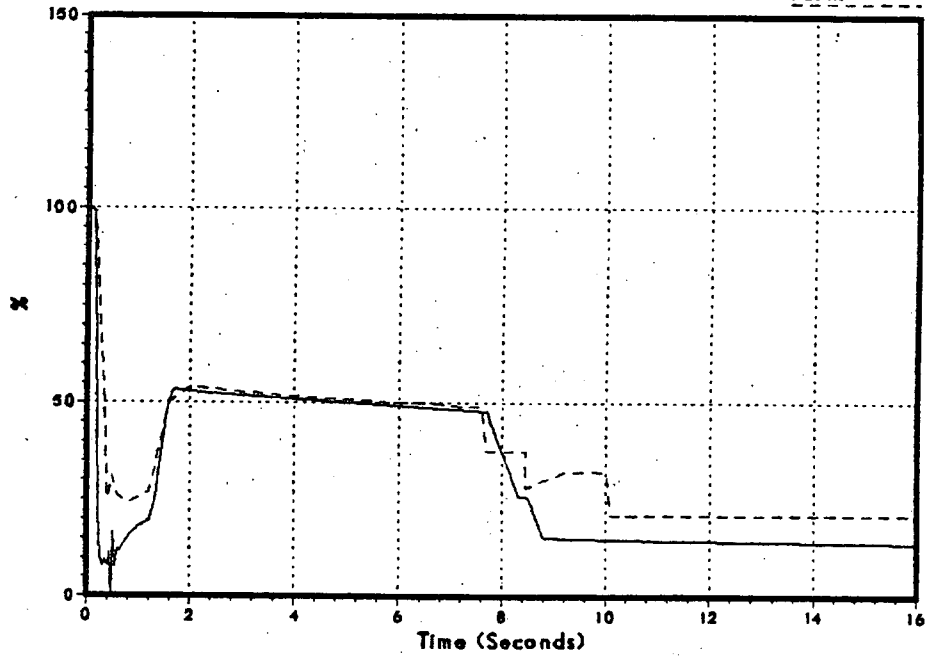


Monticello FSAR Benchmark Generator Trip w/ Bypass

Figure 3.2-21
Vessel Steam Flow

DNB069/86

FSAR



Monticello FSAR Benchmark 100% MSIV Closure

Figure 3.2-22
Steam Dome Pressure

DNB064/86

FSAR

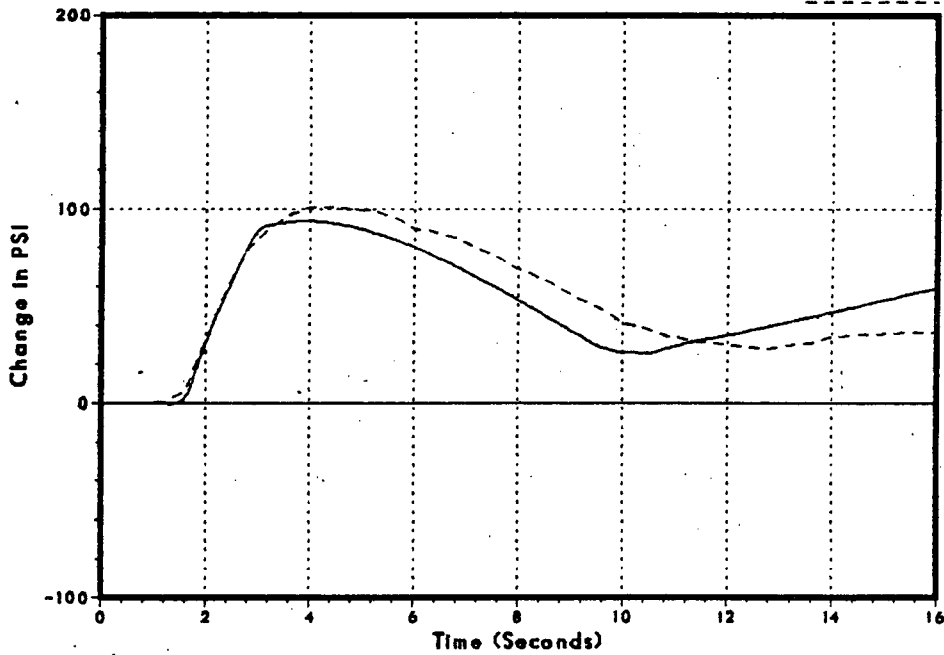
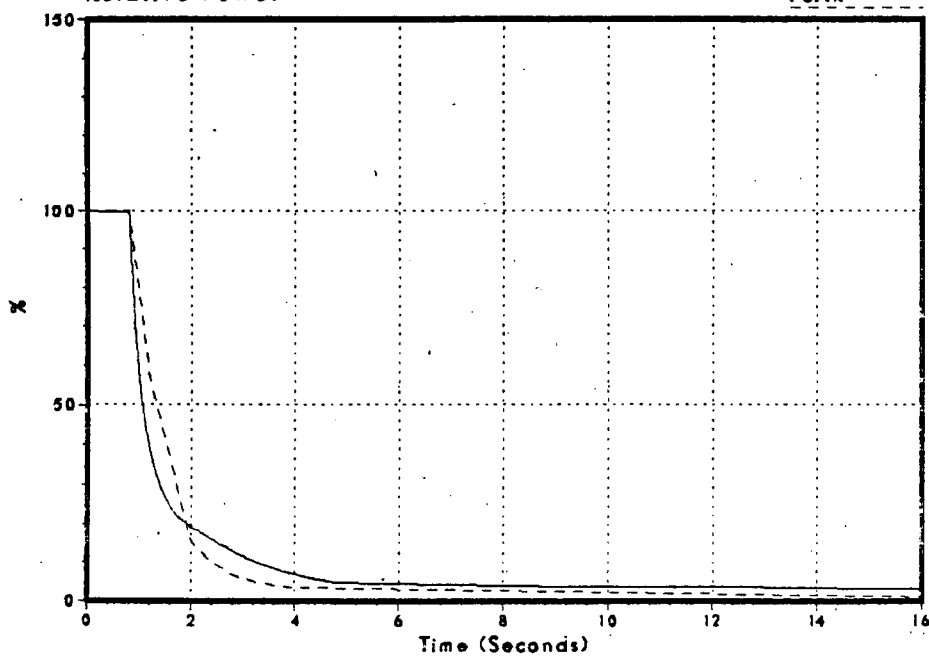


Figure 3.2-23
Relative Power

DNB064/86

FSAR



NSP

Monticello FSAR Benchmark 100% MSIV Closure

Figure 3.2-24
Core Average Heat Flux

DNB064/86

FSAR

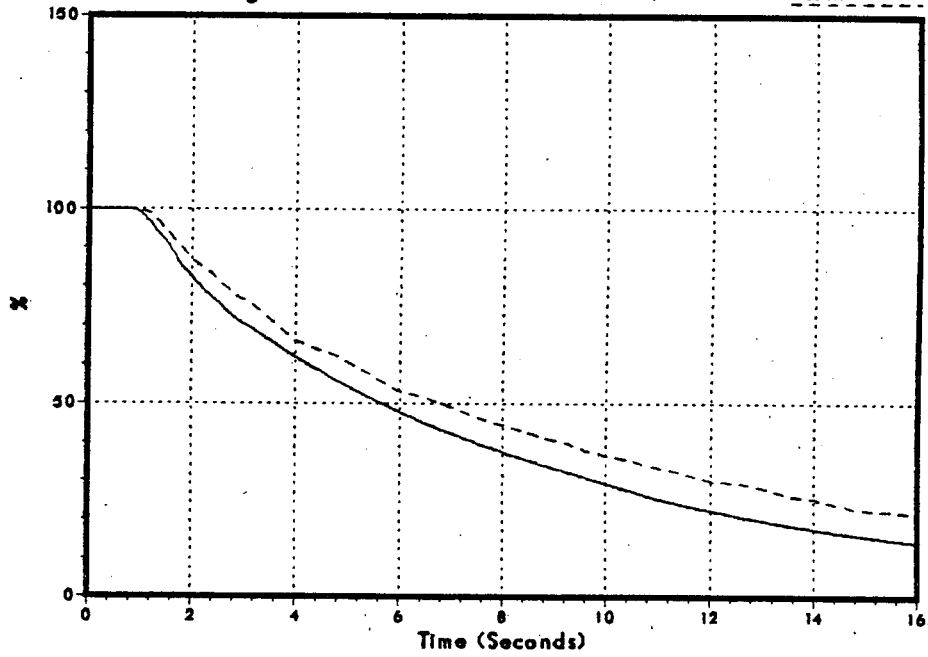
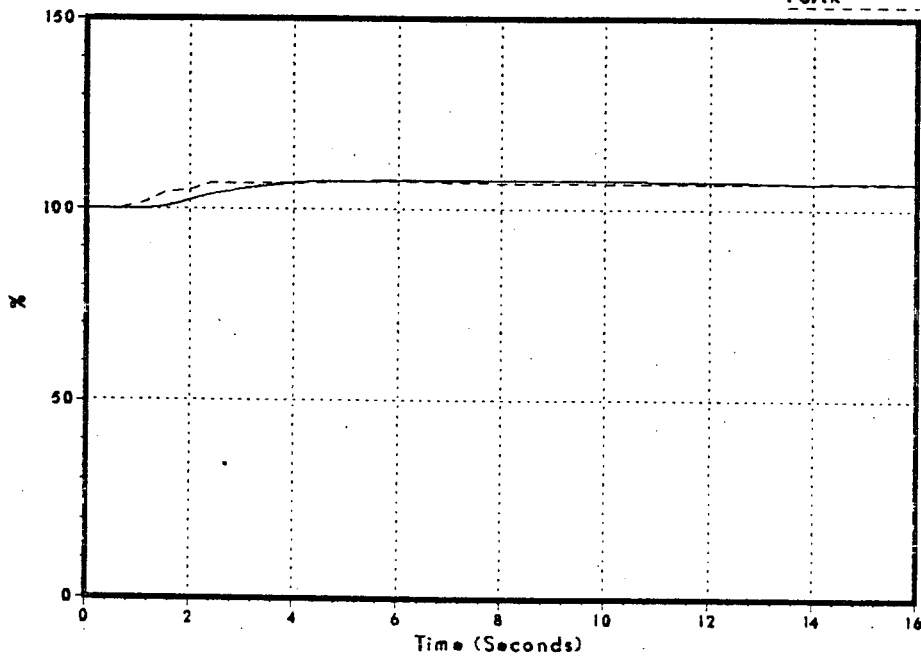


Figure 3.2-25
Core Inlet Flow

DNB064/86

FSAR



NSP

Monticello FSAR Benchmark 100% MSIV Closure

Figure 3.2-26
Main Steam Line Flow

DNB064/86

FSAR

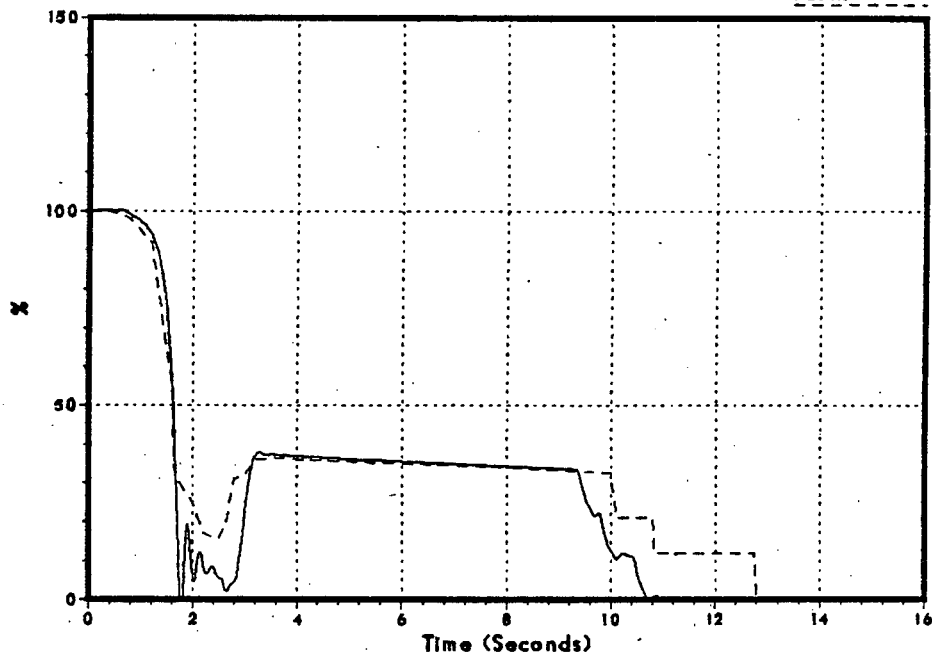
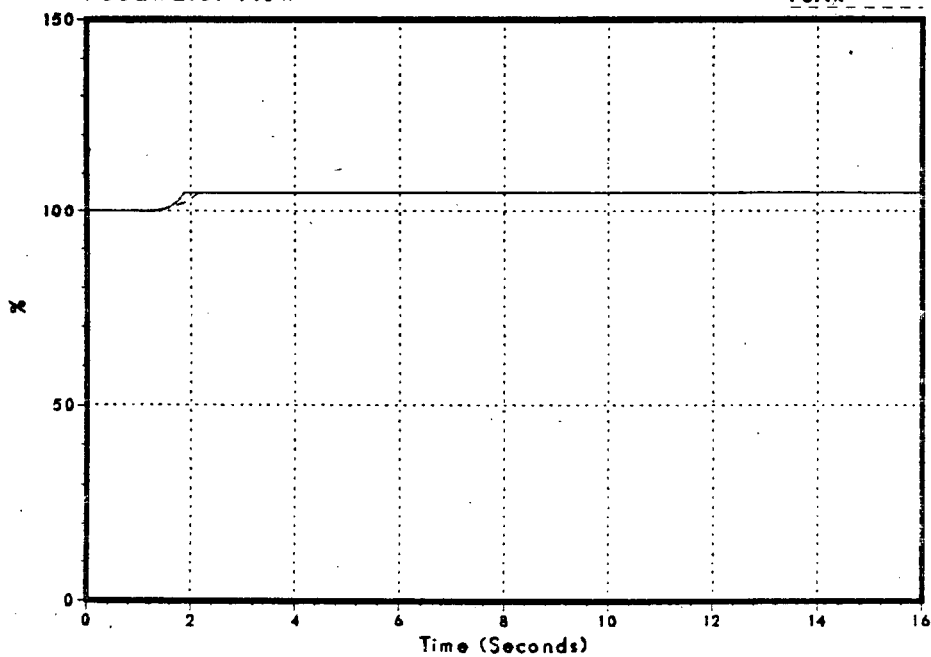


Figure 3.2-27
Feedwater Flow

DNB064/86

FSAR

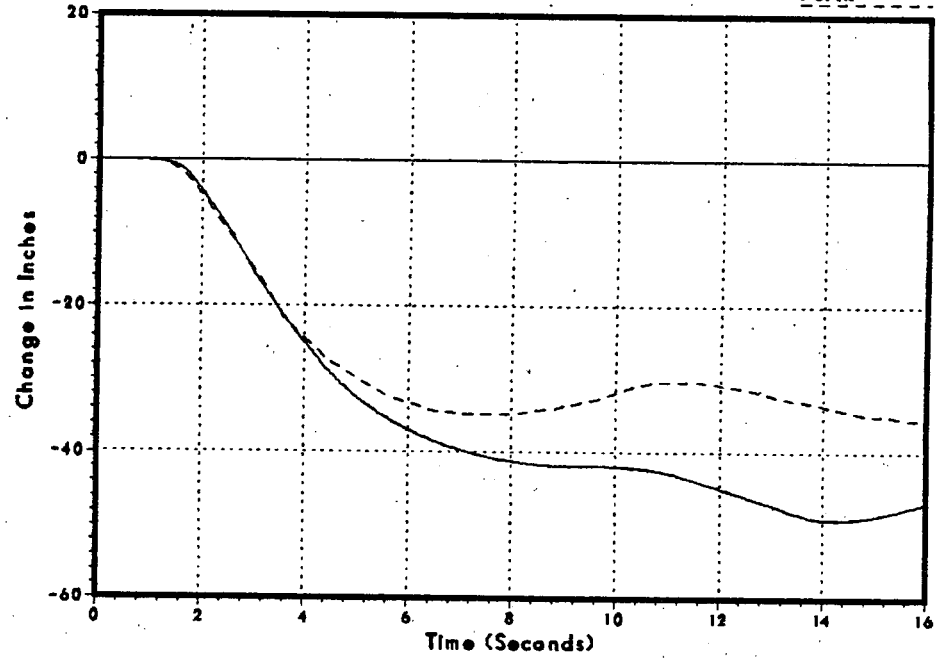


Monticello FSAR Benchmark 100% MSIV Closure

Figure 3.2-28
Sensed Level

DNB064/86

FSAR



NSP

Monticello FSAR Benchmark Feedwater Control Malfunction (Max Demand)

Figure 3.2-29
Sensed Level

DNB065/86

FSAR

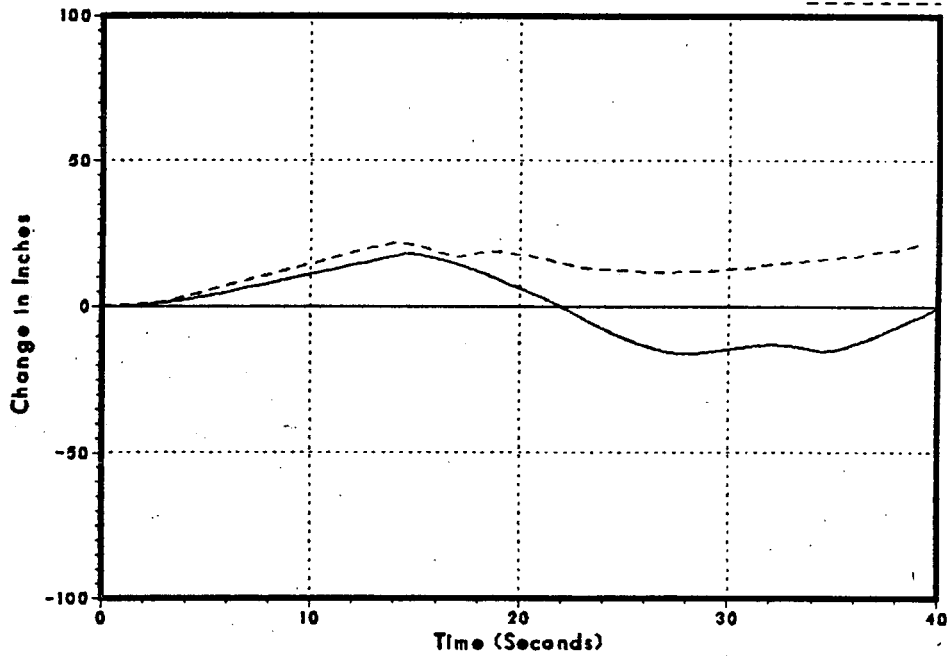
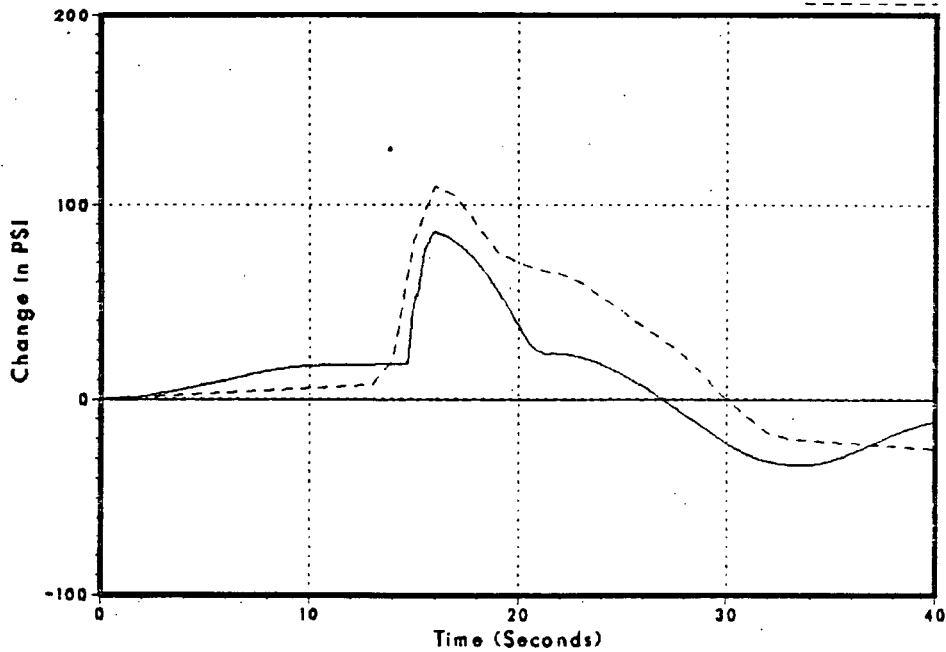


Figure 3.2-30
Steam Dome Pressure

DNB065/86

FSAR



NSP

Monticello FSAR Benchmark Feedwater Control Failure (Max Demand)

Figure 3.2-31
Core Inlet Flow

DNB065/B6

FSAR

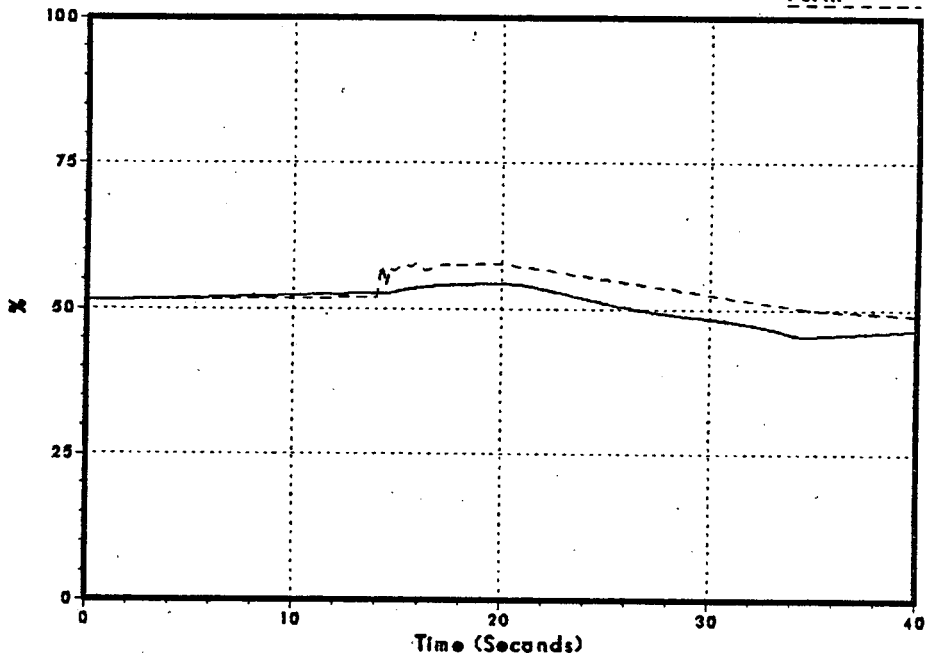
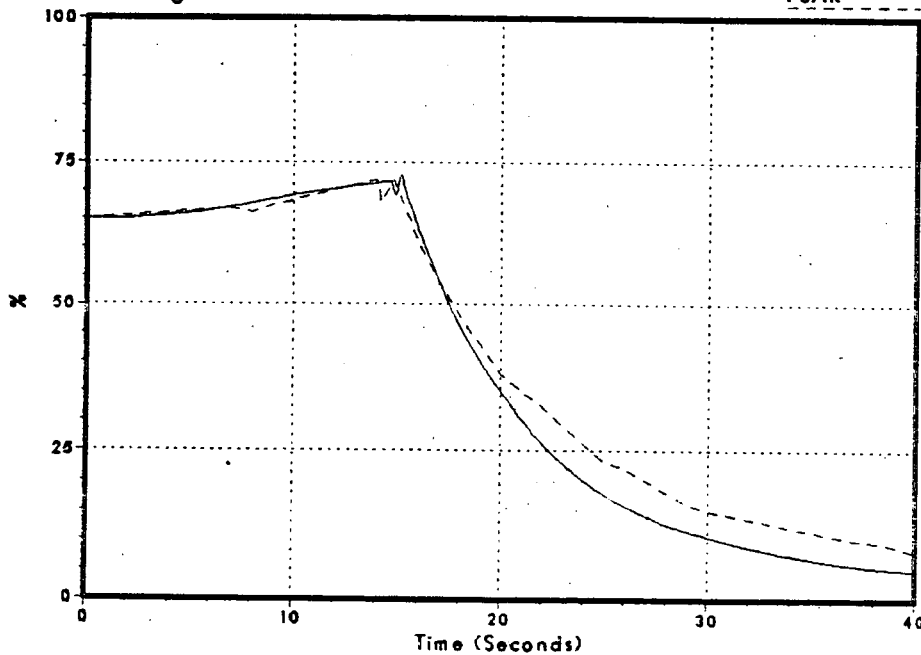


Figure 3.2-32
Average Surface Heat Flux

DNB065/B6

FSAR



NSP

Monticello FSAR Benchmark Feedwater Control Failure (Max Demand)

Figure 3.2-33
Relative Power

DNB065/86

FSAR

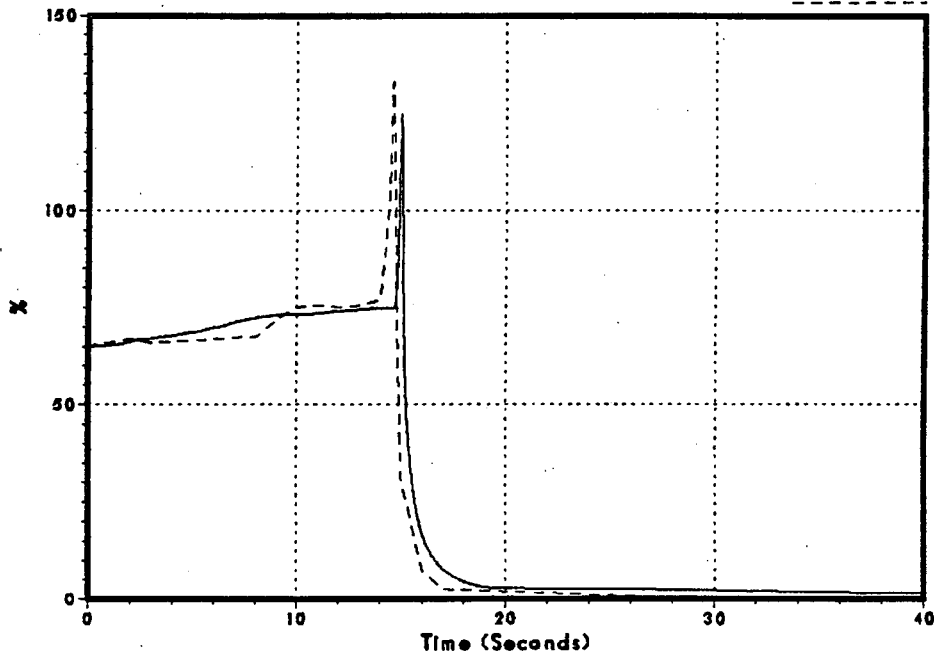
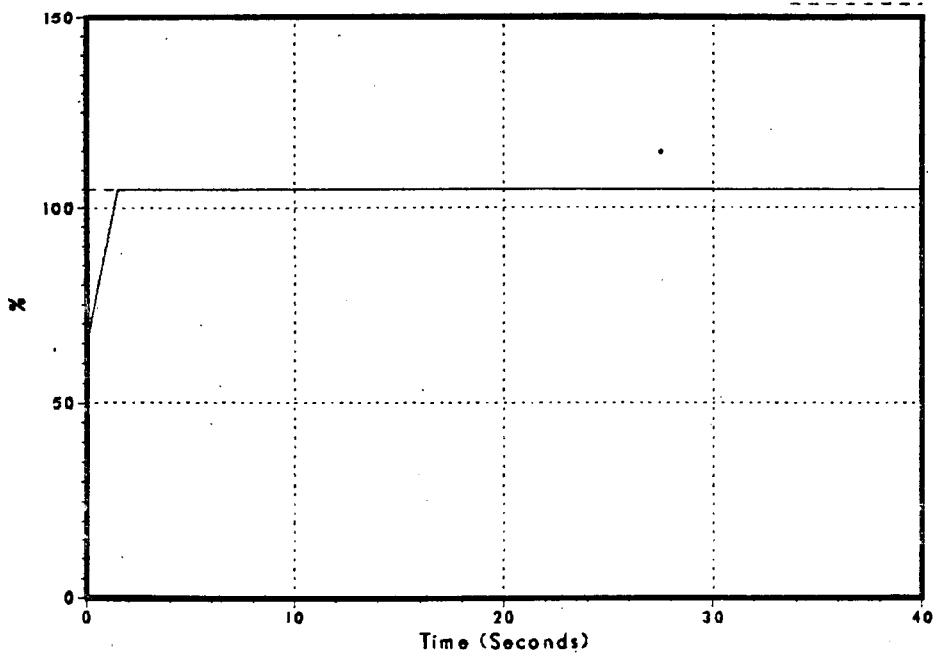


Figure 3.2-34
Feedwater Flow

DNB065/86

FSAR



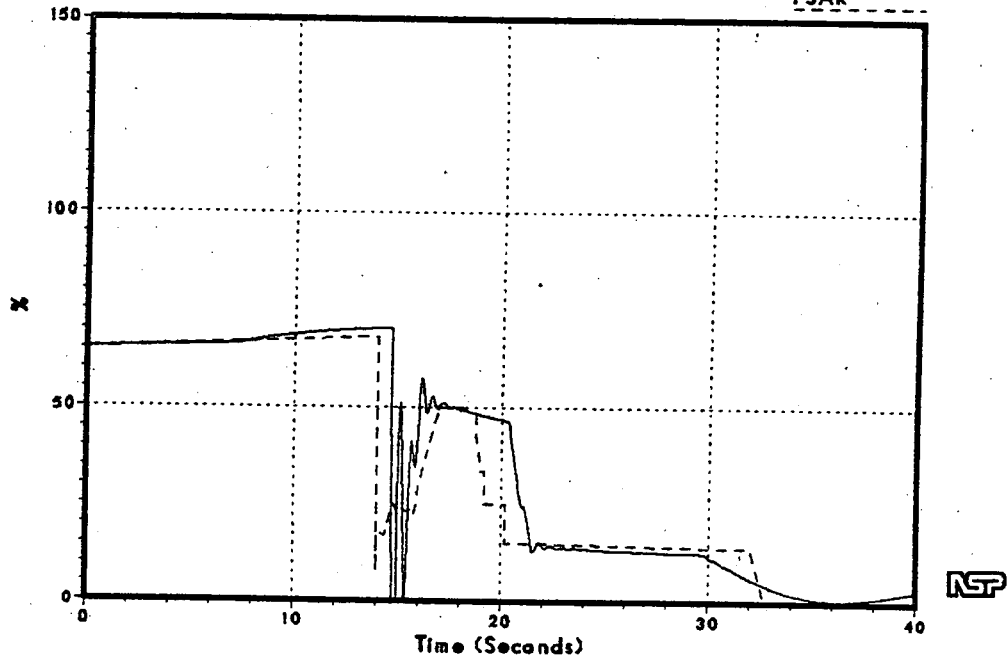
NSP

Monticello FSAR Benchmark Feedwater Control Failure (Max Demand)

Figure 3.2-35
Vessel Steam Flow

DNB065/86

FSAR



Monticello FSAR Benchmark Loss of Feedwater

Figure 3.2-36
Sensed Level

DNB066/86

FSAR

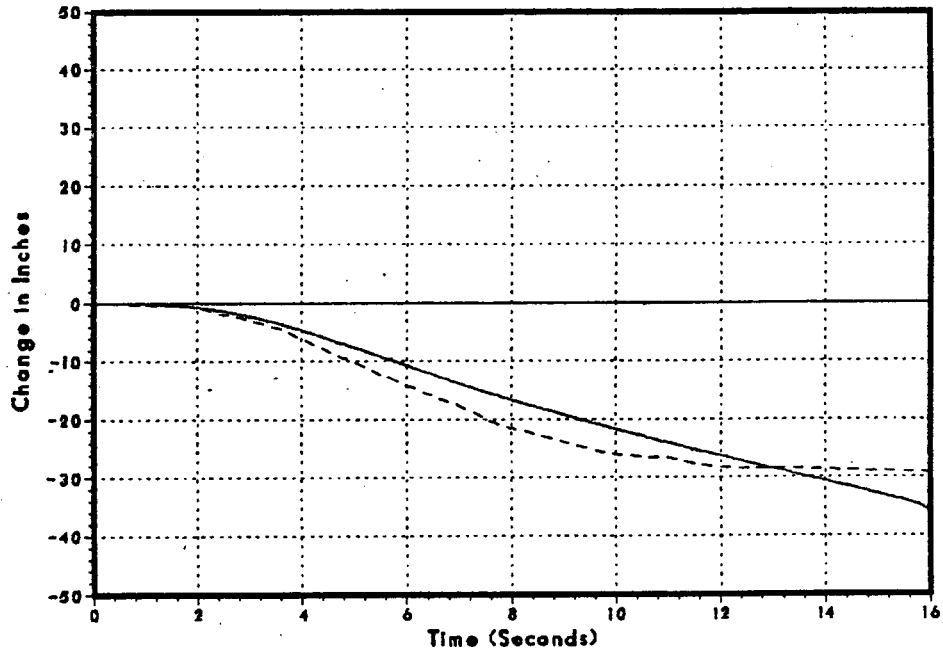
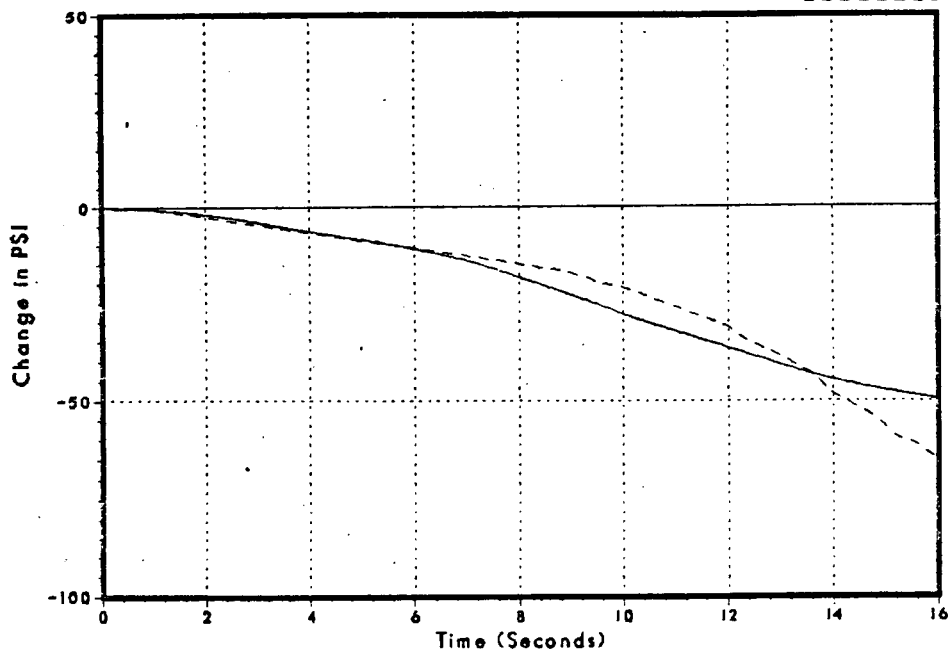


Figure 3.2-37
Steam Dome Pressure

DNB066/86

FSAR



Monticello FSAR Benchmark Loss of Feedwater

Figure 3.2-38
Core Inlet Flow

DNB066/86

FSAR

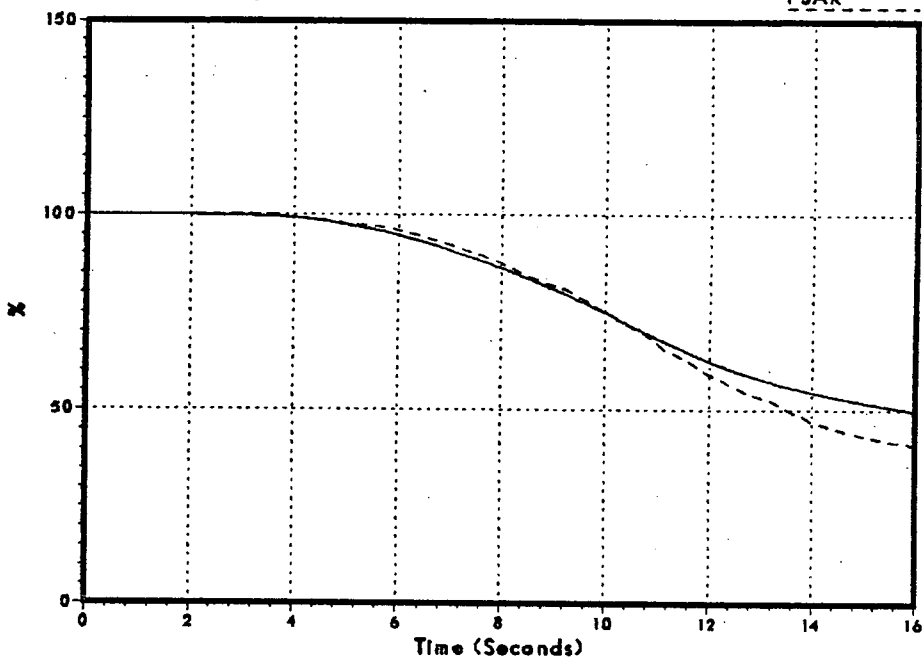
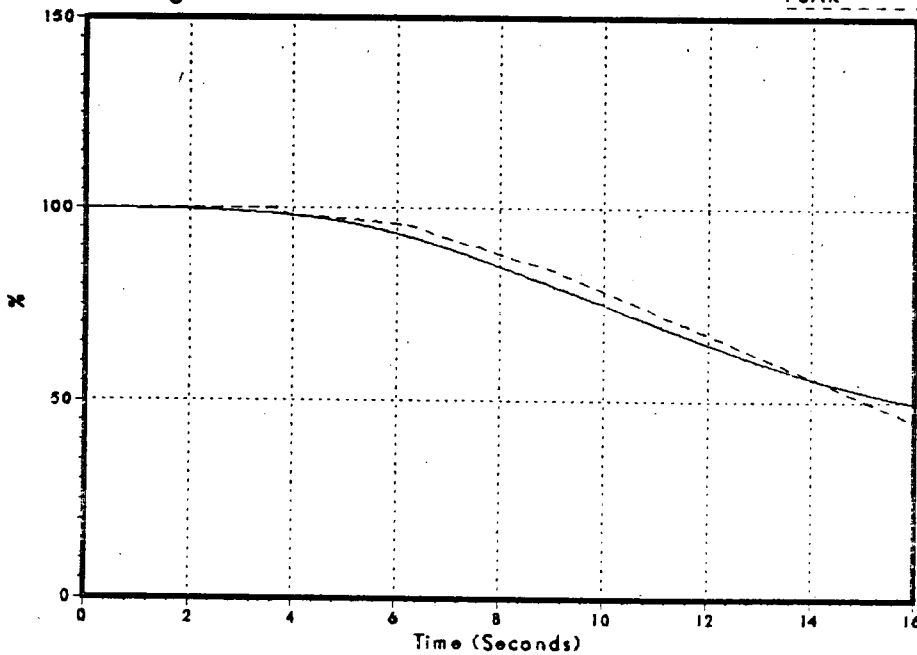


Figure 3.2-39
Average Surface Heat Flux

DNB066/86

FSAR



NSP

Monticello FSAR Benchmark Loss of Feedwater

Figure 3.2-40
Relative Power

DNB066/86

FSAR

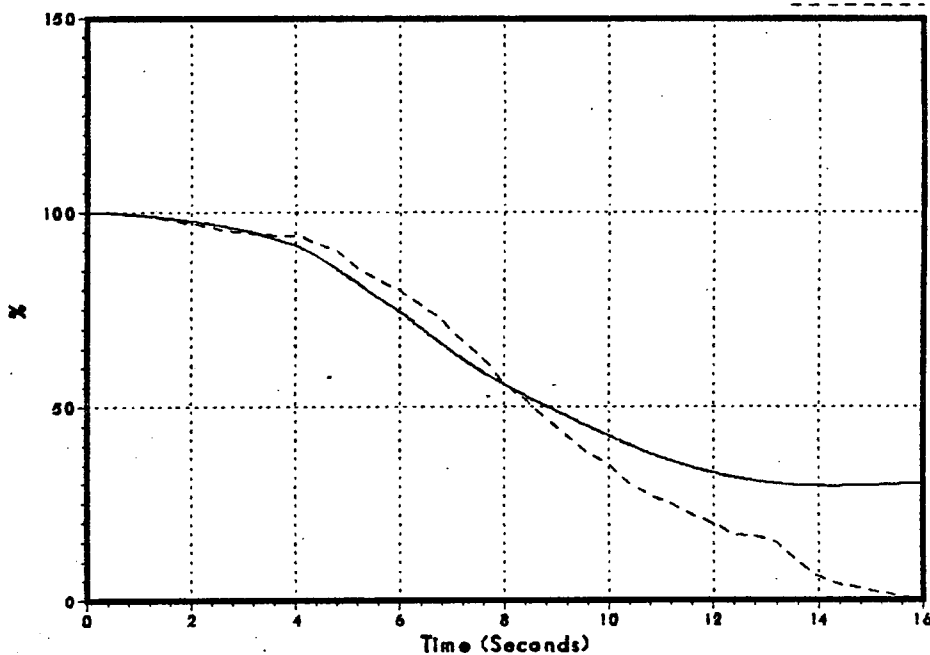
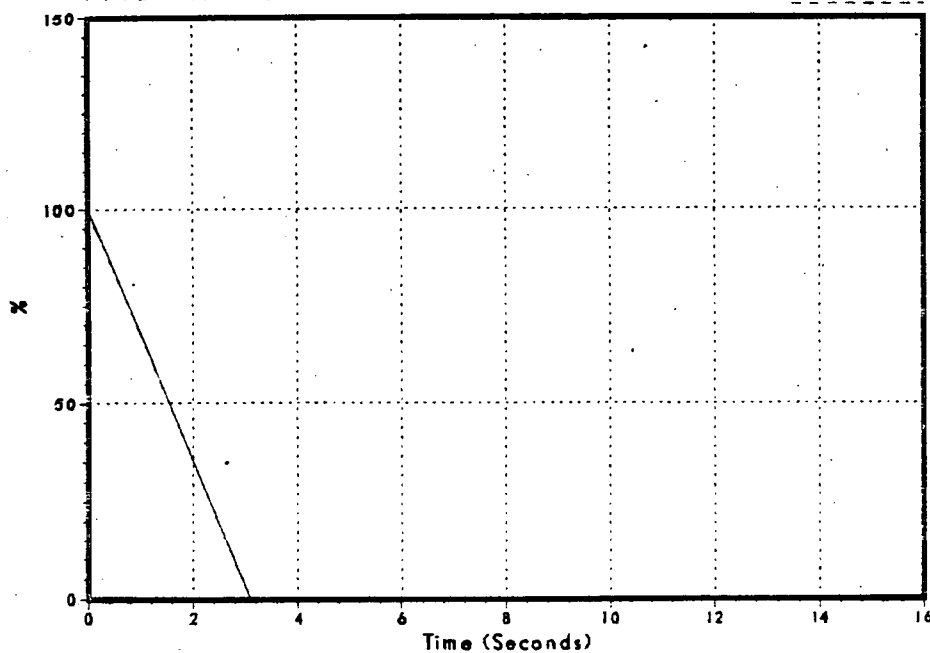


Figure 3.2-41
Feedwater Flow

DNB066/86

FSAR

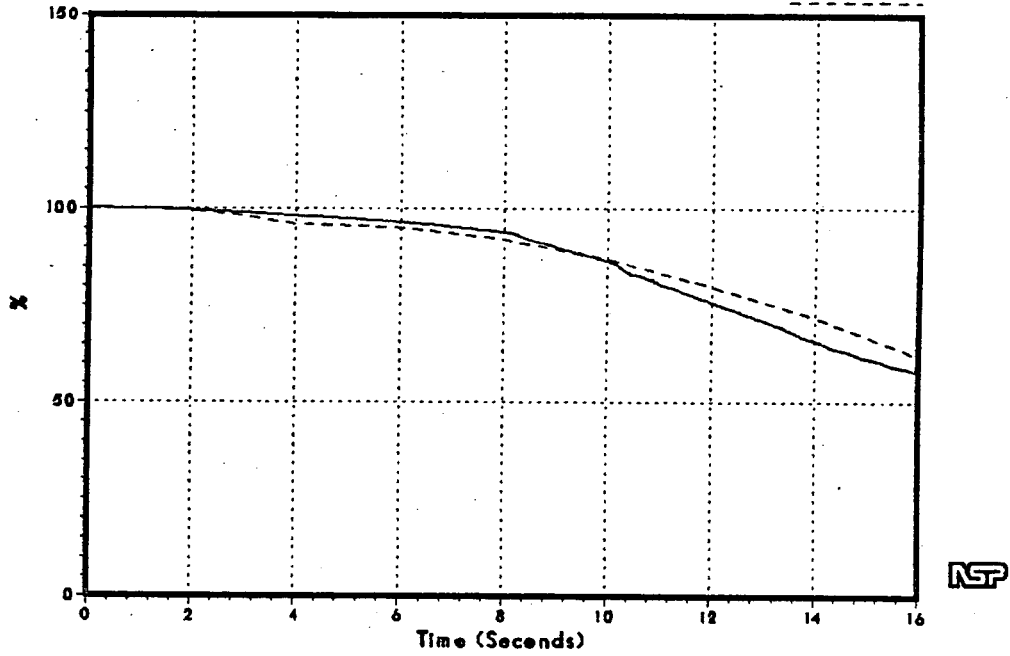


Monticello FSAR Benchmark Loss of Feedwater

Figure 3.2-42
Vessel Steam Flow

DNB066/86

FSAR



Monticello FSAR Benchmark Loss of Feedwater Heating

Figure 3.2-43
Sensed Level

DNB052/86

FSAR

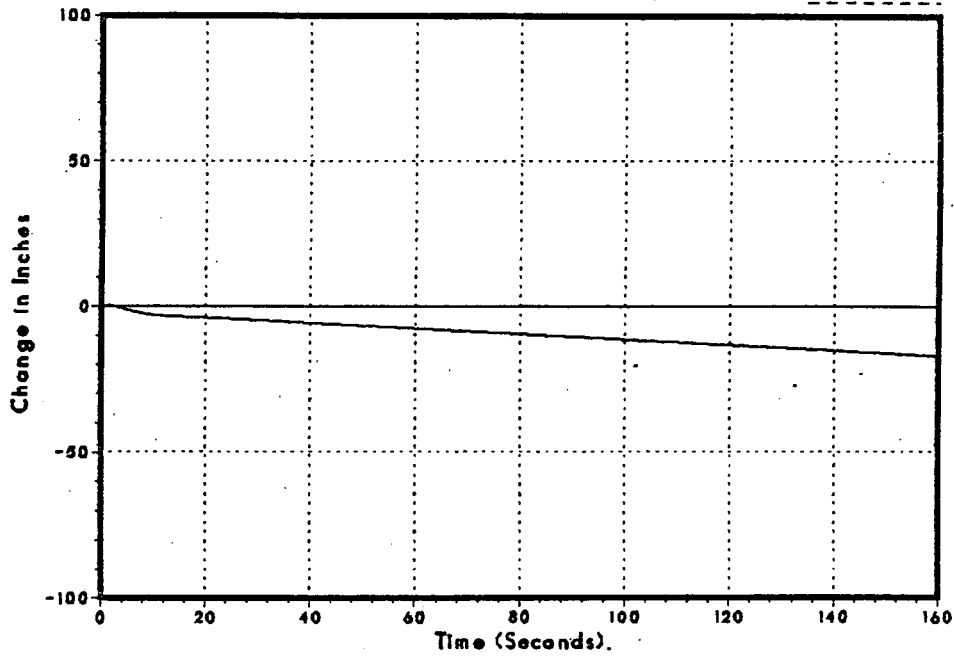
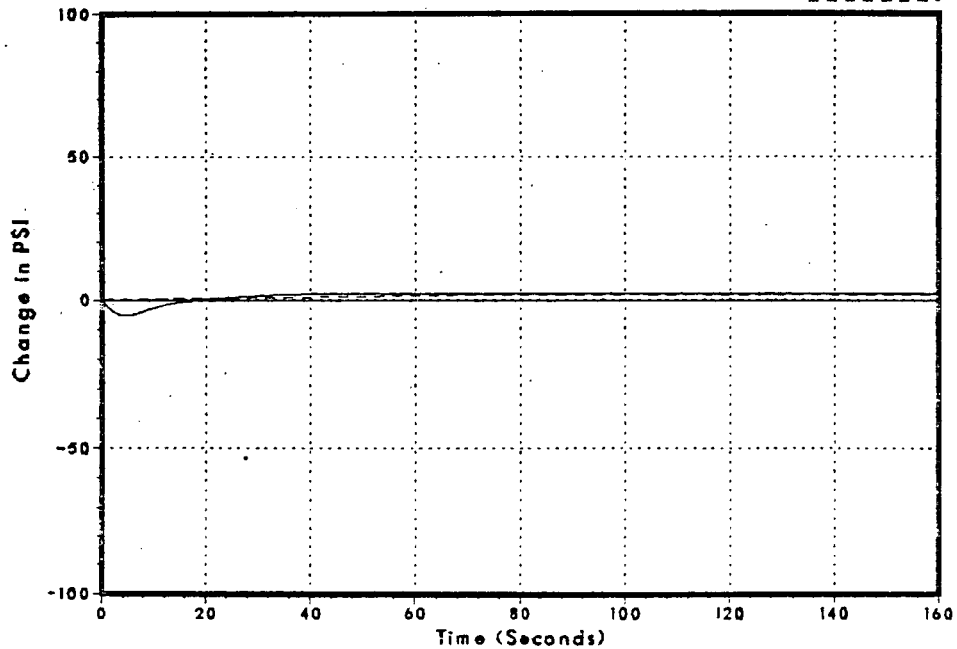


Figure 3.2-44
Steam Dome Pressure

DNB052/86

FSAR



NSP

Monticello FSAR Benchmark Loss of Feedwater Heating

Figure 3.2-45
Core Inlet Flow

DNB052/86

FSAR

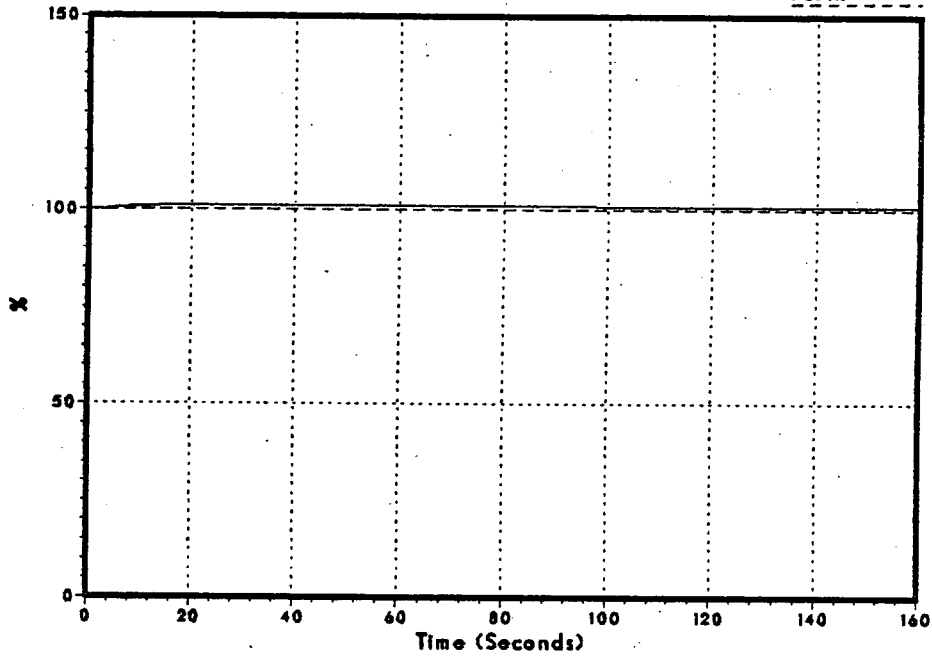
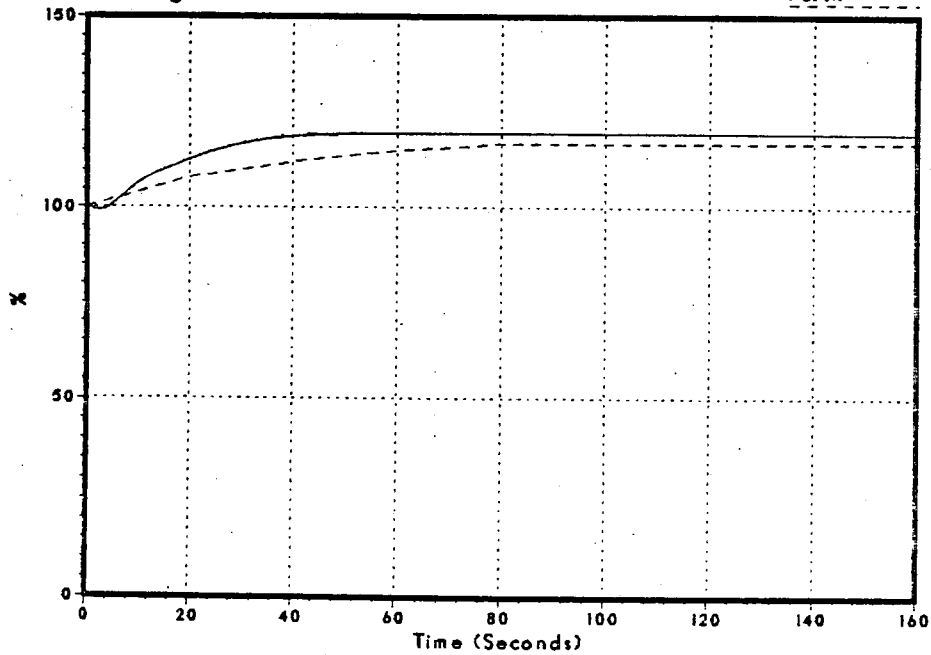


Figure 3.2-46
Average Surface Heat Flux

DNB052/86

FSAR



RSP

Monticello FSAR Benchmark Loss of Feedwater Heating

Figure 3.2-47
Relative Power

DNB052/86

FSAR

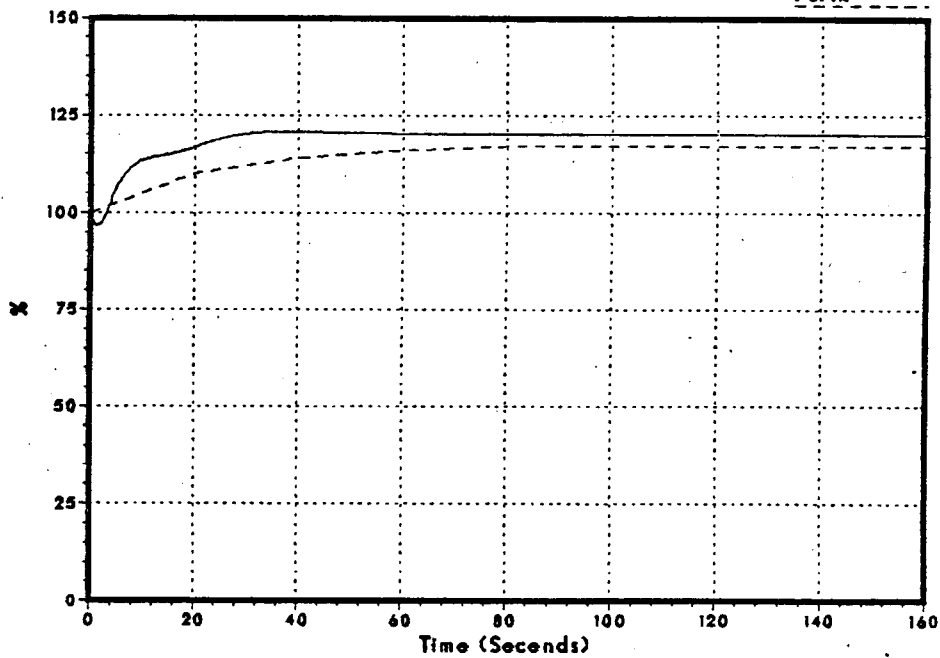
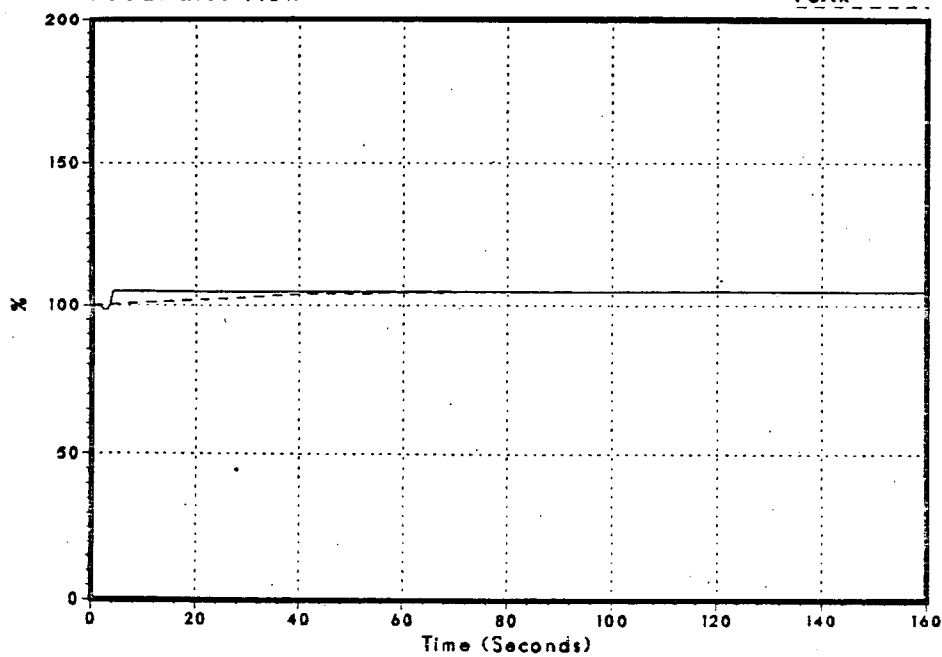


Figure 3.2-48
Feedwater Flow

DNB052/86

FSAR



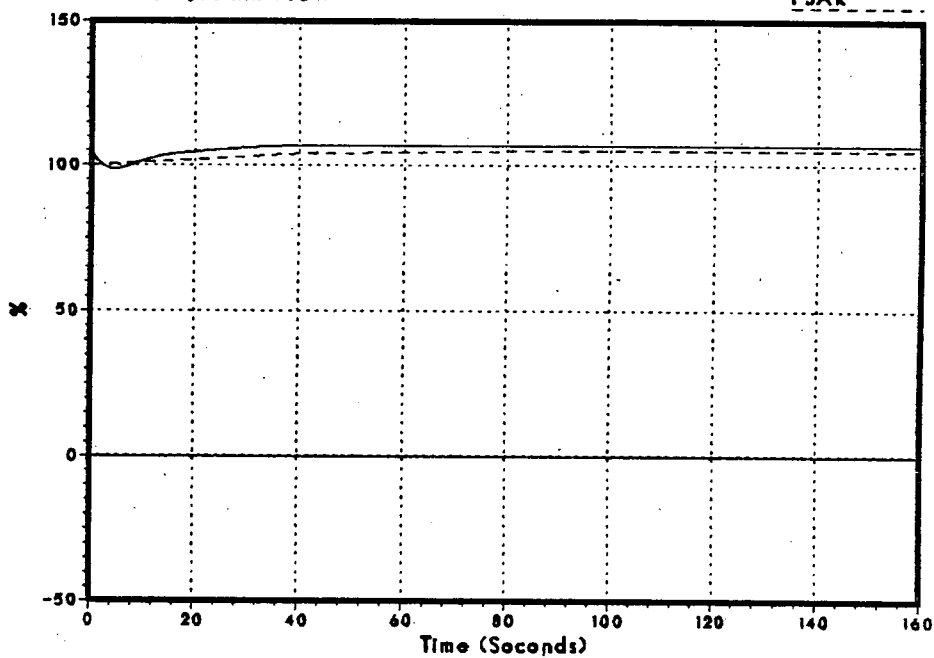
NSP

Monticello FSAR Benchmark Loss of Feedwater Heating

Figure 3.2-49
Vessel Steam Flow

DNB052/86

FSAR



Monticello FSAR Benchmark Pressure Regulator Fails Open

Figure 3.2-50
Steam Dome Pressure

DNB071/86

FSAR

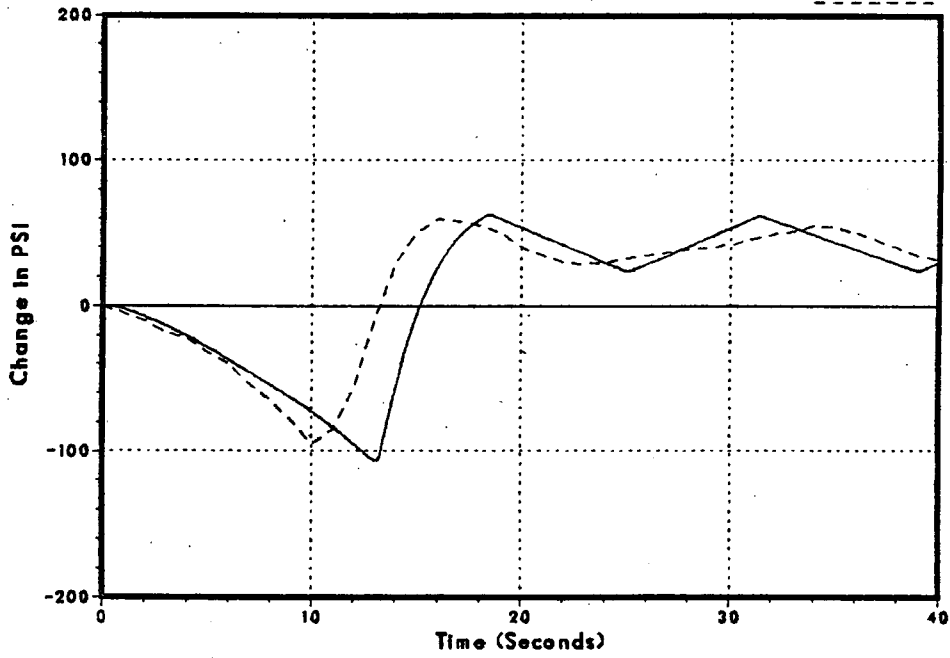
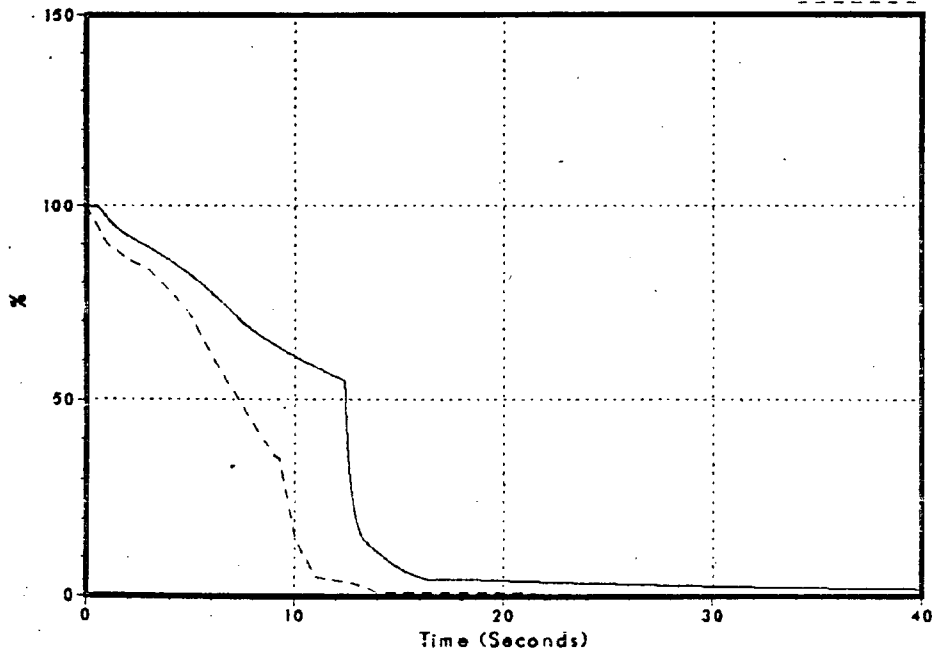


Figure 3.2-51
Relative Power

DNB071/86

FSAR



NSP

Monticello FSAR Benchmark Pressure Regulator Fails Open

Figure 3.2-52
Core Average Heat Flux

DNB071/86

FSAR

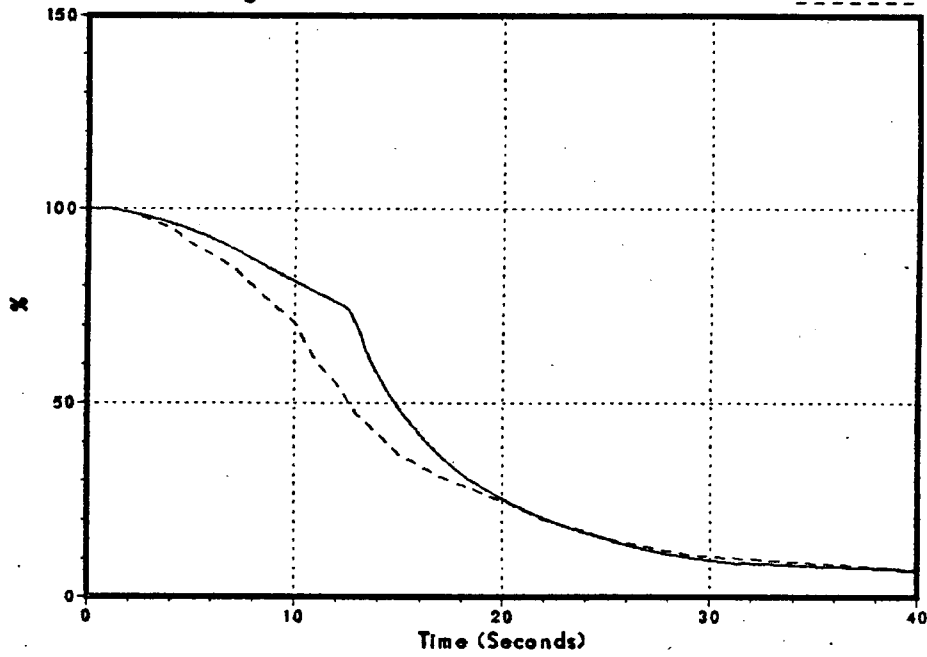
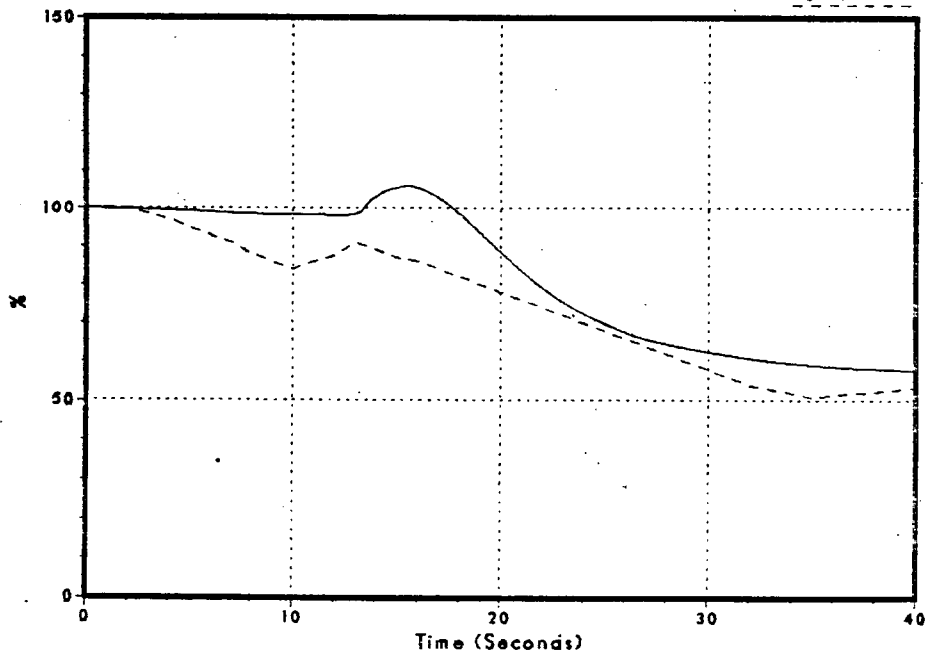


Figure 3.2-53
Core Inlet Flow

DNB071/86

FSAR



ASP

Monticello FSAR Benchmark Pressure Regulator Fails Open

Figure 3.2-54
Main Steam Line Flow

DNB071/86

FSAR

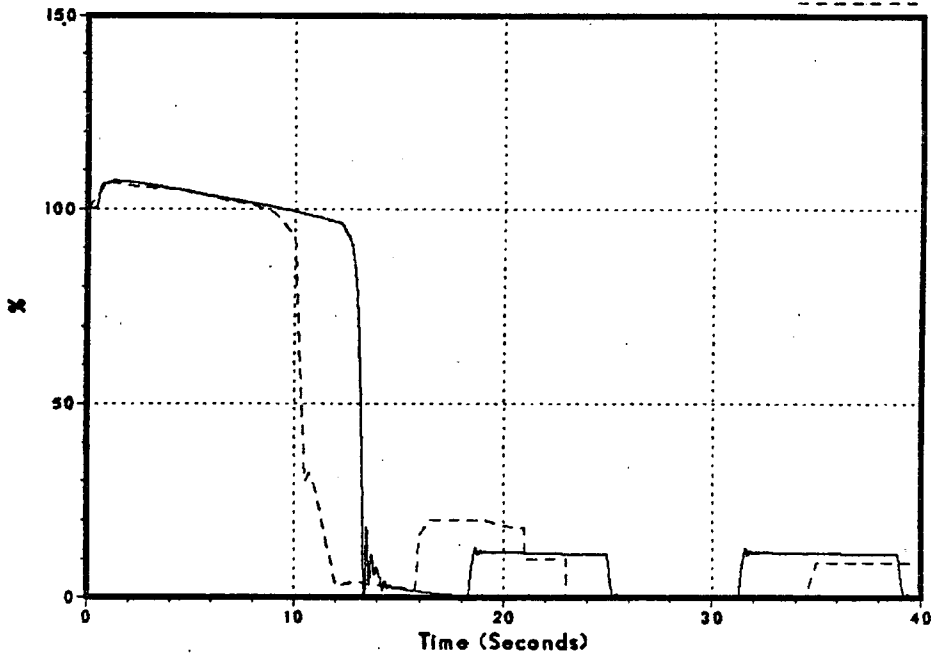
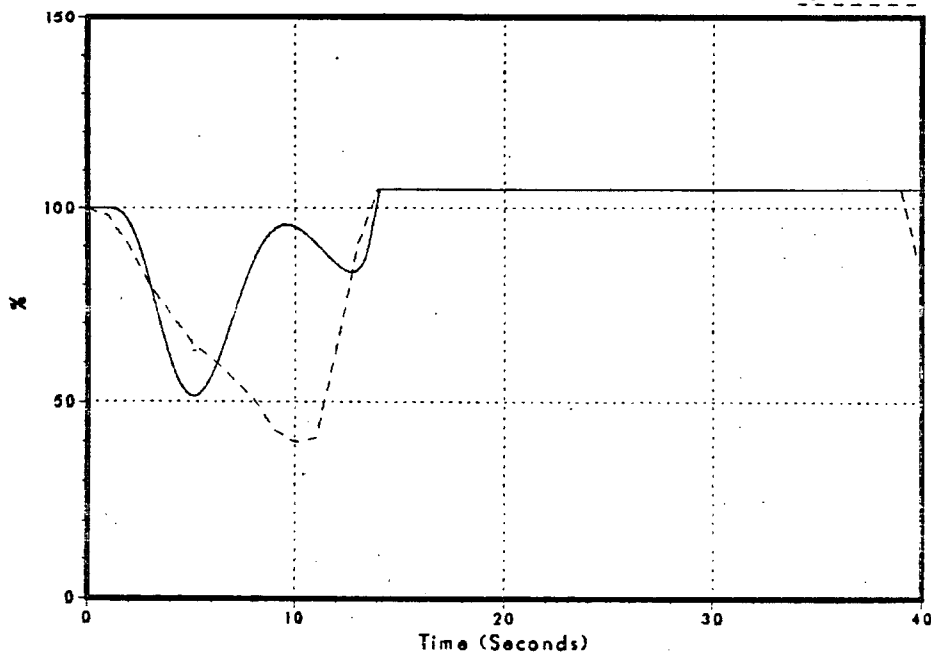


Figure 3.2-55
Feedwater Flow

DNB071/86

FSAR

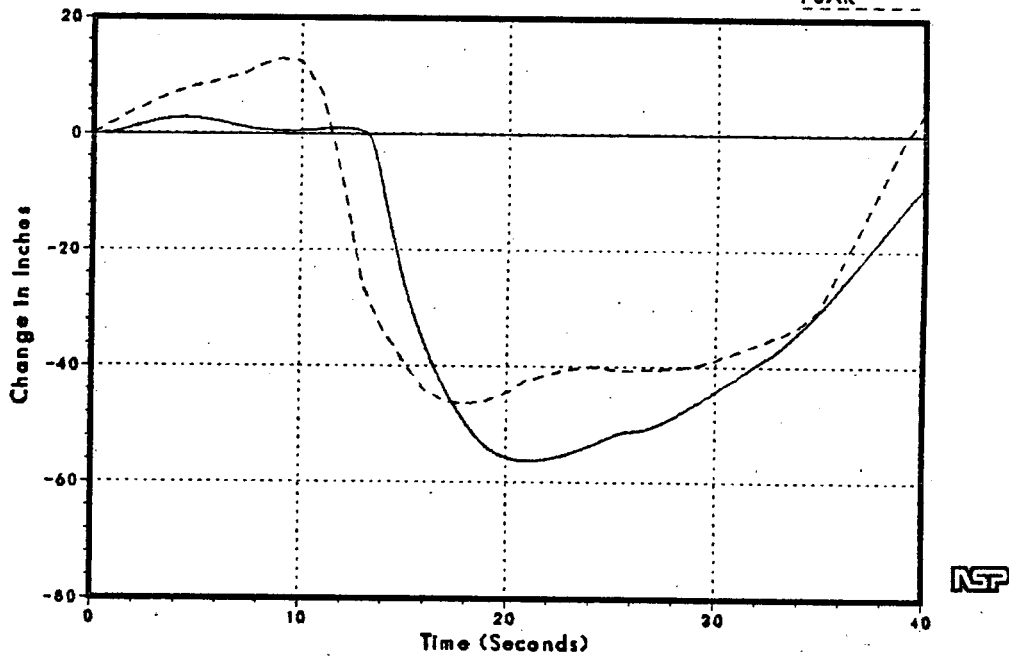


Monticello FSAR Benchmark Pressure Regulator Fails Open

Figure 3.2-56
Sensed Level

DNB071/86

FSAR



Monticello FSAR Benchmark Recirculation Pump Seizure

Figure 3.2-57
Sensed Level

DNB067/86

FSAR

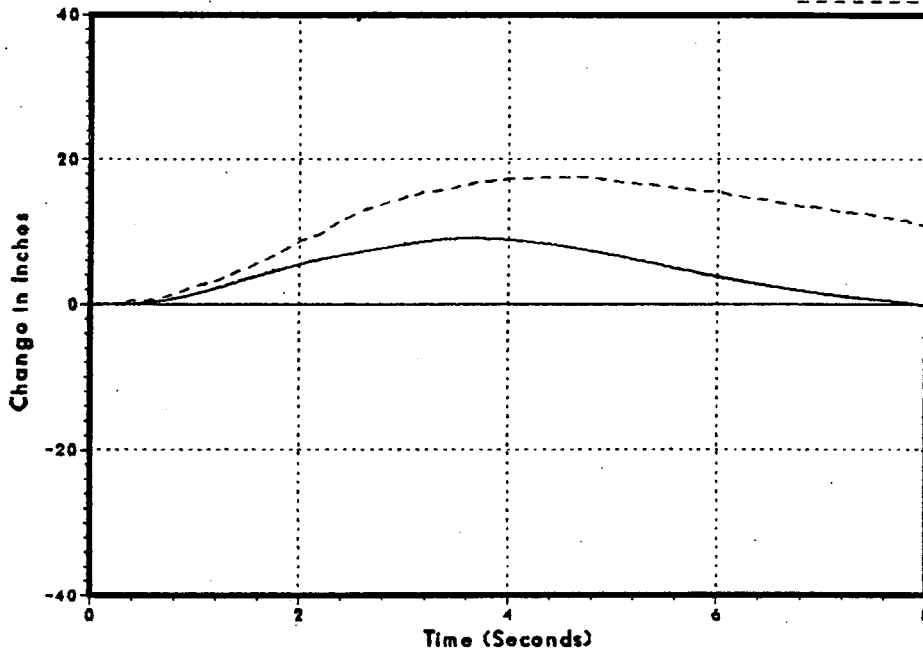
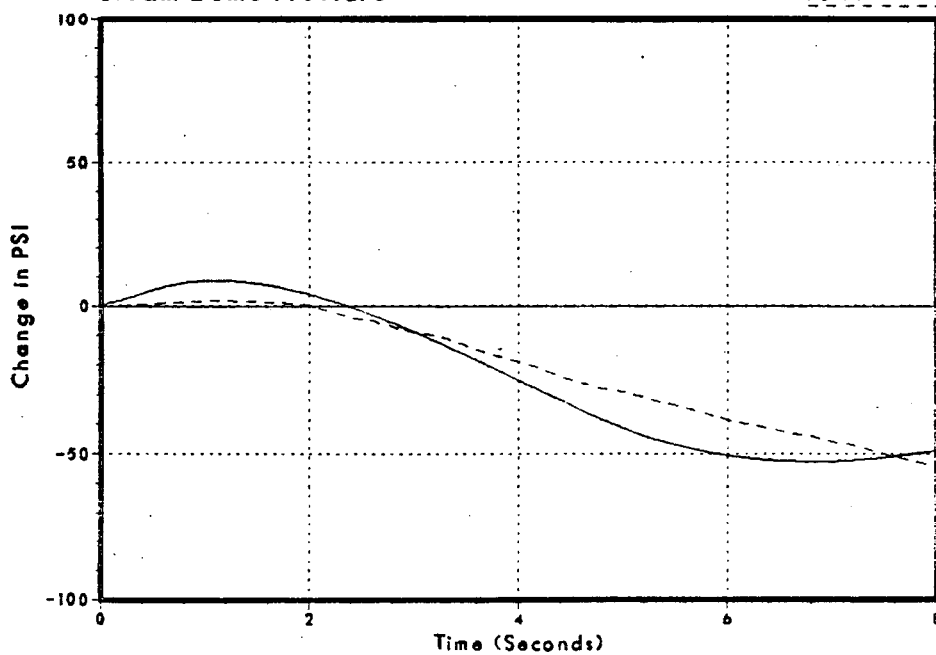


Figure 3.2-58
Steam Dome Pressure

DNB067/86

FSAR



Monticello FSAR Benchmark Recirculation Pump Seizure

Figure 3.2-59
Core Inlet Flow

DN8067/86

FSAR

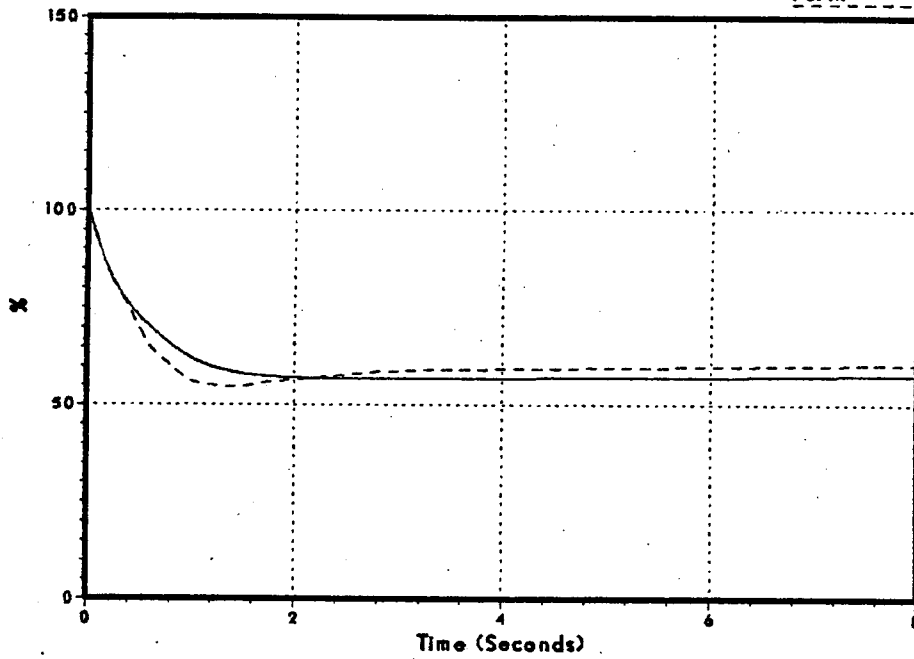
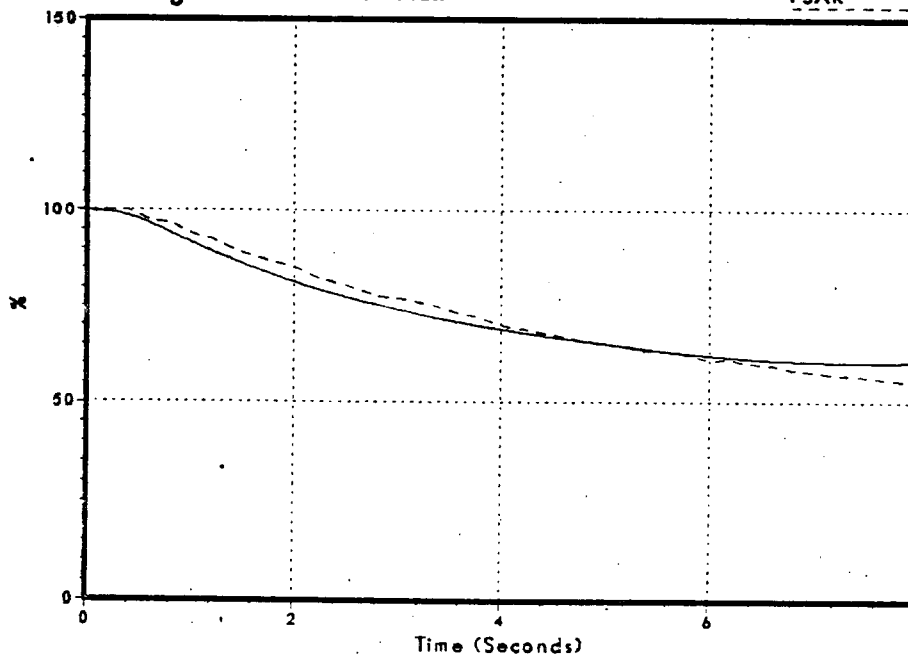


Figure 3.2-60
Average Surface Heat Flux

DN8067/86

FSAR



NSP

Monticello FSAR Benchmark Recirculation Pump Seizure

Figure 3.2-61
Relative Power

DNB067/86

FSAR

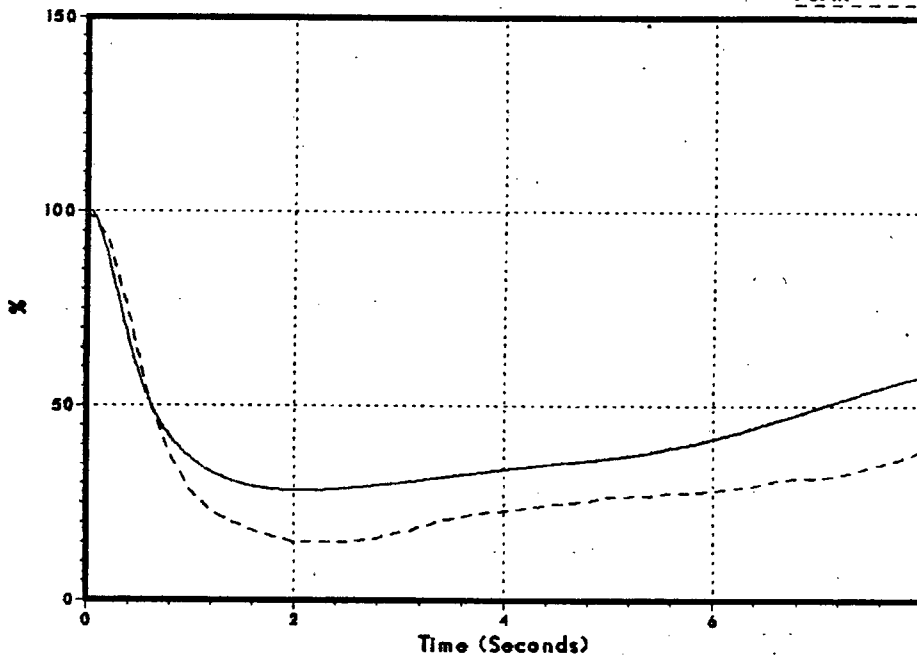
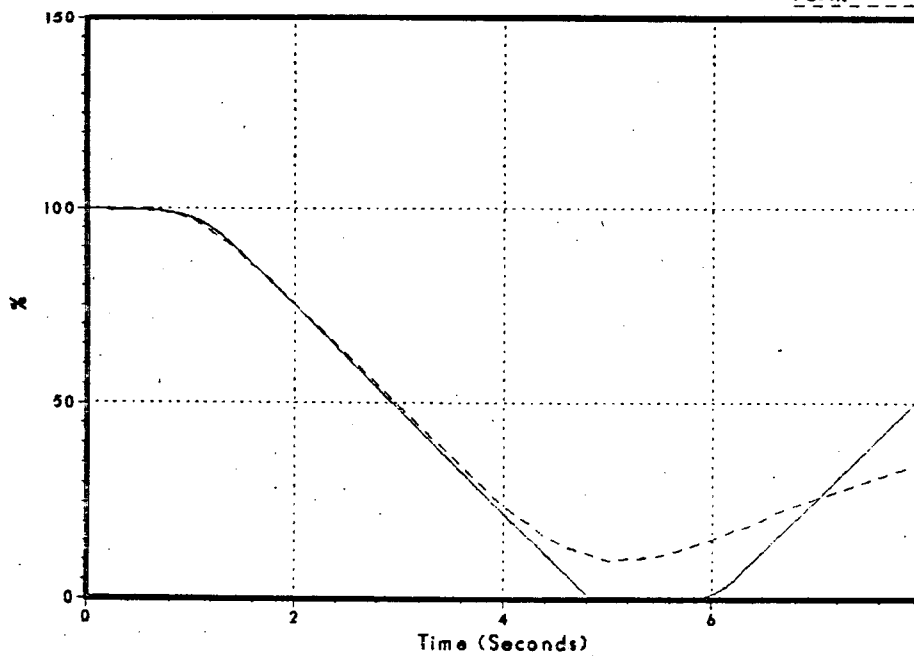


Figure 3.2-62
Feedwater Flow

DNB067/86

FSAR



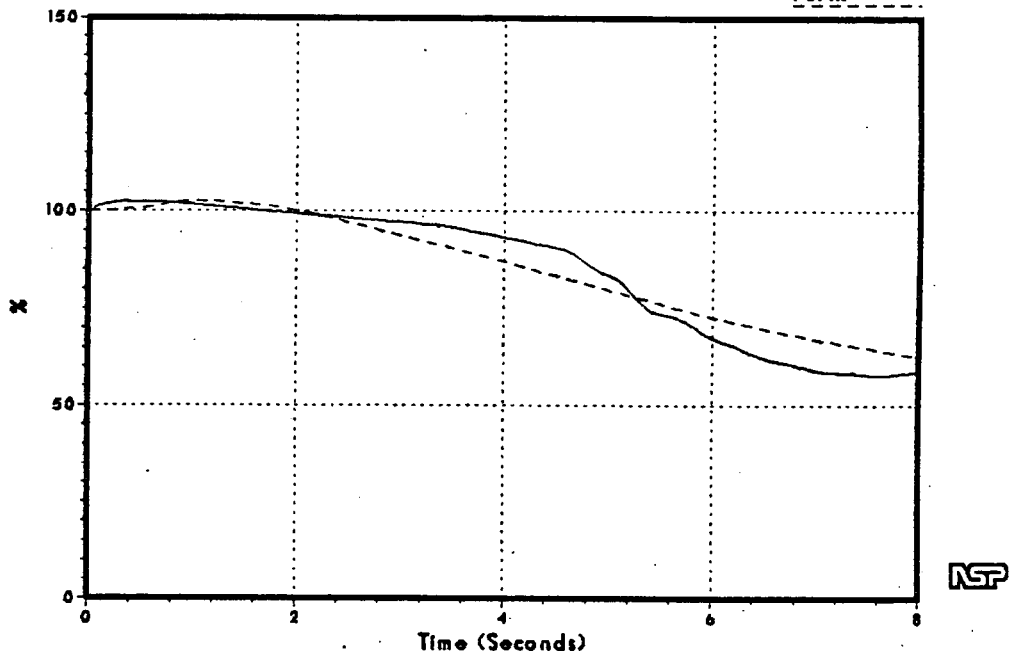
NSP

Monticello FSAR Benchmark Recirculation Pump Seizure

Figure 3.2-63
Vessel Steam Flow

DNB067/86

FSAR



Monticello FSAR Benchmark 2/2 Recirculation Pump Trip

Figure 3.2-64
Sensed Level

DNB073/86

FSAR

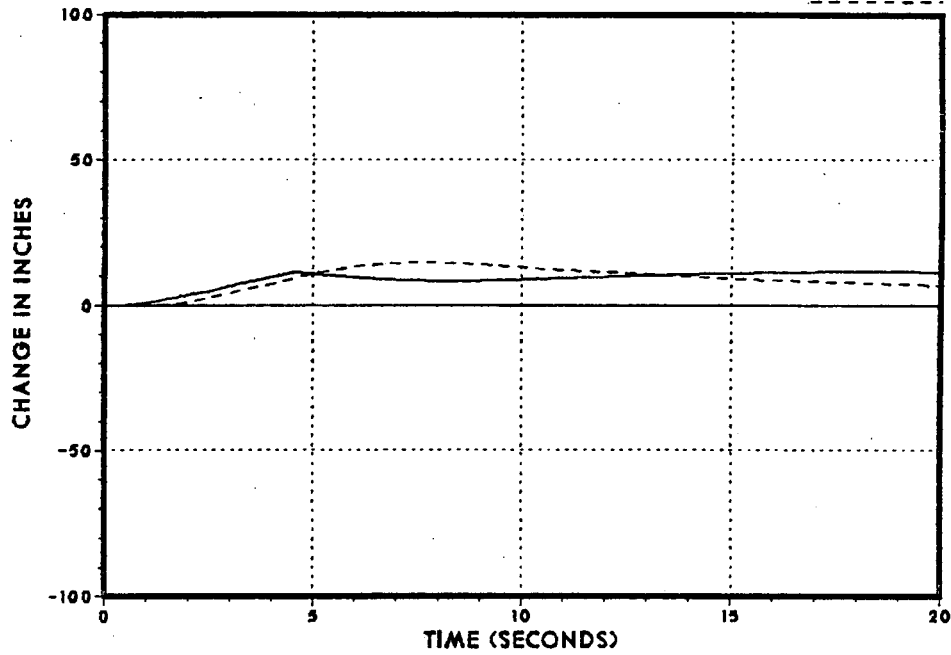
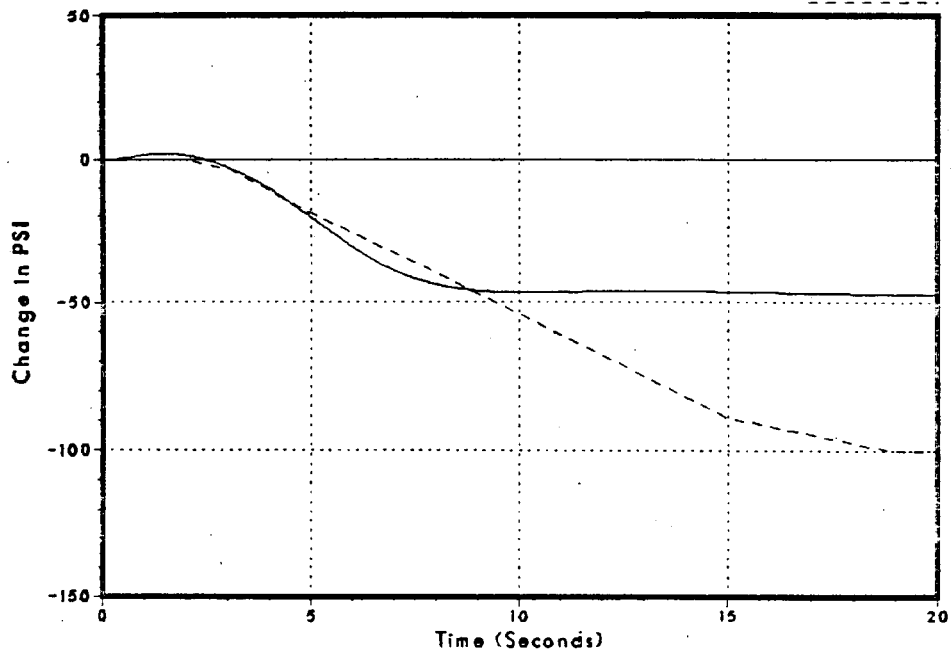


Figure 3.2-65
Steam Dome Pressure

DNB073/86

FSAR



NSP

Monticello FSAR Benchmark 2/2 Recirculation Pump Trip

Figure 3.2-66
Core Inlet Flow

DNB073/86

FSAR

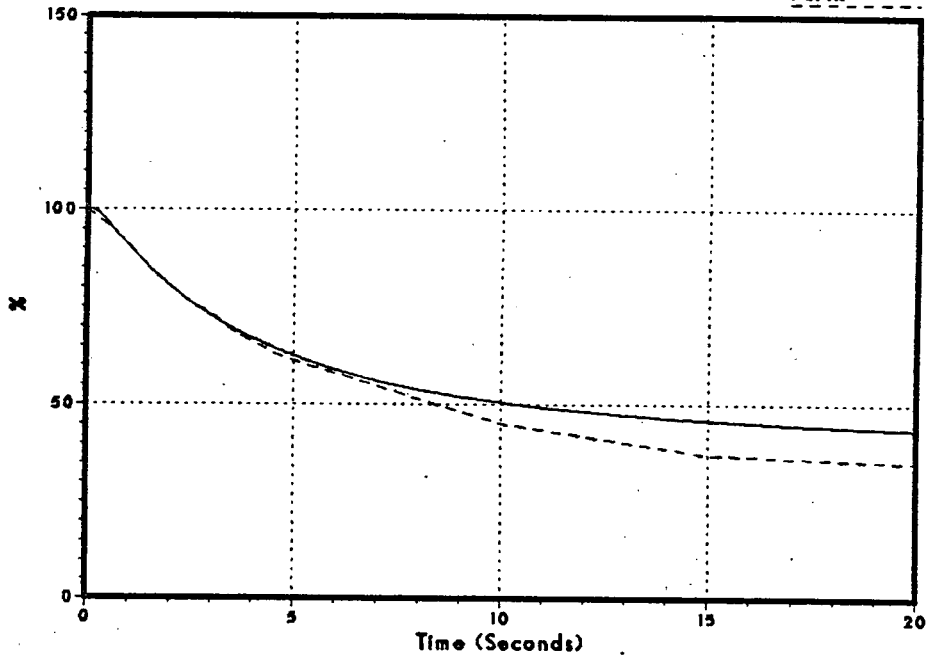
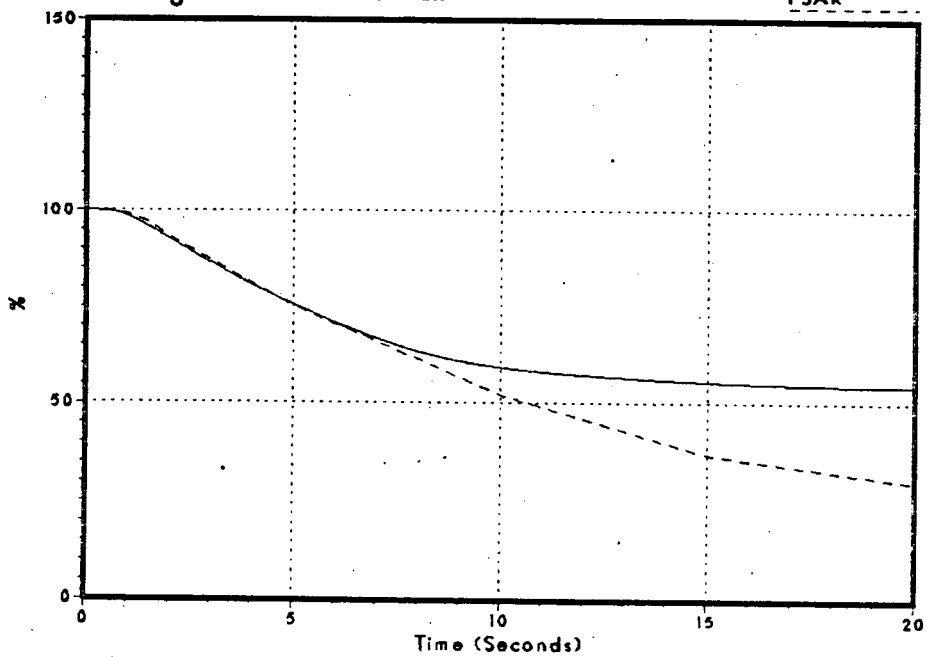


Figure 3.2-67
Average Surface Heat Flux

DNB073/86

FSAR



NSP

Monticello FSAR Benchmark 2/2 Recirculation Pump Trip

Figure 3.2-68
Relative Power

DNB073/86

FSAR

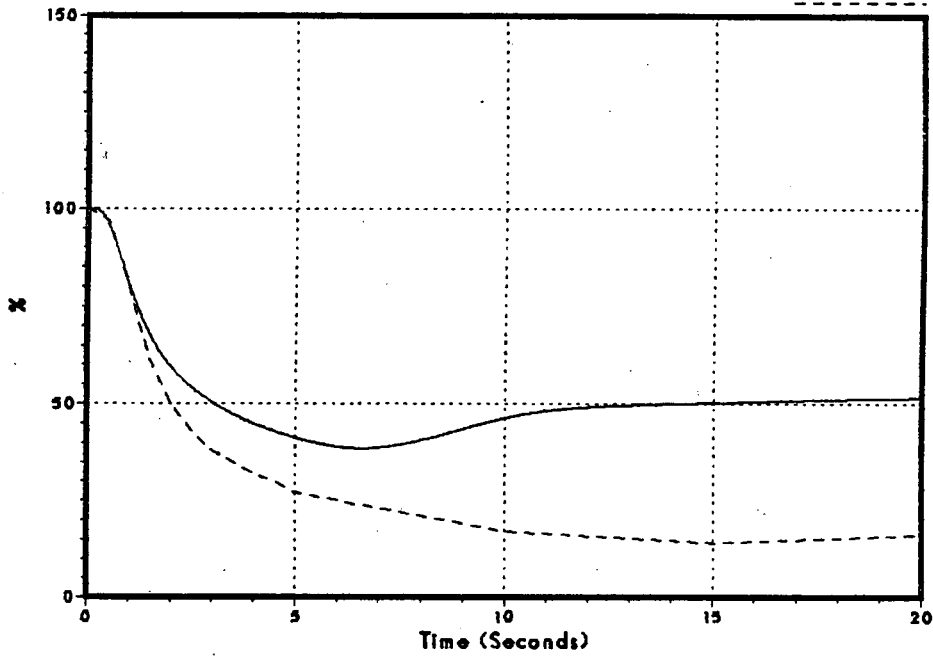
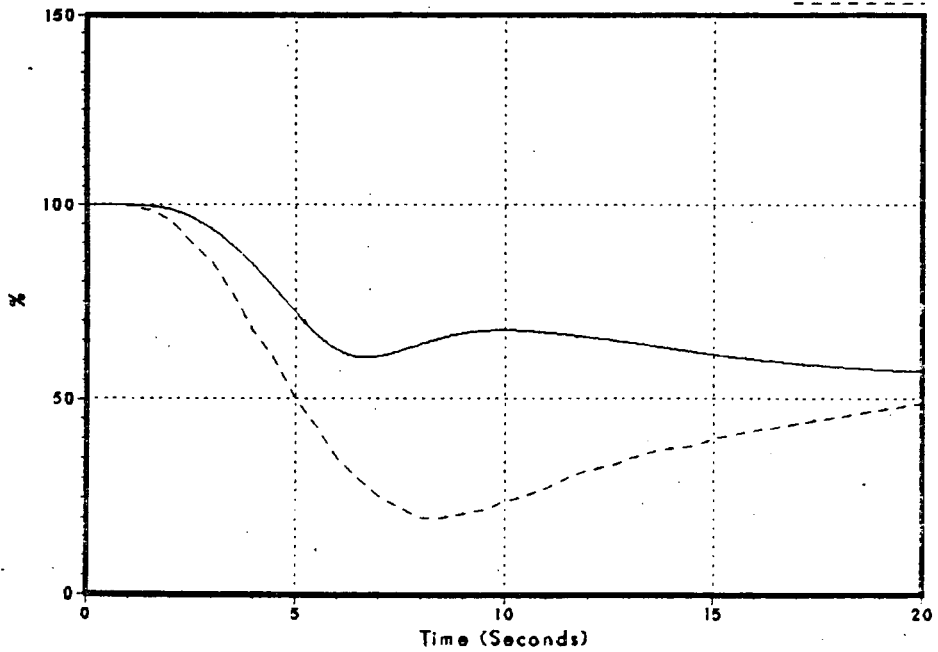


Figure 3.2-69
Feedwater Flow

DNB073/86

FSAR



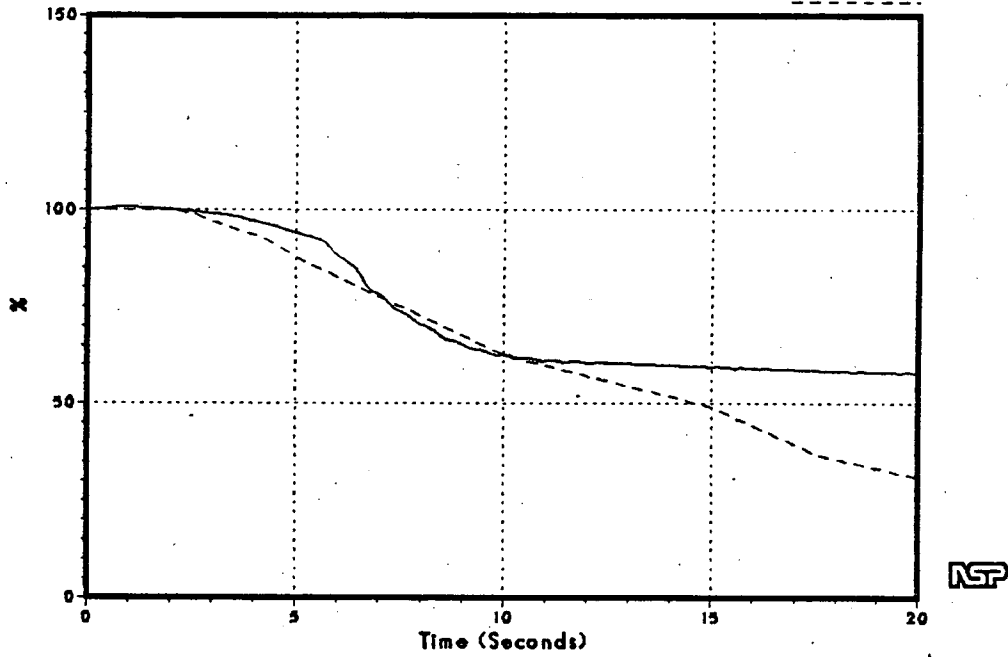
NSP

Monticello FSAR Benchmark 2/2 Recirculation Pump Trip

Figure 3.2-70
Vessel Steam Flow

DNB073/86

FSAR



NSP

Monticello FSAR Benchmark Recirculation Controller Fails (Increase)

Figure 3.2-71
Sensed Level

DNB072/86

FSAR

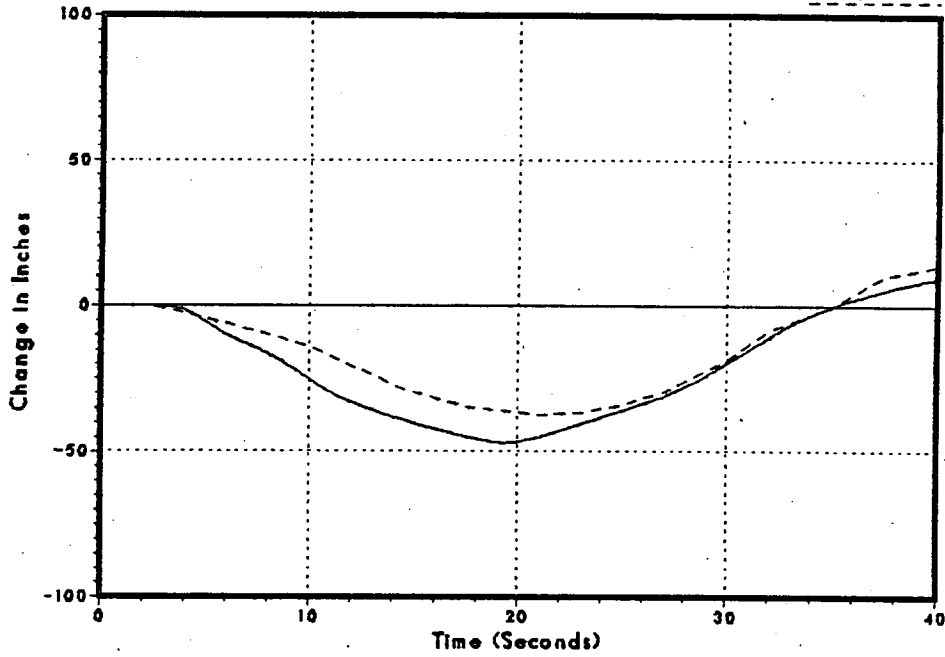
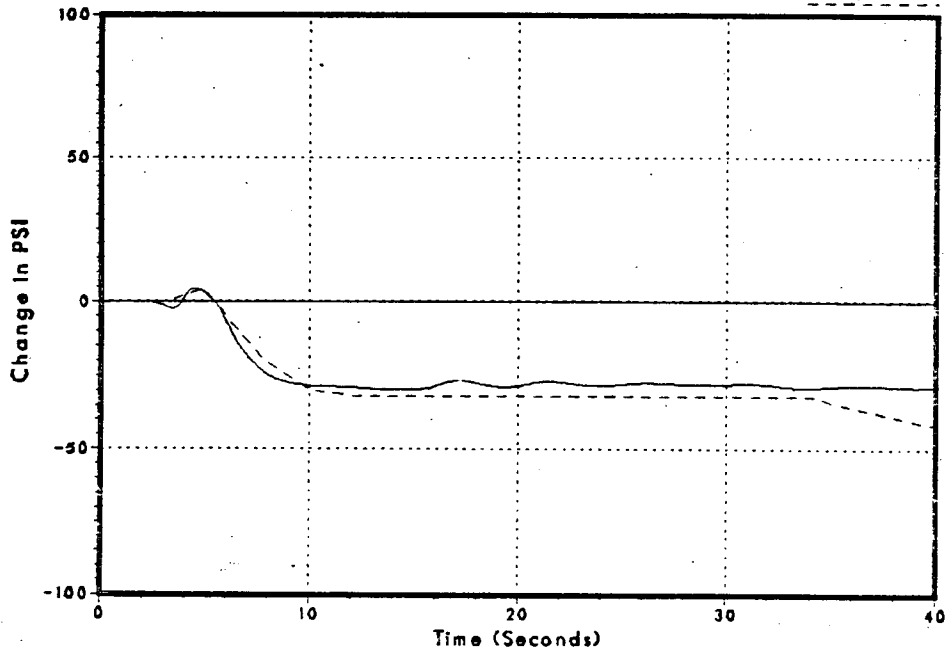


Figure 3.2-72
Steam Dome Pressure

DNB072/86

FSAR



NSP

Monticello FSAR Benchmark Recirculation Controller Fails (Increase)

Figure 3.2-73
Core Inlet Flow

DNB072/86

FSAR

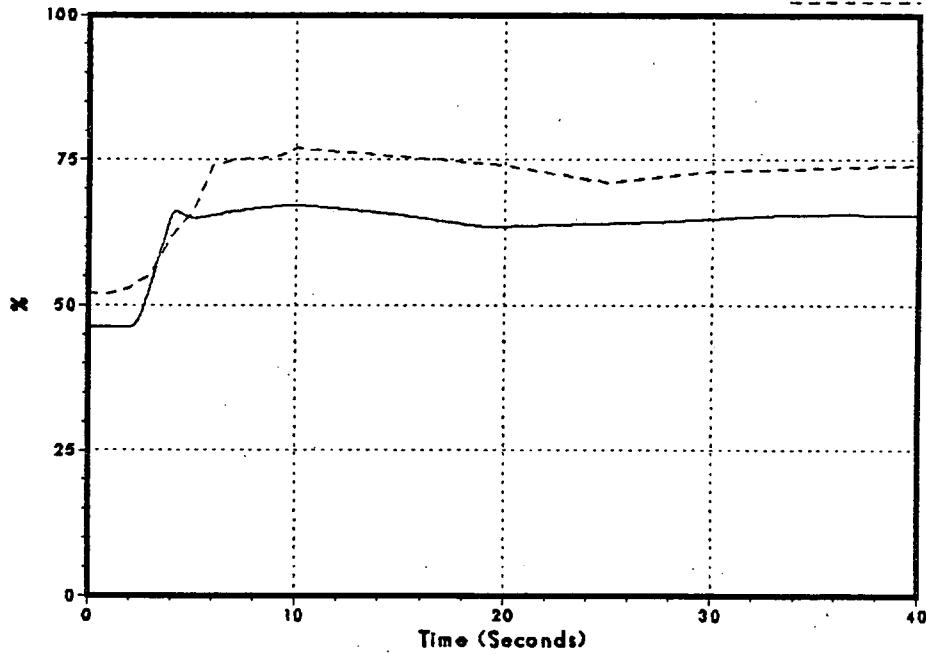
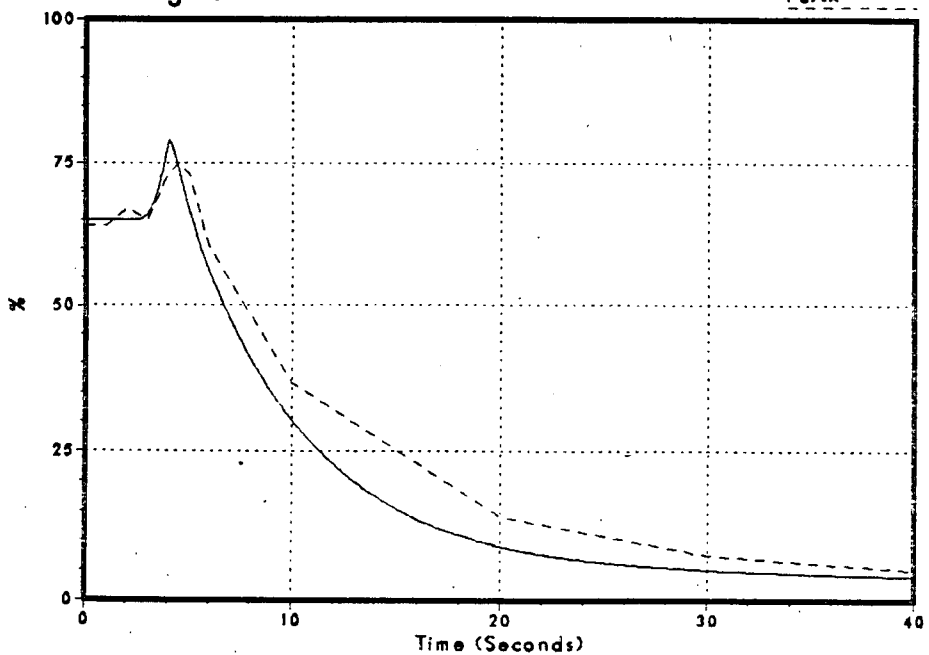


Figure 3.2-74
Average Surface Heat Flux

DNB072/86

FSAR



Monticello FSAR Benchmark Recirculation Controller Fails (Increase)

Figure 3.2-75
Relative Power

DNB072/86

FSAR

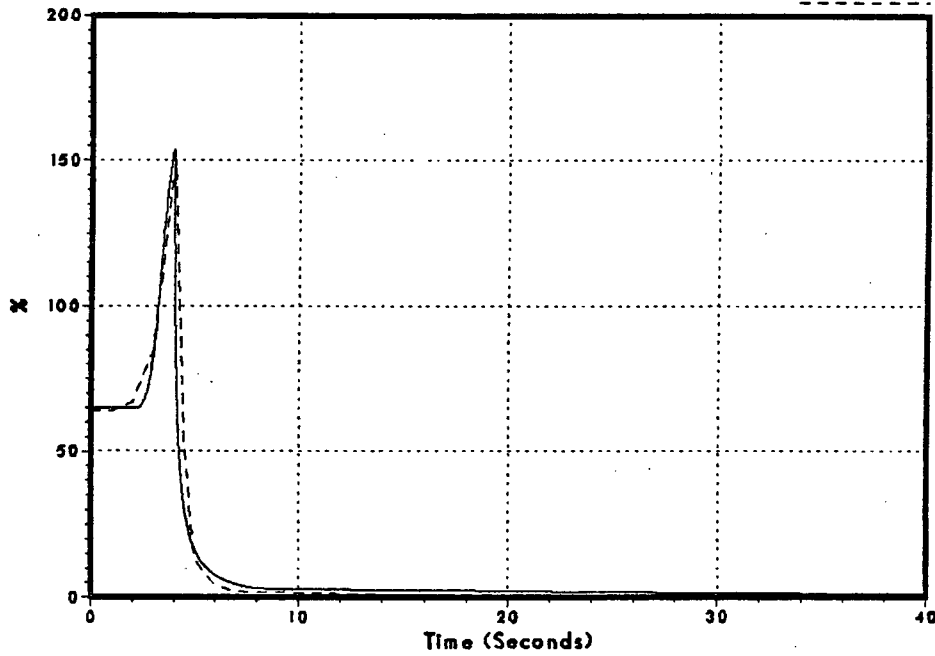
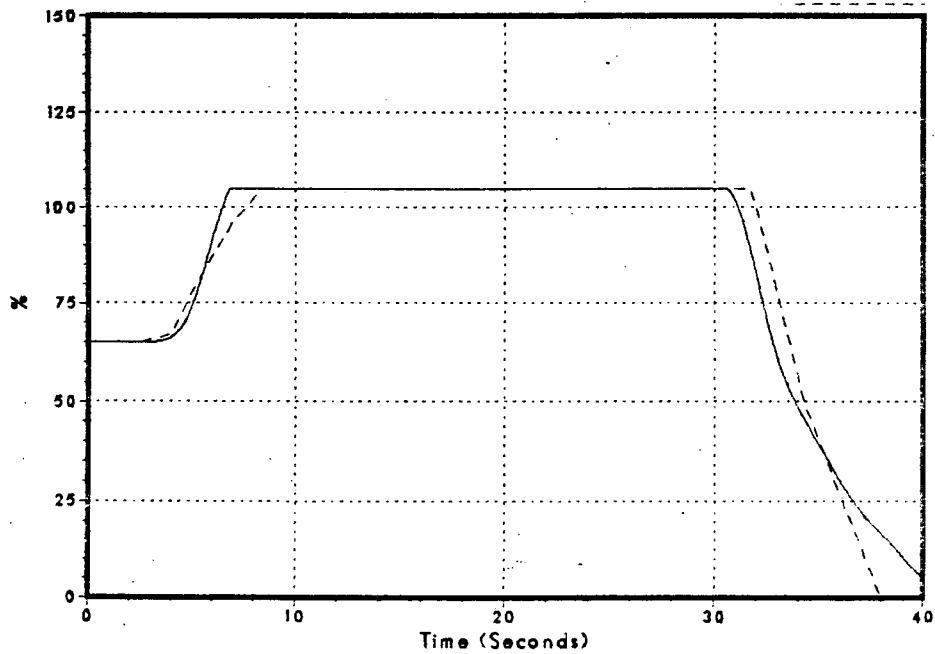


Figure 3.2-76
Feedwater Flow

DNB072/86

FSAR

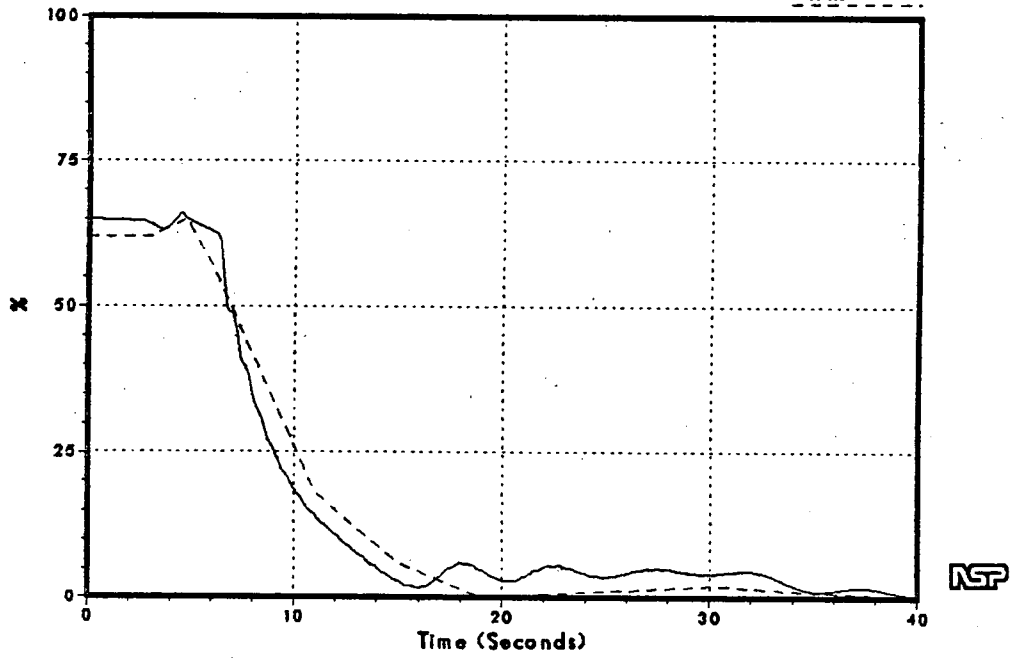


Monticello FSAR Benchmark Recirculation Controller Fails (Increase)

Figure 3.2-77
Vessel Steam Flow

DNB072/86

FSAR



Monticello FSAR Benchmark Recirculation Controller Fails (Decrease)

Figure 3.2-78
Sensed Level

No FSAR Data Available

DN8074/86

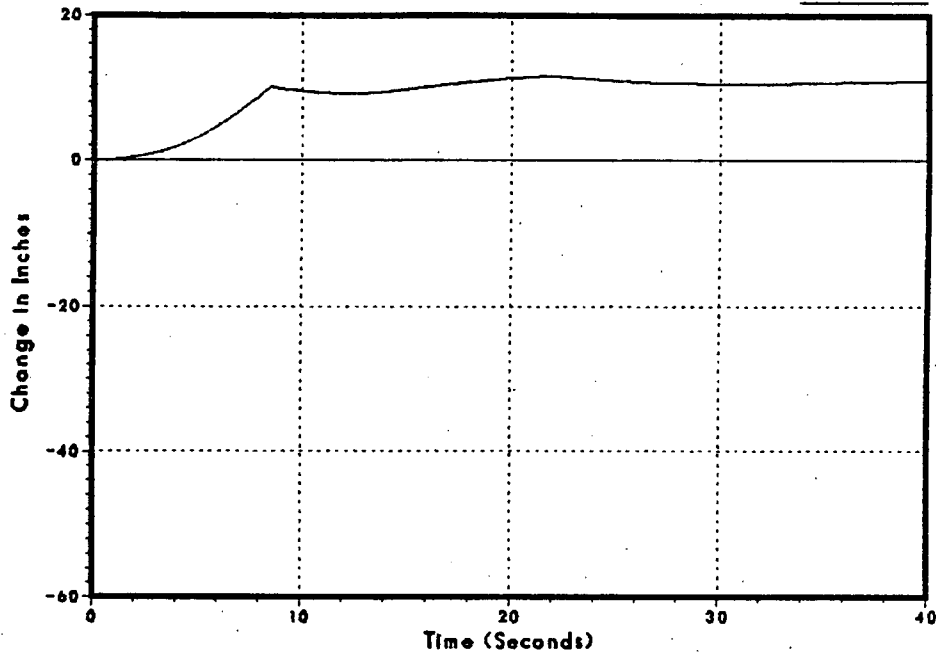
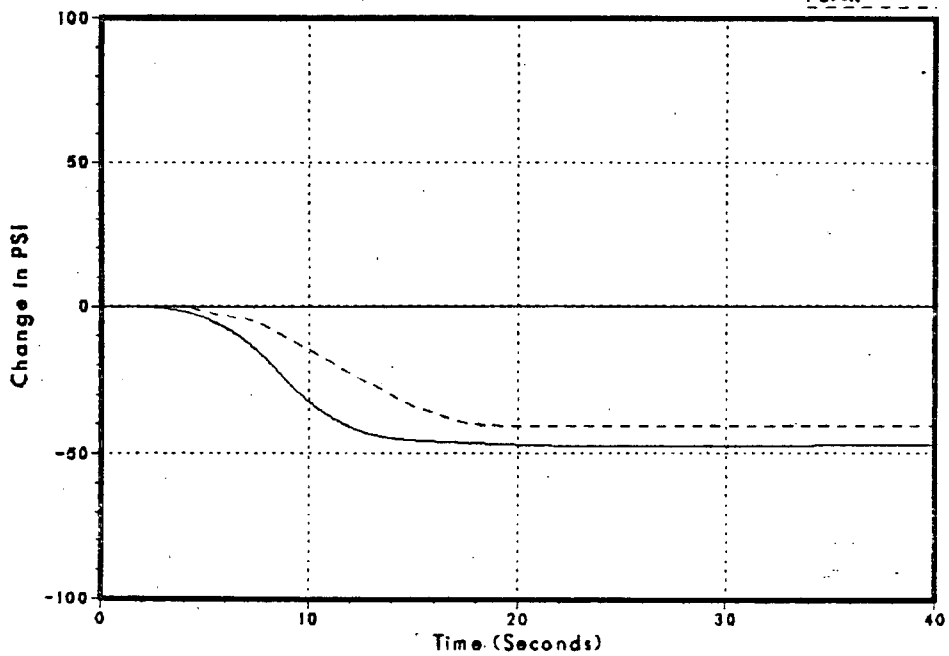


Figure 3.2-79
Steam Dome Pressure

DN8074/86

FSAR



NSP

Monticello FSAR Benchmark Recirculation Controller Fails (Decrease)

Figure 3.2-80
Core Inlet Flow

DNB074/86

FSAR

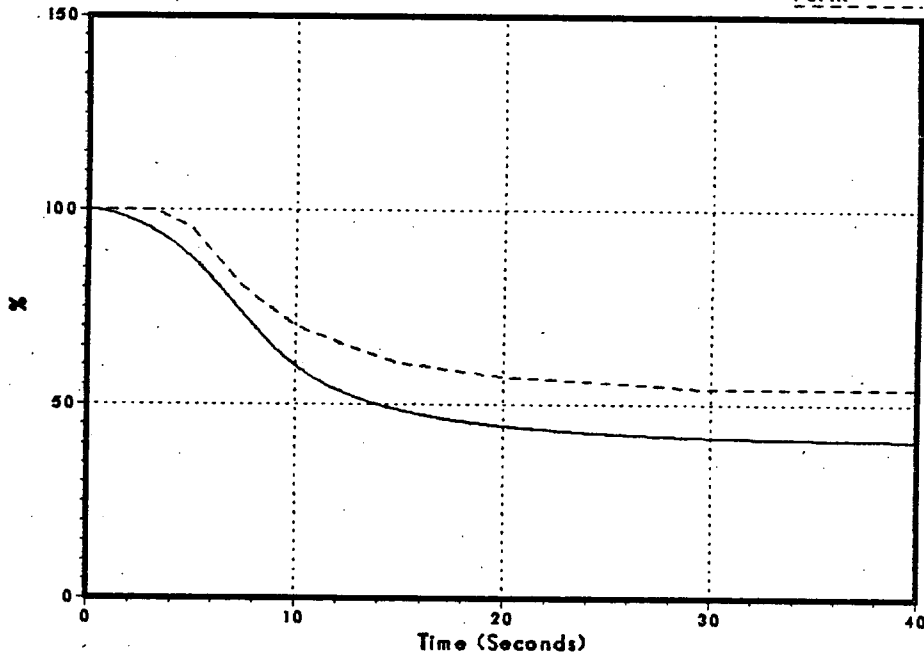
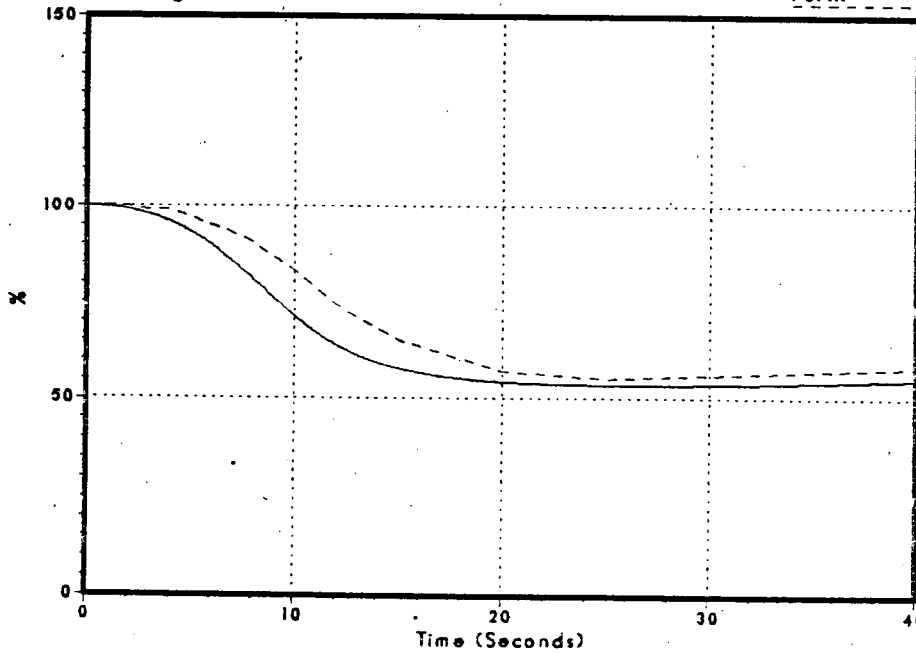


Figure 3.2-81
Average Surface Heat Flux

DNB074/86

FSAR



NSP

Monticello FSAR Benchmark Recirculation Controller Fails (Decrease)

Figure 3.2-82
Relative Power

DNB074/86

FSAR

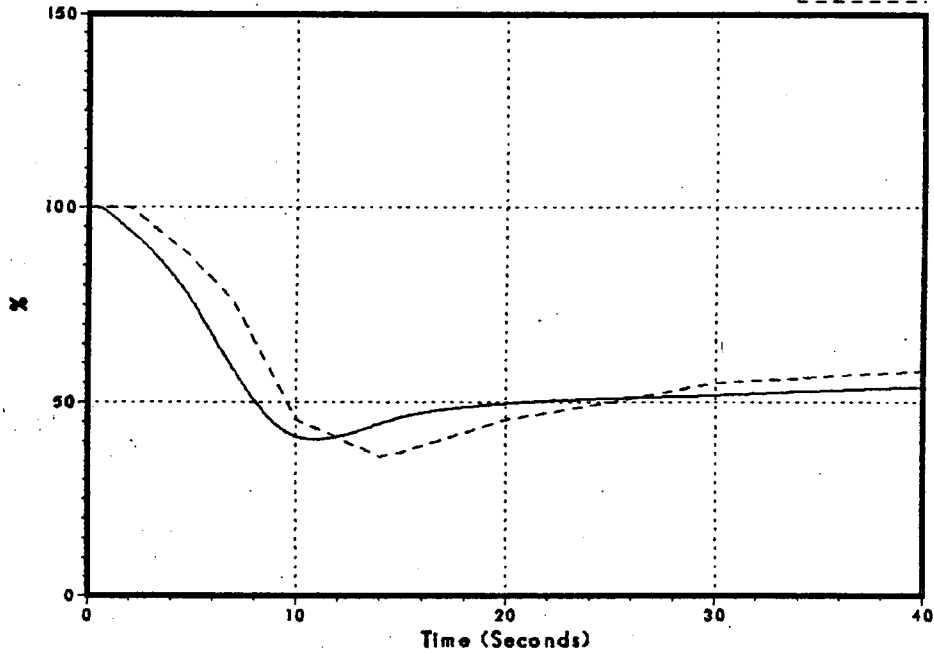
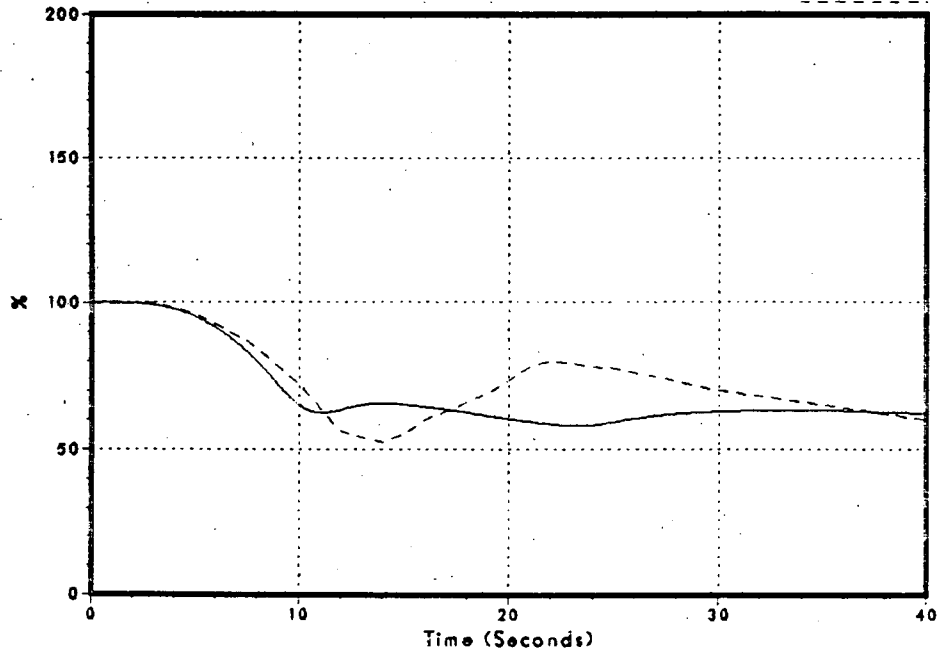


Figure 3.2-83
Feedwater Flow

DNB074/86

FSAR



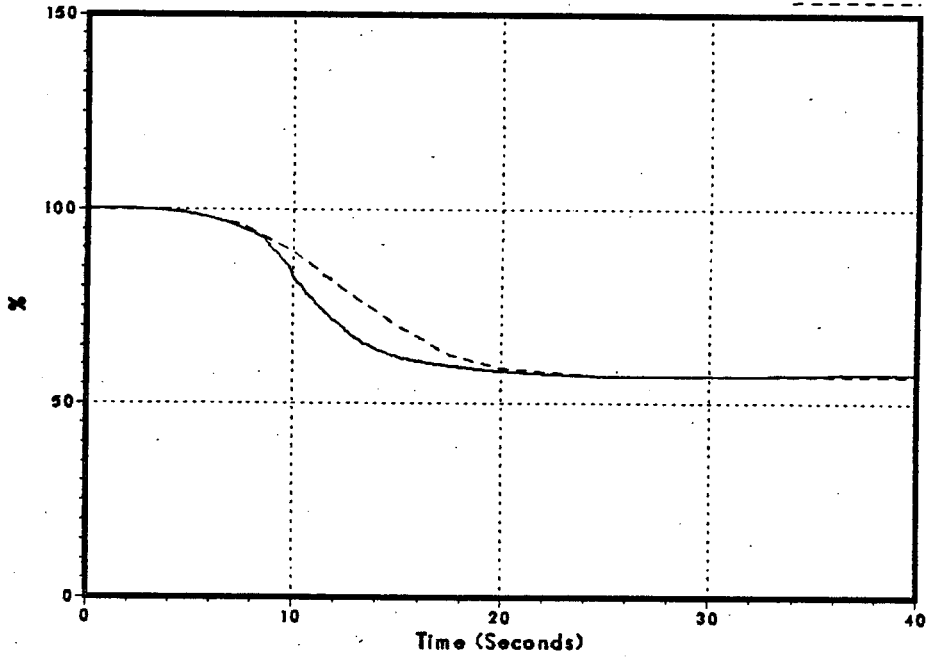
NSP

Monticello FSAR Benchmark Recirculation Controller Fails (Decrease)

Figure 3.2-84
Vessel Steam Flow

DNB074/86

FSAR



Monticello FSAR Benchmark Idle Loop Startup

Figure 3.2-85
Sensed Level

DNB068/86

FSAR

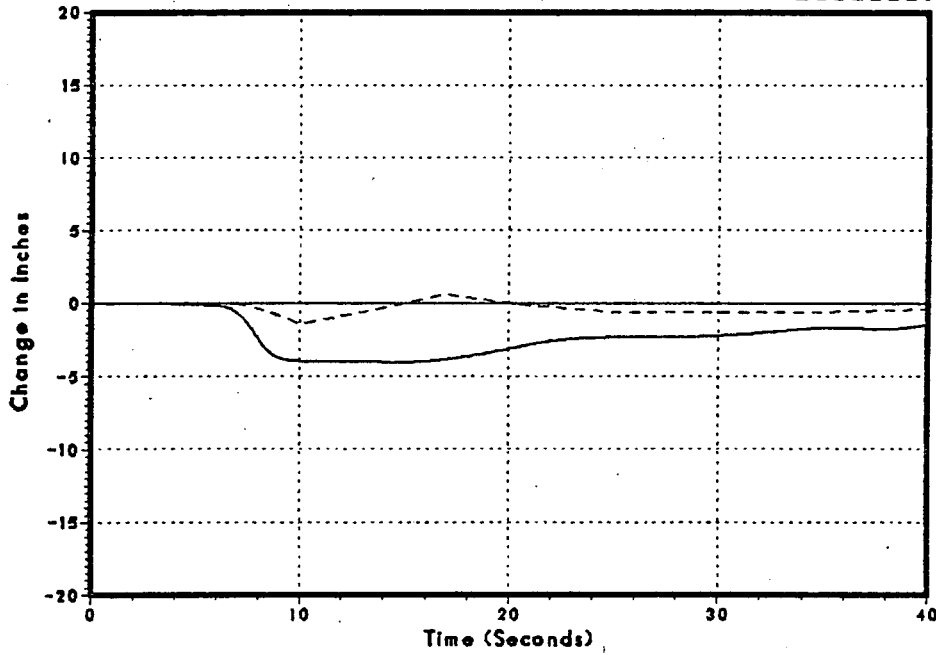
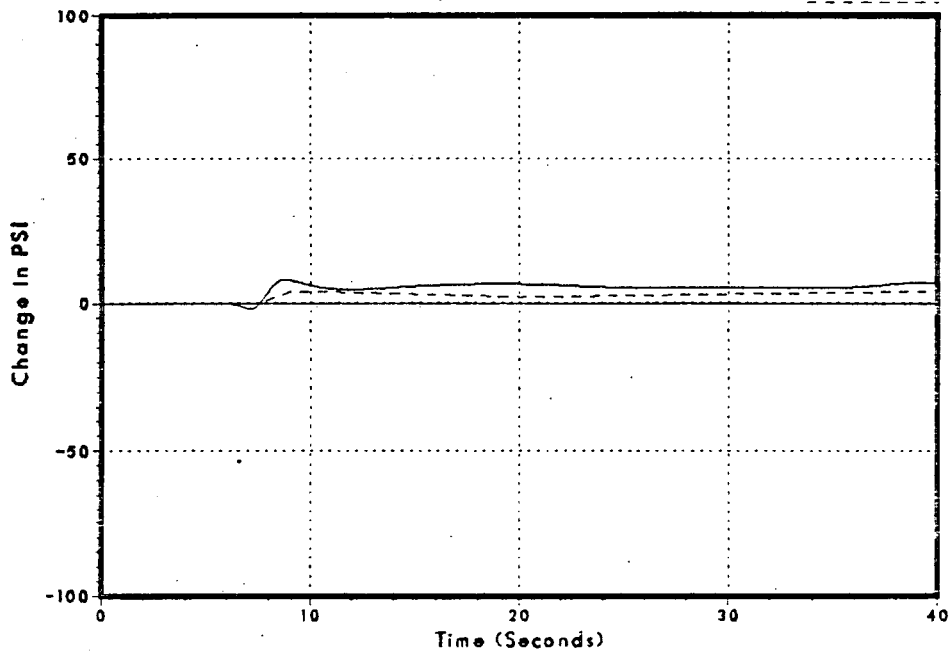


Figure 3.2-86
Steam Dome Pressure

DNB068/86

FSAR



NSP

Monticello FSAR Benchmark Idle Loop Startup

Figure 3.2-87
Core Inlet Flow

DNB068/86

FSAR

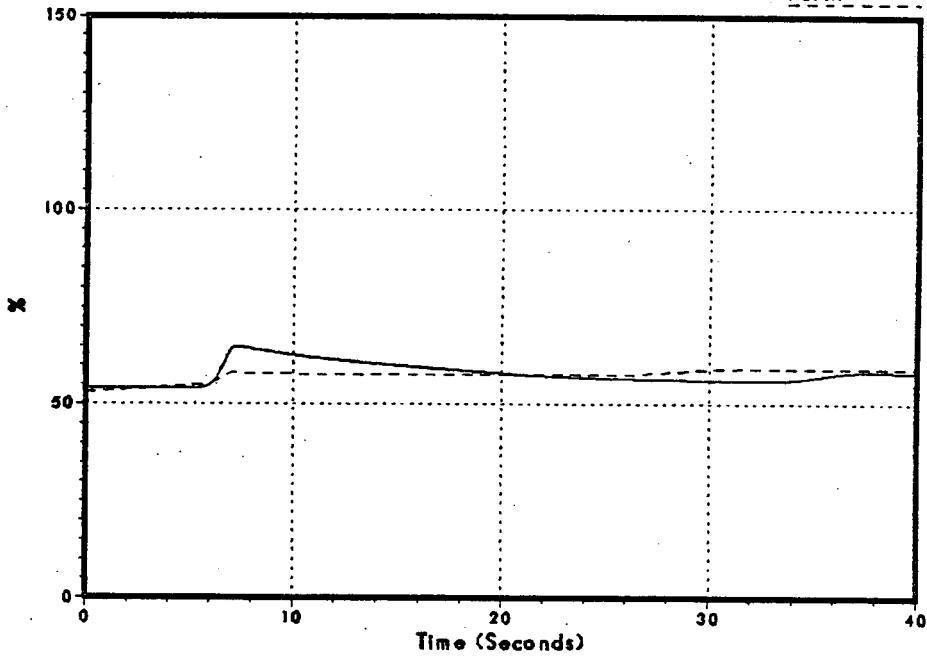
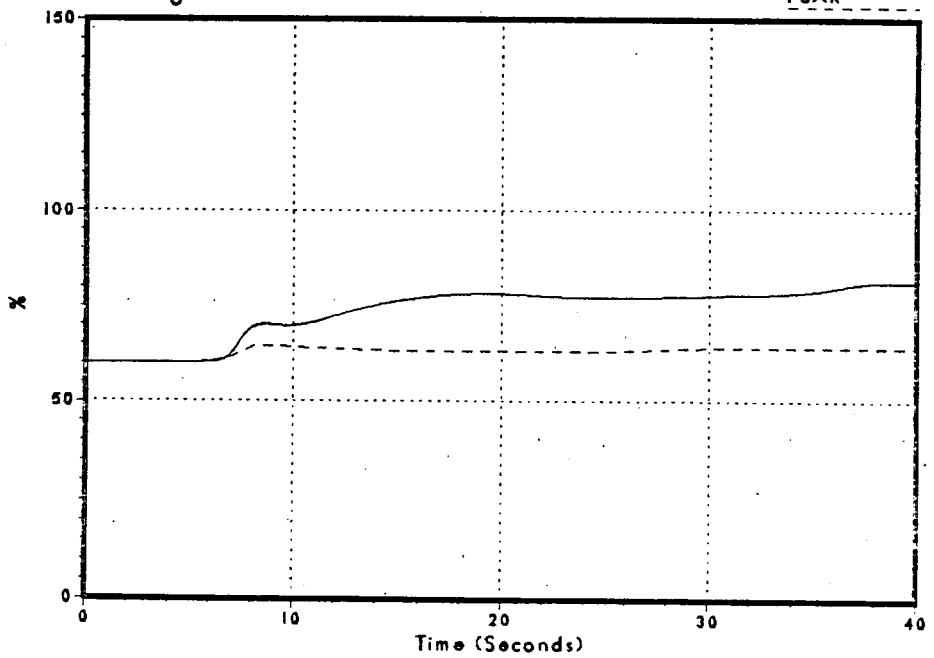


Figure 3.2-88
Average Surface Heat Flux

DNB068/86

FSAR



NSP

Monticello FSAR Benchmark Idle Loop Startup

Figure 3.2-89
Relative Power

DNB068/86

FSAR

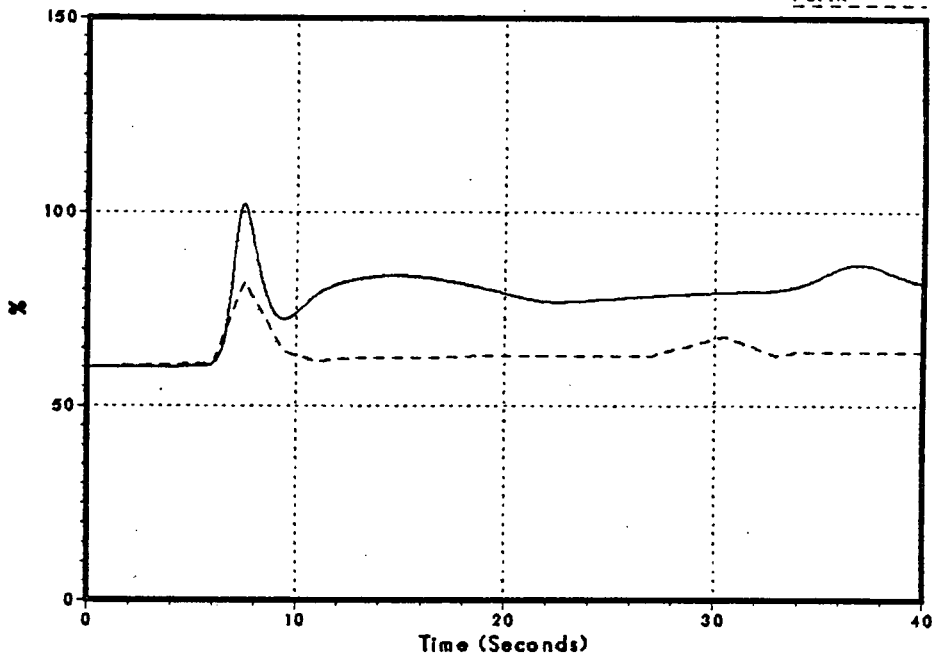
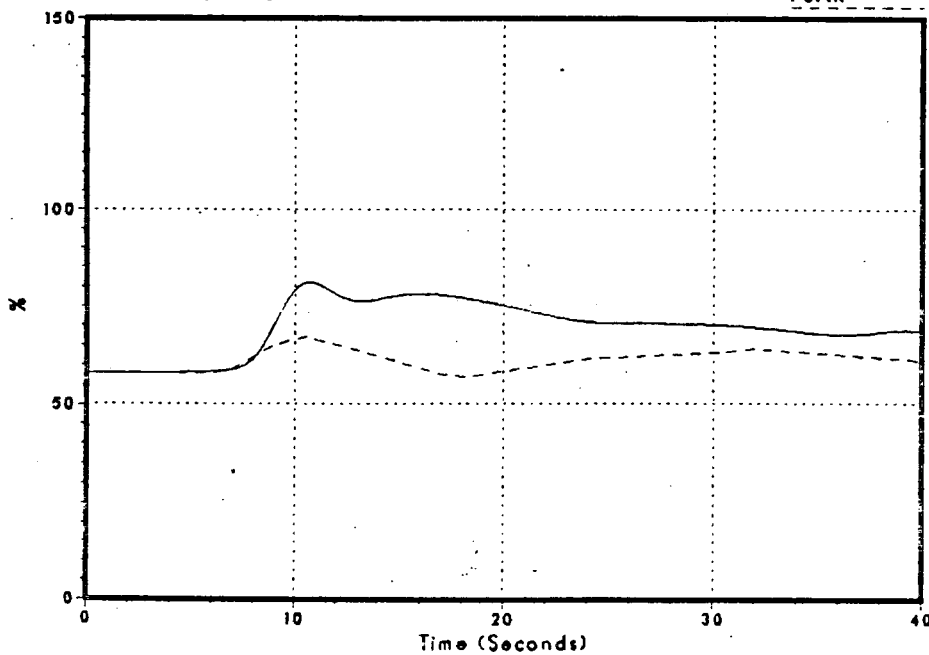


Figure 3.2-90
Feedwater Flow

DNB068/86

FSAR



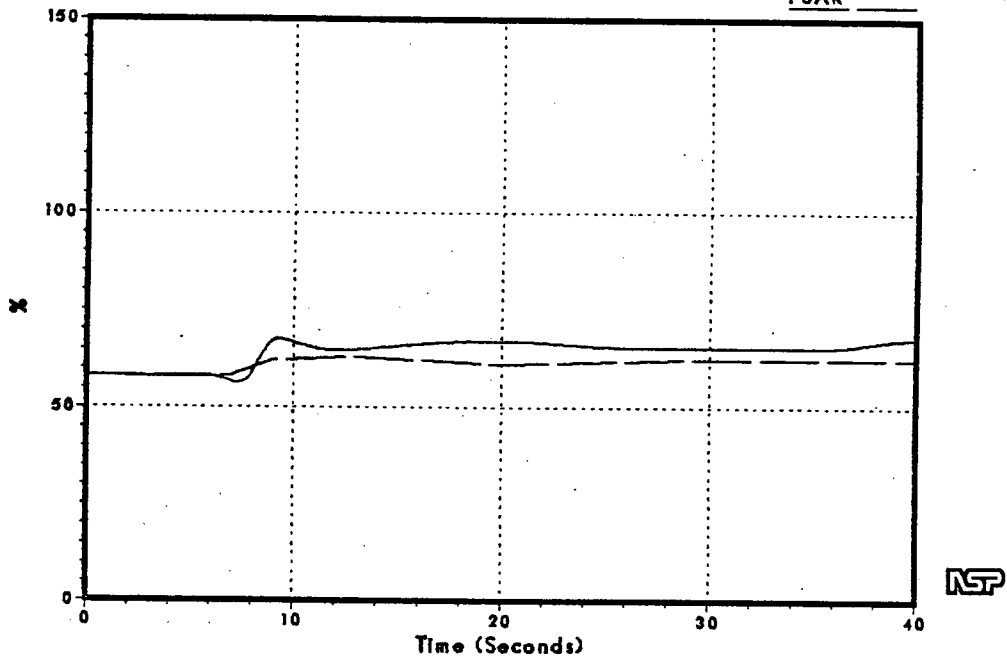
NSP

Monticello FSAR Benchmark Idle Loop Startup

Figure 3.2-91
Vessel Steam Flow

DNB068/86

FSAR



Monticello Cycle 11 Load Rejection without Bypass

Figure 3.2-92
Vessel Pressure Rise

DNB011/86

GE Analysis

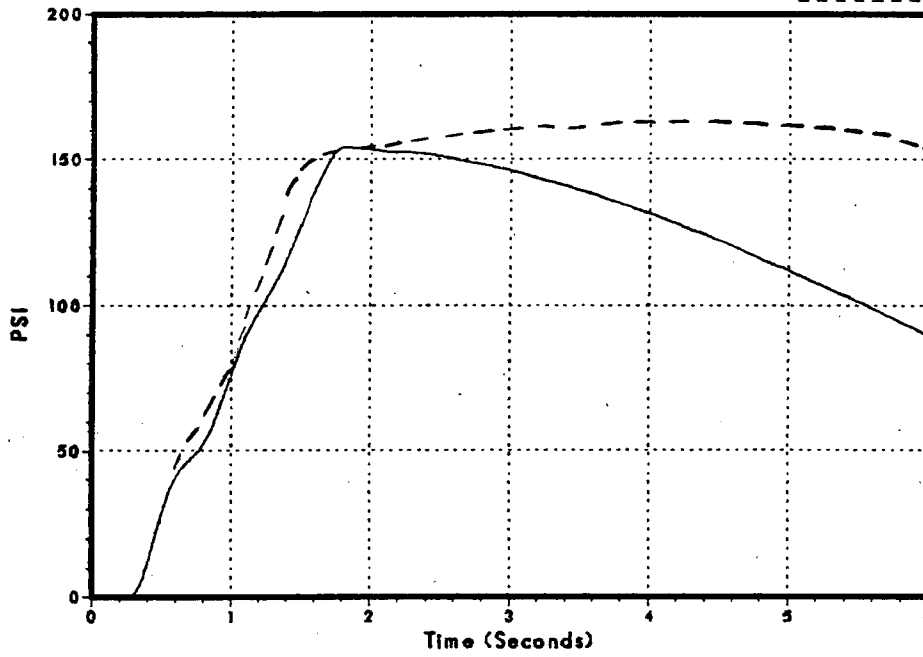
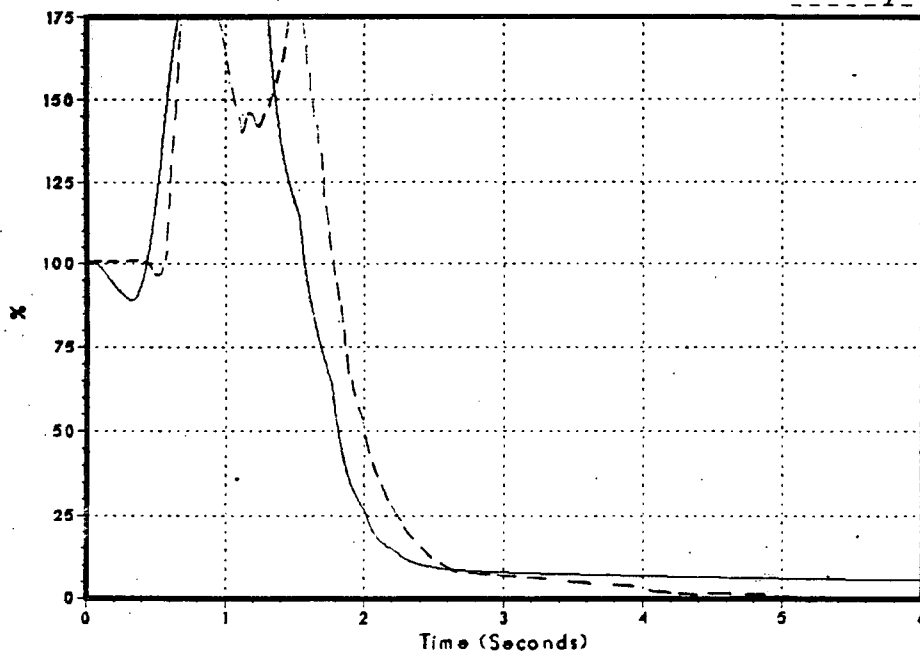


Figure 3.2-93
Relative Power

DNB011/86

GE Analysis



Monticello Cycle 11 Load Rejection without Bypass

Figure 3.2-94
Core Average Heat Flux

DNB011/86
GE Analysis

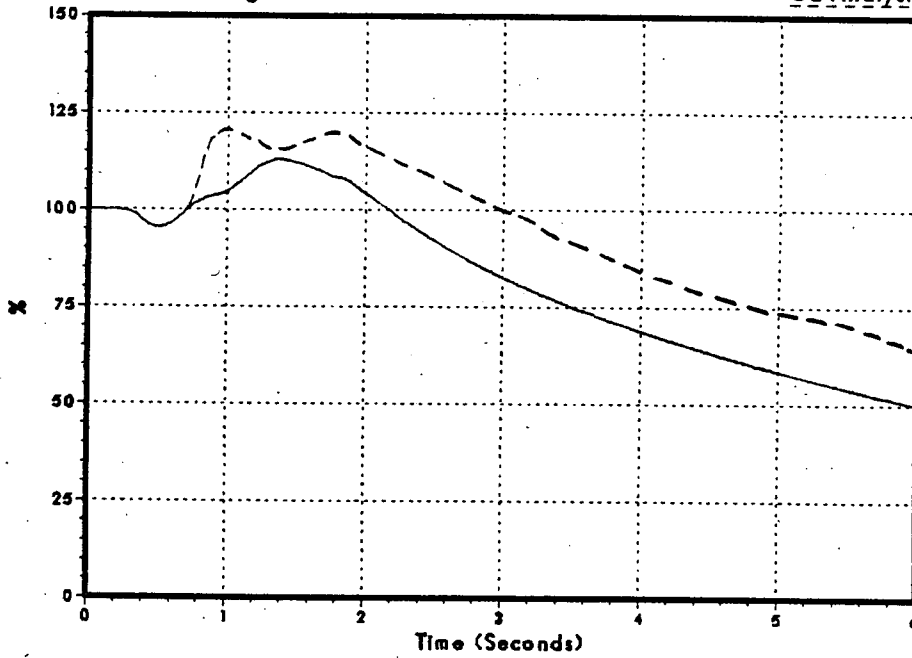
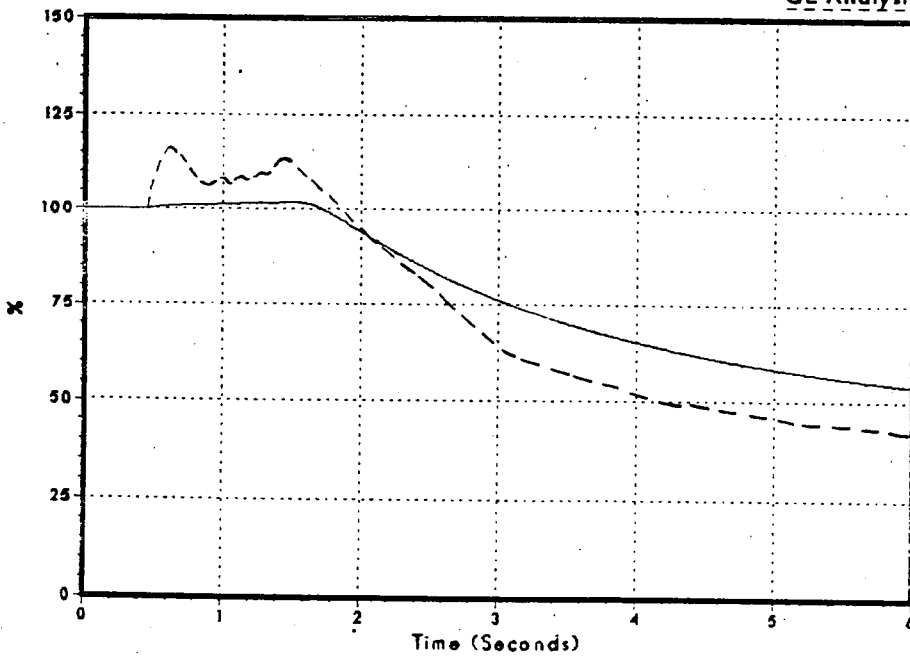


Figure 3.2-95
Core Inlet Flow

DNB011/86
GE Analysis



NSP

Monticello Cycle II Load Rejection without Bypass

Figure 3.2-96
Main Steam Line Flow

DNB011/86

GE Analysis

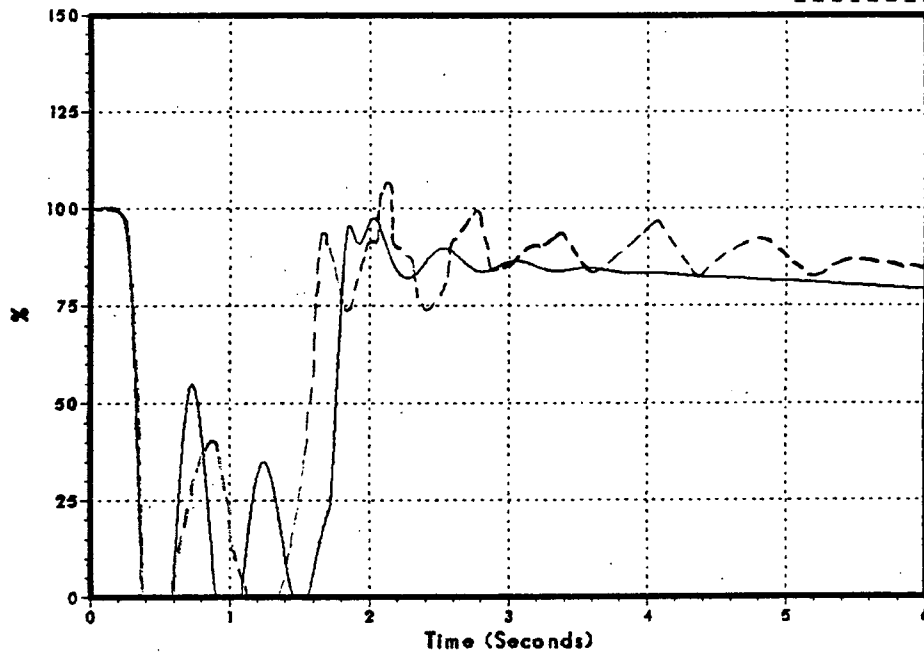
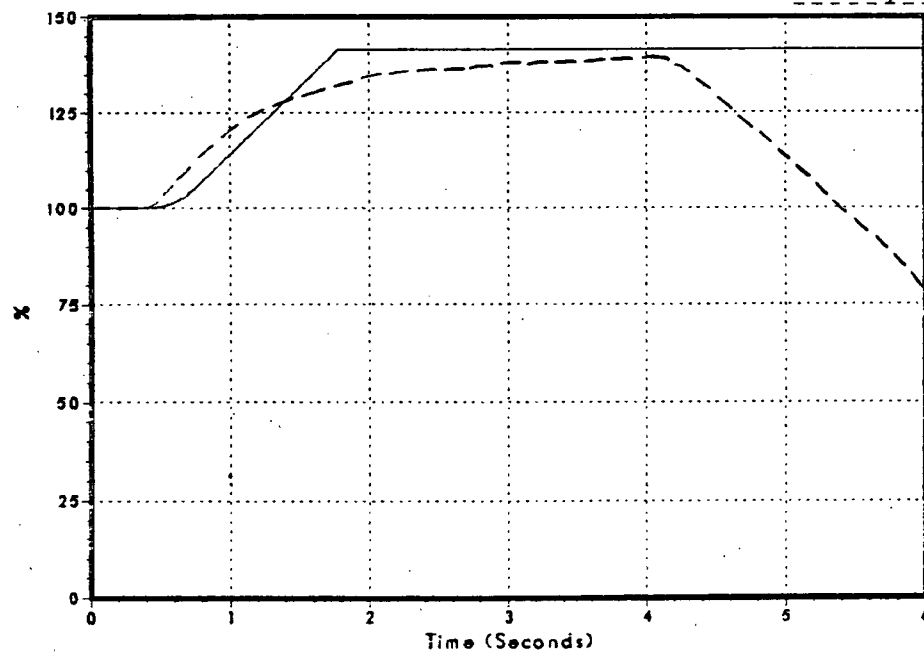


Figure 3.2-97
Feedwater Flow

DNB011/86

GE Analysis

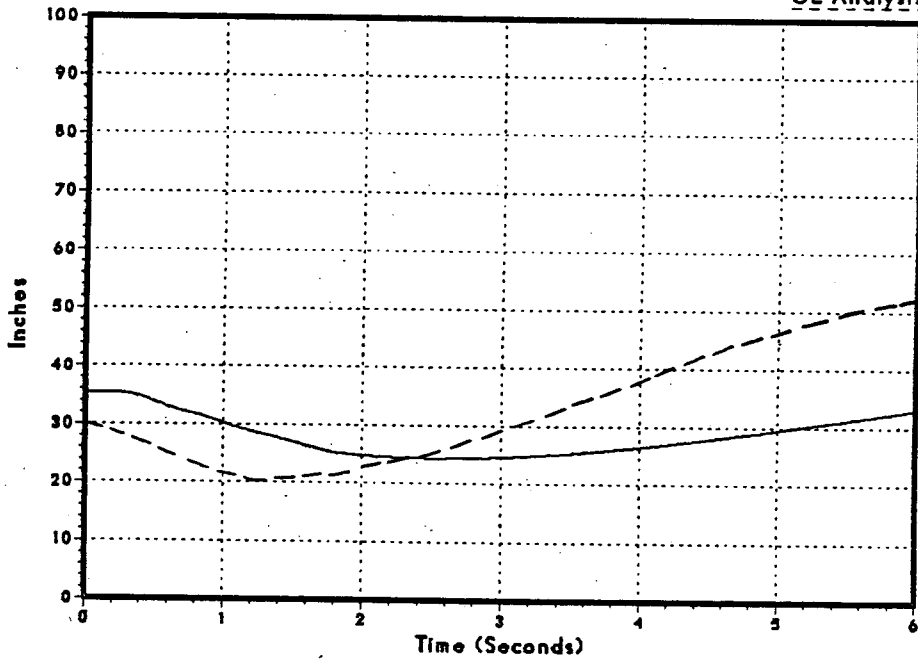


Monticello Cycle 11 Load Rejection without Bypass

Figure 3.2-98
Sensed Reactor Water Level

DNB011/86

GE Analysis



NSP

Monticello Cycle 11 Feedwater Controller Failure

Figure 3.2-99
Vessel Pressure Rise

DNB012/86
GE Analysis

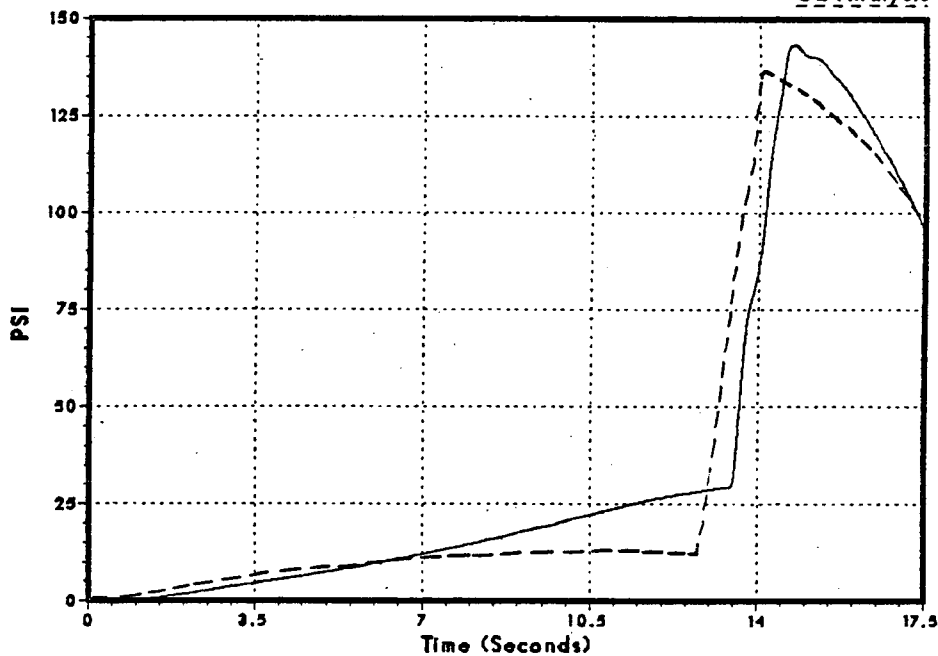
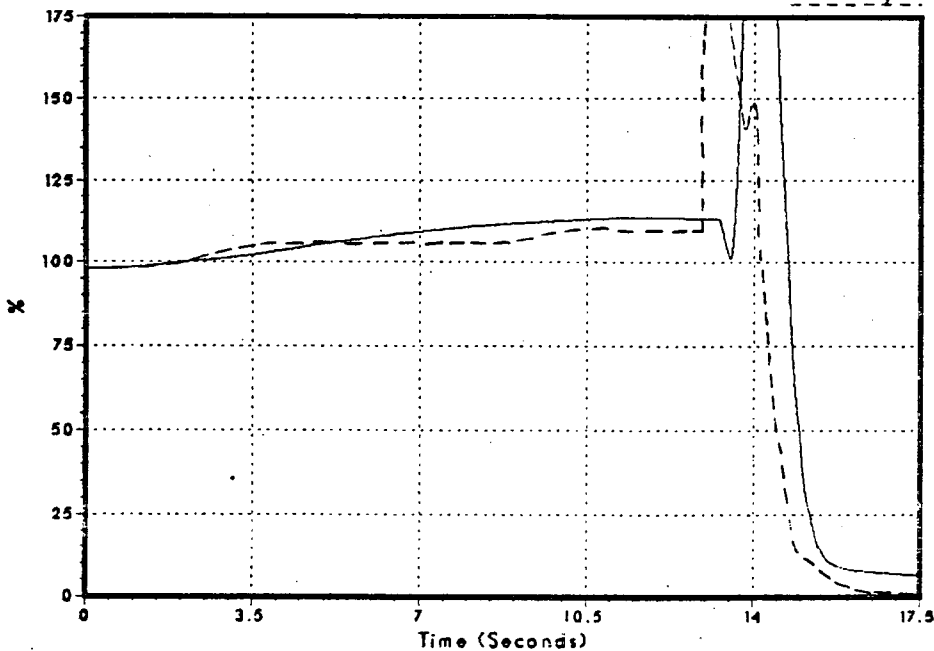


Figure 3.2-100
Relative Power

DNB012/86
GE Analysis



Monticello Cycle 11 Feedwater Controller Failure

Figure 3.2-101
Core Average Heat Flux

DNB012/86

GE Analysis

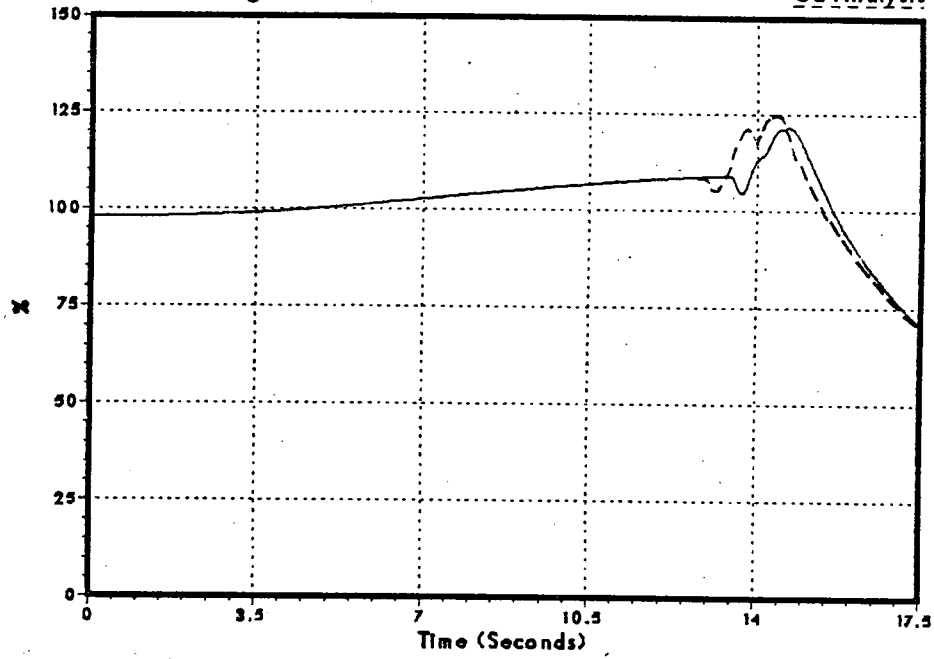
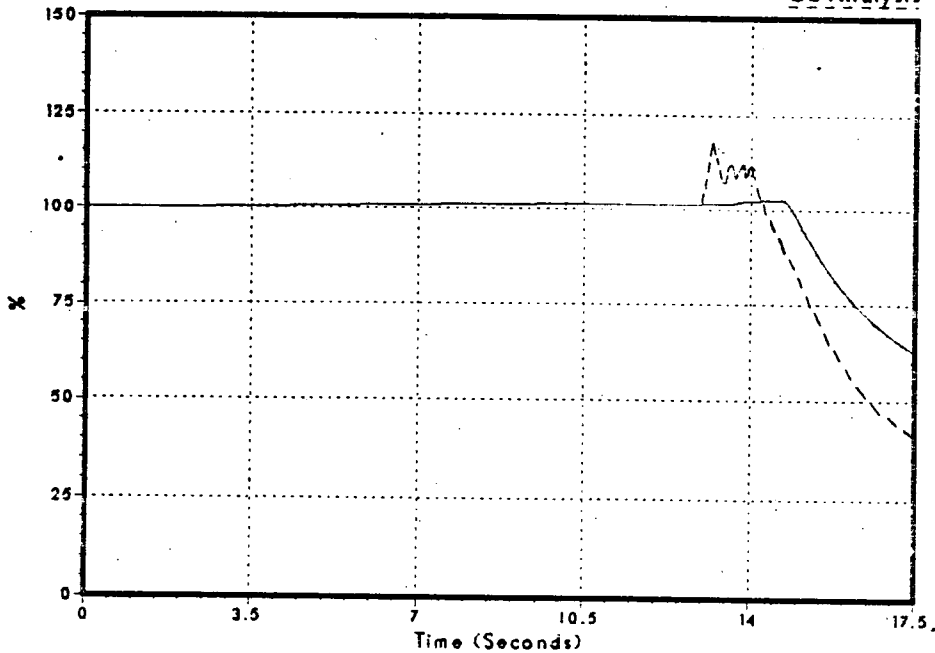


Figure 3.2-102
Core Inlet Flow

DNB012/86

GE Analysis



NSP

Monticello Cycle 11 Feedwater Controller Failure

Figure 3.2-103
Core Inlet Subcooling

DNB012/86

GE Analysis

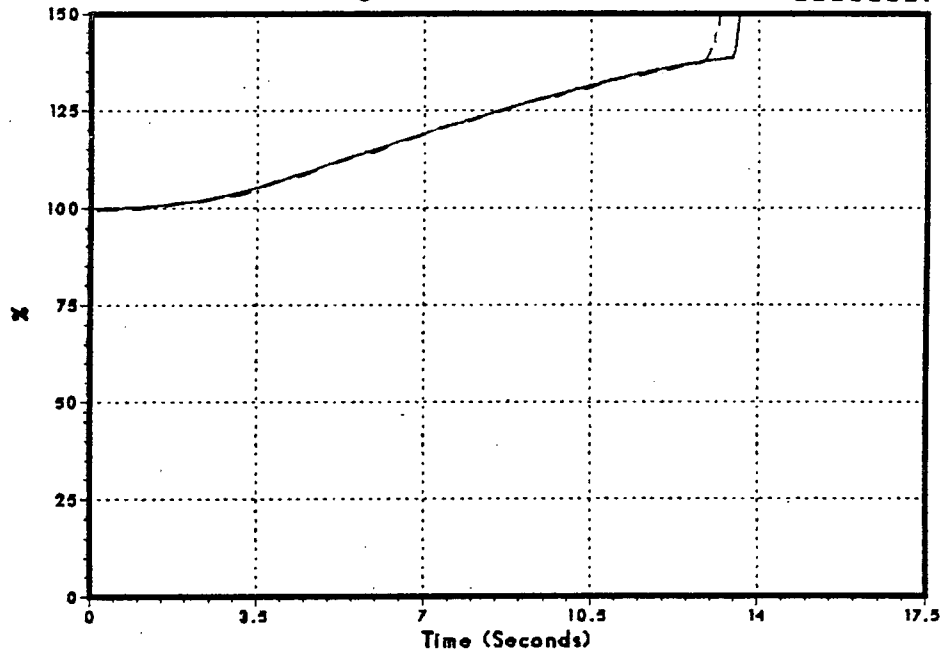
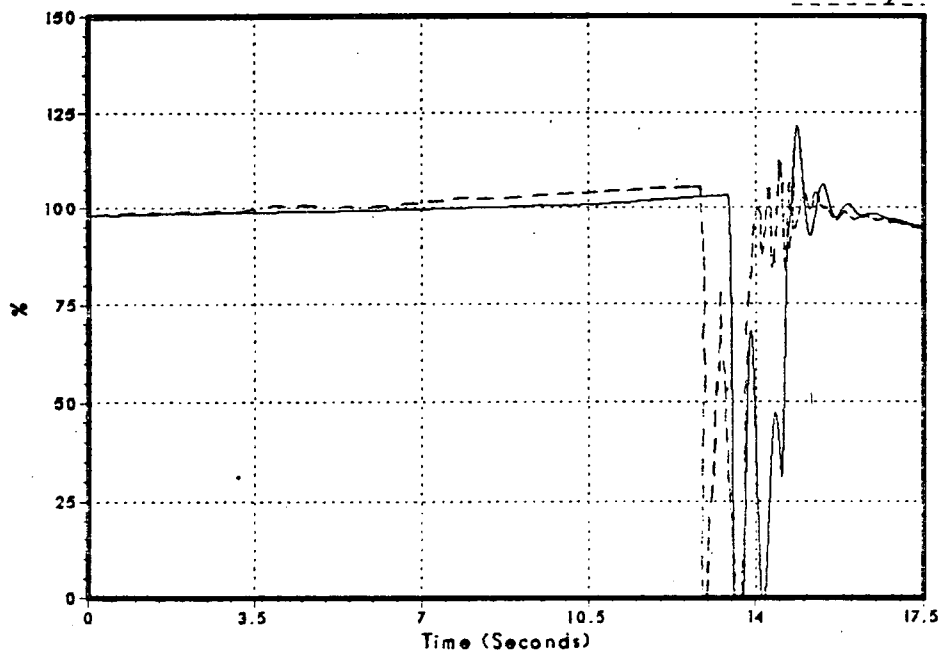


Figure 3.2-104
Main Steam Line Flow

DNB012/86

GE Analysis



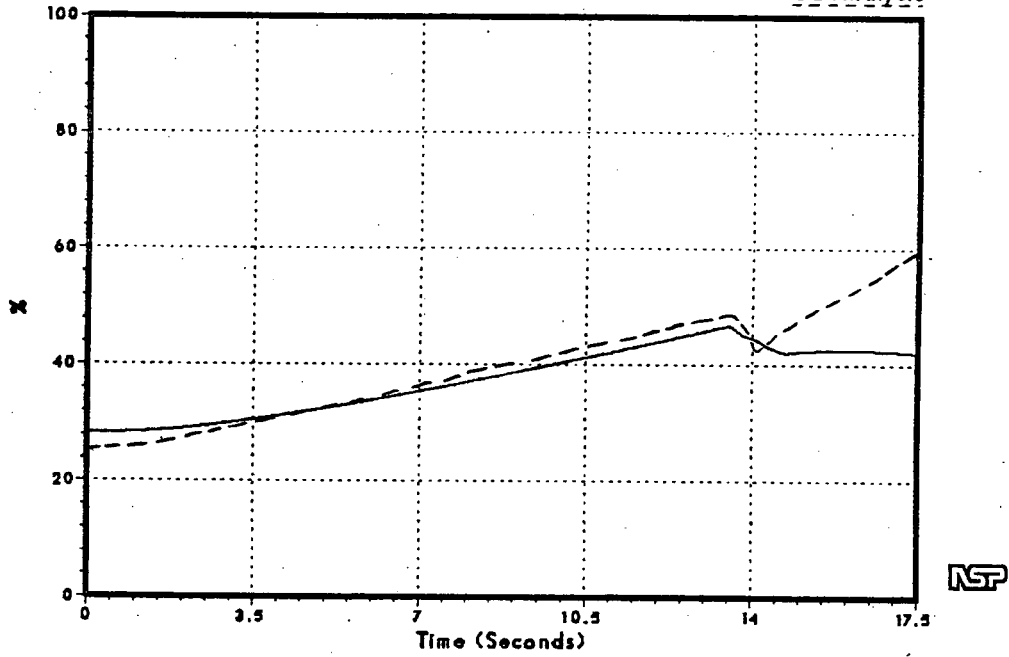
NSP

Monticello Cycle 11 Feedwater Controller Failure

Figure 3.2-105
Sensed Reactor Water Level

DNB012/86

GE Analysis



Monticello Cycle 11 100% MSIV Closure

Figure 3.2-106
Vessel Pressure Rise

DNB010/86
GE ANALYSIS

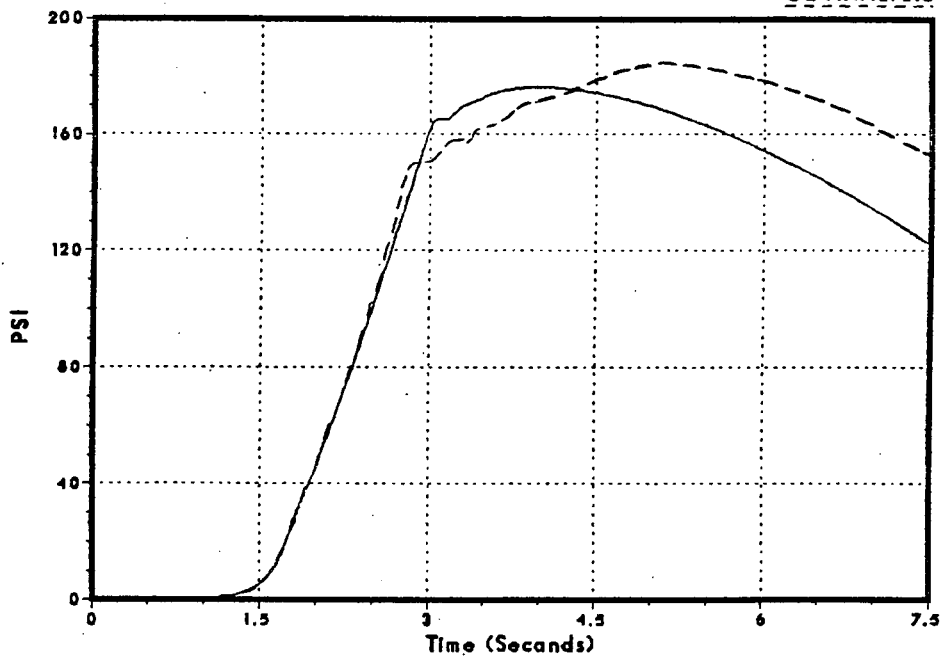
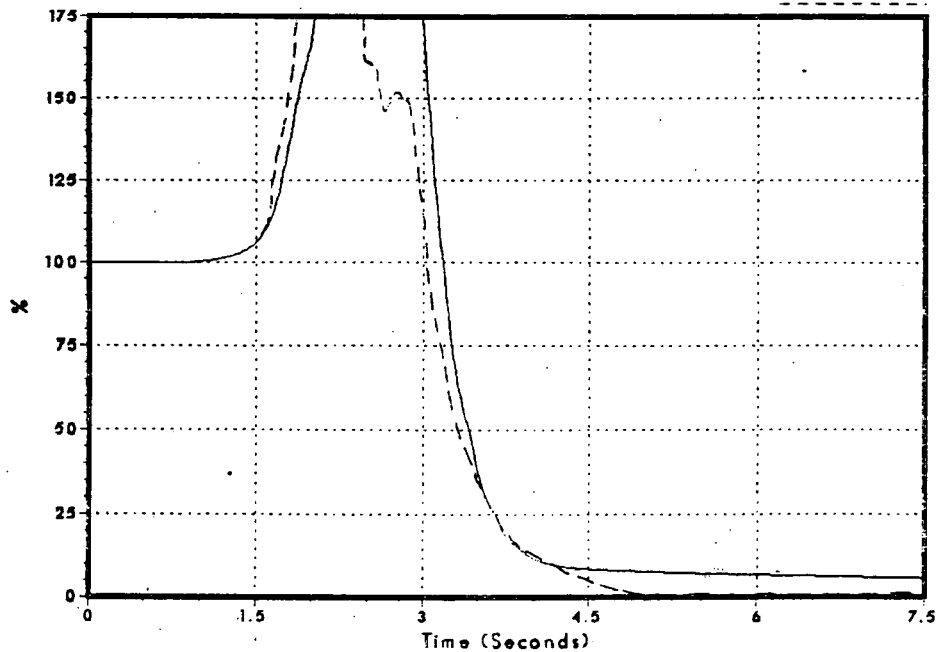


Figure 3.2-107
Relative Power

DNB010/86
GE ANALYSIS



Monticello Cycle 11 100% MSIV Closure

Figure 3.2-108
Core Average Heat Flux

DNB010/86

GE ANALYSIS

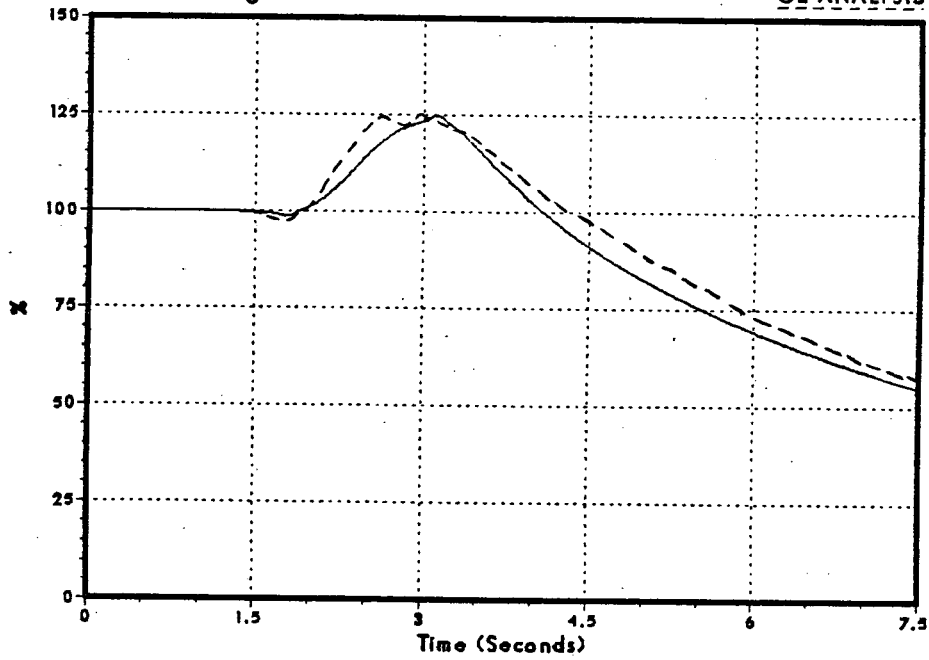
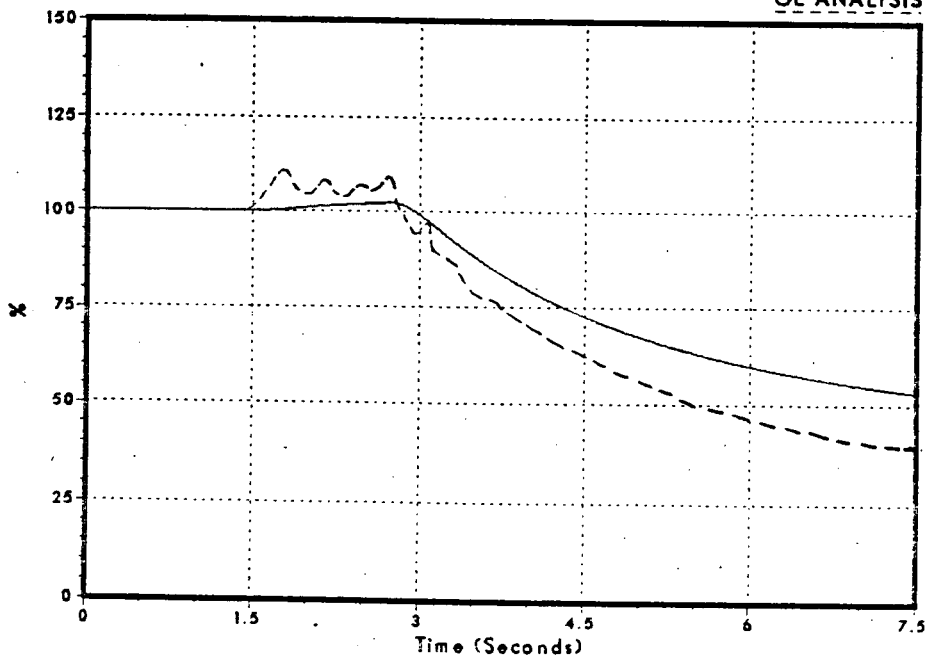


Figure 3.2-109
Core Inlet Flow

DNB010/86

GE ANALYSIS



NSP

Monticello Cycle 11 100% MSIV Closure

Figure 3.2-110
Main Steam Line Flow

DNB010/86

GE ANALYSIS

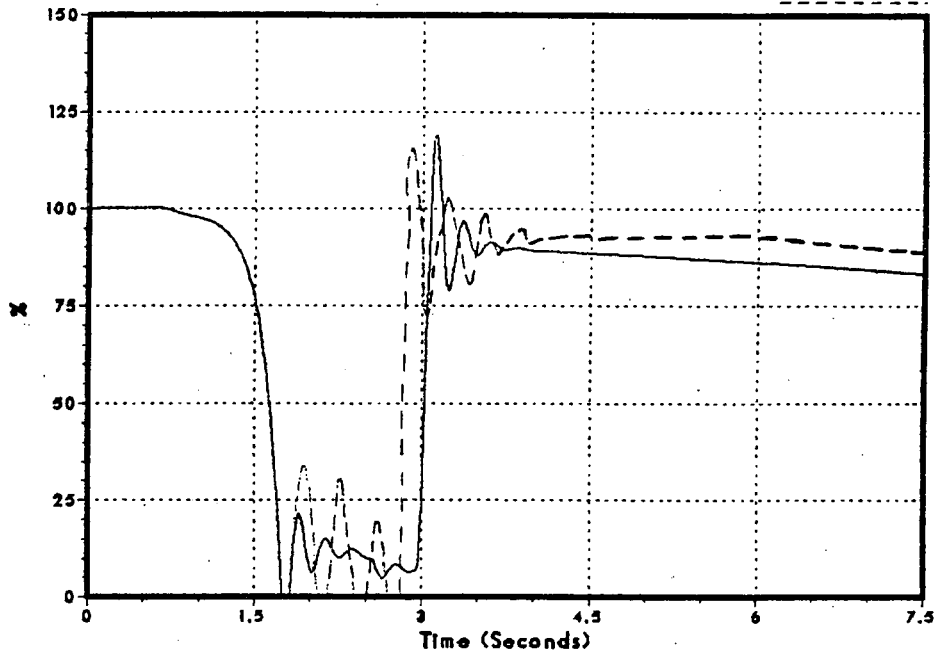
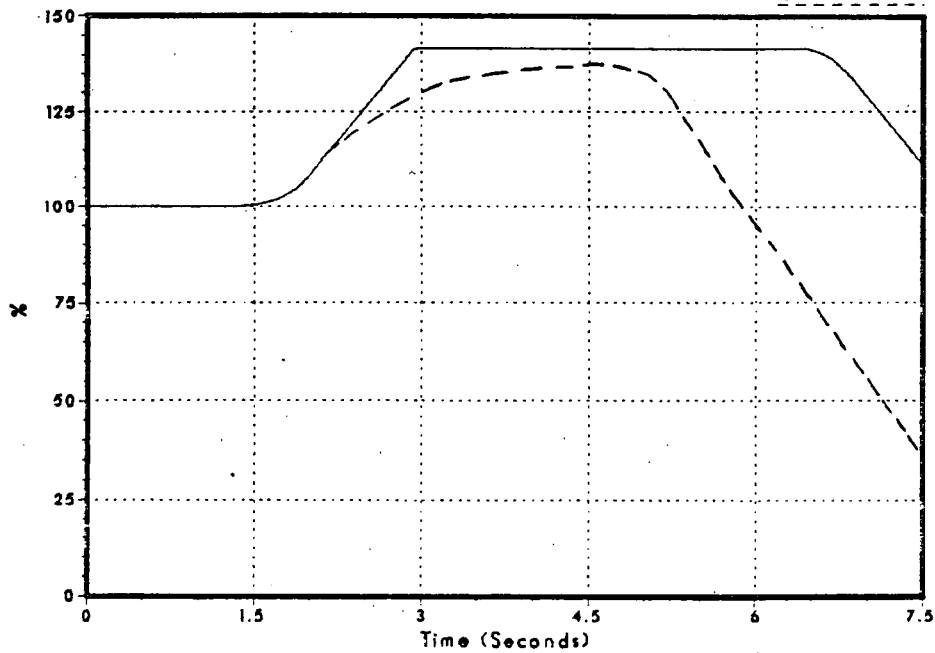


Figure 3.2-111
Feedwater Flow

DNB010/86

GE ANALYSIS



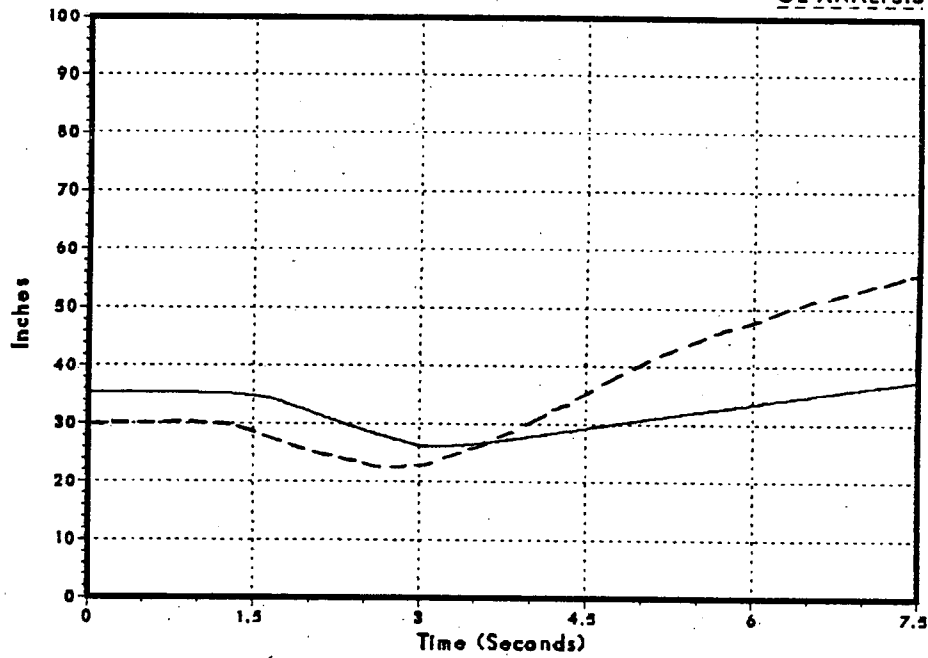
NSP

Monticello Cycle 11 100% MSIV Closure

Figure 3.2-112
Sensed Reactor Water Level

DNB010/86

GE ANALYSIS



NSP

Peach Bottom Turbine Trip Test TTI

Figure 3.2-113
Steam Dome Pressure

DNB001/86

Test Data

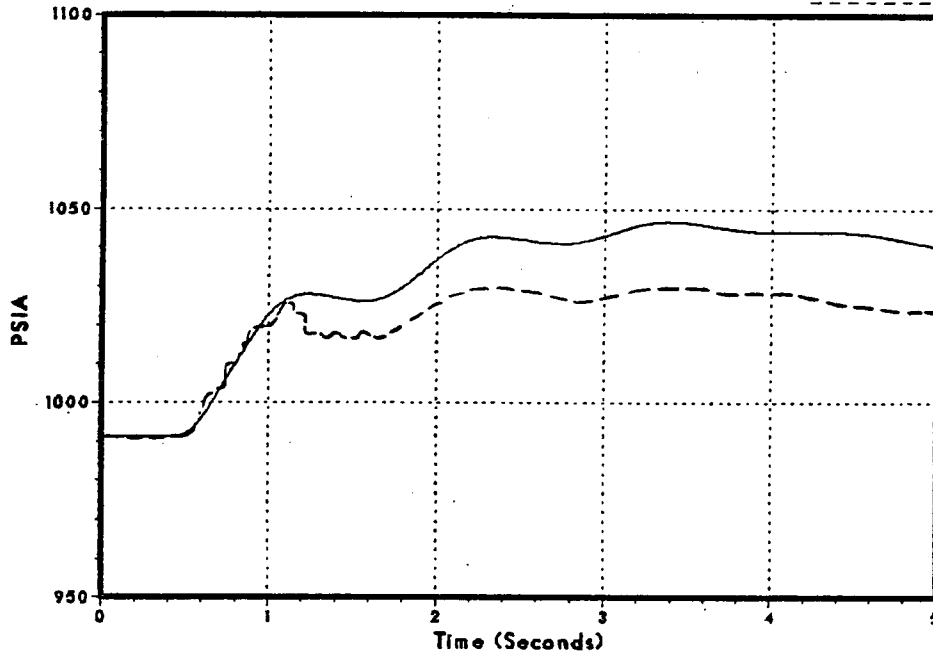
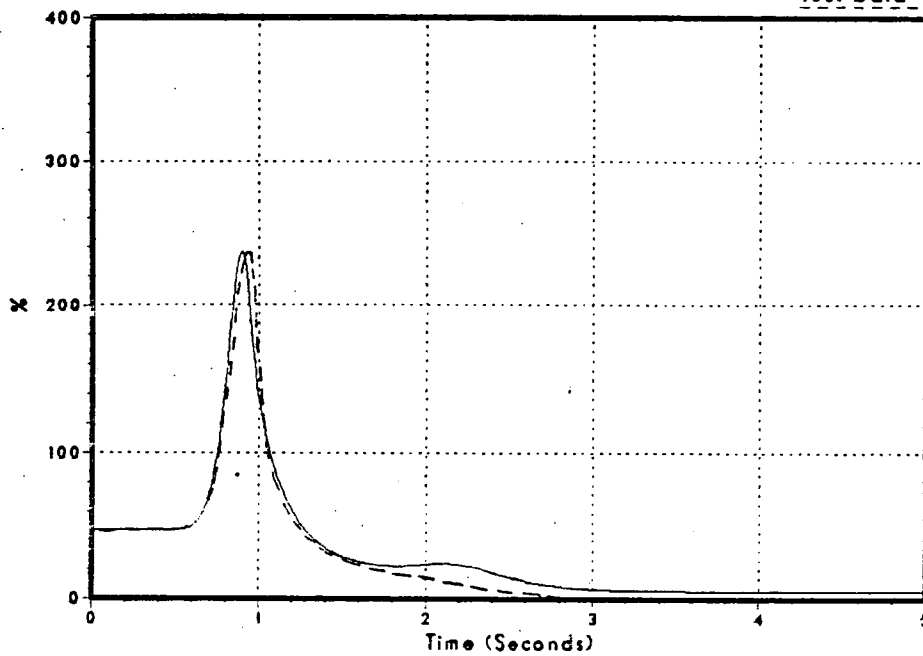


Figure 3.2-114
Relative Power

DNB001/86

Test Data



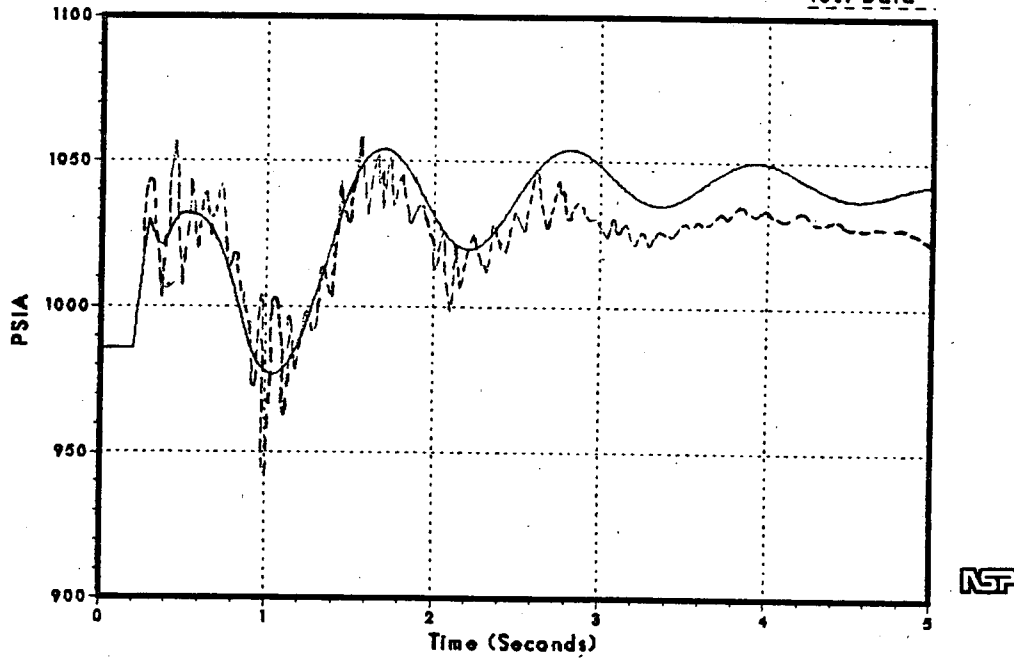
NSP

Peach Bottom Turbine Trip Test TT1

Figure 3.2-115
Turbine Throttle Pressure

DNB001/86

Test Data



Peach Bottom Turbine Trip Test TT2

Figure 3.2-116
Steam Dome Pressure

DNB002/86

Test Data

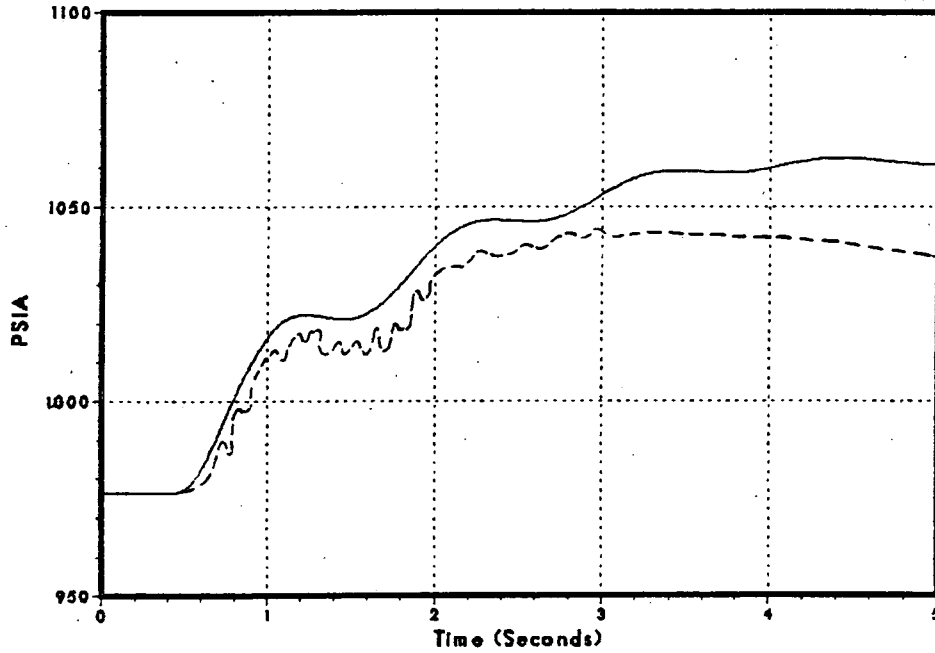
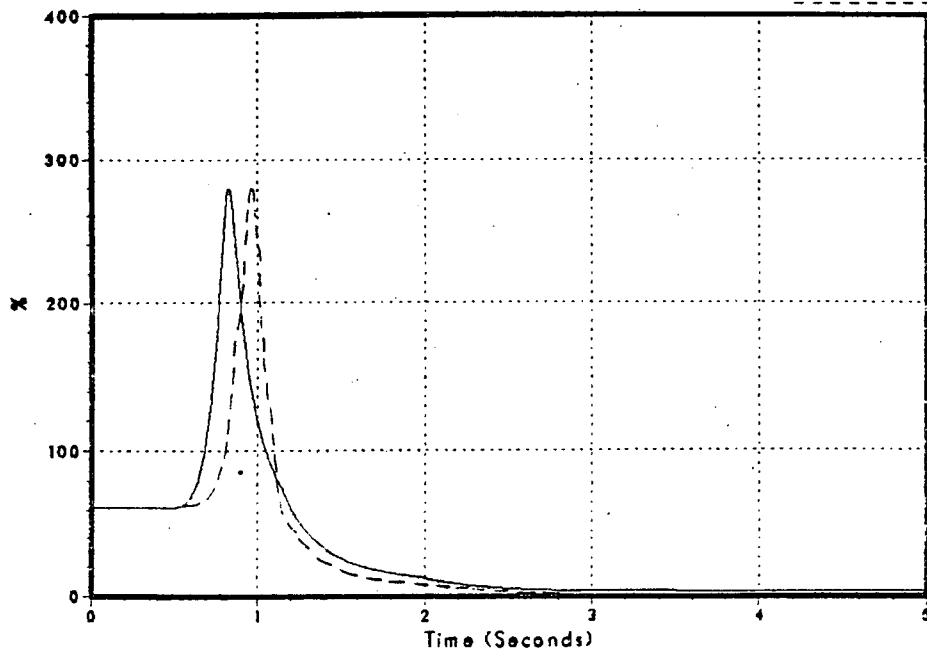


Figure 3.2-117
Relative Power

DNB002/86

Test Data



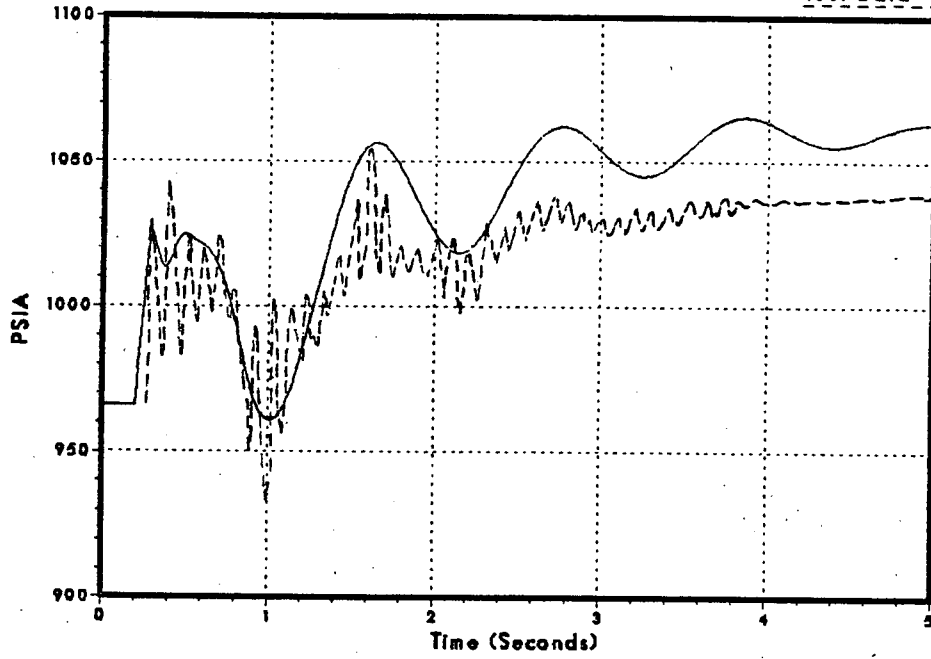
NSP

Peach Bottom Turbine Trip Test TT2

Figure 3.2-118
Turbine Thrattle Pressure

DNB002/86

Test Data



NSP

Peach Bottom Turbine Trip Test TT3

Figure 3.2-119
Steam Dome Pressure

DNB003/86

Test Data

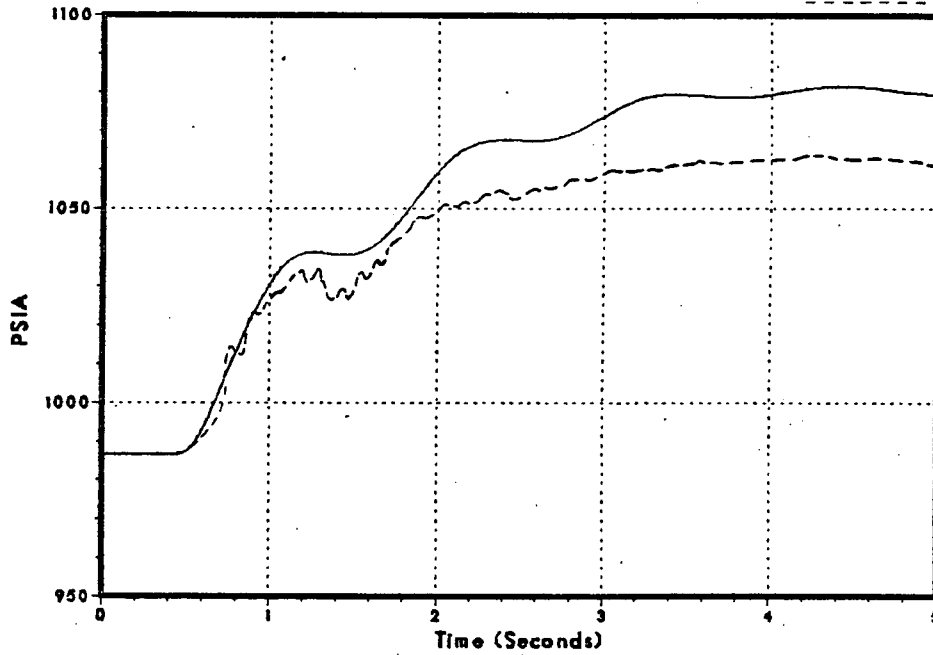
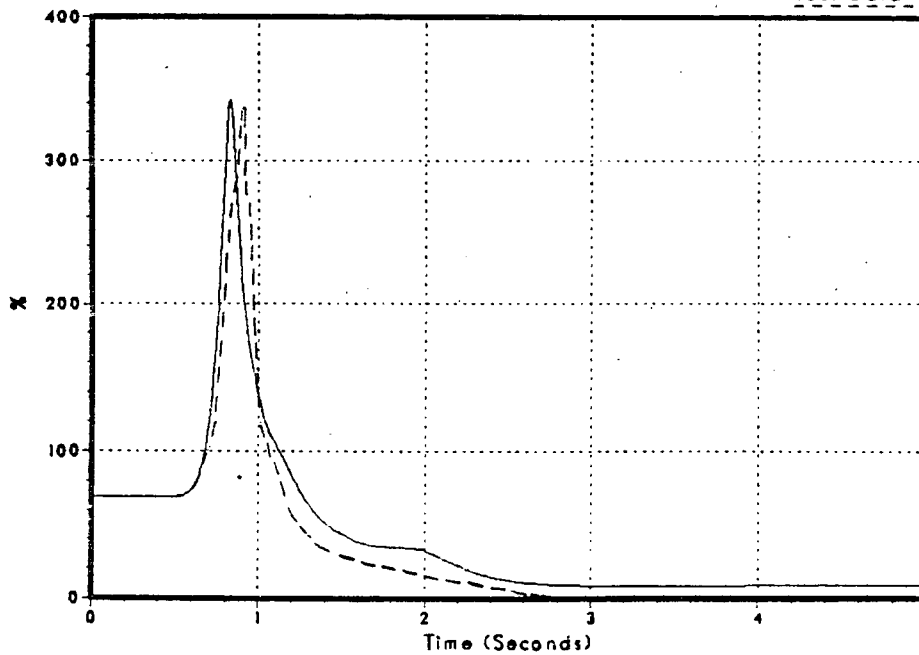


Figure 3.2-120
Relative Power

DNB003/86

Test Data



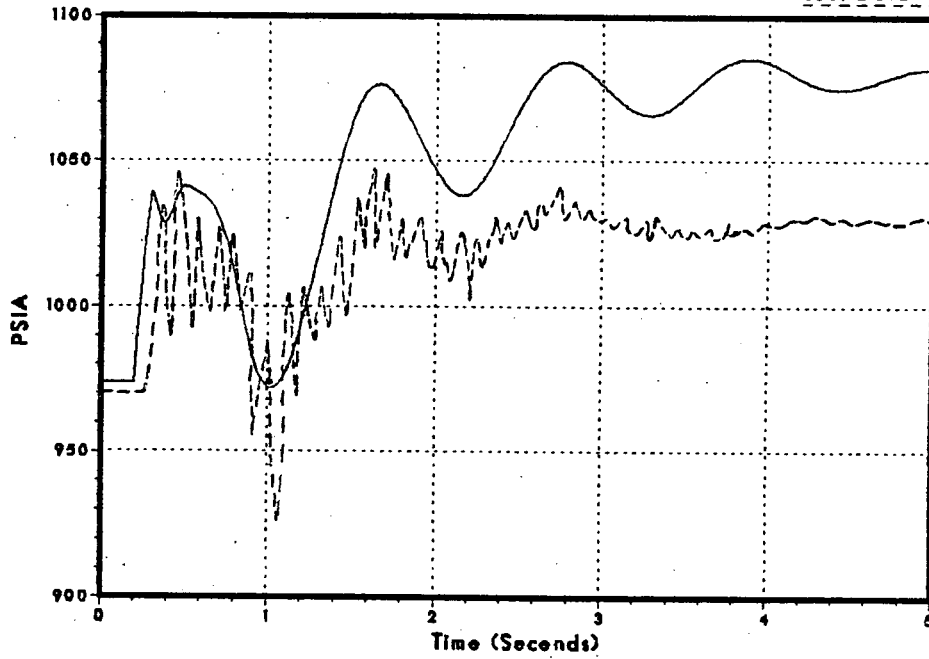
NSP

Peach Bottom Turbine Trip Test TT3

Figure 3.2-121
Turbine Throttle Pressure

DNB003/86

Test Data



NSP

Monticello Cycle 1 Turbine Trip Startup Test

Figure 3.2-122
Steam Dome Pressure

DNB038/86

Test Data

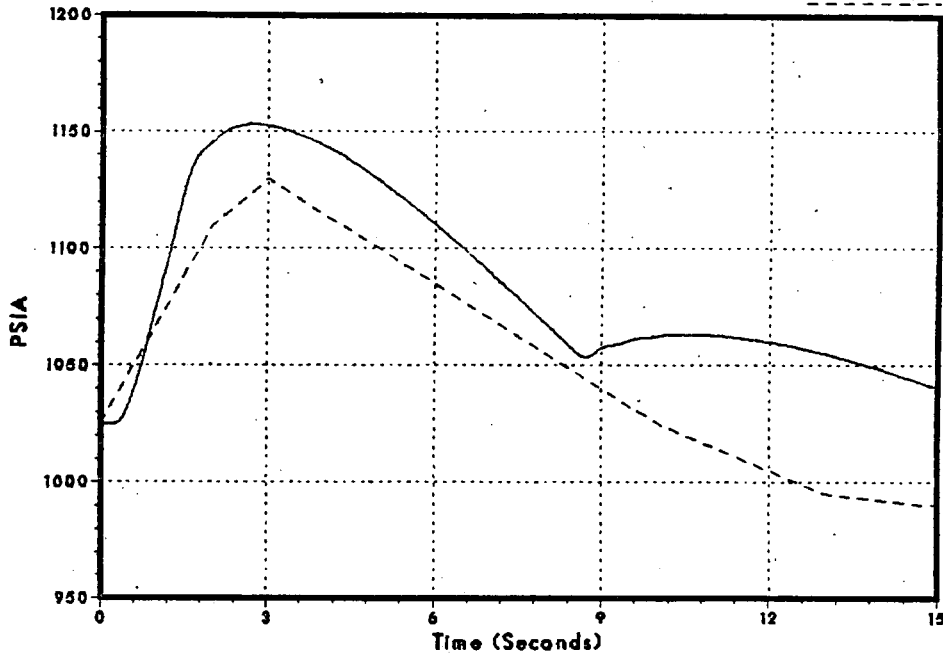
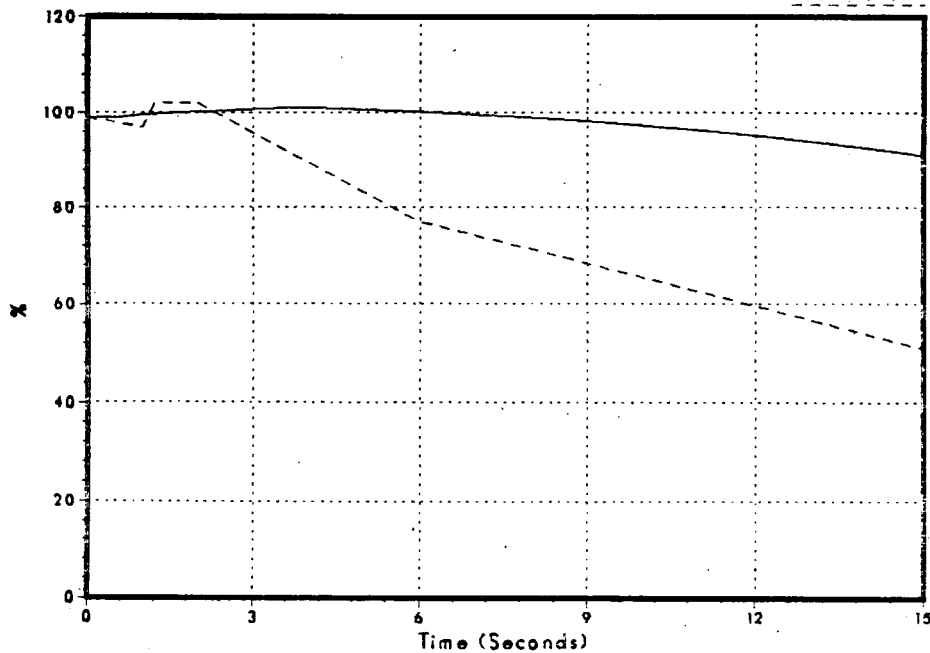


Figure 3.2-123
Total Vessel Flow Rate

DNB038/86

Test Data



Monticello Cycle 1 Turbine Trip Startup Test

Figure 3.2-124
Relative Power

DNB038/86

Test Data

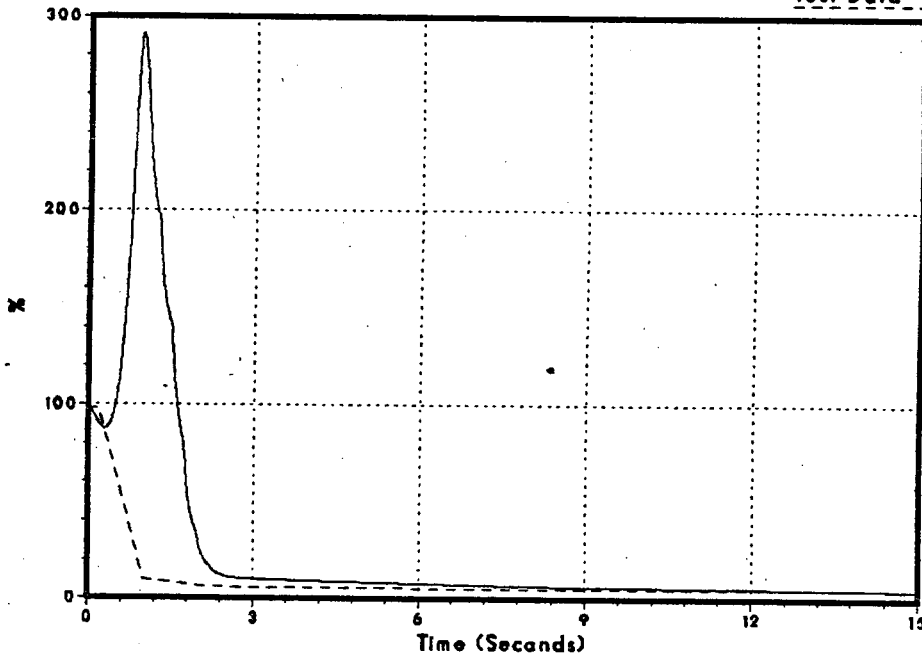
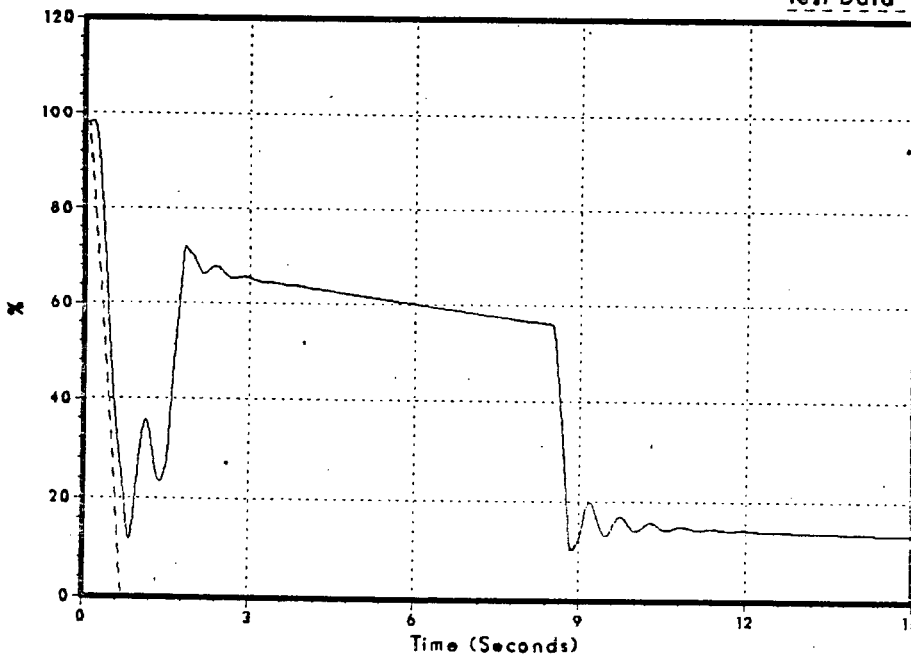


Figure 3.2-125
Main Steam Line Flow

DNB038/86

Test Data



NSP

Monticello Cycle 1 Turbine Trip Startup Test

Figure 3.2-126
Feedwater Flow

DNB038/B6

Test Data

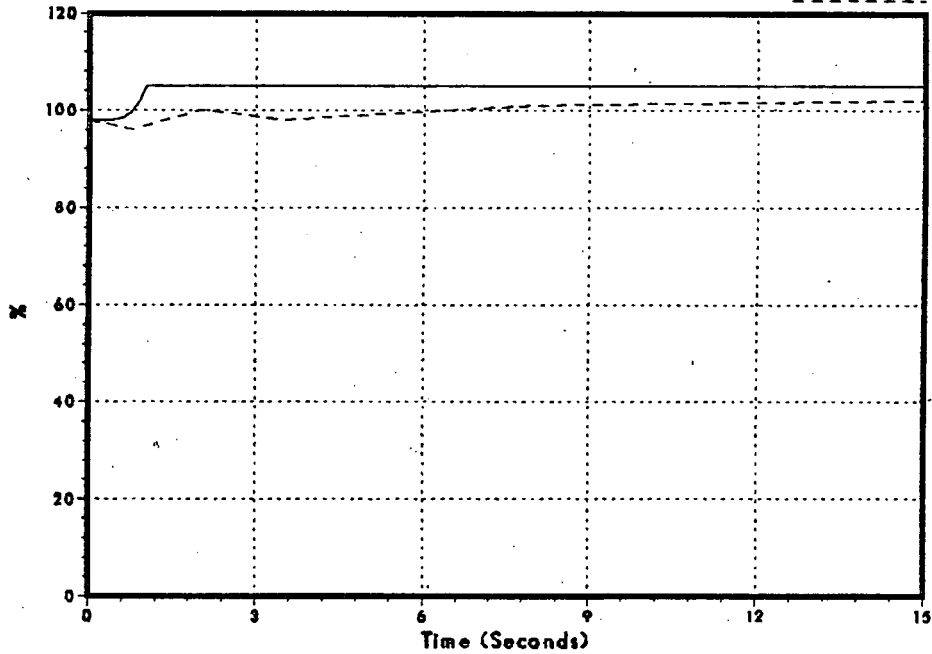
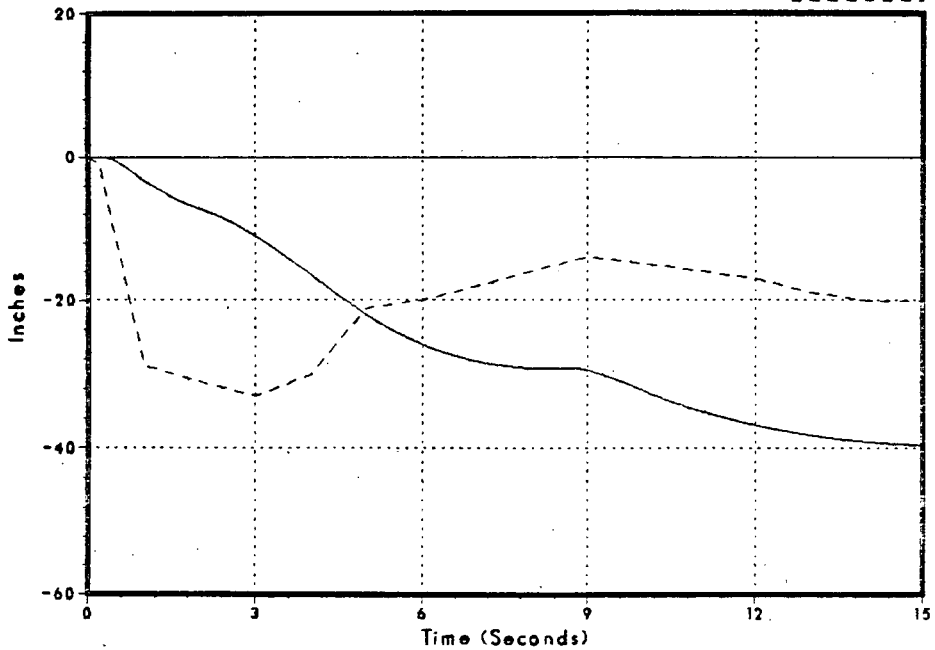


Figure 3.2-127
Sensed Reactor Water Level

DNB038/B6

Test Data



Monticello Cycle 1 4/4 MSIV Closure Startup Test

Figure 3.2-128
Steam Dome Pressure

DNB035/86

Test Data

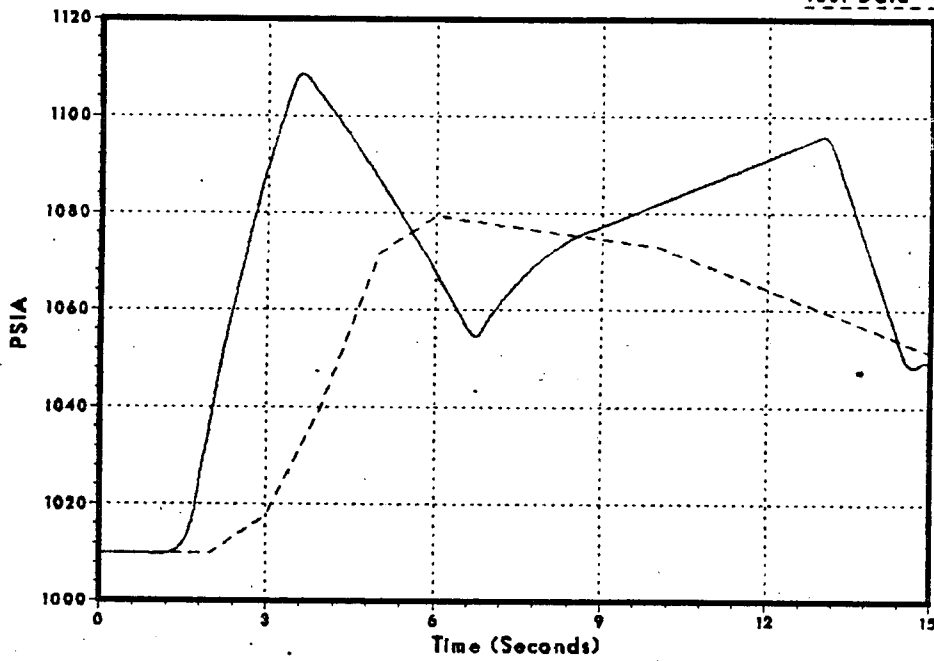
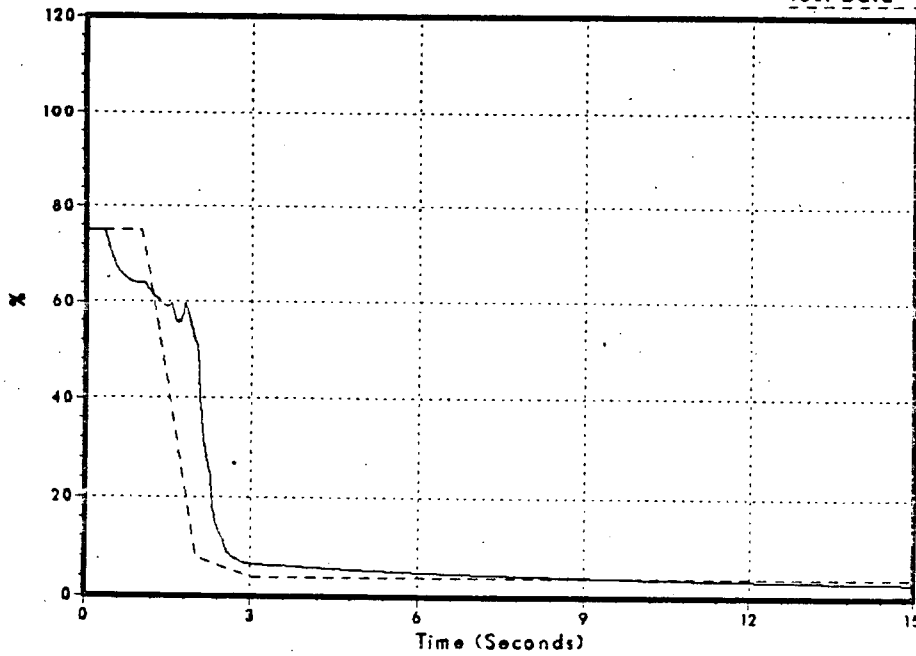


Figure 3.2-129
Relative Power

DNB035/86

Test Data



NSP

Monticello Cycle 1 4/4 MSIV Closure Startup Test

Figure 3.2-130
Steam Dome Water Level

DNB035/86

Test Data

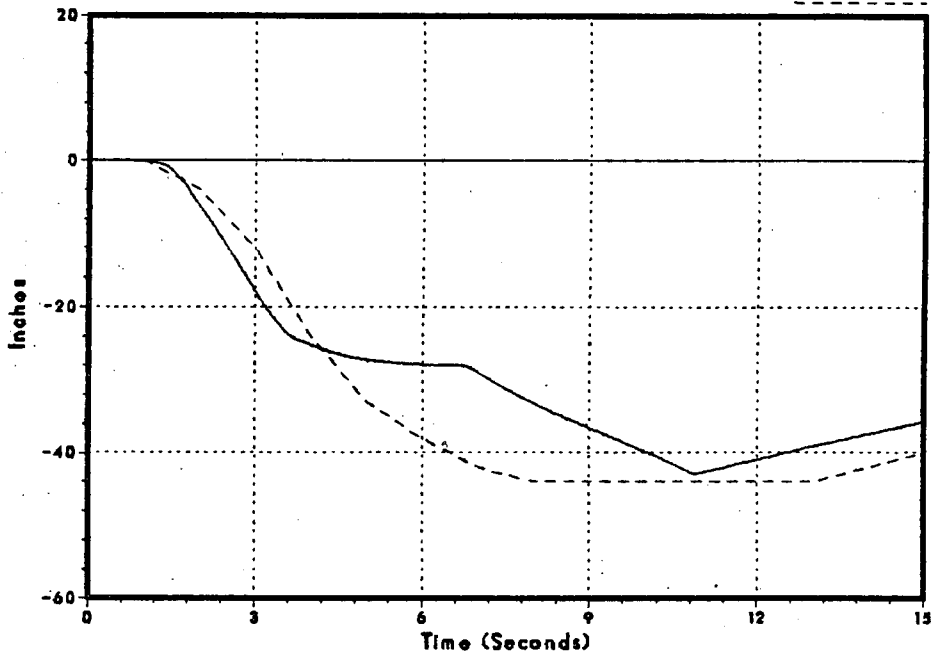
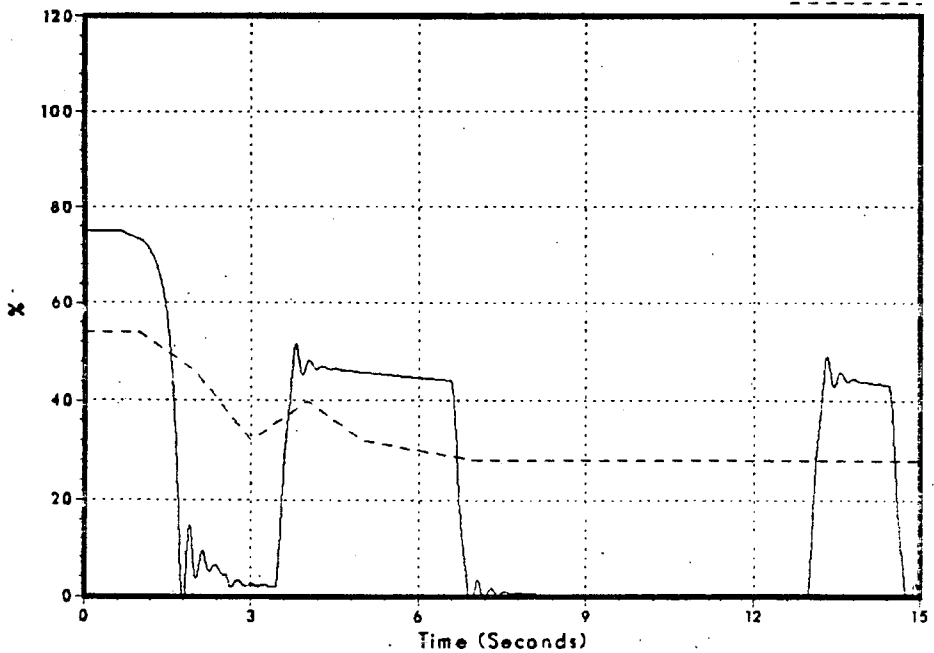


Figure 3.2-131
Main Steam Line Flow

DNB035/86

Test Data

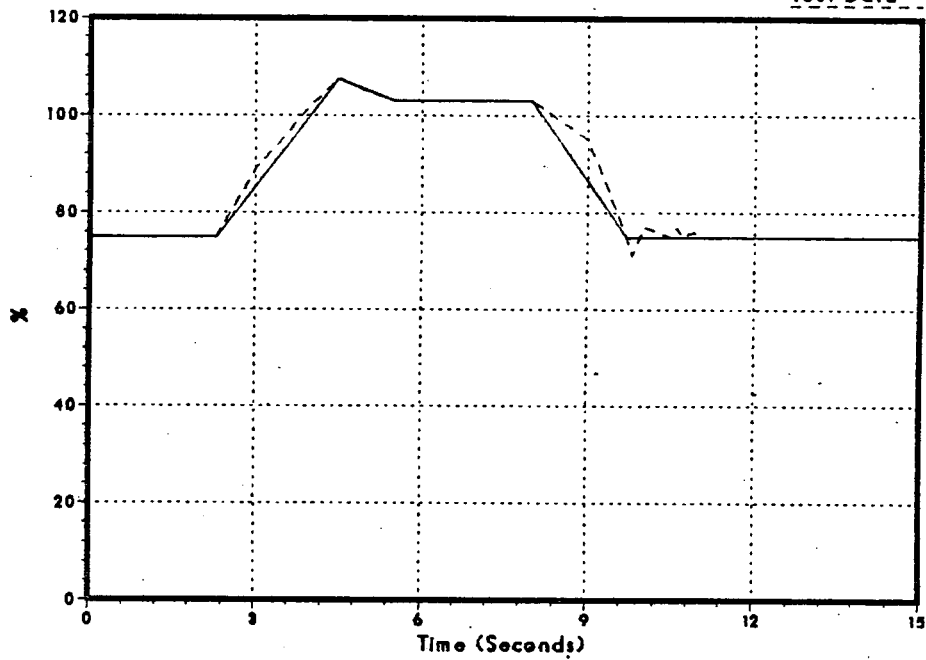


Monticello Cycle 1 4/4 MSIV Closure Startup Test

Figure 3.2-132
Feedwater Flow

DNB035/86

Test Data



Monticello Cycle 1 2/2 Pump Trip Startup Test

Figure 3.2-133
Total Vessel Flow Rate

DNB036/86

Test Data

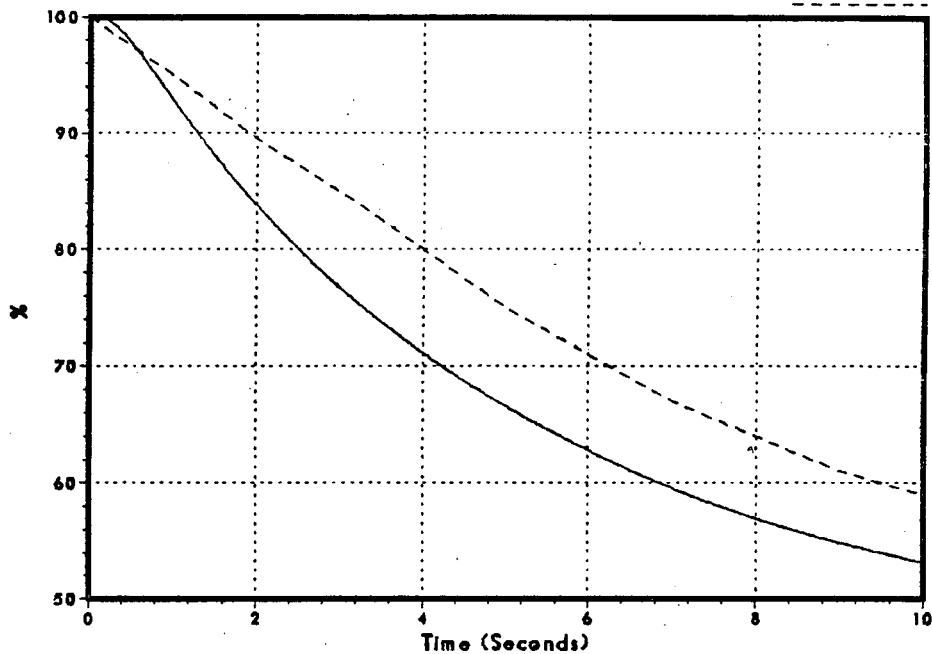
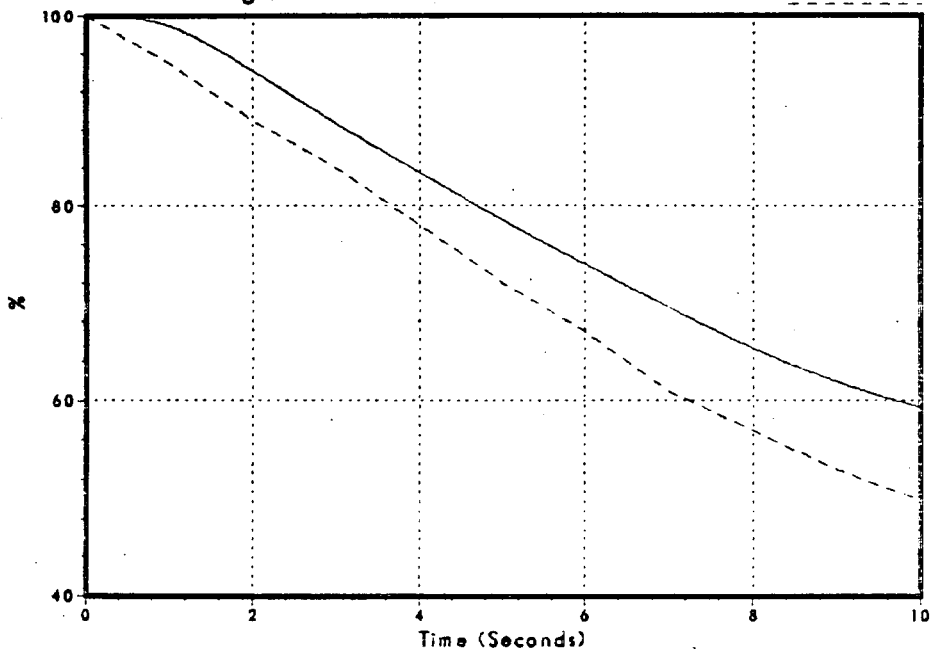


Figure 3.2-134
Core Average Heat Flux

DNB036/86

Test Data



Monticello Cycle 1 Auto Flow Decrease Startup Test

Figure 3.2-135
Steam Dome Pressure

DNB037/86

Test Data

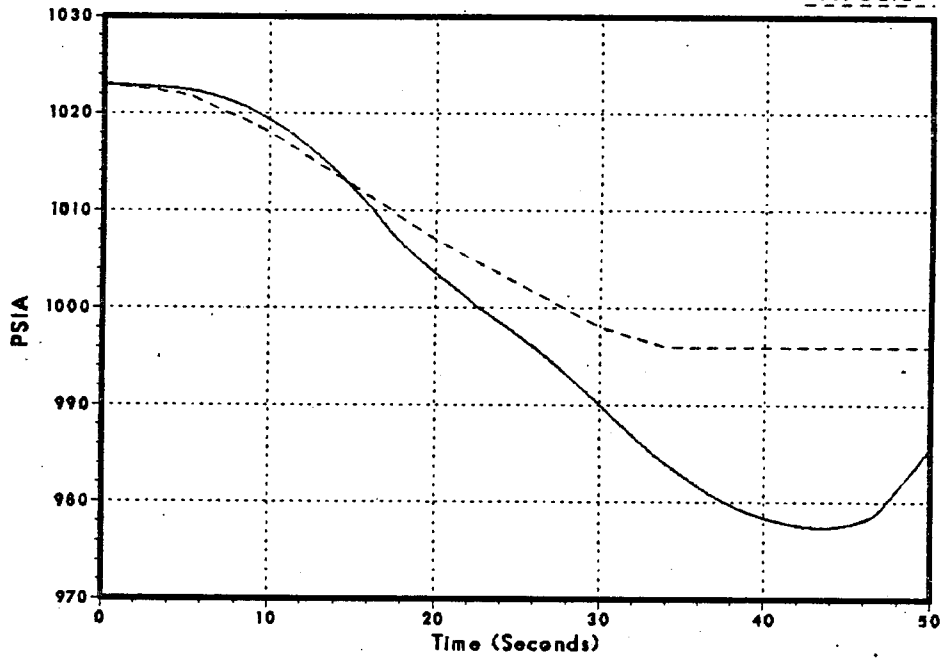
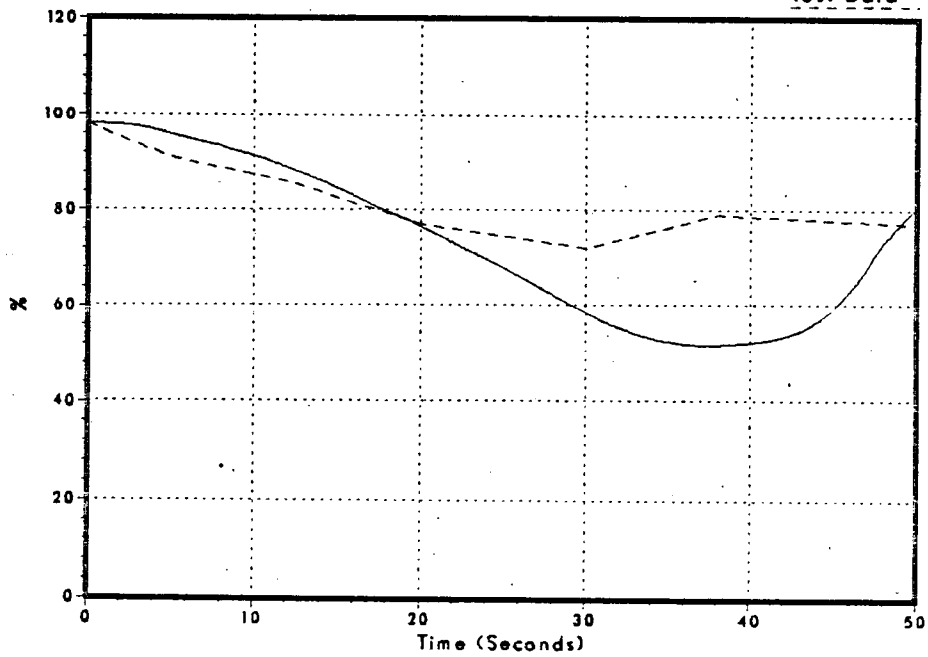


Figure 3.2-136
Relative Power

DNB037/86

Test Data



NSP

Monticello Cycle 1 Auto Flow Decrease Startup Test

Figure 3.2-137
Main Steam Line Flow

DNB037/86

Test Data

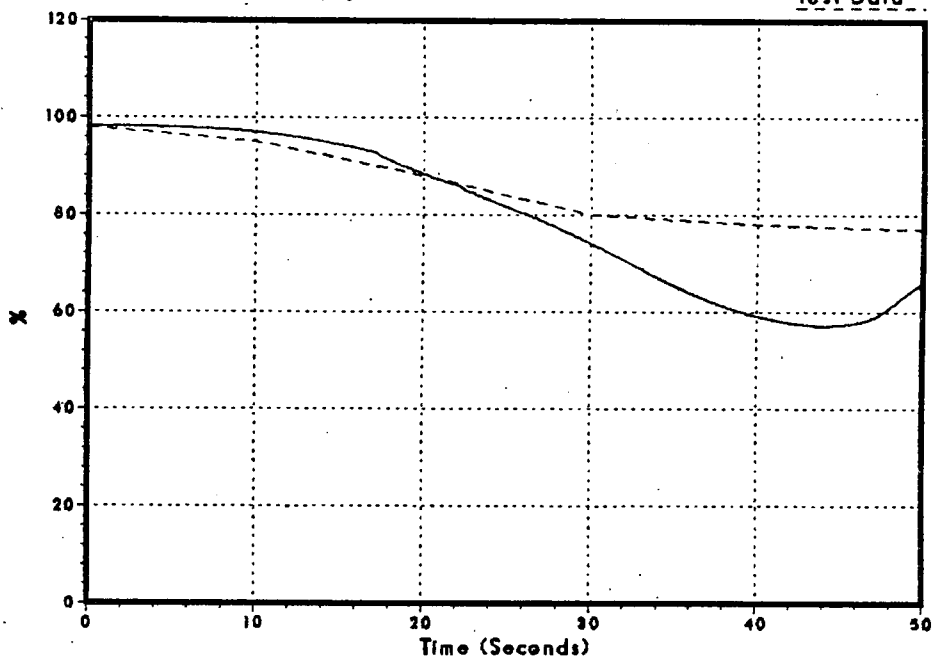
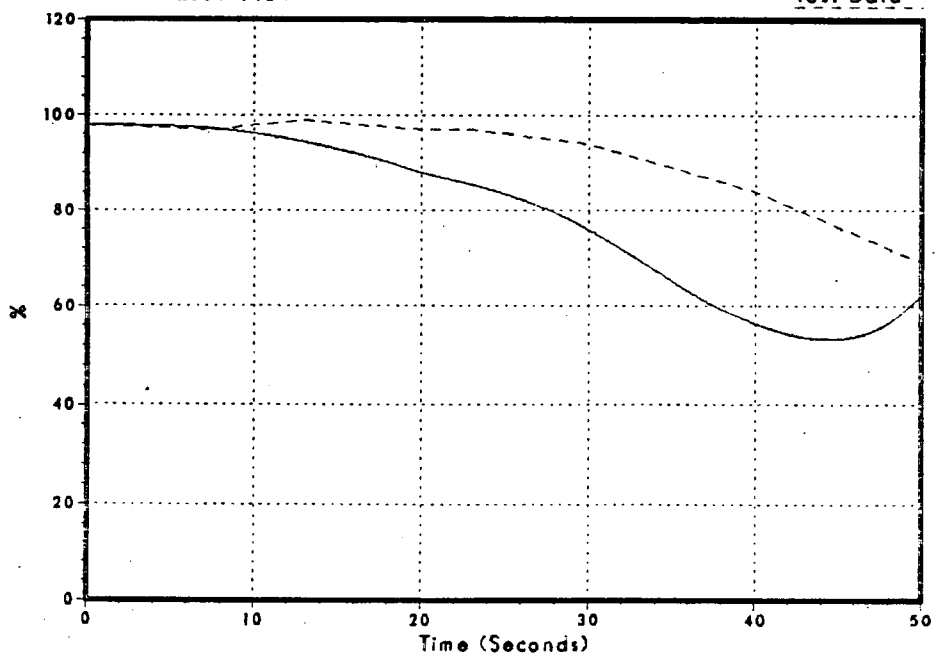


Figure 3.2-138
Feedwater Flow

DNB037/86

Test Data



NSP

Monticello Cycle 1 Auto Flow Decrease Startup Test

Figure 3.2-139
Sensed Reactor Water Level

DNB037/86

Test Data

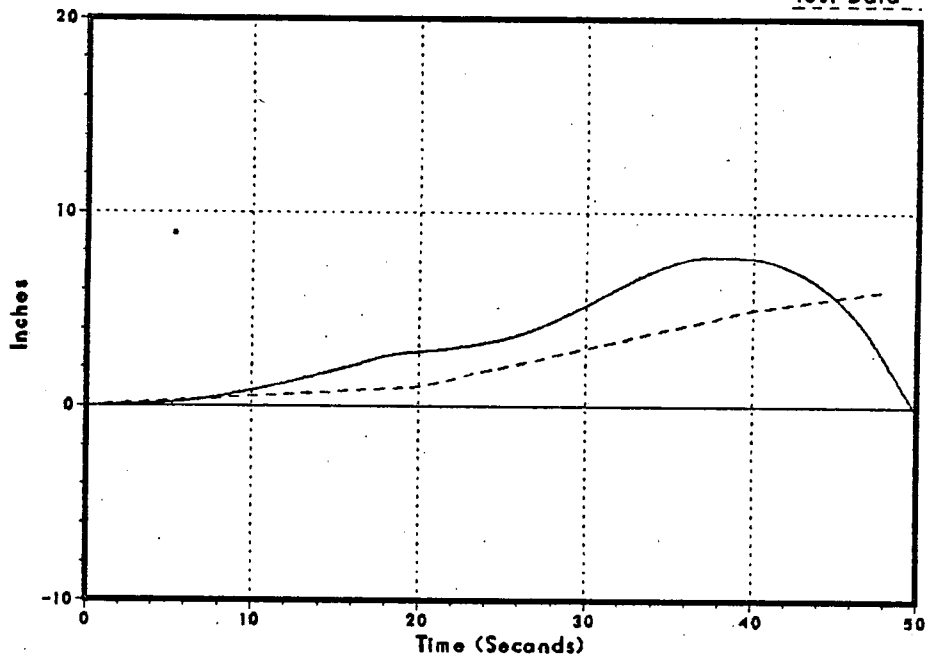
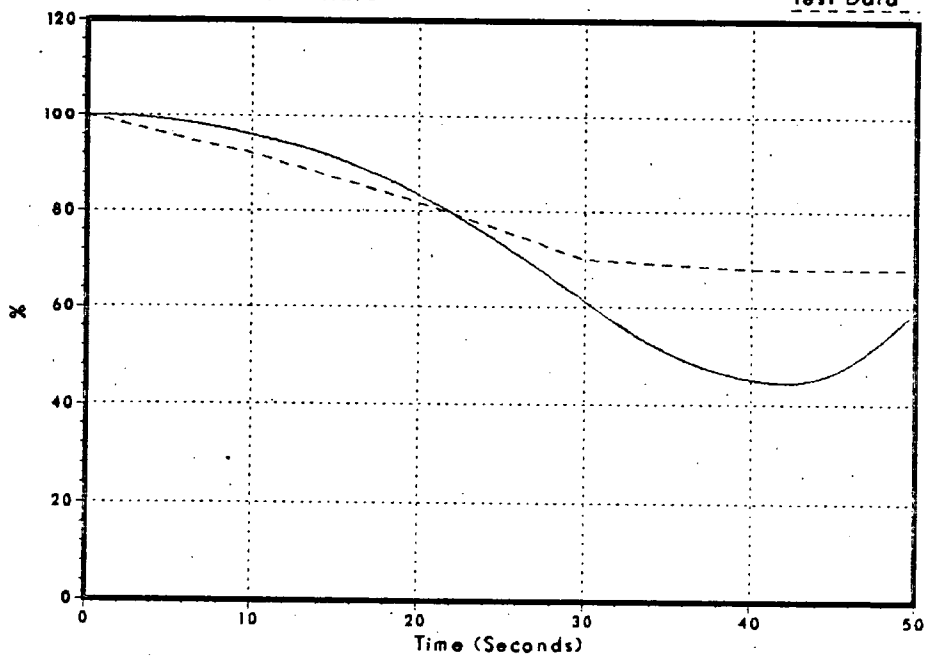


Figure 3.2-140
Total Vessel Flow Rate

DNB037/86

Test Data



NSP

Monticello Cycle 1 Pressure Step Startup Test

Figure 3.2-141
Steam Dome Pressure

DNB039/86

Test Data

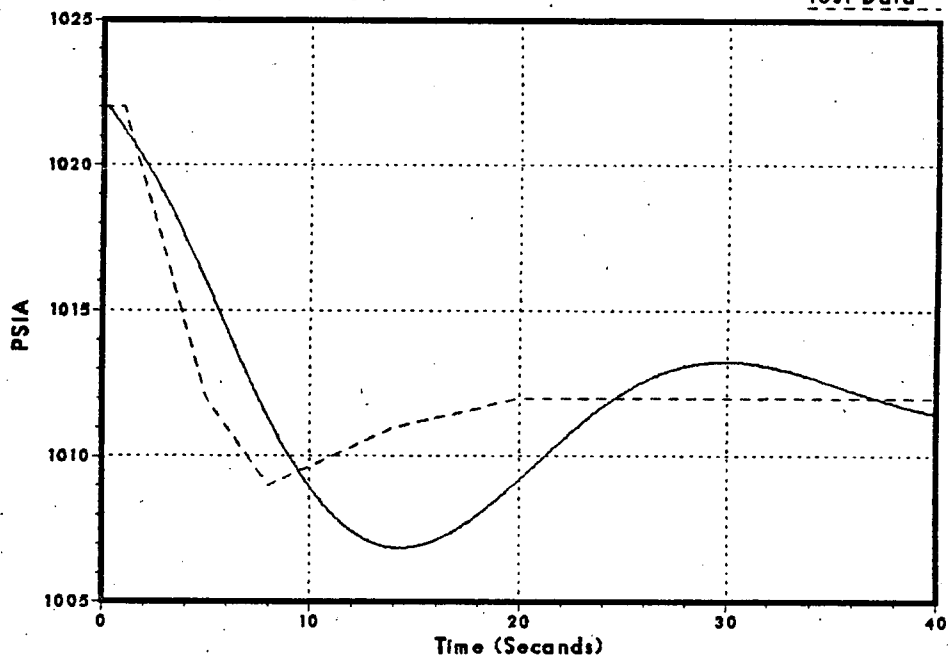
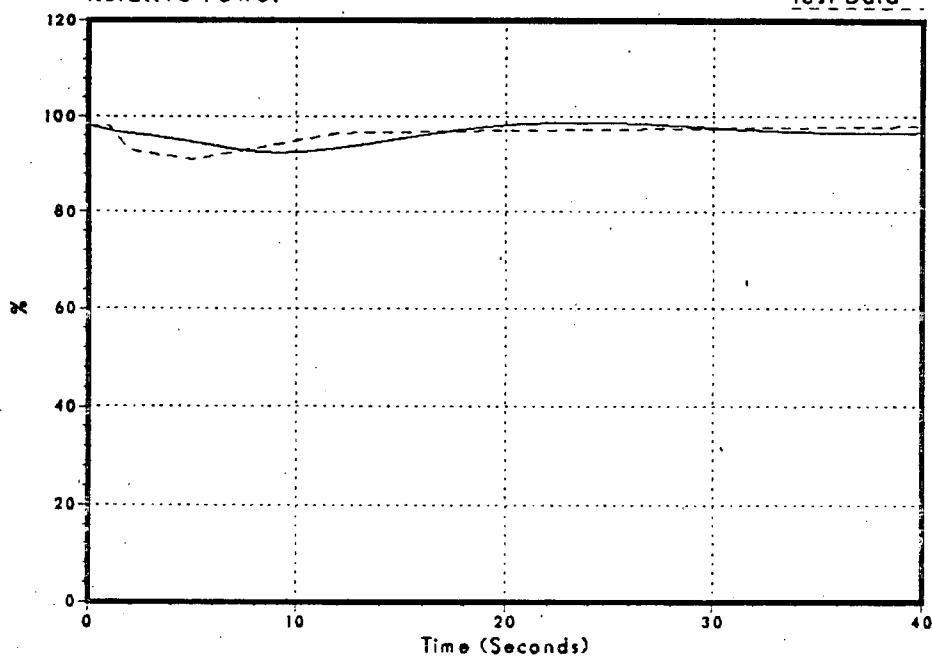


Figure 3.2-142
Relative Power

DNB039/86

Test Data



NSP

Monticello Cycle 1 Pressure Step Startup Test

Figure 3.2-143
Main Steam Line Flow

DNB039/86

Test Data

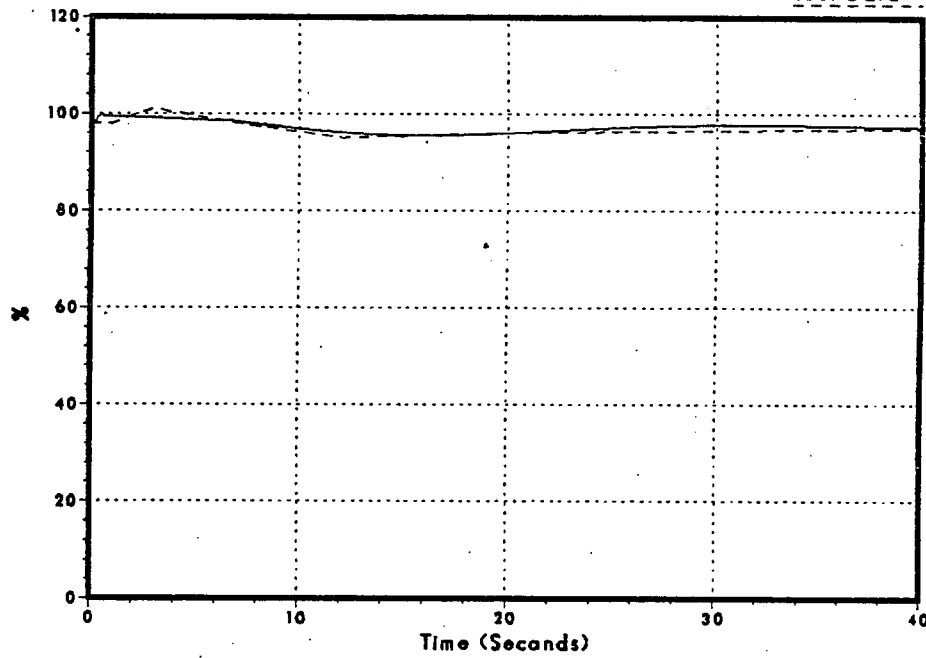
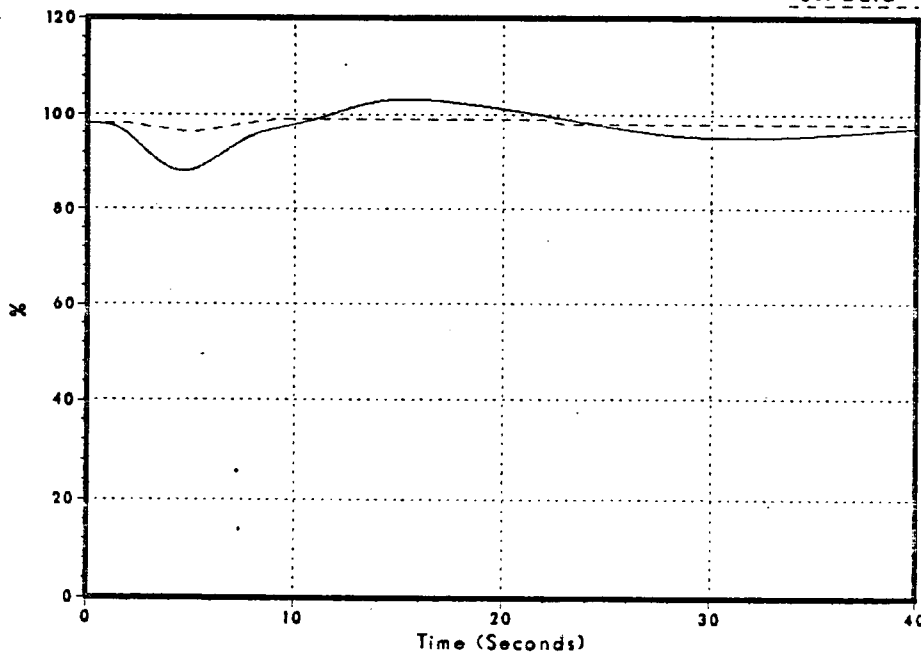


Figure 3.2-144
Feedwater Flow

DNB039/86

Test Data



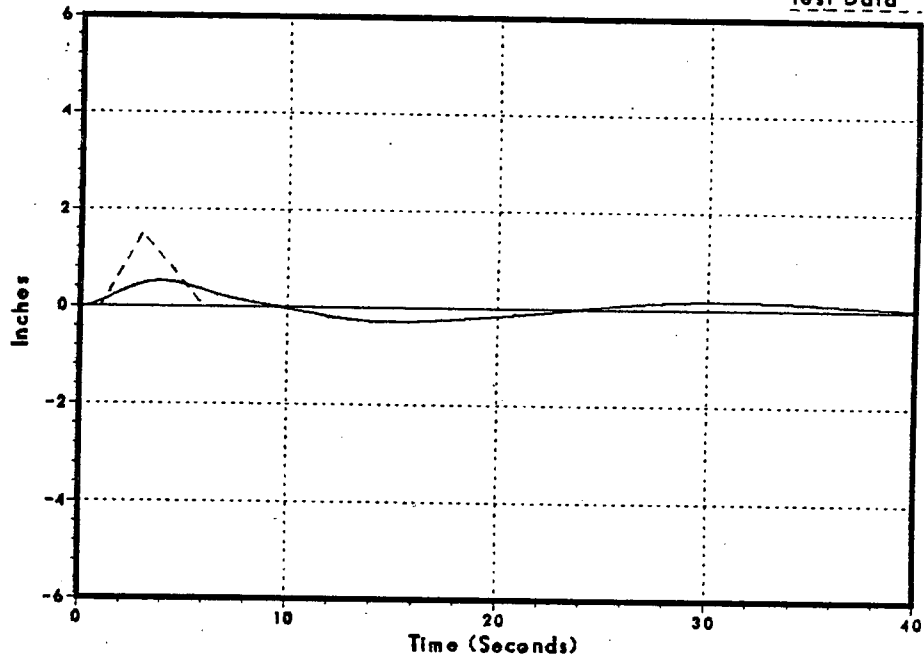
NSP

Monticello Cycle 1 Pressure Step Startup Test

Figure 3.2-145
Sensed Reactor Water Level

DNB039/86

Test Data



Monticello Cycle 1 FW Level Setpoint Step Startup Test

Figure 3.2-146
Steam Dome Pressure

DNB040/86

Test Data

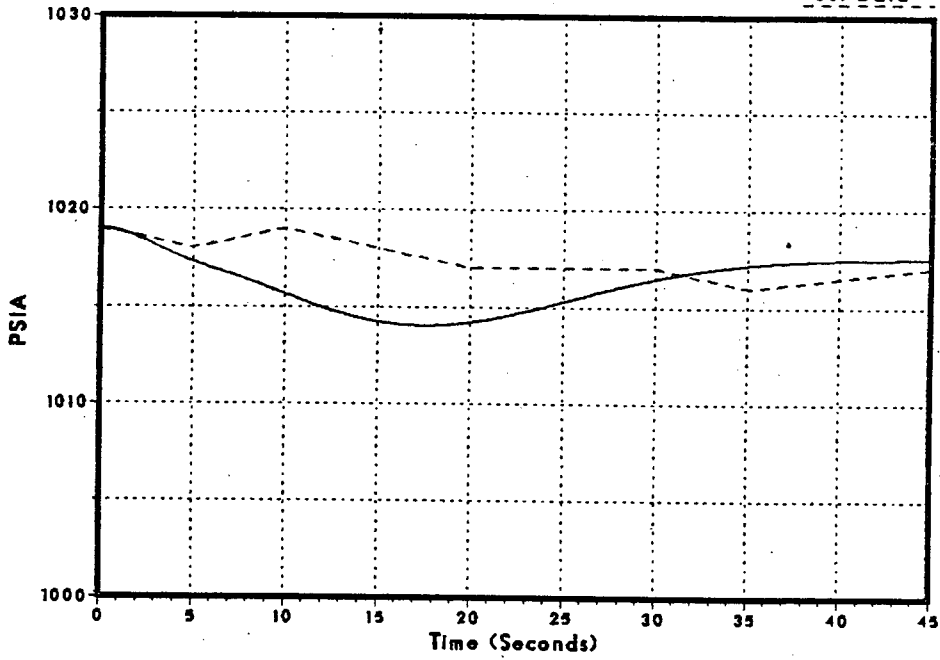
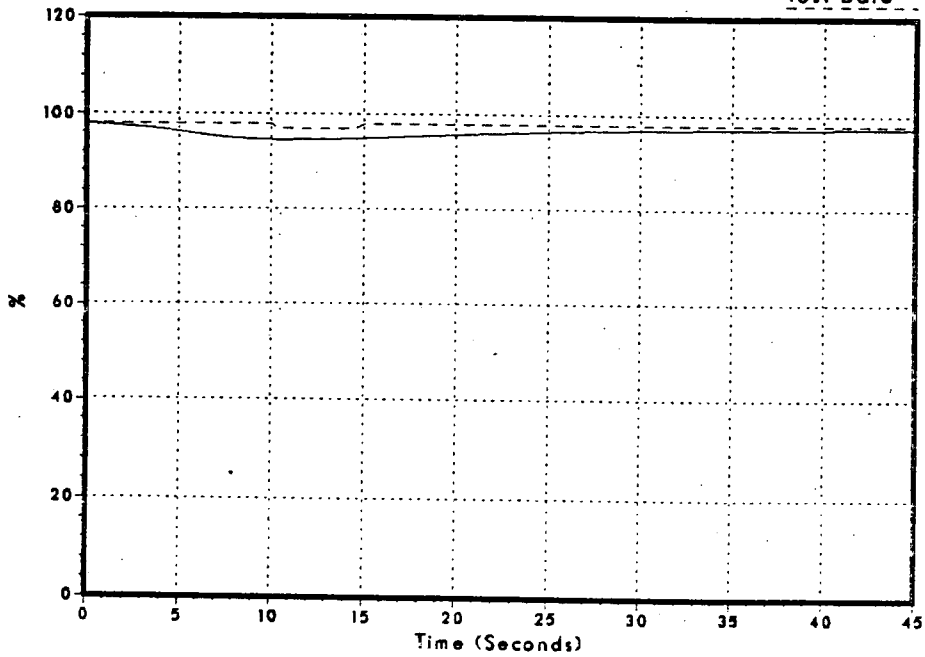


Figure 3.2-147
Relative Power

DNB040/86

Test Data



NSP

Monticello Cycle 1 FW Level Setpoint Step Startup Test

Figure 3.2-148
Feedwater Flow

DNB040/86

Test Data

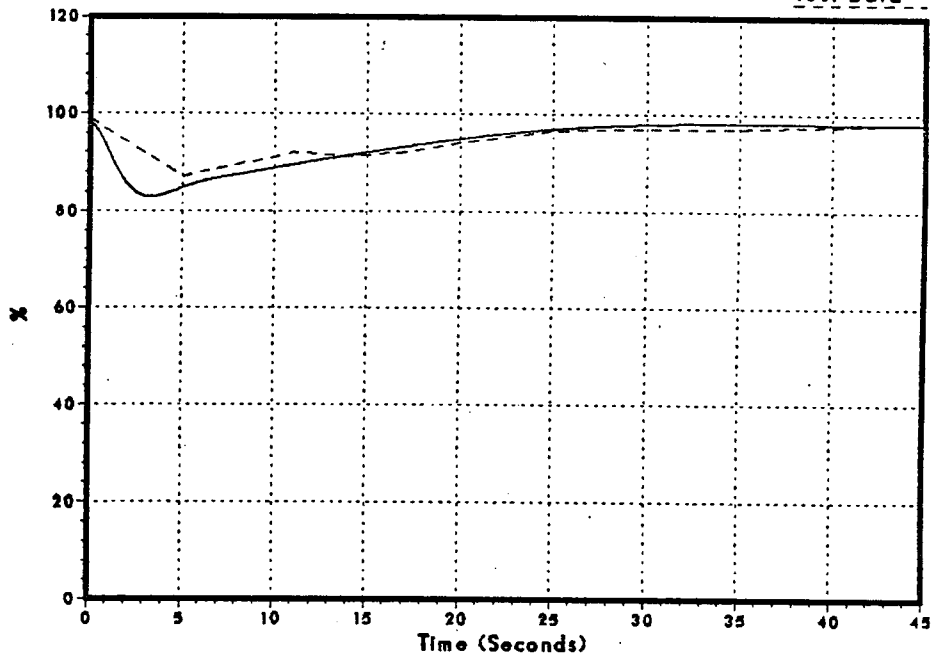
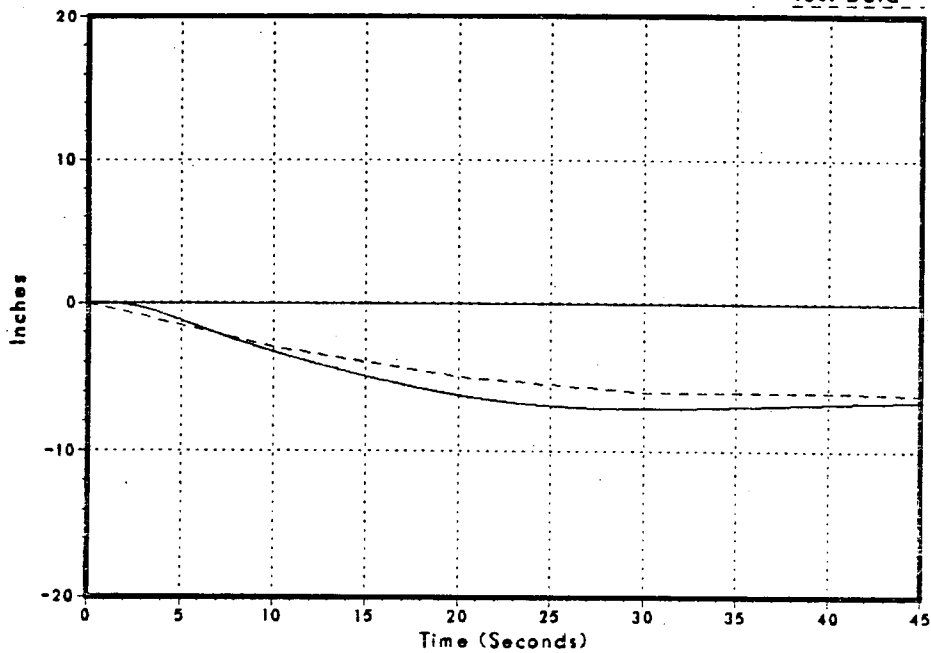


Figure 3.2-149
Sensed Reactor Water Level

DNB040/86

Test Data



NSP

4.0 RELOAD SAFETY EVALUATION METHODS

This section provides a description of the methodology used by the Northern States Power Company Nuclear Analysis Department (NSPNAD) to perform licensing analyses. These analyses will be used, in conjunction with analyses performed by the fuel vendor, to establish reactor operating limits and to demonstrate acceptable margin to established safety limits.

The NSPNAD BWR methodology is a deterministic approach which parallels the NSPNAD PWR methodology (Reference 17). The major components which describe these methods are:

- The spectrum of events covered by this submittal and the models used to simulate those events.
- The input parameters used.
- The applicable limiting acceptance criteria.
- Evaluation and application of uncertainties

These elements are discussed in detail in the following sections.

4.1 MODEL/EVENT APPLICATION

Tables 4.1-1, 4.1-2, and 4.1-3 summarize the standard spectrum of events covered by abnormal transient evaluations and the intended application of this document.

Included in Tables 4.1-1, 4.1-2, and 4.1-3 is a determination of the kinetics model used for each type of transient; i.e. point or 1-D (space-time). The kinetics model is the only code model which is dependent on event application. Table 4.1-4 summarizes the models used for licensing calculations.

The selection of a particular model, for application to licensing analysis, was based on the benchmark analyses presented in Section 3, as well as consultation with the primary code author, Dr. Richard Kern (Utility Associates International).

The philosophy used in selecting events for which the 1-D kinetics model will be applied, as opposed to the point kinetics model, was to evaluate the event phenomena with respect to the core axial behavior. Those transients which display a high degree of axial significance, e.g. overpressure transients, require a 1-D kinetics model in order to properly account for the event phenomena. The remaining transients, for which a point kinetics model will be used, do not require the more complex one-dimensional solution. Experience shows that the point kinetics model can accurately predict these remaining events.

Table 4.1-1 includes a determination of those events which are typically thermally limiting. In order to determine the limiting transient events, with respect to CPR, the relative dependency of CPR upon various thermal-hydraulic parameters was examined using the GEXL correlation. A sensitivity study was performed to determine the effect, over a range of nominal $\pm 10\%$, of changes in bundle power, bundle flow, core inlet subcooling, core pressure, and R-factor. The results of this study are presented in Table 4.1-5 for 8x8 fuel. Included in this table are the General Electric generic results from Reference 7, for the same fuel type.

As can be seen from this study, the DYNODE-B results compare favorably with the GE results, indicating the correct application of the GEXL correlation. CPR is seen to be most sensitive to changes in the R-factor and bundle power. A slight sensitivity to core pressure and core flow is also shown, as well as relative independence to core inlet subcooling.

The R-factor is a function of bundle geometry and local pin power distribution and is assumed to remain constant throughout each transient. Therefore, transients which are thermally limiting are those that produce significant increases in power. These are identified in Table 4.1-1. Previous Monticello Reload analyses, performed by GE, verify this list.

4.2 INPUT PARAMETERS

This section describes the selection of input parameters for application to licensing analyses.

Table 4.2-1 summarizes the input parameters for Monticello. Note that some transients are initiated at an operating point other than the 100% flow/100% power point indicated by Table 4.2-1. The initial operating point is selected to maximize the transient response. Measurement uncertainties are discussed in Section 4.4.

Equipment response; e.g. scram setpoints and delays, relief valve setpoints and delays, and valve closure stroke times; are set at the most conservative value specified in the Technical Specifications (Reference 12).

The kinetics parameters, CRD scram time, and CPR model inputs are discussed in the following sections.

4.2.1 KINETICS PARAMETERS

This section describes the methods used in applying conservative reliability factors and biases to the input kinetics parameters. Reference 1 describes the procedures used for determination of these factors. It is not the intent of this section to redefine the procedures used in Reference 1. However, some aspects of these procedures are presented here in order to clarify the approach taken in applying the model reliability factors and biases.

For each parameter of interest, the model reliability factor, RF_x , is applied in the conservative direction. Therefore, the direction of application is dependent on the transient being analyzed as well as on the intended licensing application. This determination is made on a case-by-case basis in order to produce the most conservative results.

In general, the magnitude and application of the reliability factor, RF_x , and bias is independent of the kinetics model used in the transient analysis, i.e., point or 1-D. However, in the case of the 1-D kinetics model, an additional uncertainty is introduced due to the collapsing procedure used in going from 3-D to 1-D. This "collapsing" uncertainty is applied to the void reactivity and the scram reactivity, since these represent the major reactivity feedback mechanisms for a BWR.

4.2.1.1 BUNOLE POWER

Bundle powers are used in the DYNODE-B hot channel model to calculate Critical Power Ratio. The bundle powers are calculated using the three-dimensional nodal model (Reference 1).

The model reliability factor and bias are applied as follows:

$$P(I,J) = P(I,J)(MODEL) * (1 + RF_{RPF}) * (1 + Bias) ;$$

where

$P(I,J)(MODEL)$ = Absolute bundle power in assembly (I,J) as calculated by the 3-D nodal model.

Bias = 0.0 (Ref. 1).

RF_{RPF} = 0.081 (Ref. 1).

The model reliability factor and bias are updated every cycle and the results documented in the Reload Safety Evaluation for that cycle.

4.2.1.2 CONTROL ROD WORTHS

Rod worths are calculated using the three-dimensional nodal model (Reference 1). Worths are determined by varying the rod position, while the independent core parameters, such as core power, flow, and void distribution, are held constant.

The model reliability factor and bias are applied as follows:

$$\Delta K_{ROO} = \Delta K_{ROD} (\text{MODEL}) * (1 + \text{Bias}) * (1 \pm \text{RF}_{ROD}) ;$$

where

$$\begin{aligned} \Delta K_{ROD} (\text{MODEL}) &= \text{Rod Worth.} \\ \text{Bias} &= 0.0 \text{ (Ref. 1).} \\ \text{RF}_{ROD} &= 0.10 \text{ (Ref. 1).} \end{aligned}$$

The model reliability factor and bias are updated every cycle and the results documented in the Reload Safety Evaluation for that cycle.

The rod worth scram reactivity is input to the transient model as a function of the total rod worth, ΔK_{ROD} , as follows:

$$\Delta K_{SCRAM_K} = \sum_I \Delta K_{ROD_I} * CF_{I,K} * \text{RWD}_K * (1 \pm \text{AF}_{\text{COLLAPSE}_{I,K}}) ;$$

where

$$\begin{aligned} \Delta K_{SCRAM_K} &= \text{Rod worth scram reactivity in axial node K.} \\ CF_{I,K} &= \text{Source weighted control fraction of bank I in axial node K.} \end{aligned}$$

$$\text{RWD}_K = \text{Relative rod worth in axial node K.}$$

$$\begin{aligned} \text{AF}_{\text{COLLAPSE}_{I,K}} &= \text{Adjustment factor to account for 3-D to 1-D} \\ &\quad \text{collapsing error of bank I in axial node K} \geq 0. \\ &= 0 \text{ for point kinetics.} \end{aligned}$$

4.2.1.3 VOID REACTIVITY

For 1-D kinetics application, void reactivity effects are modeled in DYNODE-B via changes in K^{∞} and M^2 relative to an initial transient condition.

The initial transient condition is run with the CASMO/NDH model (Reference 1). Thus the source, power, K^{∞} , and M^2 distributions are known throughout the core. The CASMO/NDH initial case is then perturbed. The differences in the values of the effective 1-D K^{∞} and M^2 distributions between the perturbed and initial cases are computed. In a similar manner, DYNODE-B is run for the initial and perturbed conditions. From the results, $\Delta K^{\infty}/\Delta U$ and $\Delta M^2/\Delta U$ are constructed as a function of U, where U is the relative water density obtained from DYNODE-B. These curves are integrated to obtain K^{∞} vs U and M^2 vs U curves which are input to DYNODE-B.

The model reliability and bias are applied to the $\Delta K^{\infty}/\Delta U$ function prior to integration, as follows:

$$\Delta K^{\infty}/\Delta H * (1 + \text{Bias}) * (1 \pm \text{RF}_{\text{VOIDS}}) * (1 \pm \text{AF}_{\text{COLLAPSE}}) ;$$

where

$$\begin{aligned} \text{RF}_{\text{VOIDS}} &= 0.10 \text{ (Ref. 1).} \\ \text{Bias} &= 0.0 \text{ (Ref. 1).} \\ \text{AF}_{\text{COLLAPSE}} &= \text{Adjustment factor to account for 3-D} \\ &\quad \text{to 1-D collapsing error } \geq 0. \end{aligned}$$

For point kinetics application, the reliability factor is applied as follows:

$$\alpha_v = \alpha_v (\text{MODEL}) * (1 + \text{Bias}) * (1 \pm \text{RF}_{\text{VOIDS}}) ;$$

where

$$\alpha_v (\text{MODEL}) = \text{Void reactivity coefficient}$$

and α_v is based on the CASMO/NDH K^{eff} changes and the corresponding DYNODE-B core average void fraction changes. The model reliability factor and bias are updated every cycle and the results documented in the Reload Safety Evaluation for that cycle.

4.2.1.4 DOPPLER COEFFICIENT

The Doppler coefficient is a measure of the change in core multiplication associated with a change in fuel temperature. Core reactivity is changed mainly due to Doppler broadening of the U-238 parasitic resonance absorption cross section due to increases in fuel temperature. For 1-D kinetics application, this effect is calculated by running CASMO/NDH cases (Reference 1) and DYNODE-B cases to develop a $\Delta K^\infty U^0 / \Delta t_f^{1/2}$ versus $t_f^{1/2}$ curve, where U^0 is the initial relative water density and t_f is the fuel temperature obtained from DYNODE-B.

The model reliability factor and bias are applied at each point as follows:

$$(\Delta K^\infty U^0 / \Delta t_f^{1/2}) * (1 + \text{Bias}) * (1 \pm \text{RF}_D) ;$$

where

$$\text{RF}_D = 0.10 \text{ (Ref. 1).}$$

$$\text{Bias} = 0.0 \text{ (Ref. 1).}$$

This distribution is then integrated to obtain the K^∞ vs $t_f^{1/2}$ curve that is input to the transient code.

For point kinetics application, the reliability factor is applied as follows:

$$\alpha_D = \alpha_D(\text{MODEL}) * (1 + \text{Bias}) * (1 \pm \text{RF}_D) ;$$

where

$$\alpha_D(\text{MODEL}) = \text{Doppler reactivity coefficient}$$

and α_D is based on the CASMO/NDH K^{eff} changes and the corresponding DYNODE-B core average fuel temperature changes. The model reliability factor and bias are updated every cycle and the results documented in the Reload Safety Evaluation for that cycle.

4.2.1.5 DELAYED NEUTRONS

For 1-D kinetics application, the delayed neutron group dependent constants; β_i and λ_j ; are assumed to be uniform throughout the core and constant in time in DYNODE-B. The total delayed neutron fraction, β , is assumed to be spatially distributed and constant in time in DYNODE-B. The use of constant delay neutron constants corresponding to the initial conditions is justified by the results in Reference 22, which show that β_{eff} does not change significantly during a transient until the scram is over. Radial source weighting is used to obtain these constants to be consistent with the transient source solution used in DYNODE-B. The local values of β_i to be used in the weighting are the values taken directly from the infinite lattice calculations (CASMO) (Reference 1) without any spectral importance weighting.

Spectral importance weighting is unnecessary because the DYNODE-B source equations relate to the integral of the source over the entire energy spectrum so that the importance of the delayed neutrons does not depend on the energy at which they are born with respect to total source.

The axial-dependent total β 's which are entered into DYNODE-B are obtained by source weighting of the $\Sigma\beta_i$ over the radial direction at each axial level so that:

$$\beta_K(\text{MODEL}) = \frac{\sum_R S_{\ell} \sum_i \beta_i^{\ell}}{\sum_R S_{\ell}}$$

The reliability factor is applied as follows:

$$\beta_K = \beta_K(\text{MODEL}) * (1 \pm RF_{\beta}) ;$$

where

$\beta_K(\text{MODEL})$ = Delayed neutron fraction at axial level K.

$RF_{\beta} = 0.04$ (Ref. 1).

For point kinetics application, the reliability factor is applied as follows:

$$\beta_{\text{eff}} = \beta_{\text{eff}}(\text{MODEL}) * (1 \pm \text{RF}_{\beta}) .$$

The model reliability factor and bias are updated every cycle and the results documented in the Reload Safety Evaluation for that cycle.

4.2.1.6 NEUTRON SOURCE LIFETIME

In the transient model for 1-D kinetics applications, the neutron source lifetime is assumed to be spatially distributed and constant in time and is defined as:

$$\ell_K^* = (1/V\nu\Sigma_f)_K$$

where V is the velocity of the source neutrons (cm/s) and source averaging over the radial plane is used for consistency with the transient source solution used in DYNODE-B.

The neutron source lifetime is calculated in the CASMO/NDH model (Reference 1) in each node ℓ from a curve fit of $(V\nu\Sigma_f)_\ell$ as a function of exposure, moderator density, and control fraction for each fuel type. ℓ_K^* is then source weighted as follows:

$$\ell_K^*(\text{MODEL}) = \frac{\sum_R S_\ell}{\sum_R (V\nu\Sigma_f)_\ell} / \frac{\sum_R S_\ell}{\sum_R}$$

The reliability factor is applied as follows:

$$\ell_K^* = \ell_K^*(\text{MODEL}) * (1 \pm \text{RF}_\ell^*);$$

where

$$\ell_K^*(\text{MODEL}) = \text{Neutron source lifetime at axial level K.}$$

$$\text{RF}_\ell^* = 0.04 \quad (\text{Ref. 1}).$$

For point kinetics applications, the reliability factor is applied as follows;

$$\ell^* = \ell^*(\text{MODEL})^* (1 \pm \text{RF}_\ell^*)$$

The model reliability factor and bias are updated every cycle and the results documented in the Reload Safety Evaluation for that cycle.

4.2.2 CRD SCRAM TIME

The mean scram time assumed in the analysis must be greater than the measured weighted cycle average scram time at a 95% confidence level for all points in the cycle. This determination is made at the 20% insertion position (~ notch 38).

That is :

$$\tau_{AVE} \leq \tau_D ;$$

where

τ_{AVE} = weighted cycle average scram time at a 95% confidence level.

τ_D = mean scram time assumed in the DYNODE-B analysis.

and

$$\tau_{AVE} = \left[\left(\sum_{i=1}^n N_i \tau_i \right) / \sum_{i=1}^n N_i \right] + \left[0.0875 \left(N_1 / \sum_{i=1}^n N_i \right)^{1/2} \right]$$

n = the number of surveillance tests performed to date in this cycle.

N_i = number of control rods measured in the i th test.

τ_i = average scram time to the 20% insertion position of all rods measured in the i th test.

N_1 = total number of active rods measured in the first test following core alterations.

$0.0875 = 1.65 * 0.053$; where 1.65 is the appropriate statistical number to provide a 95% confidence level, and 0.053 is the standard deviation of the distribution 20% position. This latter factor is based on extensive plant measurements by General Electric and is documented in Reference 21.

The transient analyses will be performed with a spectrum of scram times, allowing the plant to take full credit for the measured scram times. The spectrum of analysis scram times will be performed at small enough intervals to allow a linear interpolation of results.

4.2.3 CRITICAL POWER RATIO

Critical Power Ratio is calculated using the General Electric BWR Thermal Analysis Basis (GETAB) (Reference 18, 19 and 20). The GEXL correlation was obtained from General Electric for use by Northern States Power as a part of the current fuel contract.

The GEXL correlation has been incorporated into the DYNODE-B hot channel model. Input to this model consists of; the bundle average radial peaking factor, the relative bundle inlet flow, the bundle initial pressure and inlet enthalpy, the bundle R-factor, and the axial power distribution. The axial power distribution used in the analysis is given in Table 4.2-2 which is taken from Reference 7. The R-factors are supplied by General Electric.

The bundle average radial peaking factor and the relative bundle inlet flow factor are assumed constant throughout the transient and are calculated from the three-dimensional simulator (Ref. 1) with the appropriate uncertainties included (See Section 4.2.1.1). The GEXL correlation safety limit (See Section 4.3.1) includes an 8.7 percent (one standard deviation) uncertainty on TIP readings. As long as the NSPNAD determined bundle power model reliability factor (See Section 4.2.1.1) is less than 8.7 percent no additional uncertainty need be applied.

Proper programming and use of the GEXL correlation was tested by comparing steady state CPR values for the fuel types of interest. Small differences will exist between the GE and DYNODE-B values due to a slight difference in the water property tables used. These comparisons are shown in Table 4.2-3. Further comparisons are also shown in Table 4.1-5.

These comparisons show that NSPNAD has properly implemented the GEXL correlation and that it can be used, along with the associated safety limit (See Section 4.3.1), in licensing calculations.

4.3 LIMITING ACCEPTANCE CRITERIA

Limits on plant operation are established to assure that the plant can be safely operated and does not pose any undue risk to the health and safety of the public.

There are three limiting acceptance criteria which must be met for the spectrum of events being analyzed.

4.3.1 THERMAL LIMITS

Reference 5, Section 4.4, "Thermal and Hydraulic Design", Acceptance Criteria 1:

"SRP Section 4.2 specifies the acceptance criteria for evaluation of fuel design limits. One of the criteria provides assurance that there be at least a 95% probability at a 95% confidence level that the hot fuel rod in the core does not experience a departure from nucleate boiling (DNB) or transition condition during normal operation or anticipated operational occurrence.

Uncertainties in the values of process parameters, core design parameters, and calculational methods used in the assessment of thermal margin should be treated with at least a 95% probability at a 95% confidence level."

An acceptable approach to meet this criterion is given as:

"For DNBR, CHF or CPR correlations, the limiting (minimum) value of DNBR, CHF, or CPR is to be established such that at least 99.9% of the fuel rods in the core would not be expected to experience departure from nucleate boiling or boiling transition during normal operation or anticipated operational occurrences."

A bounding statistical analysis was performed by General Electric [7] to determine the fuel cladding integrity safety limit for 8x8, 8x8R and P8x8R fuel types. The results of the analysis show that at least 99.9% of the fuel rods in the core are expected to avoid boiling transition if the MCPR is equal to or greater than the applicable value listed in Table 4.3-1.

Thus, the thermal limits will be met if

$$\text{MCPR} = \text{ICPR} (1 + \Delta\text{CPR}/\text{ICPR}) \geq \text{MCPR limit}$$

for all normal operation or anticipated operational occurrences.

4.3.2 ASME VESSEL OVERPRESSURIZATION

Reference 5, Section 5.2.2, "Overpressure Protection", Acceptance Criteria A:

"For overpressure protection, during power operation of the reactor, the relief valves shall be designed with sufficient capacity to preclude actuation of safety valves, during normal operational transients, when assuming the following conditions at the plant:

- a. The reactor is operating at licensed core thermal power level.
- b. All system and core parameters are at values within normal operating range that produce the highest anticipated pressure.
- c. All components, instrumentation, and controls function normally.

Safety valves shall be designed with sufficient capacity to limit the pressure to less than 110% of the RCPB design pressure (as specified by the ASME Boiler and Pressure Vessel Code [15]), during the most severe abnormal operational transient and the reactor scrammed. Also, sufficient margin shall be available to account for uncertainties in the design and operation of the plant assuming:

- i. The reactor is operating at a power level that will produce the most severe overpressurization transient.
- ii. All system and core parameters are at values within normal operating range, including uncertainties and technical specification limits that produce the highest anticipated pressure.

- iii. The reactor scram is initiated by the second safety-grade signal from the reactor protection system.
- iv. The discharge flow is based on the rated capacities specified in the ASME Boiler and Pressure Vessel Code [15], for each type of valve."

Compliance with this limit requires that the reactor pressure not exceed 110% of the design pressure ($1.1 * 1250 = 1375$ psig) under upset conditions.

For Monticello, the most limiting upset condition, with respect to reactor pressure, is an MSIV closure transient with a failure of the MSIV position scram, followed by a flux scram and considering one failed S/R valve.

4.3.3 SYSTEM STABILITY

Reference 5, Section 4.4, "Thermal and Hydraulic Design", Acceptance Criteria 3."

"The reactor should be demonstrated to have sufficient margin to be free of undamped oscillations and other thermal-hydraulic instabilities for all conditions of steady-state operation (including part loop operation), and for anticipated operational occurrences."

Compliance with this limit is determined by performing setpoint step change analyses for the control systems; i.e. feedwater controller, pressure controller, and recirculation flow controller. The analyses are performed at the most limiting point along the power-flow operating map, typically the intersection of the natural circulation line and the 100% rod line. The reactor system shall be considered stable if the decay ratio X_2/X_0 is less than 1.0.

Note that the bundle channel stability analysis is performed separately by the fuel vendor.

4.4

EVALUATION AND APPLICATION OF UNCERTAINTIES

There are four areas of uncertainty which must be accounted for when performing licensing analyses. These are measurement uncertainties, code modeling uncertainties, input parameter uncertainties, and the uncertainties associated with use of a particular correlation. In general, these four categories overlap in their definitions. However, they can be used to describe all the areas of uncertainties.

Once the uncertainties have been defined, they are quantified against the available data to show conservatism and then combined deterministically within the NSPNAD methodology. That is to say, they are all applied in the conservative direction in order to produce conservative results. No attempt is made to statistically quantify the final result, but rather the conservatism of the results is assured through the compounding of the uncertainties. This methodology is similar to the PWR methods used by NSPNAD (Reference 17).

The following sections describe the evaluation and application of the four categories of uncertainties described above to the three acceptance criteria described in Section 4.3.

4.4.1 THERMAL LIMITS

Measurement Uncertainties

The GETAB methodology [18, 19, 20] generically includes uncertainties on the initial core operating conditions (See Table S.2-1 of Reference 7) in determination of the GEXL correlation safety limit. Therefore, no additional uncertainties need be applied.

Code Modeling Uncertainty

Code modeling uncertainties were quantified by comparing the calculated versus measured $\Delta\text{CPR}/\text{ICPR}$ for the Peach Bottom turbine trip tests and the Monticello turbine trip start up test (See Sections 3.2.2.1 and 3.2.2.2.1 respectively). The results are summarized in Table 4.4-1. The results show that in all cases DYNODE-B overpredicts $\Delta\text{CPR}/\text{ICPR}$ by approximately 10 percent. Therefore, no additional uncertainties need be applied.

Input Parameters Uncertainty

The application of input parameter uncertainties is described in Section 4.2. No additional uncertainties need be applied.

CPR Correlation Uncertainty

The GETAB methodology includes the GEXL correlation uncertainty in the determination of the safety limit. Therefore, no additional uncertainties need be applied for any case except the Fuel Loading Error transient. Reference 7 states that an additional penalty of 0.02 on ΔCPR must be applied to the misoriented bundle results to account for uncertainties associated with the ability of GEXL to predict CPR for an axially varying R-factor.

4.4.2 ASME VESSEL OVERPRESSURE

Measurement Uncertainties

The transient analyses used to determine compliance with the ASME Vessel Overpressure criteria are initiated from 1038 psia steam dome pressure. This initial operating pressure includes a 0.5 percent uncertainty (one standard deviation).

Code Modeling Uncertainty

Code modeling uncertainties were quantified by comparing the calculated versus measured steam dome pressures for the Peach Bottom turbine trip tests, the Monticello turbine trip start up test, and the Monticello MSIV closure start up test (See Section 3.2.2.1, 3.2.2.2.1 and 3.2.2.2.2 respectively). The results are summarized in Table 4.4-2. The results show that in all cases DYNODE-B overpredicts the peak steam dome pressure by approximately two percent. Therefore, no additional uncertainties need be applied.

Input Parameter Uncertainty

The application of input parameter uncertainties is described in Section 4.2. No additional uncertainties need be applied.

Correlation Uncertainty

No special empirical correlations are used in the calculation of vessel pressure. Therefore, this section is not applicable.

4.4.3 SYSTEM STABILITY

Measurement Uncertainties

The transient analyses used to determine compliance with the system stability criteria are initiated from an operating condition which includes a +2% uncertainty on reactor power and a -3% uncertainty on core flow. These values represent one standard deviation and are taken from Reference 16.

Code Modeling Uncertainties

Code modeling uncertainties were quantified by comparing the calculated versus measured APRM decay ratio for the Monticello feedwater controller level setpoint step, pressure regulator setpoint step, and automatic flow decrease start up tests (See Sections 3.2.2.2.6, 3.2.2.2.5, and 3.2.2.2.4, respectively). The results are summarized in Table 4.4-3. The results show that in all cases DYNODE-B conservatively overpredicts the APRM decay ratio. Therefore, no additional uncertainties need be applied.

Input Parameter Uncertainty

The application of input parameter uncertainties is described in Section 4.2. No additional uncertainties need be applied.

Correlation Uncertainty

No special empirical correlations are used in the calculation of the decay ratio. Therefore, this section is not applicable.

Table 4.1-1

SPECTRUM OF EVENTS FOR THERMAL LIMITS ACCEPTANCE CRITERIA EVALUATION

<u>Event</u>	<u>Kinetics Model to be Used for Evaluation*</u>	<u>Thermally Limiting or Near Limiting (Typically)</u>
DECREASE IN REACTOR CORE COOLANT TEMPERATURE		
Loss of Feedwater Heating	POINT	X
Feedwater Controller Failure - Maximum Demand	ONE-D	X
Pressure Regulator Failure - Open	POINT	
INCREASE IN REACTOR PRESSURE		
Pressure Regulator Failure - Closed	ONE-D	
Generator Load Rejection	ONE-D	X
Turbine Trip	ONE-D	
Main Steamline Isolation Valve Closure	ONE-D	
Loss of Condenser Vacuum	ONE-D	

Table 4.1-1 (continued)

<u>Events</u>	<u>Kinetics Model to be Used for Evaluations*</u>	<u>Thermally Limiting or Near Limiting (Typically)</u>
Loss of AC Power Transformer	POINT	
Loss of Auxiliary Power - All Grid Connections	ONE-D	
Loss of Feedwater Flow	POINT	
DECREASE IN REACTOR COOLANT SYSTEM FLOW RATE		
Recirculation Pump Trip	POINT	
Recirculation Flow Control Failure - Decreasing Flow	POINT	
REACTIVITY AND POWER DISTRIBUTION ANOMALIES		
Abnormal Startup of Idle Recirculation Pump	POINT	
Recirculation Flow Control Failure With Increasing Flow	POINT	
Control Rod Withdrawal	ONE-D	
Fuel loading Error	POINT	

Table 4.1-1 (continued)

<u>Event</u>	<u>Kinetics Model to be Used for Evaluation*</u>	<u>Thermally Limiting or Near Limiting (Typically)</u>
INCREASE IN REACTOR COOLANT INVENTORY		
Inadvertent HPCIS or RCICS actuation	POINT	
DECREASE IN REACTOR COOLANT INVENTORY		
Inadvertent Safety/Relief Valve Opening	POINT	

* Not all Transients are reanalyzed for operating plant reload applications.

Table 4.1-2

SPECTRUM OF EVENTS FOR ASME VESSEL
OVERPRESSURE ACCEPTANCE CRITERIA EVALUATION

<u>Event</u>	<u>Kinetics Model to Be Used for Evaluation</u>
MSIV Closure with Position Switch Scram Failure (i.e., MSIV Flux Scram)	ONE-D

Table 4.1-3

SPECTRUM OF EVENTS FOR SYSTEM STABILITY ACCEPTANCE CRITERIA EVALUATION

<u>Event</u>	<u>Kinetics Model to Be Used for Evaluation</u>
Level Controller Setpoint Step	POINT
Pressure Controller Setpoint Step	POINT
Flow Controller Setpoint Step	POINT

Table 4.1-4

DYNODE-B OPTION MODEL SELECTION FOR LICENSING APPLICATIONS

<u>Model Option</u>	<u>Licensing Value</u>
Number of Oxide Radial Nodes	5
Number of Cladding Radial Nodes	2
Number of Axial Nodes	24
Oxide Heat Capacity	Curve Fit
Gap Heat Transfer Coefficient	Constant
Cladding Surface Heat Transfer Coefficient	Thom
Critical Power Ratio*	GEXL
Main Steam Line Representation	Method of Characteristics
Steam Dome Pressure Model	Based on Riser and Dome Fluid. Liquid assumed to be subcooled if dome $\Delta P/\Delta t \geq 1.0$ psi/sec
Carryunder	Included
Turbine Model	Included
Pressure Regulator	Detailed
Void Model	Profile Fit
	Non-Equilibrium Flow Quality
Kinetics	See Tables 4.1-1, 4.1-2, and 4.1-3
Delayed Neutron Groups	6
Decay Heat	1971 ANS Standard
Bypass Heating	Included

* Fuel Vendor Dependent

Table 4.1-4 (continued)

<u>Model Option</u>	<u>Licensing Value</u>
Reactor Flow	Dynamic
Relief Valve	Bank
Relief Valve Stroking	Linear
MSIV Area versus Position	Non-Linear
Stop Valve Area versus Position	Non-Linear
Control Valve Area versus Position	Non-Linear
Bypass Valve Area versus Position	Non-Linear
Feedwater Controller	Detailed Three Element
Reactor Protection System Setpoints and Delays	Included
Radial Heat Generation	Included
Reactor Vessel Temperature Distribution Model	Included
M/G Flow Controller	Detailed with 2nd order Scoop Tube Servo Model
Heat Conductors	Ignored
Direct Moderator Heating	Included
Recirculation Pump Heating	Included

Table 4.1-5

SENSITIVITY OF CPR TO VARIOUS THERMAL-HYDRAULIC PARAMETERS

Parameter	[Δ CPR / Nominal CPR]	
	GE [7]	DYNODE-B
Bundle Power	-1.0	-1.01
Bundle Flow	+0.2*	+0.29
Core Inlet Subcooling	+0.1	+0.06
Core Pressure**	-0.6	-0.55
GEXL R-factor	-2.1	-2.18

NOTE: All DYNODE-B cases performed at nominal Monticello HFP conditions \pm 10%.

* Value for BWR/4

** Constant Subcooling

Table 4.2-1

INITIAL CONDITIONS AND INPUT PARAMETERS FOR
MONTICELLO RELOAD SAFETY EVALUATION MODEL

<u>Parameter</u>	<u>Licensing Value</u>
Initial Power (% NBR)	100
Initial Steam Flow (% NBR)	100
Initial Core Flow (% NBR)	100
Initial Feedwater Flow (% NBR)	100
Initial Core Inlet Enthalpy (Btu/lbm)	524.7 [18]
Initial Steam Dome Pressure (psia)	1038 [18]
Initial S/RV Steamline Pressure (psia)	1031
Initial Turbine Throttle Pressure (psia)	990
Initial Vessel Water Level (inches)	40
Core Exposure	EOC
Power Distribution	Haling
Heat Generated in Fuel (%)	96.5
Heat Deposited in Bypass (%)	1.5
Initial Core Bypass Flow Fraction (%)	10
Gap Heat Transfer Coefficient (Btu/hr ft ² °F)	1000
Void Model Parameters	Default Values
Critical Power Ratio	See Section 4.2.3
Plant Geometry	Monticello Unique
Initial Control Rod Pattern	All Rods Out
Control Rod Motion	All Rods with Same Speed
CRD Scram Time	See Section 4.2.2
Kinetics Parameters	See Section 4.2.1
Scram Setpoints	Tech Spec [12]
Reactor Protection Logic Delay	Maximum Tech Spec [12] (50 ms)
Relief Capacity	Tech Spec [12] (7/8 valves)
Relief Valve Setpoint	Tech Spec [12] (1119.1 psig)

Table 4.2-1 (continued)

<u>Parameter</u>	<u>Licensing Valve</u>
Relief Valve Response	Tech Spec [12] (400 ms delay/150 ms stroke)
Turbine Stop Valve Closure	Fastest Specified (100 ms)
Turbine Control Valve Closure	Fastest Specified (246 ms)
MSIV Closure	Fastest Tech Spec [12] (3 sec)
Flow Control	Manual
Flow Controller Setpoints	Monticello Unique
Feedwater Controller Setpoints	Monticello Unique
Pressure Controller Setpoints	Monticello Unique

Table 4.2-2

AXIAL POWER FACTORS FOR THE HOT CHANNEL MODEL

	<u>Node</u>	<u>APF</u>	<u>Node</u>	<u>APF</u>		<u>Node</u>	<u>APF</u>
(Bottom)	1	0.47	9	1.29		17	1.15
	2	0.55	10	1.34		18	1.08
	3	0.64	11	1.38		19	1.01
	4	0.74	12	1.40		20	0.93
	5	0.85	13	1.39		21	0.84
	6	0.97	14	1.36		22	0.74
	7	1.10	15	1.30		23	0.60
	8	1.21	16	1.23	(Top)	24	0.43

Table 4.2-3

STEADY STATE CRITICAL POWER RATIO COMPARISONS

<u>FUEL TYPE</u>	<u>BUNDLE POWER (MW)</u>	<u>BUNDLE FLOW (10³ lbm/hr)</u>	<u>CPR</u>	
			<u>GE</u>	<u>DYNODE-B</u>
8x8	5.320	99.2	1.34	1.347
8x8R	5.683	98.3	1.37	1.369

Inlet Conditions: $H_{in} = 524.2$ Btu/lbm
 $P = 1038$ psia

Table 4.3-1

FUEL CLADDING INTEGRITY LIMIT MCPR FOR MONTICELLO

<u>Fuel Type</u>	<u>MCPR LIMIT</u>
Reload Core 8x8	1.06
Reload Core 8x8R	1.07
Reload Core P8x8R	1.07

Table 4.4-1

COMPARISON OF MEASURED VERSUS CALCULATED TRANSIENT ΔCPR/ICPR

Transient Event	ΔCPR/ICPR		% Difference*
	Measured	Calculated	
Peach Bottom Turbine Trip Test TT1	0.170	0.187	+10.0
Peach Bottom Turbine Trip Test TT2	0.136	0.149	+ 9.6
Peach Bottom Turbine Trip Test TT3	0.132	0.149	+12.9
Monticello Turbine Trip Start-Up Test	0.003	0.156	+5000

* % Difference = $[(\text{Calculated} - \text{Measured})/\text{Measured}] * 100$

Table 4.4-2

COMPARISON OF MEASURED VERSUS CALCULATED
MAXIMUM TRANSIENT STEAM DOME PRESSURE

Transient Event	Maximum Steam dome Pressure (psia)		
	Measured	Calculated	% Difference*
Monticello Turbine Trip Start-Up Test	1130	1154	+2.0
Monticello MSIV Closure Start-Up Test	1084	1109	+2.3
Peach Bottom Turbine Trip Test TT1	1031	1047	+1.6
Peach Bottom Turbine Trip Test TT2	1038	1062	+2.3
Peach Bottom Turbine Trip Test TT3	1061	1082	+2.0

* $\% \text{ Difference} = [(\text{Calculated} - \text{Measured}) / \text{Measured}] * 100$

Table 4.4-3

COMPARISON OF MEASURED VERSUS CALCULATED
TRANSIENT POWER DECAY RATIO

Transient Event	DECAY RATIO		Difference*
	Measured	Calculated	
Monticello Feedwater Controller Setpoint Step Start-Up Test	0.0	0.0	0.0
Monticello Pressure Controller Setpoint Step Start-Up Test	0.0	0.21	+0.21
Monticello Flow Controller Setpoint Step Start-Up Test	0.25	0.89	+0.64

* Difference = Calculated - Measured

5.0 CONCLUSIONS

This report is intended to show two major conclusions:

- 1) DYNODE-B is capable of accurately modeling all of the transient phenomena of a Boiling Water Reactor Nuclear Steam Supply System during abnormal transient events.
- 2) DYNODE-B, when used in conjunction with the methodology described in Section 4, conservatively predicts the transient response of a BWR NSSS.

The first conclusion is shown in Sections 2 and 3 of this report by first describing the models used and then benchmarking those models against other licensing computer codes and against transient test data.

The second conclusion is shown in Section 4 by first describing the methodology used and then quantifying it with test data.

Based on the information presented in this report, it is concluded that the Northern States Power Nuclear Analysis Department is capable of performing BWR Transient Licensing Analyses, within the limits described herein, utilizing the DYNODE-B computer code and the methodology described in this report.

6.0 REFERENCES

1. "Monticello Nuclear Generating Plant, Qualification of Reactor Physics Methods for application to Monticello," NSPNAD-8609, Rev 0 September 1986.
2. Northern States Power Co, "Monticello Nuclear Generating Plant Final Safety Analysis Report," Docket 50-263, November 1968.
3. Northern States Power Co, "Monticello Nuclear Generating Plant Update Safety Analysis Report," Docket 50-263 October 1981.
4. "Supplemental Reload Licensing Submittal for Monticello Nuclear Generating Plant Reload 10 (Cycle 11)," 23A1673, January 1984.
5. U.S. Nuclear Regulatory Commission , "Standard Review Plan for the Review of Safety Analysis Reports for Nuclear Power Plants," NUREG-0800, July 1981.
6. Northern States Power Co, "DNB86098 Computer Code Users Manual," June 1986.
7. General Electric Co., "General Electric Standard Application for Reactor Fuel," NEDE-24011-P-A-7-US, August 1985.
8. R.B.Linford, "Analytical Methods of Plant Transient Evaluations for the General Electric Boiling Water Reactor," NEDO-10802, February 1973, and Amendments 10802-01 and 10802-02.
9. "Qualification of the One-Dimensional Core Transient Model for Boiling Water Reactors," NEDO-24154, October 1978.
10. R.C.Kern, et.al, "Best Estimate Analysis of Peach Bottom 2 Turbine Trip Tests at End of Cycle 2," NAI 77-49, August 1977.

REFERENCES (continued)

11. "Core Design and Operating Data for Cycles 1 and 2 of Peach Bottom Unit 2," EPRI-NP-0563, June 1978.
12. Northern States Power Co., "Monticello Nuclear Generating Plant Technical Specifications," Docket 50-263, License DPR-22.
13. "Monticello Nuclear Power Station Unit No. 1 Plant Transient Design Analysis Report," NEDC-10069, July 1969.
14. General Electric Co., "Monticello Unit No. 1 Startup Test Results," NEDE-10563
15. ASME Boiler and Pressure Vessel Code, Section III, Article NM-7000, "Protection Against Overpressure," American Society of Mechanical Engineers.
16. "Transient and Stability Tests at Peach Bottom Atomic Power Station Unit 2 at End of Cycle 2," EPRI NP-564, June 1978.
17. Northern States Power Co., "Prairie Island Nuclear Power Plant Reload Safety Evaluation Methods," NSPNAD-8102P Rev. 3, March 1985.
18. "General Electric BWR Thermal Analysis Basis (GETAB): Data, Correlation and Design Application," January 1977 (NEDE-10958-PA and NEDO-10958-A).
19. "Basis for 8x8 Retrofit Fuel Thermal Analysis Application," September 1978 (NEDE-24131).
20. Letter, R. E. Engel (GE) to D. G. Eisenhut and R. L. Tedesco (NRC), "Additional Information, 8x8R Fuel GETAB R-Factors," March 30, 1979.

REFERENCES (continued)

21. Letter, R. H. Buchholz (GE) to P.S. Check (NRC), "Response to NRC Request for Information on ODYN Computer Model," September 5, 1980.
22. J. M. Holzer, et.al., "A Code System to Produce Point Kinetics Parameters for LWR Calculations," ANS Trans, 39, 946-7, 1981.